Structural and Functional Studies of Caveolae in the Femoral Artery

Thesis submitted in accordance with the requirements of the University of Liverpool for the degree of Doctor in Philosophy

By

Ashraf Albrakati

July 2013

Acknowledgments

It would not have been possible to write this PhD thesis without the help and support of the kind people around me, to only some of whom it is possible to give particular mention here. Above all, I would like to thank my wife and my three angels for their support and great patience at all times.

This thesis would not have been possible without the help, support and patience of my principal supervisors, Dr. Tomoko Kamishima and Dr. John Quayle, not to mention their help, supervision, advice, and the critical reading of the manuscript. The good advice, support and friendship of my second supervisor, Dr. Caroline Dart, has been invaluable on both an academic and a personal level, for which I am extremely grateful. I also thank the Department of Cellular and Molecular Physiology for their support and assistance since the start of my postgraduate work in 2009, especially the postgraduate tutor, Dr. Alec Simpson.

Last, but by no means least, I thank my friends in the United Kingdom, Saudi Arabia, Egypt and elsewhere for their support and encouragement throughout, some of whom have already been named. For any errors or inadequacies that may remain in this work, of course, the responsibility is entirely my own.

Finally, I would also like to thank Taif University in the Kingdom of Saudi Arabia for funding this project and for granting me this scholarship.

Table of Contents

List of Tables

List of Figures

List of Abbreviation

$[Ca^{2+}]_i$ - intracellular concentration of calcium

$[cAMP]_i$ - intracellular cAMP concentration

$[cGMP]_i$ - intracellular cGMP concentration

µl - micro litre

µM - micro molar

$5\text{-}HT_{2A}$ - serotonin receptor

8-Br-cGMP - 8-bromo-cGMP

AC - adenylyl cyclase

AF-488 - alexa fluor 488

AF-594 - alexa fluor 594

ANOVA- analysis of variance

ATP- adenosine triphosphate

AVP - arginine vasopressin

Bay K-8644 - dihydropyridine

BK_{Ca} channels - large conductance calcium activated potassium channel

C - collagen fibres

Ca^{2+} - calcium

Ca^{2+}-CaM- calcium calmodulin complex

CaM - calmodulin

cAMP - cyclic adenosine monophosphate

Cav - caveolae

cav-1- caveolin-1

cav-2 - caveolin-2

cav-3 - caveolin-3

caveolae-mitochondria - caveolae and mitochondria

caveolae-SR - caveolae and sarcoplasmic reticulum

cGMP - cyclic guanosine monophosphate

Ch-MCD - cholesterol-saturated methylcyclodextrin

Cl^- - chloride ion

CSD - caveolin scaffolding domain

CTX - charybdotoxin

DAG - diacylglycerol

DMSO - dimethyl sulphoxide

ECs - endothelial cells

ECS - endothelial cells sheath

EDHF - endothelium-derived hyperpolarising factor

EEL - external elastic lamina

EGFR - epidermal growth factor receptor

EIEL - extension of IEL to sides of SMCs

EMT - electron microscope tomography

eNOS - endothelial nitric oxide synthase

ER - endoplasmic reticulum

ET1 - endothelin-1

ET_A - endothelin receptor

FA - femoral artery

FSK - frskolin

G - gap

g - gram

GPCRs - G protein-coupled receptors

GTP - guanosine-5'-triphosphate

HCAECs - human coronary artery endothelial cells

HEPES - N-2-hydroxyethylpiperazine-N-2-ethane sulfonic acid

Her2/Neu - oncogene c-erbB-2

HH - human hair

HVACs - high voltage activated channels

IBTX - iberiotoxin

ICC - immunocytochemistry

IEL - internal elastic lamina

IHC - immunohistochemistry

IK_{Ca} - intermediate conductance calcium activated K^+ channels

IP_3 - inositol trisphosphate

IP_3R - inositol 1, 4, 5-trisphosphate receptor

ISO - isoproterenol

K^+ - potassium ions

K_{ATP} - ATP-sensitive potassium channels

K_{Ca} - calcium activated potassium channel

KCl - potassium chloride

KO - knockout

KPSS - high K^+ solution

K_v - voltage dependent potassium channel

L - lumen diameter

LDL - low-density lipoproteins

LM and TEM - light and transmission electron microscope

L-NAME - L-N^G-Nitroarginine methyl ester

L-NMMA - N^G-monomethyl-L-arginine

LVACs - low voltage activated channels

M - mitochondrion

MEGJ - myoendothelial junctions

Mg^{2+} - magnesium ion

MLCK - myosin light-chain kinase

mM - milli molar

mN- milli newtons

mV – milli volts

M-β-CD - methyl-β-cyclodextrin

n - number of samples

Na^+ - sodium ion

NaCl - sodium chloride

Ne - nexus junctions

NE - norepinephrine

NO - nitric oxide

NS-1619 - 1,3-Dihydro-l-[2-hydroxy-5-(trifluoromethyl) phenyl]-5-(trifluoromethyl)-2i/benzimidazol-2-one

PBS - phosphate buffered saline

PE - phenylephrine

PIP_2 - phosphatidylinositol 4,5-bisphosphate

PKA - protein kinase A

PKC - protein kinase C

PKG - protein kinase G

PSS - physiological saline solution

RCK - conductor domains

RMSA - rat mesenteric smooth muscle arteries

ROCs - receptor-operated channels

RyR - ryanodine-sensitive Ca^{2+} release receptors

S - spanning domains

SDS - sodium dodecyl sulphate

SDS-PAGE- sodium dodecyl sulfate polyacrylamide gel electrophoresis

SEM - scanning electron microscopy

SERCA - SR Ca^{2+}-ATPase

sGC - soluble guanylyl cyclase

SK - small-conductance

SK_{Ca} - small conductance calcium-activated K^+ channels

SMCs - smooth muscle cells

SNP - sodium nitroprusside

SR - sarcoplasmic reticulum

SSC - sodium citrate buffer

STOCs - spontaneous transient outward currents

TA - tunica adventitia

TBA^+ - tetrabutylammonium ions

TBST - Tris-Buffered Saline and Tween 20

TEA^+ - tetraethylammonium ions

TEM - transmission electron microscopy

TI - tunica intima

TM - tunica media

TRPC1 - transient receptor potential channel 1

U44619 - thromboxane analogue

V - caveosomes

V_1 - vasopressin receptor

VDCCs - voltage-dependent calcium channels

v-rsc - Rous sarcoma viral oncogene

vWF - Von Willebrand factor

Abstract

Structural and Functional Studies of Caveolae in the Femoral Artery

Caveolae are important microdomains found in the plasma membrane, which act as signalling hubs in endothelial cells (ECs) and smooth muscle cells (SMCs). Thus, disruption of caveolae by membrane cholesterol depleting agents such as methyl β-cyclodextrin (M-β-CD) has various functional effects on arteries, including impairment of endothelium-dependent relaxation and augmentation of smooth muscle cell contraction independently of the endothelium.

The aim of this study was to test the hypotheses that caveolae modulate contractility in rat femoral artery, and more specifically the response to BK_{Ca} channel activity. Different methods were used in the study including; transmission electron microscopy (TEM), immunohistochemistry, immunocytochemistry and Western blot, and myography. M-β-CD was used in this work to disrupt caveolae from the plasma membranes of SMCs and ECs of rat femoral artery.

TEM examination showed that caveolae were present throughout the plasma membrane of the SMCs and ECs in femoral artery. TEM examination also showed that treatment of the artery with M-β-CD, causes removal of caveolae from most of plasma membrane of the SMCs and ECs. Immunohistochemistry and immunocytochemistry results showed that cav-1, cav-3 and BK_{Ca} channels are co-expressed in SMCs, and cav-1 and BK_{Ca} channels are present in ECs. The presence of these proteins in femoral artery tissue lysate was confirmed by Western blot. Femoral artery contraction studies using myography showed that caveolar disruption by M-β-CD caused a significant increase in the contraction in endothelium-intact artery rings in response to 20 mM K^+ and 100 nM BayK-8644 (20 K/ Bay K). In endothelium-denuded artery rings and/or after incubation of endothelium-intact artery rings with L-NAME (an eNOS inhibitor), there was a non-significant increase in the contraction in response to 20K/ BayK. Incubation of endothelium-intact artery rings with TEA^+ or IBTX, both BK_{Ca} channel inhibitors, caused a significant increase in the contraction to 20 K/ Bay K. Incubation of endothelium-intact artery rings with L-NAME, reduced the contraction to TEA^+ and IBTX. These results provide evidence that contraction of rat femoral artery is inhibited by basal nitric oxide release from the endothelium, and BK_{Ca} channels in the SMCs might have a role in this vasorelaxation.

Further femoral artery relaxation studies showed that the integrity of caveolae was important for the vasorelaxation of arteries (pre-contracted with 20 K/ Bay K) when BK_{Ca} channels were directly activated by NS-1619. In contrast, vasorelaxation by isoproterenol and forskolin in endothelium-denuded artery was not significantly altered after caveolae were disrupted.

These data together suggest that caveolae are an important factor in maintaining Ca^{2+} homeostasis in SMCs in rat artery femoral due to regulation of contractile activation.

Chapter 1 Introduction

The vascular system consists of vessels of varying size and function designed to transport blood, hormones, oxygen, vitamins, glucose, minerals and waste (Mulvany and Aalkjaer, 1990). There are three major types of blood vessel: arteries, veins and capillaries (Aaronson and Ward, 2007). Arteries are further divided into three types according to their size: elastic conducting arteries, muscular distributing arteries and resistance arteries/arterioles. Elastic conducting arteries include the largest artery, the aorta, and the most important characteristic of these arteries is their low resistance due to their large diameter (0.3 cm to 1 cm) (Mulvany and Aalkjaer, 1990, Mulvany and Halpern, 1977). They are richer in elastin and collagen fibers than any other type of vessel to allow them to withstand high pressure (Aaronson and Ward, 2007). Muscular distributing arteries such as femoral arteries are the second largest arteries. The most important function of these arteries is the delivery of blood to target organs. These arteries are important in vasoconstriction and vasodilation as they have a lot of smooth muscle. Finally, resistance arteries and small arterioles are the smallest arteries that deliver blood to capillaries. Control of blood flow through capillary beds is achieved by changing the lumen size of arterioles (Mulvany and Aalkjaer, 1990). Blood flow through a given blood vessel depends directly on the pressure difference between the two ends of the blood vessel, and indirectly on the resistance to blood movement. Blood flow to tissues is regulated by the ability of arteries to constrict (vasoconstriction) or dilate (vasodilation). This property is dependent on the state of contraction of the smooth muscle cells within the arterial wall (Mulvany and Aalkjaer, 1990, Mulvany and Halpern, 1977). Maintained contraction of arterial smooth muscle (smooth muscle tone) causes a sustained

alteration in arterial diameter. Vascular smooth muscle tone is regulated by a diverse range of mechanisms including neuronal, hormonal, biochemical and bioelectrical stimuli (Mulvany and Aalkjaer, 1990, Mulvany and Halpern, 1977). Many of these signals ultimately influence free intracellular Ca^{2+} concentration within the smooth muscle cells (SMC), leading to contraction or relaxation of arteries.

I selected the femoral artery to study as it is an important artery that supplies blood to the groin and thigh area to allow walking, running and other everyday activities. It is also relevant as it susceptible to peripheral arterial disease, mainly through an atherosclerotic process (Dieter et al., 2002).

1.1 Anatomy of the femoral artery

The femoral arteries receive blood from the external iliac artery (Ohayon et al., 2012). The femoral artery is located a little beneath the groin area and continues down along the front of the thigh (Ohayon et al., 2012). Once it crosses the middle of the thigh it merges to become the popliteal artery. The femoral artery is one of muscular distributing arteries with a large lumen, and therefore offers little resistance to the flow of blood. The femoral artery walls are made up of three layers: tunica intima, tunica media and tunica adventitia **(figure 1.1)**. The intimal layer (tunica intima) is composed of a single layer of endothelial cells (ECs) which have a squamous structure and form fenestrations (Zhang, 1999). The medial layer (tunica media) is made up of SMCs embedded within a matrix of elastin and collagen fibres. The tunica media is bound by the internal and external laminae and provides the vessel with the ability to contract. For this reason, this layer has the ability to stretch up to 1.5 times its length and back to their normal length when not under tension (Zhang, 1999). The adventitial layer (tunica adventitia) in the arteries is mainly made

of connective tissue (collagen and elastin), macrophages, mast cells, fibroblasts and Schwann cells and nerve axons (Mulvany and Aalkjaer, 1990), which are mainly adrenergic nerves.

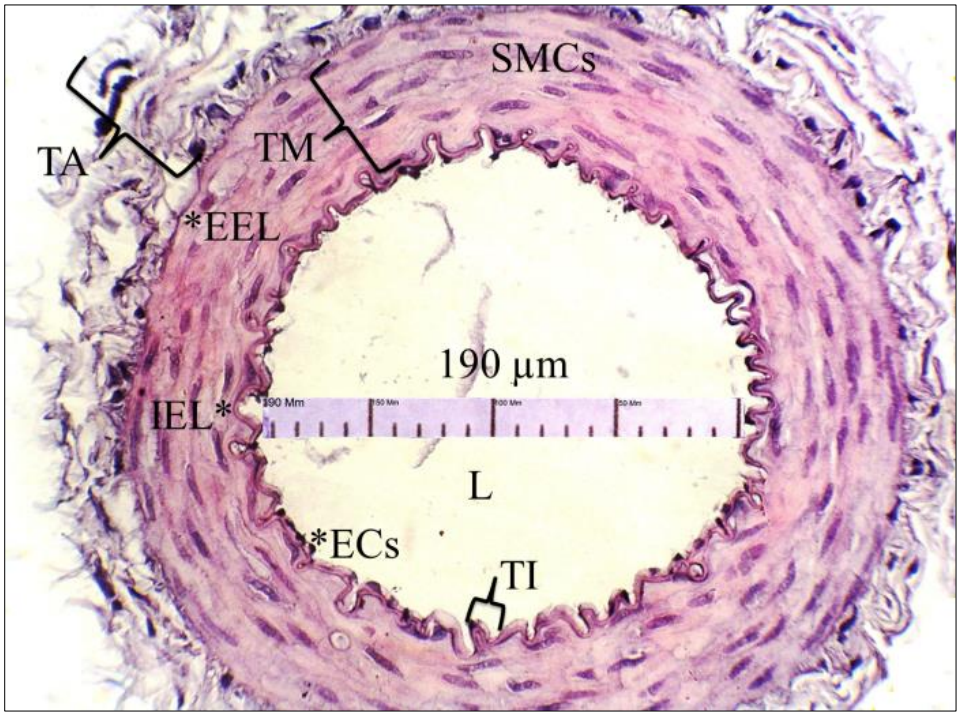

Figure 1.1. A histological preparation of a rat femoral artery showing the three layers; tunica intima (TI), which include ECs; tunica media (TM), which include SMCs; and the tunica adventitia (TA). The internal elastic lamina (IEL) and external elastic lamina (EEL) are also shown. The lumen diameter (L) is about 190 µm. Haematoxylin and eosin staining, X400 magnification.

1.2 Caveolae

1.2.1 Initial discovery

In the 1950s, morphologically-identified caveolae were first described using electron microscopy as flask-shaped, 50-100 nm diameter invaginations in the plasma membrane of endothelial cells (Palade, 1953). After that, Yamada in 1955 observed similar ‘cave-like’ structures in the epithelial cells of the gall bladder of a mouse

(Yamada, 1955). Caveolae are classically described as small omega-shaped invaginations (50-100 nm diameter) in the plasma membrane (**figure 1.2 A and B)** (Palade, 1953, Yamada, 1955). Later studies revealed that caveolae are a special type of a lipid raft, highly enriched in cholesterol and sphingolipids (Brown and London, 1998, Simons and Toomre, 2000). Further investigations identified caveolae in most mammalian cell types with notable abundance in adipocytes (Fan et al., 1983, Scherer et al., 1996), endothelial cells (Feron et al., 1996) and smooth muscle cells (Forbes, 1979).

Forty years later, researchers have identified the most important structural protein of caveolae, known as caveolin (Glenney and Soppet, 1992). Caveolin was re-classified to caveolin-1 (cav-1) after the discovery of two additional members of the caveolin gene family, caveolin-2 (cav-2) and caveolin-3 (cav-3) (Glenney and Soppet, 1992, Way and Parton, 1995, Scherer et al., 1996). Over the course of several years, different studies showed that caveolae are implicated in cellular cholesterol homeostasis, endocytosis, transcytosis, potocytosis, cell signalling and tumour suppression (Razani et al., 2002). More recent studies investigated caveolin-deficiency and how it can cause diseases such as diabetes, cancer, muscular dystrophies and cardiovascular disease (hypertension and atherosclerosis) (Cohen et al., 2004).

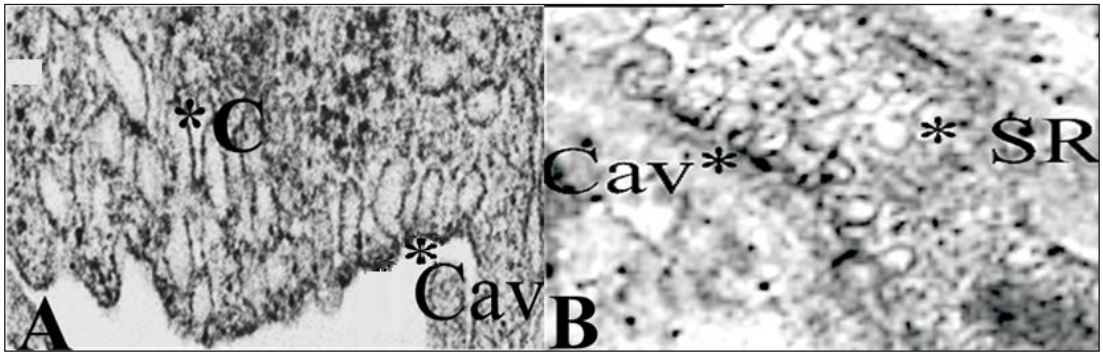

Figure 1.2. Transmission electron micrographs of intact rat femoral artery. A, Endothelial cell. Caveolae (Cav) cover most of the EC membrane. Caveosomes (C) are also abundant. **B**, Smooth muscle cell. Omega-shaped caveolae cover most of the SMC membrane. Also shows the peripheral SR.

1.2.2 Lipid rafts

In 1972, Singer and Nicolson first proposed the fluid-mosaic model to describe the construction of plasma membranes (Singer and Nicolson, 1972). In this model, they suggested that proteins were "floating" within the lipid bilayer like a "liquid" surface cell membrane **(figure 1.3)** (Singer and Nicolson, 1972). Although it is a useful conceptualisation, this model had limitations in explaining several function of the plasma membrane including signal transduction. Additionally, this model ignored the presence of caveolae in the plasma membrane. This model was expanded by Henderson and Unwin in 1975 where they proposed the presence of integral membrane proteins within the cell membrane (Henderson and Unwin, 1975). They also alternated hydrophobic and hydrophilic parts of trans-membrane loops of these proteins. Additionally, they suggested that glycoprotein carbohydrate groups were on the extracellular surface.

In 1997, Simon and Ikonen proposed the modern concept of cell membrane structure. They explained that the plasma membrane is composed of a combination of protein receptors and glycosphingolipids organised in glycolipoprotein microdomains, known as lipid rafts (Simons and Ikonen, 1997). The movement of

the clustering of sphingolipids and cholesterol laterally or sideways within the fluid bilayer leads to raft formation. They also suggested that the rafts function as platforms for the attachment of proteins to allow movement in the membranes laterally or sideways, and to facilitate signal transduction. Plasma membranes have also been re-described by more recent studies on the standard lipid bilayer and lipid rafts within them **(figure 1.4)** (Alberts 2002). Lipid rafts are more tightly-packed than the standard lipid bilayer (Korade and Kenworthy, 2008) and can float freely in the membrane bilayer (Simons and Ehehalt, 2002).

The original concept of rafts was used as an explanation for several cell membrane functions such as the embedding of macromolecules in the phospholipid matrix, the transport of proteins selectively included or excluded in lipid rafts, the regulation of neurotransmission, and receptor trafficking for signal transduction (Korade and Kenworthy, 2008, Pike, 2009).

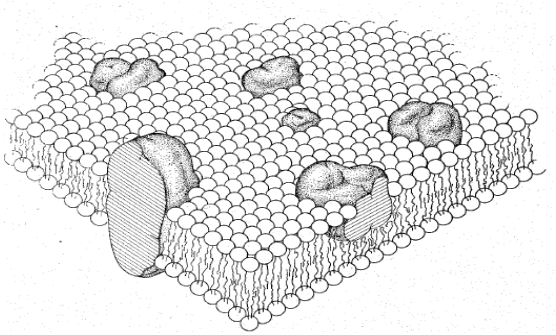

Figure 1.3. The original fluid-mosaic model of the plasma membrane (Singer and Nicolson, 1972).

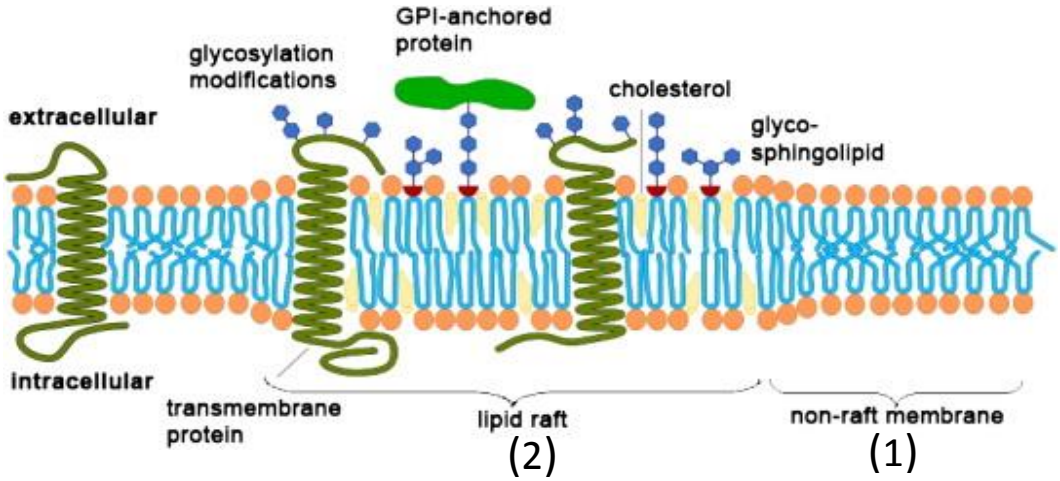

Figure 1.4. The new concept of lipid raft organisation. Area (1) is the standard lipid bilayer, whereas area (2) is a lipid raft. Adapted from Alberts (2002).

1.2.3 Caveolae structure

Caveolae can be described as a cholesterol-rich and clathrin-free invaginated microdomain in the cell membrane (Anderson, 1998) **(figure 1.5 A)**. Morphologically, caveolae have been shown to be a flask-like membrane structure. However, this shape can be changed according to the physiological condition of the cells (Razani and Lisanti, 2001b, Simionescu et al., 1975). Originally, caveolae were identified as a sub-type of lipid raft. However in contrast with lipid rafts, caveolae contain a family of small proteins called caveolins and another family of proteins

called cavins. It has been shown that each caveola contains of approximately 140-150 caveolin molecules (Pelkmans and Zerial, 2005). In addition, caveolae are rich in cholesterol, sphingolipids, receptors and ion channels as well as lipid raft (Lisanti et al., 1994a, Anderson, 1998).

1.2.3.1 Caveolins

Caveolins are considered to be the main structural protein units of caveolae. They are a family of small proteins (18-24 kDa) that are embedded in the cell membrane with both N- and C-terminals reside in the cytosol. Caveolins are comprised of three types: cav-1, cav-2 and cav-3 (Lisanti et al., 1994a, Anderson, 1998). Caveolins are synthesised in the rough endoplasmic reticulum (ER) and subsequently trafficked via the Golgi complex to the cell surface (Hayer et al., 2010).

Caveolins are essential in mediating the invagination of caveolae. Furthermore, caveolins can be oligomerised into a complex of 14-16 subunits and become larger mega-complexes (Minami et al., 1995, Sargiacomo et al., 1995). It is believed that the high affinity of caveolins for cholesterol, oligomerisation and the oligomer-oligomer interactions may facilitate the formation of the 50-100 nm caveolar invaginations (Sargiacomo et al., 1995). A 33 amino acid hydrophobic domain of each caveolin is believed to anchor the protein in the cell membrane (Anderson, 1998).

1.2.3.1.1 Caveolin scaffolding domains

Various studies have identified a 20 amino acid domain that is located in the membrane side of the cytosolic N-terminal domain of caveolin, termed the caveolin scaffolding domain (CSD) (**Table 1**) (Couet et al., 1997). One of the most important

functions of CSDs is their interaction with several binding partners such as G protein α-subunits and Src family kinases (Cohen et al., 2004). Through CSDs, caveolins are able to bind and regulate caveolin-associated signalling proteins. Couet et al. identified the possible binding motifs in these caveolin-associated proteins using a glutathione S-transferase-fusion protein containing the CSD to screen a peptide phage display library (Couet et al., 1997). In this study, the researchers found a high-binding affinity of a selected group of peptides to the CSD, with the sequences of these motifs as following: ΦXΦXXXXΦXXΦ, ΦXΦXXXXΦ and ΦXXXXΦXXΦ where Φ is an aromatic residue (Phe, Tyr, or Trp) and X is any amino acid (Couet et al., 1997).

Table 1. Scaffolding domain sequences and residues of caveolin 1, 2 and 3.

Caveolin	CSD sequence	Residues
Cav-1 D G I W K	A S F T T F T V T K	Y W F Y R 82-101
Cav-2 D K V W I	C S H A L F E I S K	Y V M Y K 54-73
Cav-3 D G V W R	V S Y T T F T V S K	Y W C Y R 55-74

1.2.3.1.2 Caveolin-1

Cav-1 was originally identified by Glenney and co-workers as a component of caveolae in Rous sarcoma virus-transformed chicken fibroblasts (Glenney and Soppet, 1992). Cav-1 has two isoforms, cav-1α (178 amino acid peptide) and cav-1β (147 amino acid peptide); both isoforms have been reported to show overlap with slight differences in their distribution in mammalian cells (Scherer et al., 1995), where cav-1α is the predominant isoform (Hnasko and Lisanti, 2003). The expression of cav-1 is reported in most cell types of the vascular system (Bernatchez

et al., 2005).

Cav-1 has been implicated in a wide range of signal transduction processes (Razani et al., 2002). This protein has a major role in physiological mechanisms that regulate vascular reactivity. In this regard, cav-1 has been shown to be co-expressed with endothelial nitric oxide synthase (eNOS) and has a negative regulatory role in eNOS activity. Consequently, cav-1 association inhibits the release of nitric oxide (NO) (Sowa et al., 2001).

1.2.3.1.3 Caveolin-2

Caveolin-2 (162 amino acid peptide) was identified for the first time in adipose tissue by Scherer et al. using microsequencing of adipocyte-derived caveolin-enriched membranes (~20 kDa) (Scherer et al., 1996). Cav-2 has multiple isoforms: cav-2α, cav-2β and cav-2γ (Hnasko and Lisanti, 2003), and it has been shown that cav-2 co-express with cav-1 in caveolae. The interactions of cav-2 with G proteins in adipose tissue is different from that of cav-1, and maybe explains why cav-1 and cav-2 are co-expressed within a single cell (Scherer et al., 1996).

1.2.3.1.4 Caveolin-3

Caveolin-3 (or M-caveolin) was identified as a muscle-specific isoform through an analysis of a cDNA library screening for cav-1 homologous genes (Way and Parton, 1995). The cav-3 protein (151 amino acid peptide) is organised by two coding exons (Anderson, 1998, McMahon et al., 2009) and is split into four parts: N-terminus (1–53 amino acids), CSD (54–73 amino acids), transmembrane (74–106 amino acids), and C-terminus (107–151 amino acids) (Parton, 1996, Galbiati et al., 2001).

1.2.3.1.5 Caveolin distribution

Tissue expression profile studies have shown expression of both cav-1 and cav-2 in several cell types, with the highest level in adipocytes, endothelial cells, pneumocytes and fibroblasts. Cav-3 expression is limited to muscle (cardiac, skeletal and smooth muscle cells) (Scherer et al., 1994, Scherer et al., 1996, Anderson, 1998). Cav-1 and cav-3 have been shown to be co-expressed in the smooth muscle cells of some specific tissues (Glenney and Soppet, 1992, Razani and Lisanti, 2001b, Razani et al., 2002, Scherer et al., 1996). Furthermore, in other studies, it has been shown that CSDs of both cav-1 and cav-3 bind with same caveolin biding motifs of partner proteins (Okamoto et al., 1998). Expression of both of cav-1 and cav-3 might explain their contribution in the formation of distinct caveolae in smooth muscle cells (Kogo et al., 2006).

1.2.3.1.6 Cavins

Cavins modulate caveolin function and organization by acting as scaffolding proteins and by regulating the availability of caveolins (Chidlow and Sessa, 2010). Four cavin isoforms have been discovered: cavin-1, cavin-2, cavin-3 and cavin-4. Cavins are closely related in primary structure and possess a highly conserved N-terminal domain. Moreover, cavins are distributed in different tissues (Chidlow and Sessa, 2010) suggesting that each member regulates tissue-specific caveolae function.

1.2.3.1.6.1 Cavin-1

Cavin-1, also known as polymerase transcript release factor, is one of the proteins that supports caveolin as it plays an important role in the regulation of caveolin expression and caveolae formation and organisation (caveolae morphology) (Liu and Pilch, 2008, Chidlow and Sessa, 2010). The importance of cavin-1 in caveolae

formation has been demonstrated in adipose tissue (Aboulaich et al., 2004). The co-expression of cavin-1 with cav-1 has been demonstrated in lipid rafts (Aboulaich et al., 2004). Importantly, the interaction between cavin-1 and cav-1 seems indirect as loss of caveolae disrupts the association of cavin-1 and cav-1. The role of cavin-1 appears to be stabilizing shape of caveolae by acting as its molecular anchor to cytoskeletal proteins (Liu and Pilch, 2008). Moreover, the importance of cavin-1 for the stability of cav-1 has been confirmed in vitro as over-expression of cavin-1 has been shown to cause increased levels of cav-1 (Hill et al., 2008).

These findings were further supported by Hayer et al. using live-cell imaging to demonstrate that cav-1 scaffolds are trafficked to the plasma membrane independently from cavin-1. The trafficking of cav-1 alone to the plasma membrane without cavin-1, suggest that the interaction between cavin-1 with cav-1 might only assist in the formation of caveolae (Hayer et al., 2010).

1.2.3.1.6.2 Cavin-2

Cavin-2, also known as a serum deprivation-response protein, has been demonstrated to directly bind with cavin-1 and recruit it to the plasma membrane (Hansen et al., 2009). It has also been shown that cavin-2 is necessary for the expression of cav-1 and cavin-1 proteins in the cell membrane and subsequent formation of caveolae (Hansen et al., 2009). Over-expression of cavin-2 in vitro has been reported to cause the formation of elongated tubular caveolae that might be involved in channel formation (Gustincich et al., 1999, Hansen et al., 2009). These studies also highlighted the importance of cavin-2 in caveolae signalling and compartmentalisation of PKC to caveolae. Cavin-2 has also been shown to be

important for pleckstrin (a protein found in platelets), a platelet PKC substrate when bound to cavin-2 (Baig et al., 2009).

1.2.3.1.6.3 Cavin-3

It has been shown that cavin-3 is expressed only when cav-1 is expressed in the same cells although the expression of cav-1 was detected alone without cavin-3 in some tissues. This suggests that the expression of cavin-3 might be linked to the expression of cav-1 (McMahon et al., 2009). Furthermore, it has been shown that down-regulation of cavin-3 occurs as a result of depletion of cav-1. This also indicates that cav-1 is necessary for cavin-3 stability (McMahon et al., 2009). Another study demonstrated the presence of cavin-3 in caveolae and endocytic vesicles (Mundy et al., 2002), and that it traffics with cav-1 to different places in the cell (McMahon et al., 2009). This might indicate that cavin-3 plays an important role in caveolae budding or movement of the endocytic vesicles beside microtubules. On the other hand, intracellular trafficking has been impaired when cavin-3 was absent. Together, these results suggest that cavin-3 is important for caveolae budding to form vesicles (Izumi et al., 1997).

1.2.3.1.6.4 Cavin-4

Cavin-4 has been shown to be expressed in muscle, with an extremely high expression in skeletal and cardiac muscle (Tagawa et al., 2008, Bastiani et al., 2009). Bastiani et al. (2009) have shown that cavin-4 is localised with cav-3 and interacts with cavin-2. Furthermore, cavin-4 may influence the differentiation of skeletal muscle, and so it may play a role in caveolae-associated muscle disease (Bastiani et al., 2009).

1.2.4 Formation of caveolae

The formation and function of caveolae has mainly been attributed to the caveolin family (Rothberg et al., 1992) **(figure 1.5 B)**. Cav-1 and cav-2 are expressed in non-muscle and smooth muscle tissues (Parolini et al., 1999). However, cav-3 is specifically expressed in cardiac, skeletal and vascular smooth muscle (Tang et al., 1996). Cav-1 and cav-3 have been shown to be essential in the formation of caveolae in muscle. Deleting cav-1 or cav-3 in mice was shown to result in a loss of caveolae (Drab et al., 2001, Galbiati et al., 2001). Moreover, it has been shown that introducing the expression of cav-1 in cells in which caveolae or caveolins are not normally detectable results in *de novo* formation of caveolae in these cells (Fra et al., 1995). The importance of caveolin in the biogenesis of caveolae has also been demonstrated in a prokaryotic host lacking any intracellular membrane system. In this simple model system, introducing recombinant caveolins induced the formation of caveolae-like structures (Walser et al., 2012). Although cav-2 is associated with cav-1 in various cell types and is a component of caveolae structure, it is redundant in caveolae formation, and thus its role is still elusive (Scherer et al., 1996). The recent model of caveolae biogenesis proposes that assembly is linked to the biosynthetic trafficking of cav-1(Kirkham et al., 2008). Cav-1 is synthesised and oligomerised in the endoplasmic reticulum. After the transportation of the cav-1 oligomers to the Golgi complex, they form larger complexes and associate with cholesterol (Hayer et al., 2010). Following trafficking of caveolin complexes to the plasma membrane, cavins are recruited to stabilise the caveolin oligomers. Loss of cavin-1 in cultured cells was shown to cause depletion of caveolae (Hill et al., 2008). Deleting cavin-1 in mice resulted in caveolae loss and reduced levels of caveolins (Liu and Pilch, 2008). Therefore, cavin-1 is a crucial component for caveolae

generation and maintenance. Cavin-2 has been shown to be an important element in the formation of the caveolar membrane curvature (Hansen et al., 2009). However, the precise roles of other cavins have not yet been elucidated.

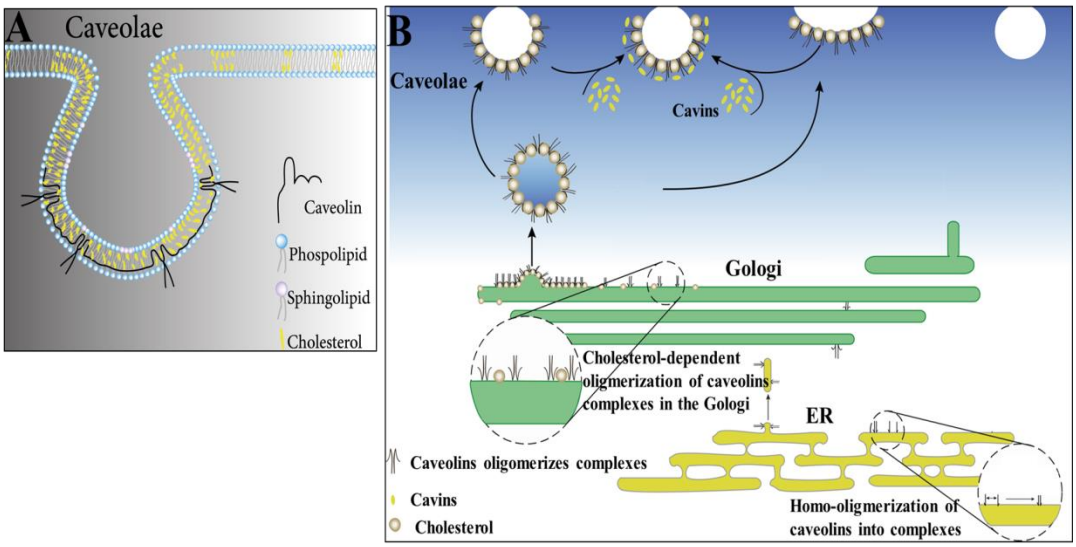

Figure 1.5. Schematic diagram; A. Main features of caveolae and caveolins. **B**. Caveolae formation and membrane trafficking of cav-1. Figure B is modified from Hayer et al. (2010).

1.2.5 Roles of caveolae/caveolins

Since their discovery in 1953, several functional roles have been attributed to caveolae and caveolins in numerous cell types. In this section, I will focus on the most important functional roles of caveolae and caveolins.

1.2.5.1 Vesicular transport

At the level of the vascular endothelium, most molecules internalise through endocytosis. Endocytosis can be mediated via three different pathways: clathrin-coated pits (receptor mediated); pits (fluid-phase); and caveolae-vesicles system transport (receptor mediated) (Moore, 2006). The endocytosis by clathrin-coated pits

and/or pits (fluid-phase) might lead to the transfer of materials to endosomal and/or lysosomal compartments whereas the caveolae-vesicles system can transport macromolecules into the cell (endocytosis) to the endoplasmic reticulum and/or Golgi apparatus complex, or across it through the cell (transcytosis) (Schnitzer, 2001, Razani et al., 2002). In addition to the use of the caveolae-vesicles system for cellular entry, it allows macromolecules to avoid classical digestion in the cell by enzymes in the endosomal and lysosomal compartments (Pelkmans and Helenius, 2002, Na et al., 2003, Panyam et al., 2003). Furthermore, several studies have shown that the caveolae-vesicles transcytosis/endocytosis system transfers macromolecules such as albumin (Ghitescu et al., 1986), insulin (King and Johnson, 1985), low-density lipoproteins (LDL) (Frank et al., 2009), and chemokines (Ge et al., 2008) from the lumen of blood vessels to the sub-endothelial space. Generally, the caveolae-vesicles system can transport molecules through three different pathways: transcytosis, endocytosis and potocytosis.

1.2.5.2 Transcytosis

Transcytosis is considered to be one of the most important functions of the endothelial caveolae where macromolecules from the luminal surface are transferred to the abluminal surface through trans-endothelial channels. These channels might be formed as a result of the connection of free vesicles (caveosomes) to each other and ultimately to caveolae at the other surface (Clough and Michel, 1981) **(figure 1.6 A)**. This mechanism might allow macromolecules to completely and rapidly cross the artery wall via caveolae.

Transcytosis via caveolae is exploited by various viral pathogens as shown in nanotechnology experiments where labelled ‘tracer’ serum proteins were used to

track their dynamic interaction with endothelial cells using electron microscopy (Razani et al., 2002). Furthermore, in another study, antibodies were used to label specific proteins in the capillary lumen. Results of this experiment showed that pathogens completely and rapidly crossed the capillary wall directly via caveolae (Schnitzer, 2001). These studies suggest that caveolae have the ability to select specific proteins to be transported via the transcytosis pathways (Razani et al., 2002).

1.2.5.2.1 Endocytosis

Endocytosis is a process where small and large molecules are taken up by cells from artery lumen and then transported into the intracellular compartments ER and/or Golgi apparatus complex. This occurs exclusively by caveosomes rather than clathrin-coated pits (Razani et al., 2002) **(figure 1.6 B)**. Caveolae also contain dynamin (Henley et al., 1998), a GTPase that mediates the internalisation of caveolar vesicles. Although the complete mechanism of endocytosis is still not clear, several findings suggest that the activation of tyrosine kinases is key in this process (Pelkmans and Helenius, 2002). Certainly, activation of this kinase through phosphorylation leads to active endocytosis through caveolae. Also, the binding of several pathogenic agents, which have receptors in caveolae, leads to the activation of kinase signalling pathways (Norkin, 2001, Norkin et al., 2002). These properties might provide a mechanism to inhibit several pathogens by blocking pathogenesis receptors which are present in caveolae.

1.2.5.3 Potocytosis

It has been shown that caveolae are involved in cellular drinking (solute uptake), also known as potocytosis (Anderson et al., 1992). Through this pathway, the

endothelium can transport small molecules without having to use endosomal/lysosomal compartments, allowing them to avoid classical digestion in the cell (Anderson et al., 1992, Razani and Lisanti, 2001b).

1.2.5.4 Cholesterol homeostasis

Cholesterol homeostasis is attributed to the ability of cav-1 to bind cholesterol in the ER and transport it to caveolae at the plasma membrane. At this stage, the cholesterol molecules can be transferred to extracellular (abluminal surface) lipoproteins or be used for building the plasma membrane. Cav-1 can repeat this cycle through return to the ER/Golgi compartments (Razani and Lisanti, 2001b) **(figure 1.6 C)**. Further analysis found that each cav-1 molecule forms a complex with ~1-2 cholesterol molecules in vitro (Murata et al., 1995). Later, a similar result was reported in vivo (Thiele et al., 2000). Additionally, cav-1 has been shown to transport cholesterol from the ER directly to caveolae, which subsequently flowed to a non-caveolae membrane region (Smart et al., 1996). Moreover, the scavenger receptor B1 (responsible for the influx of LDL particles into the endothelium) has been identified to co-express with cav-1 in caveolae (Graf et al., 1999). These results might indicate a wide and varied interrelationship between cav-1/caveolae and cholesterol in the endothelium.

1.2.5.5 Tumour suppression

The association between caveolins and tumour suppression was first investigated in 1989 by Glenney (1989). He demonstrated that cav-1 is a predominant phosphoprotein in v-src-transformed embryonic chicken fibroblasts. For example, cav-1 was highly expressed, as detected using immunohistochemical and Western

blot analysis, in a non-tumorigenic human fibroblast cell line (IMR-90). On the other hand, in human fibrosarcoma cells (HT-1080), cav-1 expression is greatly reduced. Cav-1 is up-regulated in HT-1080 cells when the mitogen activated protein kinase signalling pathway is inhibited by PD 98059 (Wiechen et al., 2001).

Cav-1 has also been investigated to act as a scaffold for several proteins with a capacity to interact and inhibit various signalling pathways which could activate oncogenes (Razani et al., 2002). Cav-1 has been shown to have suppressor effects on oncogenes such as c-Neu and c-Myc (Engelman et al., 1998a, Park et al., 2001). Further work reported that cav-1 can have similar inhibitory effects on several other receptor tyrosine kinases such as EGFR, Her2/Neu, and PDGF receptor tyrosine kinases, which are localised to caveolae and may act as pro-proliferative/anti-apoptotic signals (Razani et al., 2002). Therefore, cav-1 may be a critical member of cellular tumour suppressors that inhibit the action of tumorigenic signals.

1.2.5.6 Signal transduction

Under control conditions, caveolin binds with other protein molecules in caveolae. Additionally, caveolae can serve to compartmentalize signal transduction molecules in order to influence the function of other proteins (Razani and Lisanti, 2001b) **(figure 1.6 D)**. In this regard, there are several proteins, such as receptor tyrosine kinases, G protein-coupled receptors and ion channels that have been shown to localise to caveolae, as reviewed by (Razani and Lisanti, 2001b). This observation led other authors to suggest that cav-1 might serve to compartmentalise certain signalling molecules within caveolae, focusing on the localisation of these elements within the cell with possibility of selectively modulating cell signalling events (Lisanti et al., 1994a). Therefore, caveolae may serve as a platform for various

receptors and proteins that have a role in signal transduction. When activated by ligand binding, they could be recruited to caveolae.

This suggestion was confirmed by several studies showing the GTPase activity of G protein α-subunits could be inhibited by a 20-amino acid peptide derived from the cav-1 N-terminal domain (residues 82-101, CSD, see **Table 1**) (Li et al., 1995). Further work confirmed the interaction between cav-1 and other proteins including Src family tyrosine knases, PKC isoforms and eNOS (Engelman et al., 1998a, Okamoto et al., 1998, Smart et al., 1999). This confirmed that cav-1 interacts with other proteins through this CSD.

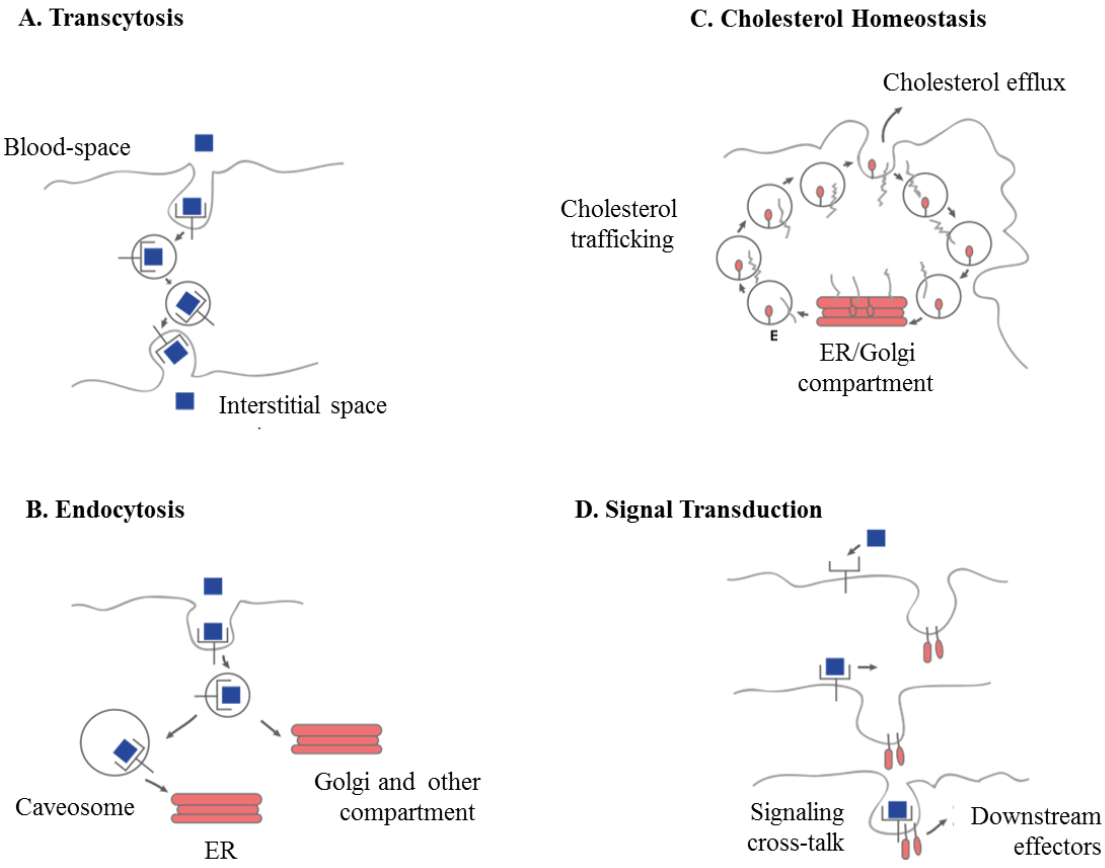

Figure 1.6. Schematic diagram illustrating the physiological functions of caveolae and the caveolins. Modified from Razani and Lisanti (2001). **A**. Transcytosis-transport of proteins from the luminal side to the abluminal surface through trans-endothelial channels. These channels might be formed as a result of the connection of free vesicles (caveosomes) to each other and ultimately to caveolae at the other surface. **B**. Endocytosis is a process for uptake of small and large molecules and their subsequent transport into the intracellular compartments ER and/or Golgi apparatus from the artery lumen exclusively by caveosomes. **C**. Cholesterol homeostasis is attributed to the ability of cav-1 to bind cholesterol in the ER and transport it to caveolae at the plasma membrane. Caveolin can repeat this cycle through return to the ER/Golgi compartments. **D**. Signal transduction; caveolin under control conditions binds with other protein molecules in caveolae. Additionally, caveolae can serve to compartmentalize signal transduction molecules in order to regulate other proteins function.

1.2.5.7 Regulation of endothelial nitric oxide synthase (eNOS)

Caveolae are the key organiser of vascular relaxation via modulation of eNOS activity (Chidlow and Sessa, 2010). eNOS is an isoform of the NOS enzyme and is localised to the caveolae domain at the plasma membrane of endothelial cells (Xu et

al., 2008). The association between cav-1 and eNOS leads to inhibition of eNOS activity and therefore of NO release (Chidlow and Sessa, 2010).

eNOS is targeted to caveolae through co-translocation, N-myristoylation and post-translocation palmitoylation (Ju et al., 1997, Okamoto et al., 1998). eNOS has two binding sites (oxygenase and reductase) which facilitate the direct interaction with the two cytoplasmic domains of cav-1 to form an eNOS-caveolin heteromeric complex (Garcia-Cardena et al., 1997). The caveolin binding motifs (CBMs) of eNOS (FXAAPFXXW) that recognises the CSD of cav-1 is in the oxygenase domain (Garcia-Cardena et al., 1997). The interaction of cav-1 with eNOS causes inhibition of the NO signal until there is an increase in the influx of Ca^{2+}, resulting in formation of the Ca^{2+}-calmodulin complex. The interaction between cav-1 and eNOS is regulated by this Ca^{2+}-calmodulin complex (Michel et al., 1997). Ca^{2+}-calmodulin triggers dissociation of eNOS from cav-1, leading to the oxidisation of L-arginine to generate NO and L-citrulline (Fleming and Busse, 2003, Minshall et al., 2003). NO, in combination with other vasodilatory factors, regulates vascular tone and maintains normal blood vessel function and integrity (Rosselli et al., 1998). Generation of NO by eNOS is regulated by three possible mechanisms: direct interaction of the heteromeric complex of caveolin and Ca^{2+}-calmodulin with eNOS, reversible phosphorylation, and differential localisation of the eNOS-isoenzyme within the endothelial cells. Subcellular eNOS distribution is mediated by lipid modification, for example, myristoylation and dual palmitoylation have the ability to induce the association of the enzyme with the Golgi and cell membrane, respectively (Govers and Rabelink, 2001).

Xu et al. found that disruption of caveolae in the aorta of rats by cholesterol depleting agents, such as methyl-β-cyclodextrin (M-β-CD) and filipin, caused an

impairment of NO function in acetylcholine-induced relaxation (Xu et al., 2007). The reduced NO-mediated relaxation after caveolae disruption might be due to an enhanced "scavenging" of eNOS by cav-1 freed from caveolae, possibly accompanied by internalisation (endocytosis) (Michel, 1999). eNOS and cav-1 translocation from plasma membrane caveolae to the endoplasmic reticulum or Golgi apparatus occurs in cholesterol depleted cells (Blair et al., 1999). eNOS internalises in association with caveolin without the usual agonist-stimulated activation events occurring (Michel, 1999). These results suggest that alterations in plasma membrane cholesterol might alter caveolin–eNOS activity, and subsequently cause endothelial dysfunction. The results from this model show the importance of caveolae in maintaining appropriate regulation of eNOS activity, and therefore NO production.

1.2.5.8 Regulation of ion channel function

Several types of ion channels localise to caveolae and associate with caveolins (Dart, 2010). Cholesterol depletion from lipid rafts, including caveolae, can alter the function of the ion channels that are localised to caveolae, and therefore have an effect on the physiological function of these channels, as summarised in **Table 2**. Cholesterol depletion by cholesterol depleting agents led to altered ion channel function in vascular tissue in response to several types of agonists (Dreja et al., 2002, Prendergast et al., 2010).

1.2.5.8.1 Regulation of large conductance Ca^{2+}-activated K^+ (BK_{Ca}) channel function

In vascular SMCs, BK_{Ca} channels are considered to be the key regulator of artery tone through their inhibitory effect on L-type Ca^{2+} channels. Opening of BK_{Ca} channels reduces L-type (voltage-dependent) Ca^{2+} channel (VDCC) opening, and

therefore decreases Ca^{2+}influx into SMCs, causing vasodilation (Dopico et al., 2012). BK_{Ca} channels belong to a family of Ca^{2+}-dependent K^+ channels in vascular SMCs and have been investigated by biophysical techniques and primary sequence analysis (Cui et al., 1997, Horrigan and Aldrich, 1999).

In vascular SMCs, BK_{Ca} channels can be activated (opened) by several factors, such as locally produced Ca^{2+} transients (sparks) from ryanodine-sensitive Ca^{2+} releasing receptors (RyR) in the sarcoplasmic reticulum (SR) see, Bolton and Imaizumi (1996), agonist stimulation (Ganitkevich and Isenberg, 1990), phosphorylation by protein kinase G (PKG) activation by NO (through the activation of sGC) (Mistry and Garland, 1998) or direct interaction of NO with BK_{Ca} channel proteins (Bolotina et al., 1994). Furthermore, BK_{Ca} channels have been reported to have a large number of potential phosphorylation sites, so regulation could be exerted through the channel phosphorylation by a number of protein kinases (including PKA, PKG, PKC and Src), as reviewed in Hill et al. (2010).

Activation of voltage-dependent Ca^{2+} channels (VDCCs) by depolarization of the SMC cell membrane by high extracellular potassium ion (K^+) concentration or by direct binding by the Ca^{2+} channel agonist Bay K 8644 (Prendergast et al., 2010) can increase bulk cytosolic $[Ca^{2+}]_i$, consequently causing SMCs contraction (Levick, 2010). In contrast to the action of bulk changes in cytosolic $[Ca^{2+}]_i$, local, sub-membrane $[Ca^{2+}]_i$ increases can result in relaxation. Thus, Ca^{2+} sparks through local release of micromolar concentrations of Ca^{2+} from SR via RyR receptors, result in a local increase in Ca^{2+}. The sparks are distributed in regions of close apposition of the plasma membrane to the SR membrane. The distance between the plasmalemma and the superficial SR is about 20 nm in SMCs (Somlyo et al., 1978). SMC contraction does not occur as a result of Ca^{2+} sparks as amount of Ca^{2+} released is insufficient to

raise global Ca^{2+}. Rather, Ca^{2+} sparks activate BK_{Ca} channels in the spark microdomain, thus generating spontaneous transient outward currents (STOCs), inducing membrane hyperpolarisation (the membrane potential becomes more negative), thereby closing VDCCs and causing relaxation (Lacinova, 2005). This mechanism is very important in vascular reactivity and the reduction of myogenic tone (Fallet et al., 2001, Gschwend et al., 2003). Several immunostaining studies have shown that mammalian BK_{Ca} channels are co-expressed with cav-1 and cav-3 (Wang et al., 2005, Riddle et al., 2011). Furthermore, inhibition of BK_{Ca} channels by blockers causes membrane depolarisation, leading to vasoconstriction (Wulf et al., 2009).

In mouse cerebral artery SMCs, BK_{Ca} channels, L-type Ca^{2+}channels and RyR form a functional unit that regulates smooth muscle contractility (Cheng and Jaggar, 2006). Under control conditions, Ca^{2+} influx through L-type Ca^{2+}channels causes release of Ca^{2+} from a cluster of RyRs (a Ca^{2+} spark) resulting activation of BK_{Ca} channels **(figure 1.7 A)** (Sones et al., 2010). Cheng and Jaggar demonstrated that the genetic ablation of cav-1 abolishes caveolae and decreases BK_{Ca} channel opening frequency (Cheng and Jaggar, 2006). Disrupting caveolae in SMCs of the cerebral artery by M-β-CD also leads to decreased spark frequency and amplitude (Lohn et al., 2000). These results suggest that the changes in Ca^{2+} sparks and transient BK_{Ca} channel current might be due to the disruption of the local coupling between BK_{Ca} channels and RyR channels **(figure 1.7 B)**. Similar results have been reported in another paper (Sones et al., 2010). The authors reported that the disruption of caveolae by M-β-CD leads to an inhibition of BK_{Ca} channels in murine portal vein myocytes using patch clamp technique. They found that the application of paxilline (a BK_{Ca} channel blocker) caused inhibition of outward BK_{Ca} channels current and

depolarisation of the cell membrane. A similar result was found when they applied M-β-CD. These results suggest that BK_{Ca} channels in vascular myocytes are inhibit indirectly by caveolar disruption by cholesterol depletion.

The effect of cholesterol depletion in regulating ion channels has been studied by Prendergast et al.(Prendergast et al., 2010). The effects of M-β-CD and cholesterol oxidase (to replenish cholesterol) on Ca^{2+}signals were examined in rat coronary artery myocytes in response to high K^+ solution (KPSS), caffeine (to activate SR Ca^{2+} release) and agonist-induced Ca^{2+} signals. Agonists included 5-HT, endothelin-1 and phenylephrine. Bay K 8644 was also used to stimulate L-type Ca^{2+} channels. Ca^{2+} transients were measured from single SMCs of the coronary artery in response to 5-HT, endothelin-1 and phenylephrine. The authors concluded: (i) application of KPSS, Bay K-8644 or agonists led to an increase in $[Ca^{2+}]_i$ in the SMCs before cholesterol manipulation. (ii) The Ca^{2+} signals generated in response to KPSS or with caffeine were not altered by cholesterol depletion. (iii) Ca^{2+} signals generated by endothelin-1, phenylephrine and 5-HT were significantly decreased after cholesterol depletion. (iv) Application of cholesterol oxidase on M-β-CD treated cells led to a recovery of agonist-induced Ca^{2+} signals.

In the same study, the effect of cholesterol depletion on BK_{Ca} channel function was examined (Prendergast et al., 2010). To examine the effect of M-β-CD on BK_{Ca} channel function, three selective K channel blockers were used before and after incubation with M-β-CD: iberiotoxin (IBTX) to block BK_{Ca} channels, TRAM-34 to block intermediate conductance K channels (IK_{Ca}), and apamin to block small conductance K channels (SK_{Ca}). Results showed that increase in outward current observed with M-β-CD was significantly inhibited by IBTX but not by TRAM-34 or apamin. These results suggest that cholesterol extraction and caveolae disruption by

M-β-CD caused a selective alteration of ion channel function, with L-type Ca^{2+} channel activity unchanged while BK_{Ca} channel activity was positively altered. These results suggest that contraction is a result of a wide range of signalling proteins that are associated with caveolae (Prendergast et al., 2010).

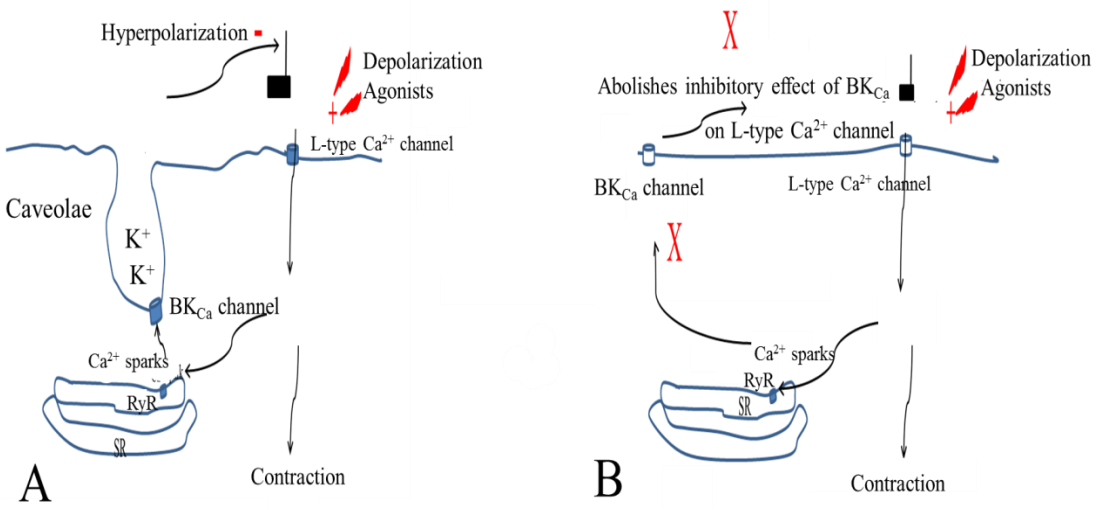

Figure 1.7. Schematic diagram illustrating the physiological role of BK_{Ca} channels in vascular SMCs and activation of these channels by SR-mediated Ca^{2+} sparks. A; in vascular SMCs, BK_{Ca} channels are within the caveolae microdomains. L-type Ca^{2+} channels can activate transient Ca^{2+} rises in the form of Ca^{2+} sparks from the SR via ryanodine-sensitive mechanisms. Presence of SR near to Cav microdomains allows Ca^{2+} sparks to activate BK_{Ca} channels. The efflux of K^+ ions subsequently inhibits L-type Ca^{2+} channels. This promotes SMC relaxation. **B**; Cav depletion by M-β-CD leads to re-distribution of BK_{Ca} channels away from peripheral SR. Consequently, abolishing the inhibitory effect of BK_{Ca} channels on L-type Ca^{2+} channel, resulting from the absence of activation of BK_{Ca} channels by Ca^{2+} sparks.

Table 2. Vascular ion channels associated with caveolae. +: yes; -: not shown; TRPC1: transient receptor potential channel 1; EDHF: endothelium-derived hyperpolarising factor.

Channel	Tissue	Biochemical isolation	Electron microscope	Association caveolin	Functional effect	References
TRPC1	Endothelium-denuded caudal artery	+	+	+	Cholesterol depletion inhibits the TRPC1-store operated Ca^{2+} signal.	(Bergdahl et al., 2003)
L-type Ca^{2+}	Cerebral artery	+	+	-	Cav-1 ablation attenuates the coupling between L-type Ca^{2+}channels and RyR channels.	(Cheng and Jaggar, 2006)
BK_{Ca}	Endothelial (cell lines)	+	-	+	BK_{Ca} channels are inactive under control conditions but can be activated by cholesterol depletion or knockdown of cav-1.	(Wang et al., 2005)
BK_{Ca}	Aorta	-	-	+	Under normal conditions, cav-1 limits the contribution of the BK_{Ca} channels to EDHF-mediated relaxation. Reduced expression of cav-1 leads to greater channel activity to the EDHF- mediated response, which seems essential for maintained coronary dilation.	(Feher et al., 2010)
$K_{ir6.1}$	Vascular smooth muscle cells; HEK293 cells	+ -	+ -	+ -	Cholesterol depletion eliminates cAMP/PKA-dependent regulation of channel. PKC-mediated caveolin-dependent internalisation.	(Jiao et al., 2008)
BK_{Ca}	Gracilis artery endothelium	+	-	+	BK_{Ca} channels are inactive under control conditions but can be activated by cholesterol depletion or exposure of the tissue to chronic hypoxia.	(Riddle et al., 2011)

1.2.5.8.2 Role of caveolae in regulation of artery contraction

A large number of signalling molecules are associated with caveolin as discussed above (Shaul and Anderson, 1998, Razani and Lisanti, 2001b). Furthermore, other molecules that are important in vascular physiology including eNOS, Ca^{2+}-ATP-ase, and the endothelin receptor (Fujimoto et al., 1998) may be regulated by caveolins. For example, the impaired endothelin receptor-induced vascular contractility in cav-1 knockout (KO) mice shows further support for a role of caveolae and caveolins in GPCRs signalling.

Normally, but not exclusively, artery contraction occurs as a response to graded membrane depolarisation which induces elevation of intracellular Ca^{2+} concentration in SMCs by opening of VDCCs (Klabunde, 2004). In contrast, there are a number of negative feedback mechanisms that decrease Ca^{2+} concentration in SMCs including the activation of BK_{Ca} channels (Hill et al., 2010). For example NO, which is released by endothelial cells and diffuses to SMCs, can activate BK_{Ca} channels and consequently decreases Ca^{2+} influx through VDCCs through the inhibitory effect of BK_{Ca} channels on VDCCs. However, several studies have shown that the cholesterol depletion from lipid rafts including caveolae is associated with impairment of both NO and Ca^{2+} signalling in the cardiovascular system, causing aberrations in endothelium dependent-relaxation and contractility, and consequently defects in myogenic tone, as summarised in **Table 3**.

The effects of caveolae disruption by cholesterol depletion agents (such as filipin or M-β-CD) on endothelium-dependent relaxation in different vascular beds have been studied by Xu et al. using an organ bath technique (Xu et al., 2007). They reported that caveolae disruption in the rat aorta, small renal arteries and mesenteric arteries

caused impaired endothelium-dependent relaxation and reduced release of NO and endothelium-derived hyperpolarising factor (EDHF). Consequently, there was decreased NO-dependent relaxation after treatment by either filipin or M-β-CD (Xu et al., 2007). In the same experiment, the inhibition of NOS was examined by N^G-monomethyl-L-arginine) (L-NMMA). In the aorta, treatment with either filipin or M-β-CD only inhibited the NO component, whereas in the renal artery both NO and EDHF pathways were affected. In contrast, in mesenteric arteries, filipin treatment only reduced EDHF-dependent response.

The functional inhibition of caveolae in SMCs by cholesterol depletion with M-β-CD has provided insights to the regulation of arterial contractility. Dreja et al. provided a useful model to explain why contraction was increased after M-β-CD treatment (Dreja et al., 2002) using rat tail artery devoid of endothelium. Contractions were induced using calyculin A (an inhibitor of myosin light chain phosphatase), KPSS (60 mM K^+ to depolarize the cell membrane), cirazoline (α_1-adrenergic agonist), 5-HT (serotonin receptor 5-HT_{2A} agonist), arginine vasopressin (AVP, vasopressin receptor V_1 agonist), endothelin-1 (endothelin receptor ET_A agonist), or AlF_4 (a direct activator of G-proteins) before and after cholesterol depletion by M-β-CD. The cytoplasmic Ca^{2+} concentration of individual smooth muscle cells from the tail artery was also measured before/after cholesterol depletion (Dreja et al., 2002). In cholesterol-depleted preparations, the force response to calyculin A, high K^+, cirazoline and AlF_4 were unaffected. In contrast, responses to 5-HT, AVP and endothelin were significantly reduced. Furthermore, analysis of sucrose density fractionation of non-treated tail artery showed an enrichment of 5-HT_{2A} receptors, but not α1-adrenergic receptors, with cav-1. This result could explain the persistence of the cirazoline-induced response after cholesterol depletion

(Dreja et al., 2002). The contractile response to 5-HT was dependent on extracellular Ca^{2+} and L-type Ca^{2+} channels as verapamil, an L-type Ca^{2+} channel blocker, completely blocked 5-HT–induced contraction. As L-type Ca^{2+} channel activation by membrane depolarisation with KPSS was unaffected after cholesterol-depletion, the impaired 5-HT response after cholesterol depletion seems to be due to a reduced membrane depolarisation in response to 5-HT, leading to a compromised L-type Ca^{2+} channel activation (Dreja et al., 2002).

Dreja et al. also suggested that the Ca^{2+} wave activity, originating from the SR, was selectively affected by cholesterol extraction, with a larger decrease for 5-HT than for cirazoline stimulation. This suggests that inositol trisphosphate (IP_3) formation by 5-HT stimulation may have been impaired by cholesterol depletion. Also, Dreja et al. reported cholesterol depletion caused an increase in basal $[Ca^{2+}]_i$, with a possible consequence of increased Ca^{2+} loading to the SR. Indeed an increased response to caffeine (which opens RyR receptors) was observed after cholesterol depletion. Because Ca^{2+} release by cirazoline was also increased after cholesterol depletion whereas that by 5-HT was not, it may be inferred that IP_3 production by the latter agonist had been reduced. In addition, the artery contraction to 5-HT was restored by exogenous cholesterol, which also restored caveolae formation. So, these results together conclude that the signalling pathways that regulate smooth muscle contraction depend on cholesterol, and serotonergic signalling depends on the integrity of caveolae (Dreja et al., 2002).

The importance of the relationship between caveolae and SR on the contractility of rat mesenteric smooth muscle cells has been studied by Shaw et al. using pressure myography (Shaw et al., 2006). They used M-β-CD to disrupt caveolae, while calyculin-A was used to “de-associate SR and caveolae” (see below). Calyculin A is

a myosin phosphatase inhibitor and so produced maximum and practically irreversible contraction. Mesenteric arteries were stimulated with phenylephrine or U44619 (a thromboxane analogue) before and after M-β-CD treatment. Significantly reduced agonist contractility was observed for both agonists after M-β-CD treatment. In addition, electron microscopy of control mesenteric artery sections showed prominent peripheral SR in close juxtaposition to caveolae of the plasma membrane, as well as central SR close to mitochondria and the nucleus. However, electron microscopy examination of smooth muscle after the treatment with calyculin-A showed SR was no longer in close apposition to caveolae. With M-β-CD treatment, caveolae were absent, although peripheral SR localisation close to the plasmalemma remained visible. Microscope examination of the artery smooth muscle that received cholesterol supplementation following M-β-CD showed a return of the close association of the peripheral SR with caveolae. Calyculin-A treatment markedly decreased Ca^{2+} oscillations in response to phenylephrine or U46619 (Shaw et al., 2006). These results support the idea of the co-expression of caveolae and underlying peripheral SR in smooth muscle cells of mesenteric arteries regulates Ca^{2+} oscillations and contraction.

The effects of caveolae disruption on vascular BK_{Ca} channels and contraction of rat femoral arteries are the main part of my study, and I will discuss this further in chapter 5 and 6.

Table 3. Vascular contractility associated with caveolae. + : yes; - : not shown; PE: phenylephrine.

Vessel type	Cholesterol depletion agent type	Electron microscopy	Force measurement	Physiological effects	References
Aorta, renal artery and mesenteric artery of rat	M-β-CD and filipin	+	Organ bath	In the aorta, treatment with either filipin or M-β-CD only inhibited the NO component whereas in the renal artery, both NO and EDHF component were affected. In mesenteric arteries, filipin treatment only reduced EDHF component.	(Xu et al., 2007)
Rat tail artery devoid of endothelium	M-β-CD	+	Organ bath	Enrichment of cav-1 occurred in the same fraction of sucrose gradient with 5-HT_{2H} receptors, but not α1-adrenergic receptors. The contraction was inhibited in response to 5-HT, arginine vasopressin (AVP) and endothelin-1 after disruption of caveolae, but responses to KPSS, calyculin A, cirazoline or AlF_4 were not affected.	(Dreja et al., 2002)
Rat mesenteric arteries	M-β-CD	+	Pressure myograph	Under normal conditions, SMCs exhibited a prominent peripheral SR that often encircled individual caveolae. Disruption of caveolae in SMCs caused decreased contractile force in response to PE or U46619. Electron microscopy investigation suggested that the disruption of the caveolae–SR associations with calyculin-A or M-β-CD treatment may explain the impaired Ca^{2+} oscillation triggered by PE or U46619.	(Shaw et al., 2006)
Intact aorta and fatty streak area of rabbit	M-β-CD and filipin	+	Organ bath	Disruption of aortic endothelial caveolae caused reduced acetylcholine-induced relaxation. Caveolae disruption did not affect contraction with PE or relaxation responses to A23187 or the NO donor, sodium nitroprusside. L-NAME pre-treatment increased PE-induced contraction in a similar degree for both control and M-β-CD treated rings suggesting cholesterol depletion did not alter basal eNOS activity. Electron microscopy provided the evidence that the fatty streak deposit, observed in the animals fed with hypercholesterolemic diet, is associated with a decrease in caveolae 'transductosomes' abundance, which appears to represent a novel mechanism of endothelial dysfunction.	(Darblade et al., 2001)

1.2.6 Caveolin knockout mice

Cav-1 and cav-3 single and double knockout mice have been generated (Cohen et al., 2004, Insel and Patel, 2007). Use of these animals as a model can aid the understanding of the caveolin signalling hypothesis (Insel and Patel, 2007). The importance of cav-1 in the formation of caveolae in vascular SMCs was studied by Drab et al. (2001). They demonstrated the absence of caveolae in cav-1 knockout mice, although cav-3 was still present in these animals. Furthermore, the most predominant phenotypes were detected in cardiac, vascular and pulmonary tissues and might be due to the loss of caveolae in multiple cells types (Murata et al., 2007). The tissue specific phenotypes exhibited by knockout mice are useful in examining the role of caveolae and caveolins at organ level. For example, cav-1 knockout mice showed blunted artery contractility, and this is consistent with the hypothesis that cav-1 tonically inhibits eNOS under normal conditions (Razani and Lisanti, 2001a). It has to be said, however, that use of knockout mice may have complications. Side effects of protein ablation may unexpectedly occur as the result of compensatory mechanisms in vivo. Thus, the outcome of cav-1 knockout is not necessarily expected to be exactly the same as that of M-β-CD or filipin treatment in vitro. Furthermore, while knockout of caveolins abolish the protein expression per se, drugs such as M-β-CD are “functional antagonists” of caveolins and will have no effect on caveolins expressed outside of caveolae.

1.2.7 Caveolins outside of caveolae

Caveolin signalling has been shown to act independently of caveolae with other proteins in cells that do not have caveolae, such as leukocytes (Millan et al., 2006). Furthermore, caveolin has been shown to interact with other proteins outside of caveolae in cells such as cardiac myocytes (Head and Insel, 2007). Several studies have reported that caveolins outside of caveolae can regulate numerous signalling pathways, for example cAMP production (Head and Insel, 2007), cell adhesion (del Pozo et al., 2005), T cell activation (Ohnuma et al., 2004) and leukocyte diapedesis (movement of the cells through intact capillary walls into surrounding tissue (Millan et al., 2006)). Other studies have implicated caveolins in the trafficking of signalling molecules from and to the cell membrane (Head and Insel, 2007). Furthermore, although it has been shown that cav-1 is linked with eNOS outside of caveolae, it is also reported that non-caveolar cav-1 fails to exert its inhibitory effect on eNOS. The physical proximity of cav-1 to eNOS within caveolae, therefore, is crucial in inhibiting NO release (Sowa et al., 2001).

1.2.8 Methods to study caveolae

Several approaches have been used to study caveolae as a subset of lipid rafts, using biochemical, microscopic, pharmacological and molecular biological techniques. In the case of a biochemical approach, lipid rafts and caveolae are extracted by subcellular fractionation after disruption of cells with or without detergents (Ostrom and Insel, 2006, Patel et al., 2008a). Subsequently, lipid rafts and caveolae are separated using centrifugation of fractions with continuous (Optiprep) or discontinuous (sucrose) gradients, and can be isolated using immunoprecipitation, especially with anti-caveolin

antibodies. Without immunoprecipitation, one may not be able to distinguish between lipid rafts and caveolae due to the common properties shared by both (Ostrom and Insel, 2006, Insel and Patel, 2007, Patel et al., 2008a). Pharmacological methods are also used to study caveolae, typically by treating cells with cholesterol depleting agents such as M-β-CD or filipin (Schnitzer et al., 1994, Lam et al., 2004, Xu et al., 2007). These agents are capable of removing the cholesterol from caveolae due to their ability to isolate lipophiles in their hydrophobic core by using cyclic oligomers of glucose (cyclodextrins) (Pitha et al., 1988). Several studies have reported that treatment with M-β-CD led to the removal of cholesterol and then the disruption of caveolae structure (Prendergast et al., 2010).

Microscopy studies can complement and validate the results of biochemical or pharmacological studies by determining the location of raft components (Ostrom and Insel, 2006). One of the most important aspects of microscopic techniques when combined with immunocytochemistry and immunohistochemistry is to show the expression of specific proteins in cells and tissues. Confocal microscopy, in particular, is a powerful tool as the co-expression of two proteins in a tissue or in an individual cell can be investigated (Riddle et al., 2011). In addition to confocal microscopy, electron microscopy was a giant leap forward in our understanding of cell structure, as it can magnify cells or a section of tissue up to X100,000, and can distinguish objects as small as 0.2 nm. Furthermore, in some cases, electron microscopy can be used for high resolution subcellular immunocytochemistry using immuno-gold labelled antibodies. In general, electron microscopy includes transmission electron microscopy (TEM), scanning electron microscopy (SEM) and electron microscope tomography (EMT).

TEM can be used to explore the internal structure of a cell. SEM can study the detailed architecture of the surface of a cell (Brodusch et al., 2013). EMT was used for decades and is used for three-dimensional imaging of the sub-cellular structures of a cell (Frey et al., 2006). All of these electron microscope types have been used in studies to describe caveolae shape, to show the localisation of a specific protein to caveolae, and to show caveolae disruption from the plasma membrane of several types of cells after treatment with a cholesterol depletion agent (Frey et al., 2006, Riddle et al., 2011).

Gene knockout in mice is an alternative approach to study caveolae. Caveolin- knockout mice (cav-1, -2, -3 and cav-1/3 double KO mice) have been generated (Cohen et al., 2004, Insel and Patel, 2007). Several diseases including cardiomyopathies and pulmonary arterial hypertension have been shown in cav-1 KO mice as a result of a lack of cav-1, as well as a lack of cav-2 and caveolae (in certain cell types) (Cohen et al., 2004, Insel and Patel, 2007). However, it is not possible to say whether the loss of expression of caveolins in KO mice directly or indirectly caused these diseases, as discussed earlier.

In addition to the methods described above, myography is a useful method to assess the effects of the removal of cholesterol using M-β-CD (Adebiyi et al., 2011) where contraction of arteries can be measured before and after treatment.

1.3 Ion channels in vascular SMCs

1.3.1 Calcium channels

Vascular contractile force is regulated mainly by cytoplasmic free Ca^{2+} concentration of SMCs (Bolton and Imaizumi, 1996, Wellman and Nelson, 2003). In vascular SMCs,

neurotransmitters, membrane depolarisation and hormones can stimulate an increase in the cytoplasmic Ca^{2+} concentration due to the release of stored intracellular Ca^{2+} from the SR and/or an influx of extracellular Ca^{2+} due to the activation of Ca^{2+} channels in the cell membrane (Guibert et al., 1996). The Ca^{2+} entry pathways through Ca^{2+} channels into vascular SMCs can be classified into: (i) VDCCs such as L- and T-type Ca^{2+} channels; and (ii) voltage-independent Ca^{2+} channels such as receptor-operated channels (ROCs), which are regulated by agonist-receptor interactions, as reviewed by (Spedding and Paoletti, 1992).

1.3.1.1 Classification of voltage-dependent calcium channels

Voltage-dependent Ca^{2+} channels represent the major Ca^{2+} entry pathway in vascular SMCs. VDCCs were first identified in 1953 by Fatt and Katz in crustacean muscle (Fatt and Katz, 1953). Later, VDCCs were also recognised in many cells types including vascular SMCs (Lacinova, 2005). VDCCs were initially classified based on their pharmacological and electrophysiological properties into (i) high voltage activated channels (HVACs) such as L-type Ca^{2+} channels, and (ii) low voltage activated channels (LVACs) such as T-type Ca^{2+} channels. The membrane potential required by HVACs for activation, such as L-type Ca^{2+} channels, is around -30 mV, whereas the membrane potential required by LVACs for activation is around -50 mV (Lacinova, 2005).

1.3.1.1.1 L-type Ca^{2+} channel in vascular tissue

In vascular SMCs, VDCCs are particularly important because influx of extracellular Ca^{2+} is essential for SMCs contraction (Fransen et al., 2012). L-type Ca^{2+} channel activity is a key regulator of vascular SMCs contractile state, and Ca^{2+} influx pathways

mainly depend on this channel type (Yamamura et al., 2013). The L-type VDCCs are the classic target of Ca^{2+} channel blockers extensively prescribed as antihypertensive drugs (Cribbs, 2001). Ablation of the L-type Ca^{2+} channel gene (CACN1C) in vascular SMCs in mice shows this channel has a dominant role in development of SMC tone (Moosmang et al., 2003). Knockdown of the channel using siRNA reduces blood pressure in a hypertensive rodent model (Rhee et al., 2009). L-type Ca^{2+} channels can be activated by several ways: (i) directly through depolarisation of the membrane by solutions such as high extracellular K^{+}, which opens VDCCs, increasing Ca^{2+} entry (Nelson and Quayle, 1995). L-type Ca^{2+} channels can also be activated by dihydropyridine agonists such as Bay K-8644 (Yamamura et al., 2013) that bind to the channel. (ii) indirectly by activating G-proteins and cellular signal transduction pathways in response to an agonist, such as noradrenaline (Nelson et al., 1988).

Calcium entry through the L-type Ca^{2+} channel is important in maintaining the basal tone of smooth muscle, especially in the arteries of spontaneously hypertensive rats, as reviewed by (Karaki et al., 1997). It has also been demonstrated that stretching vascular tissues activates L-type Ca^{2+} channels and increases basal tone in basilar artery (Langton, 1993). In my work, I have chosen to directly activate L-type Ca^{2+} channel to induce rat femoral artery contraction.

1.3.1.1.2 L-type Ca^{2+} channel blockers

L-type calcium channels are responsible for regulating the influx of calcium into muscle cells, which in turn stimulates smooth muscle contraction and cardiac myocyte contraction (Hess et al., 1984). Calcium channels blockers bind to L-type Ca^{2+} channels

located on the vascular smooth muscle and inhibit calcium influx into the cells. Therefore, these cause vascular smooth muscle relaxation (vasodilation). The most forceful and specific of the Ca^{2+} channel blockers are the dihydropyridines group, such as nifedipine, amlodipine and felodipine (Dube et al., 1985). On the other hand, the drug, Bay K8644 is a structural analogue of the dihydropyridines, which has effects opposite to those of nifedipine and other similar Ca^{2+} antagonists (Schramm et al., 1983). This compound causes vasoconstriction by competing for the nifedipine binding site, suggesting that it acts by increasing Ca^{2+} influx through VDCCs (Schramm et al., 1983).

1.3.2 Potassium channels

Potassium channels play a critical role in the regulation of electrical potential across the membrane of SMCs. The SMC membrane potential is essential in regulating contractile force by controlling Ca^{2+} influx, as well as indirectly regulating the release of intracellular Ca^{2+}. Therefore, changes in SMC membrane potential will lead to a decrease or increase in cytosolic Ca^{2+} concentration, and therefore contraction. Factors that regulate the activity of K^+ channels can have an effect on SMC contraction and therefore on vascular resistance, blood flow and blood pressure (Ko et al., 2008).

As K^+ channels regulate the membrane potential in SMCs, they control the probability of VDCCs being open, and hence regulate Ca^{2+} entry into the SMCs (Nelson et al., 1995). Furthermore, it has been demonstrated that decreased K^+ currents lead to a depolarised SMC membrane, which in turn gives rise to increased Ca^{2+} influx into the

SMC: this may play an important role in stimulating SMC contraction (Nelson and Quayle, 1995).

1.3.2.1 Classification of vascular potassium channels

In general, SMCs have four main types of K^+ channels classified by their electrophysiological and pharmacological properties (Cook, 1988, Nelson and Quayle, 1995). Voltage-activated K^+ channels (K_v) are encoded by the K_v gene family, BK_{Ca} channels by the *Slo* gene, inward rectifiers (K_{IR}) by Kir2.0s, and ATP-sensitive K^+ channels (K_{ATP}) by Kir6.0s (Hu and Zhang, 2012). Furthermore, Ca^{2+}-dependent K^+ channels (K_{Ca}) have been subdivided into three distinct classes based on their conductance. They are the large conductance BK_{Ca} channels, which are blocked by charybdotoxin (CTX) and IBTX (Miller, 1995), the intermediate-conductance (IK) channels, which are inhibited by TRAM-34 (Gaete et al., 2012), and the small-conductance (SK) apamin-sensitive K^+ channels (Burnham et al., 2002).

1.3.2.1.1 Large-conductance (BK_{Ca}) channels

The large-conductance, Ca^{2+}-activated K^+ channels (BK_{Ca}, also called *Slo* or MaxiK) were first identified by Marty 1981 (Marty, 1981). These channels are abundant in vascular SMCs (Hu and Zhang, 2012) and are characterised by their large conductance of K^+ (Hu and Zhang, 2012). BK_{Ca} channels play an important role in many cellular functions, such as action potentials, hyperpolarisation and the modulation of vascular tone under physiological conditions. The major role of vascular SMC BK_{Ca} channels in the regulation of arteriolar tone is to hyperpolarise the SMC plasma membrane, which

consequently would decrease the opening of L-type Ca^{2+} channels and relax the blood vessel.

BK_{Ca} channels are a tetramer composed of pore-forming α-subunits and a family of tissue-specific accessory β-subunits. The α-subunit is abundantly expressed in SMCs and encoded by a single gene (KCNMA1) with various spliced isoforms; β-subunits are encoded by four genes (KCNMB1-4) (Lee and Cui, 2010). The α-subunit consists of seven transmembrane-spanning domains (S0–S6). S4 contributes to voltage-sensing and S5–S6 make up the pore-forming region **(figure 1.8)** (Latorre and Brauchi, 2006, Lee and Cui, 2010). In addition, a transmembrane S0 domain leads to an extracellular N-terminus (Lee and Cui, 2010). The large cytosolic tail domain of the α-subunit includes two conductor domains (RCK1 and RCK2) forming an intracellular C-terminus. These conductor domains are believed to be Ca^{2+}-sensing because they have high affinity Ca^{2+} binding sites on both RCK1 and RCK2 domains (Yuan et al., 2010). RCK1 and RCK2 are therefore believed to provide the structural basis for Ca^{2+} sensitivity and form a gate ring to stimulate channel opening in response to increases in intracellular Ca^{2+} (Dopico et al., 2012).

The β-subunits comprise of two transmembrane-spanning domains (S1 and S2). Both ends of the β-subunits (N- and C-terminals) are intracellular (Ledoux et al., 2006). These domains are believed to contribute to their sensitivity to cytosolic Ca^{2+} concentration. SMC BK_{Ca} channels contribute to the regulation of membrane potential, and therefore vascular tone, and function as a negative feedback mechanism to decrease vasoconstriction (Brayden and Nelson, 1992). As well as being modulated by several vasodilators and vasoconstrictors, these channels are a potential therapeutic target for

several artery diseases, such as hypertension and atherosclerosis. BK_{Ca} channels are considered to be promising candidate because little expression of these channels is found in cardiomyocytes, offering vascular selectivity. Additionally, the ability of BK_{Ca} channels to allow efflux of K^+ is greater than any other K^+ channel present in SMCs due to their large conductance (Ghatta et al., 2006). Furthermore, the sensitivity of BK_{Ca} channels to voltage-dependent opening is weaker than other voltage-dependent K^+ channels in SMCs (Ghatta et al., 2006).

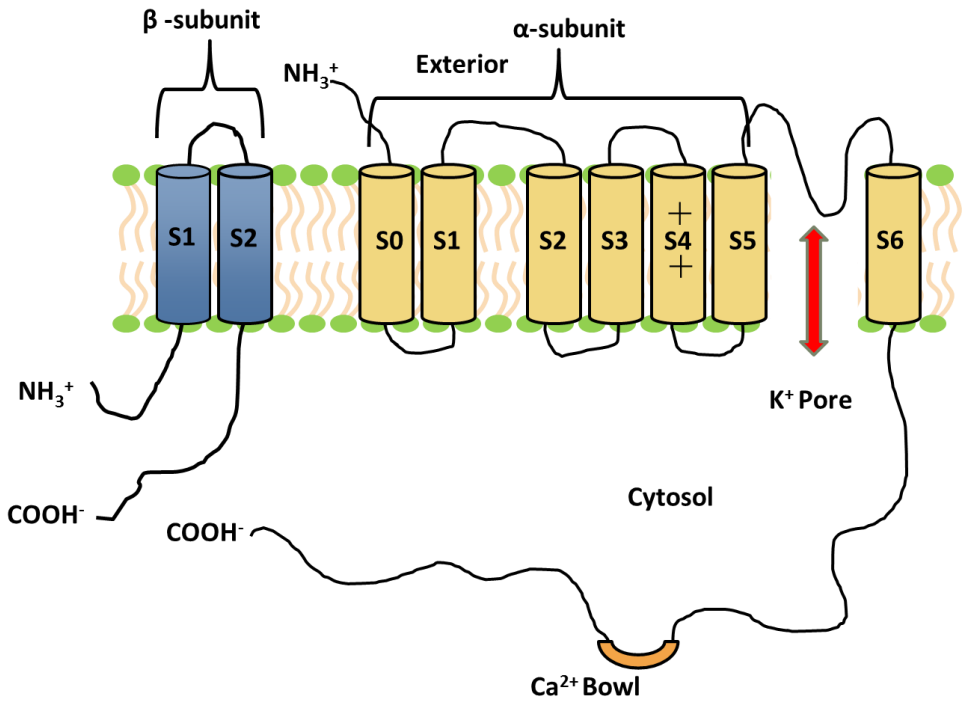

Figure 1.8. Diagram showing the components of the BK_{Ca} channel. BK_{Ca} channels consist of channel-forming (α) and accessory (β) subunits. The α-subunit is made of seven membrane-spanning domains (S0 to S6). The K^+ pore is located between S5 and S6. S4 contributes to voltage-sensing. The α-subunit contains an extracellular N-terminal and intracellular C-terminal domain. The cytoplasmic tail domain contains RCK1 and RCK2 as intracellular Ca^{2+} binding domains. The β-subunits are made of two membrane-spanning domains (S1 and S2), with both the N-terminal and C-terminal located in the cytoplasm.

1.3.2.1.1.1 BK_{Ca} channel openers

The BK_{Ca} channel openers are made up of a big group of synthetic benzimidazolone derivatives, such as NS-004 and NS-1619, and biaryl amines, such as mefenamic and flufenamic acids (Hill et al., 2010). The activation mechanism of both NS-004 and NS1619 on BK_{Ca} channels is to target the α-subunits and (i) enhance the Ca^{2+} binding sites (RCK1 and RCK2) at the C-terminal of the α-subunit, and (ii) support the interaction between the α- and ß-subunits. The action of NS-1619 was first identified by Olesen et al. in 1994 in aortic SMCs (Olesen et al., 1994) where it induced hyperpolarisation of SMCs. In addition, BK_{Ca} channels in vascular SMCs can also be activated by other physiological BK_{Ca} channels openers such as isoproterenol (White et al., 2000).

1.3.2.1.1.2 BK_{Ca} channels blockers

BK_{Ca} channels blockers are made up from a large group of agents and toxins such as IBTX, charybdotoxin and quaternary ammonium compounds including tetraethylammonium ions (TEA^+) (Langton et al., 1991) and tetrabutylammonium ions (TBA^+) (Kwok et al., 1998). Some of these blockers, such as IBTX and TEA^+, are relatively selective for the BK_{Ca} channel, while charybdotoxin also inhibits other K^+ channels such as IK_{Ca} and SK_{Ca}. IBTX and charybdotoxin act by blocking the movement of K^+ by binding to a site in the external vestibule of the pore and occluding the extracellular side of the pore (Giangiacomo et al., 1992). All the above BK_{Ca} channels blockers lead to the depolarisation of SMCs and activate VDCCs, leading to vasoconstriction (Giangiacomo et al., 1992). Additionally, several studies showed that

application of vasoconstrictors such as 5-HT, phenylephrine, angiotensin II (Alioua et al., 2002) and endothelin-1(Minami et al., 1995) was accompanied by a suppression of BK_{Ca} channel activity.

1.4 Contraction and relaxation mechanisms of intact arteries

In the vascular SMCs of resistance arteries, vasoconstrictor stimuli initiate SMC contraction by causing an increase in the intracellular Ca^{2+} concentration (Aaronson and Ward, 2007). An increase in intracellular Ca^{2+} concentration leads to Ca^{2+} binding to the cytoplasmic regulatory protein calmodulin, thus forming Ca^{2+}/calmodulin complexes. An increase in Ca^{2+}/calmodulin complexes leads to the activation of the enzyme myosin light-chain kinase (MLCK). The activation of MLCK leads to the phosphorylation of myosin light chain heads, which in turn leads to myosin-actin cross-bridge formation, causing the contraction of SMCs (Aaronson and Ward, 2007). A change in Ca^{2+} concentration in SMCs is mediated by: (i) an influx of extracellular Ca^{2+} via VDCCs, such as L-type Ca^{2+} channels, and receptor-operator channels (ROCs); (ii) the release of stored Ca^{2+} from the SR due to the activation of GPCRs by vasoconstrictors such as norepinephrine (NE) and endothelin-1 (ET1); and (iii) decreased removal of intracellular Ca^{2+} via Ca^{2+}-ATPase pumps (Levick, 2010). The main Ca^{2+} entry pathway in SMCs is through L-type Ca^{2+} channels (Moosmang et al., 2003). In contrast, increased concentrations of cytoplasmic Ca^{2+} lead to the activation of K^+ channels such as BK_{Ca} channels. Activation of BK_{Ca} channels causes an efflux of K^+, therefore causing membrane hyperpolarisation and thus decreasing contraction due to the switching off of L-type Ca^{2+} channels.

Endothelial cells regulate local vascular tone via the diffusion of several vasodilatory factors from ECs into SMCs. Nitric oxide is one of these factors. Activated muscarinic-3 receptors (M_3) in the ECs cause an influx of Ca^{2+} via ROCs and release Ca^{2+} from the ER due to increases in IP_3. Both lead to an increase in intracellular Ca^{2+} concentration. An increase in intracellular Ca^{2+} concentration leads to the interaction of Ca^{2+} with cytosolic calmodulin, thus forming Ca^{2+}/calmodulin complexes. An increase in intracellular Ca^{2+}/calmodulin complexes leads to the dissociation of eNOS from cav-1, thereby increasing eNOS activity and promoting the conversion of L-arginine to L-citrulline and the production of NO **(figure 1.9)** (Griffith and Stuehr, 1995).

For resistance artery SMCs, NO diffuses from ECs into SMCs, leading to the activation of guanylyl cyclase (GC). The activation of GC leads to the conversion of guanosine-5'-triphosphate (GTP) to cGMP. cGMP activates protein kinase G (PKG), which has multiple vasodilating effects: (i) it activates K^+ channels, causing membrane hyperpolarisation that inhibits Ca^{2+} influx by switching off L-type Ca^{2+} channels; (ii) it stimulates the sequestration and extrusion of Ca^{2+} via Ca^{2+}-ATPase; and (iii) it stimulates myosin phosphatase by inhibiting Rho kinase **(figure 1.9)**.

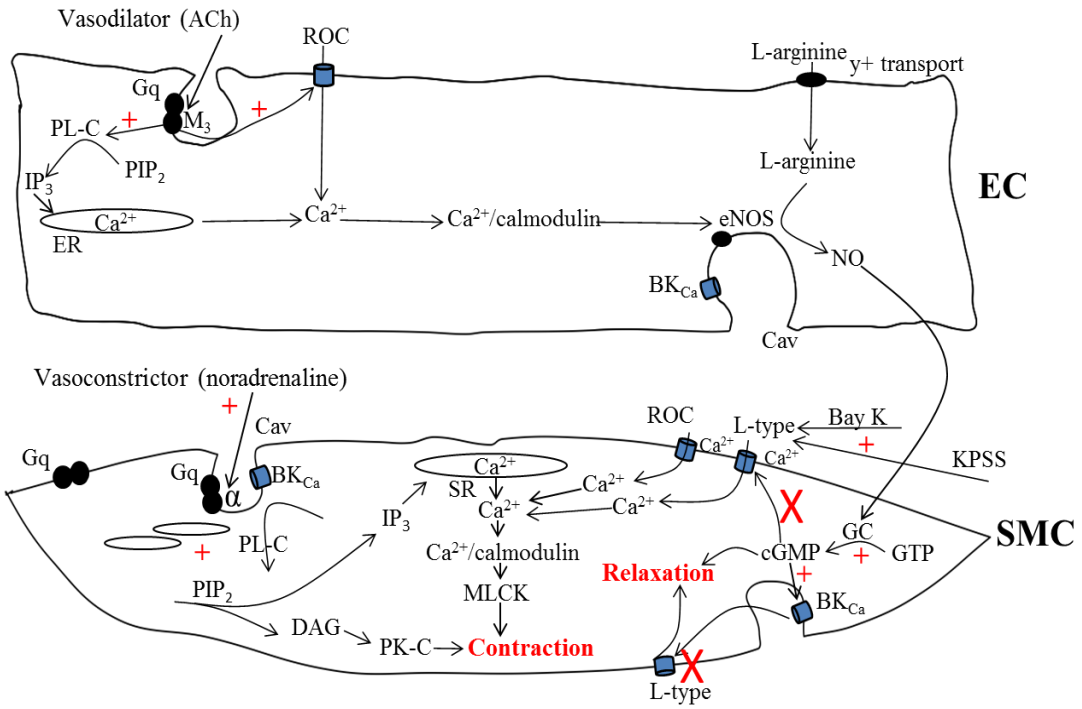

Figure 1.9. A schematic representation of the signalling mechanisms in both SMC and EC which regulate the normal contraction and relaxation of intact arteries.

1.5 Hypothesis

The role of caveolae and caveolins in regulating arterial contractility is the main subject of my thesis. We hypothesise that BK_{Ca} channels are co-expressed to caveolae in vascular cells of the rat femoral artery. The specific aims of this project are to: (i) examine the structural properties and distribution pattern of caveolae, caveolins and BK_{Ca} channels in rat femoral artery using electron microscopy and confocal microscopy; and (ii) study the role of caveolae and BK_{Ca} channels in regulation of the contraction and relaxation in femoral artery rings using myography.

Chapter 2 General Materials and Methods

2.1 Dissection of the femoral arteries and tissue preparation

Male Wister rats (200-250 g) were humanely killed while unconscious, having been made so by exposure to a gradually raised concentration of CO_2, followed by cervical dislocation and exsanguination by trained personnel in accordance with Schedule 1 of the UK Animals (Scientific Procedures) Act, 1986. The legs were cut off, and femoral arteries were carefully dissected from the surrounding fat and connective tissues and placed into the physiological salt solution (PSS) (see 2.5.5 in this chapter).

2.2 Reagents and kits

All general chemicals were purchased from Sigma-Aldrich Ltd (The Old Brickyard, New Road, Gillingham, Dorset, SP8 4XT) or Fisher Scientific (Bishop Meadow Road, Loughborough, LE11 5RG) or VWR International (Hunter Boulevard, Magna Park, Lutterworth, Leicestershire, LE17 4XN). Derails of specialised chemicals are given in corresponding sections.

2.2.1 Primary antibodies

Mouse monoclonal anti-cav-1 (cat no. 610406) and anti-cav-3 (cat no. 610420) antibodies were purchased from BD Biosciences (Edmund Halley Road, Oxford Science Park, Oxford, OX4 4DQ). Mouse monoclonal anti-actin and anti-α-actin antibodies were purchased from Sigma-Aldrich Ltd. Rabbit polyclonal anti-vWF antibody was purchased from Dako UK Ltd (Cambridge House, St Thomas Place, Ely, Cambridgeshire, CB7 4EX). Rabbit polyclonal anti-BK_{Ca} channel antibody was bought

from Alomone Labs (Jerusalem, Israel). Dilutions used for primary antibodies were as follows. Anti-cav-1, 1:200; anti-cav-3, 1:500; anti-BK_{Ca}, 1:500; anti-actin and anti-α-actin, 1:300; anti-vWF, 1:300. All the primary antibodies were diluted using antibody diluting solution.

2.2.2 Secondary antibodies

Anti-mouse Alexa Fluor 488 (green)/ Alexa Fluor 594 (red) and anti-rabbit Alexa Fluor 488 (green)/ Alexa Fluor 594 (red) were used as secondary antibodies (Life Technologies Ltd**,** 3 Fountain Drive, Inchinnan Business Park, Paisley, PA4 9RF). All secondary antibodies were diluted in 1:500 using antibody diluting solution.

2.2.3 Slide preparation for histology, immunohistochemistry and immunocytochemistry

The slides were washed with soap, rinsed with running tap water then distilled water, and then dried. For immunohistochemistry experiments, the slides were then rinsed with 100% ethanol and dried for 100 minutes at room temperature. They were then dipped in the gelatine-coating solution (gelatine (0.8 g) and chromium potassium sulfate (0.08 g) dissolved in 400 ml of warm distilled water) for 3 minutes. Afterwards, the gelatin-coated slides were air-dried overnight. Gelatin-coating was necessarily in order to prevent the tissue slices coming off from the slides during the staining procedure.

2.3 Ultrastructure study of femoral artery using transmission electron microscopy and histology techniques

The purpose of transmission electron microscopy (TEM) was to investigate the topological relationship between caveolae and sarcoplasmic reticulum (SR) (caveolae-SR) or caveolae and mitochondria (caveolae-mitochondria) in the SMCs and ECs of intact and methyl β-cyclodextrin (M-β-CD) treated femoral arteries.

The purpose of histological technique was to show the microscopic structure of rat femoral artery and to confirm the removal of endothelial cells from the intima of the femoral artery.

2.3.1 Transmission electron microscope preparation of rat femoral arteries

Femoral arteries were treated with 5 mM M-β-CD (*n*=5) and matched with a control group of arteries (*n*=5). Both groups were cut into small pieces (about 0.5 mm^3). The segments were immediately fixed (4% paraformaldehyde and 2.5% glutaraldehyde) in 0.1 M sodium cacodylate (pH 7.4) overnight at room temperature. Next day, the samples were rinsed three times in 0.1 M sodium cacodylate and then post-fixed in 1% (w/v) osmium tetroxide (OsO_4) in 0.1 M sodium cacodylate for 1 hour. The samples were then rinsed with 0.1 M cacodylate for 30 minutes each, and then incubated with 0.1 M cacodylate overnight. The next day, the samples were washed with distilled water and ethanol, for 30 minutes each, and incubated in 2% aqueous uranyl acetate for 60 minutes before routine embedding in resin. The samples were dehydrated through a graded series of alcohol (60, 70, 80, 90 and 100%), five minutes for each. Afterwards, the segments were immersed in 100% acetone to remove water from the tissues. The samples were

then embedded in resin (30% resin:70% acetone; 70% resin:30% acetone and 100% resin) for 1, 1 and 2 hours, respectively. The samples were left in the oven at 60°C to polymerise overnight (Kuo et al., 2001). Ten sections were cut from each group (control group and M-β-CD treated group) at a thickness of 70-90 nm using an ultramicrotome, Leica EM FC6 (Ernst-Leitz-Straße 17-37, Wetzlar, D-35578, Germany). Ultrathin sections were picked up on coated copper grids of 300-mesh, with 0.3% Pioloform. Subsequently, the grids were dried out overnight at room temperature. The grids were double stained with 2% aqueous uranyl acetate, four minutes each, and thereafter the grids were rinsed with distilled water for one minute; the grids were re-stained again with 0.1 M lead citrate for four minutes. Afterwards, the grids were washed with distilled water for a minute and left overnight at room temperature to dry.

2.3.2 Histological preparation of rat femoral arteries

Intact and endothelium-denuded arteries were used (n=5 in each group). The endothelium was removed from artery rings by gently rubbing the intimal surface with a human hair. Arteries were cut into small pieces and then fixed in 10% formaldehyde fixative. In an automatic tissue processor (Shandon Elliott duplex processor, Type SCE-0545, Shandon LTD, Camberley), the tissues were dehydrated in 60%, 70%, 80% and 100% ethanol for 30 minutes each. After the dehydration, the samples were cleared with xylene for 90 minutes and embedded in paraffin wax for three hours. During this process the tissue samples were placed into molds along with liquid embedding wax, which then hardened. The blocks were sectioned at a thickness of 5 microns using a Leica microtome (RM2245). The sections were mounted onto slides coated with 2%

gelatin. For histological examination, 20 sections from endothelium-denuded and endothelium-intact arteries were stained with Ehrlich Hematoxylin and Eosin (Culling, 1974). Cytoplasm showed up as a pink colour whereas nuclei were stained a blue/purple colour.

2.4 Studies using immunohistochemistry, immunocytochemistry and Western blotting techniques

Immunohistochemical technique was used to identify the localisation of cav-1, cav-3 and BK_{Ca} channels at the tissue level of the rat femoral artery. Immunocytochemical technique was used to examine expression pattern of these proteins in the individual smooth muscle cells of rat femoral arteries and cultured human coronary artery endothelial cells (HCAEC) (PromoCell GmbH, Handschuhsheimer Landstr.12, D-69120 Heidelberg, Germany). vWF and α-actin were labelled as specific markers for ECs and SMCs, respectively. The size of proteins that were recognized by primary antibodies against cav-1, cav-3, BK_{Ca} channels and α-actin were examined by Western blotting. In some cases, double staining was performed. If two primary antibodies were from different species, we conducted dual indirect staining. If two primary antibodies were from the same species, we used the combination of indirect and direct staining techniques.

2.4.1 Immunohistochemical preparation of rat femoral arteries

Femoral arteries of rats were dissected and immediately placed in PSS (see 2.5.5 in this chapter). Then, the arteries were cut into approximately 4 mm lengths and embedded in CRYO-M-BED embedding media (Bright Instrument Limited, St Margarets Way,

Huntingdon, PE18 6EB) on a cork disk. The blocks were frozen in isopentane cooled in liquid nitrogen and were cut using a cryostat (Bright Instrument Limited) at 11 µm thickness. The cut section was placed in the middle of a gelatine-coated slide and, using a DAKO pen, a circle was drawn around the section in order to confine the liquid on the slice. The slice was fixed in 2% paraformaldehyde in PBS solution containing (in mM): KCl 2.7, KH_2PO_4 1.5, NaCl 137, and Na_2HPO_4 8 (pH 7.4). Aldehyde forms cross links between reactive end-groups of adjacent protein chains, thereby fixing the preparations. Fixing solution was added carefully inside the circled area and left for 5 minutes; afterwards the fixative was removed. A 100 mM glycine buffer (pH 7.4), which quenches paraformaldehyde reaction in the tissue, was added carefully and left for 10 minutes at room temperature. The section was then permeabilized using 0.1% Triton X100 in PBS to make holes in the cell membrane so that antibodies, which are large molecules, can get in to the cells and bind to their epitopes. The permeabilizing solution was removed, and the slide was washed three times using PBS, 5 minutes each time, at room temperature. The PBS solution was then removed and an antibody diluting solution, containing 2% goat serum, 1% bovine serum albumin (BSA) and 0.05% Triton X100 in a sodium citrate buffer (SSC) containing (in mM) NaCl 150 and Na_3 citrate 15 (pH 7.2), was applied to block non-specific binding of antibodies for 30 minutes at room temperature in the humidifier (Ramos-Vara, 2011).

2.4.1.1 Indirect staining

The indirect method of immunolabelling was used when only one primary antibody was used, or when two primary antibodies raised in different host species were used. The

tissue sections were incubated with the diluted primary antibodies in a humidifier overnight at 4 °C. After overnight incubation, the primary antibodies were removed, and the slides were washed 3 times, for 10 minutes each time, at room temperature, using an antibody washing solution which contained (in mM) NaCl 150, Na_3 citrate 15 and 0.05% Triton X100 (pH 7.2). The antibody wash solution was then removed and diluted secondary antibody was added and left for 90 minutes at room temperature in a humidifier. The humidifier was kept in the dark to avoid any bleaching of the fluorophore. The slides were then washed 3 times with an antibody wash solution, for 10 minutes each time at room temperature to remove un-bound secondary antibody. Finally, slices were washed twice consecutively with distilled water, and then left in the dark to dry. A small drop of mounting media (Bright Instrument Limited) was added on the slide, and covered with a clean cover slip (13 mm diameter, thickness 1), and kept in dark overnight to dry (Ramos-Vara, 2011).

2.4.1.2 Direct staining

For double immunolabelling with two primary antibodies from the same host species, the direct staining method was used for the second primary antibody. In my work, this was only required when co-staining with rabbit anti-BK_{Ca} channels and rabbit anti-vWF. The slices were incubated with diluted rabbit anti-BK_{Ca} primary antibody, and then labelled with anti-rabbit secondary antibody. A Zenon IgG antibody labelling kit (Molecular Probes) was used to directly conjugate rabbit anti-vWF primary antibody with anti-rabbit secondary Fab fragments (fragment with antigen binding site) tagged with fluorophore. Any excess un-bound Fab fragments were neutralised by the addition

of goat serum before the primary-secondary antibody complex was applied to the slices. After washing of the primary-secondary antibody complex, the slices were post-fixed to compensate for lower avidity of the Fab fragment (Ramos-Vara, 2011).

2.4.1.3 Negative control

For the negative control, two methods were used: (i) secondary antibodies were mis-matched against primary antibodies (eg. anti-rabbit secondary used for mouse primary). (ii) secondary antibodies were applied without primary antibody incubation (Ramos-Vara, 2011).

2.4.2 Preparation of rat femoral arteries SMCs

Femoral arteries were dissected under a microscope and cut into small pieces (2-4 mm). Single cells were obtained using an enzymatic digestion procedure. Arteries were first incubated for 40 minutes at 35 $^{\circ}$C in a low (0.1 mM) Ca^{2+} buffer containing 1.4 mg ml^{-1} papain (Sigma), 0.9 mg ml^{-1}dithioerythritol (Sigma) and 0.9 mg ml^{-1} bovine serum albumin. The 0.1 mM Ca^{2+} buffer contained (in mM) :137 NaCl, 0.44 $NaH_2PO_4.H_2O$, 0.42 Na_2HPO_4, 4.17 $NaHCO_3$, 5.6 KCl, 1 $MgCl_2$, 10 HEPES and 0.1 $CaCl_2$ (pH 7.4). Arteries were further digested for 20 min at 35 $^{\circ}$C in the low Ca^{2+} buffer containing 1.7 mg ml^{-1} collagenase (Type F, Sigma) and 1 mg ml^{-1} hyaluronidase (Type I-S, Sigma). After enzyme treatment, the artery was rinsed in the low Ca^{2+} buffer, and single cells were dispersed in this solution by trituration of the digested tissue using a fire-polished Pasteur pipette (Skoog and Tani, 2011).

2.4.2.1 Fixation

A suspension of SMCs was added onto size-1 cover slips placed in the bottom of the wells of a 24-well plate, and cells were allowed to settle. SMCs were fixed with 2% paraformaldehyde in PBS solution (pH 7.4) for 10 minutes at room temperature. Quenching and permeabilising were performed in the same manner as described in 2.4.1.

2.4.2.2 Blocking and staining

Blocking and staining of the single cells were performed in the same way described in 2.4.1 and 2.4.1.1 for frozen tissue sections.

2.4.3 Immunohistochemical preparation of HCAECs

2.4.3.1 Fixation

HCAECs (PromoCell) were cultured on sterilised coverslips in 24 well plates with MV2 media (PromoCell). When ready to start experiments, the entire medium was removed and the wells were washed with PBS (pH 7.4). In order to fix the cells, 1 ml of 2% paraformaldehyde in PBS solution was added to each well and left for 10 minutes. Afterward, the same process described for rat femoral artery smooth muscle cells (2.4.2.1) was followed.

2.4.3.2 Blocking and staining

The same process described for rat femoral artery smooth muscle cells (2.4.2.2) was followed.

2.4.4 Confocal microscope

The most notable advantage of confocal microscopy compared to conventional fluorescent microscope is the elimination of out-of-focus signal. Thus, the confocal images are sharper and so more detailed information regarding the origin of signal can be obtained. In addition, the confocal technique allows the users to collect serial optical sections from thick specimens thereby re-constructing the 3-D images. The disadvantage of confocal microscopy is it requires a powerful excitation light (usually laser) that may bleach fluorophore although this problem is largely overcome due to the development of fade-resistant probes such as Alexa Fluor. Alexa 488 is excited by 488 nm light and Alexa 594 is excited by 594 nm light. Light is directed by a dichroic mirror towards a pair of rotating mirrors. Then the excitation light excites the fluorescent sample after passing through the microscope objective. The same mirrors are used to descan emitted light due to specimen fluorescence. The light then passes through the dichroic mirror through a pinhole placed in the conjugate focal plane of the sample. The dichroic mirror is used to allow light above a certain wavelength to pass while the pinhole rejects all out-of-focus light arriving from the sample. Finally, the light is measured by a detector such as a photomultiplier tube. The reconstruction of a 2D image of the object is done by scanning the illumination beam across the specimen. At the same time, this image is built up, pixel by pixel, using a computer that is attached to the detector **(figure 2.1)**.

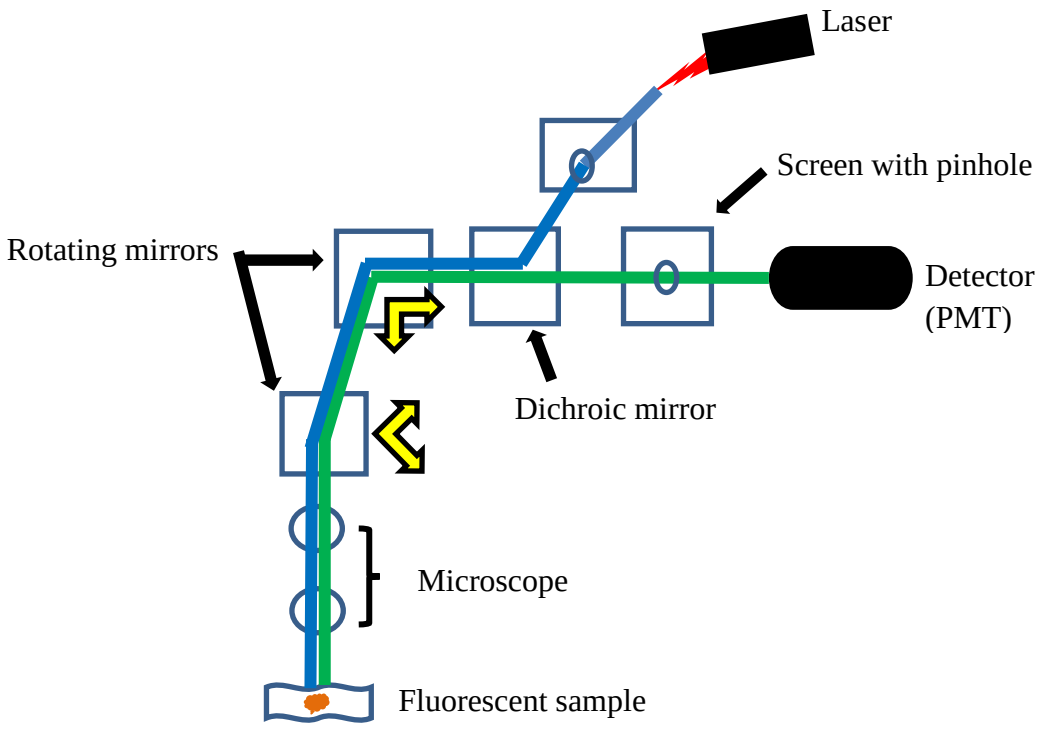

Figure 2.1. Schematic layout of the confocal microscope. Laser is scanned across the specimen by scanning mirrors. Pinholes serve to reject out-of-focus light.

2.4.5 Data analysis of immunostaining

An immunofluorescence microscopic analysis of fluorescence intensity was semi-quantified using Leica confocal software (LCS) Lite in an attempt to profile the relative strength of light along the line of interest. The intensity profile was then plotted using OriginPro 8.6.

2.4.6 Western blotting

Western blot is often used along with immunohisto- and immuno-cytochemistry. The former assess the size of detected proteins (but not necessarily where the protein is expressed) and the latter identify the location of protein expression (but not necessarily confirming that the primary antibody is binding to the right protein). In my work, antibodies were used mainly for the immunohisto- and immunocyto-chemical work, but Western blotting technique was also used to confirm the protein expression of cav-1, cav-3, and α-actin in rat femoral artery lysates, as well as to confirm protein expression of BK_{Ca} channels in both the brain and femoral artery.

2.4.6.1 Tissue sample preparation

Rat femoral arteries were homogenized in a lysis buffer (3 mM EGTA, 250 mM NaCl, 3 mM EDTA and 20 mM TrizmaHCl) in the presence of protease inhibitors (Sigma) on ice. Thereafter, the samples were centrifuged at 13000 rpm for 10 minutes at 4°C, and the supernatant was collected and pellet was discarded. Supernatant protein extracts were mixed with X2 sample buffer and heated for 10 minutes at 98 °C for protein denaturation.

2.4.6.2 Acrylamide gel

7 µl of rainbow molecular weight marker (GE Healthcare Life Sciences, Amersham Place, Little Chalfont, Buckinghamshire, HP7 9NA) and 25 µl of protein lysates were loaded to the wells of a 4 % stacking gel. Protein samples were separated in 10% resolving gel.

2.4.6.3 Electrophoresis

Gel cassette containing 2 gels was placed in the gel tank, and filled to the top with SDS running buffer (25 mM Tris base, 192 mM glycine and 3.5 mM SDS). Remaining running buffer was poured into the gel tank, outside of the gel cassette. Gel was then run at 120V for 60 minutes.

2.4.6.4 Transfer

The proteins separated on acrylamide gel were then transferred onto a nitrocellulose membrane in the gel tank surrounded by crushed ice. The transfer buffer consisted of 25 mM Tris base, 192 mM glycine and 20% methanol, and protein transfer was achieved by providing 110 V for 1 hour.

2.4.6.5 Blocking and detection

The membranes were removed from the cassette and rinsed with TBST containing (in mM) Trizma 20, NaCl 137 and 0.1% Tween 20 (pH 7.6). The membranes were then stained in Ponceau S (Sigma-Aldrich) to check the separation of proteins and transfer efficiency before moving on to the next step. If the membranes were deemed fit for proceeding, Ponceau S staining was removed by washing the membranes with TBST on a rocking platform. Membranes were then blocked in a TBST solution containing 1 % or 5 % non-fat milk (to block non-specific binding) for one hour at room temperature on the rocking platform.

2.4.6.5.1 Antibodies

2.4.6.5.1.1 Primary antibodies

The membranes were probed with mouse monoclonal anti-cav-1 (dilution, 1:200), mouse monoclonal anti-cav-3 (1:500), rabbit polyclonal anti-BK_{Ca} channels (1:300) and mouse monoclonal anti α-actin (1:300). All the primary antibodies were diluted with TBST with 1 % or 5 % non-fat milk, and membranes were incubated with diluted primary antibodies at the volume of 1 ml in the fridge overnight.

2.4.6.5.1.2 Secondary antibodies

Membranes were washed quickly several times with TBST to remove most of primary antibodies and then further washed in a TBST solution 3 times 10 min each. The membranes were then incubated with secondary antibodies for 90 minutes at room temperature. The secondary antibodies used were: anti-rabbit IgG conjugated with horseradish peroxidise (HRP), diluted with 1 % or 5 % non-fat milk-TBST to 1:5000, and anti-mouse IgG conjugated with HRP, diluted with 1% or 5 % non-fat milk-TBST to 1:10000.

2.4.6.6 Western blot-stripping

In some cases, stripping of the antibodies from the original blot was performed to allow re-blotting of the membrane against actin, a house-keeping protein, to check for equal gel loading among wells. After the first experiment, the membranes were rehydrated with TBST and then washed using the stripping solution consisting of 100 mM β-mercaptoethanol, 2% SDS and 62.5 mM Tris base (pH 6.7) 2 times for 10 min each at

room temperature. After this, the membranes were rinsed several times with TBST, and blocked with a TBST with 5% non-fat milk solution. The membranes were incubated with mouse monoclonal anti-actin primary antibody diluted with TBST with 5 % non-fat milk overnight, and rest of the procedure was followed as normal Western technique.

2.4.6.7 Visualisation

Presence of HRP-conjugated secondary antibodies was detected using an enhanced chemiluminescence (ECL) technique, and light was captured using auto-radiographic Hyperfilm (Amersham) in a hyper-cassette. Exposure time was varied depending on the strength of the signal, and the Hyperfilm was developed and fixed and the image was scanned so that bands can be sized against pre-stained rainbow ladder.

2.5 Femoral artery contraction and relaxation studies

Femoral artery contraction (measured in mN) was induced using KPSS or 20 mM K/Bay K 8644 under the different conditions mentioned in chapters 5 and 6 using myography. Values were expressed as means $\pm$ SEM. Vasorelaxant responses of the vasodilators were expressed as the fraction of the maximal contraction to either KPSS and/or 20 mM K/Bay K 8644.

2.5.1 Myography

Wire myography (Dual Wire Myograph System 510A, DMT A/S, Aarhus, Denmark) is an in vitro technique which allows small arteries with a diameter of 100-500 μm to be studied under isometric condition (Mulvany and Halpern, 1977, Mulvany and Aalkjaer,

1990). Arteries were dissected, cleaned, and then mounted onto a two-channel myograph. Each artery was then normalised to determine its maximum active tension development. This allows for the standardisation of the initial experimental condition. This is the technique I used for my study to obtain a functional read-out after manipulation of cholesterol/caveolae.

The myograph contains two jaws, on which the artery was mounted **(figure 2.2)**. One jaw was attached to a micrometre and the other to a piezo-electric isometric force transducer. Piezo-electric force transducers have a linear output over a wide range of force up to 50 mN and can compensate for changes in temperature. The wire myograph, including a sensor probe, was connected to a Myo-interface, which gives a visual read-out of force and temperature. The Myo-interface had an analogue output that was converted to a digital signal by a minidigi converter and signal recorded with a PC using the Axoscope software (Axon Instruments, Union City, California, USA) with an acquisition rate of 20Hz.

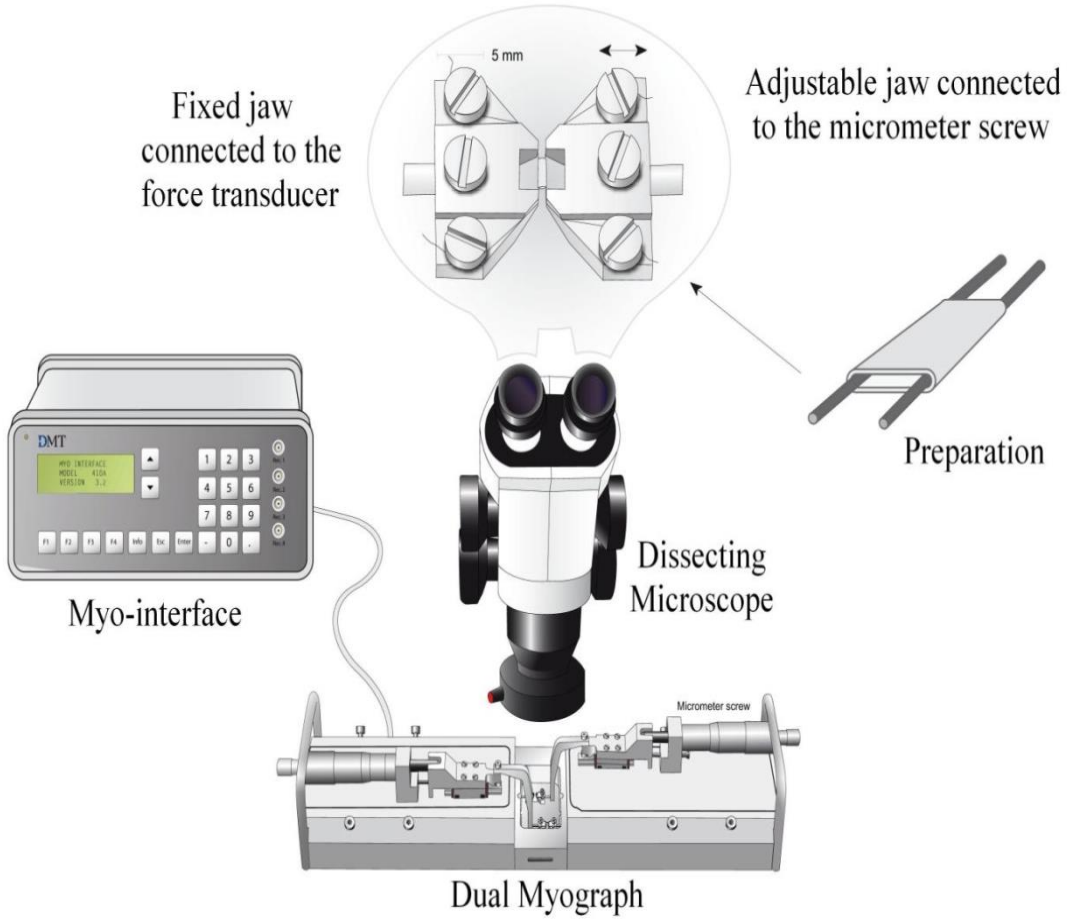

Figure 2.2. Dual wire myograph system (410M). Adapted from the DMT website (www.dmt.dk).

2.5.2 Mounting of artery

Each strip of artery was mounted on two 40 μm diameter stainless steel wires, where one wire was attached to the force transducer and the other to the micrometre (Mulvany and Halpern, 1977). Wire was first secured underneath one screw on the upper surface of the stainless steel jaw that was connected to the micrometre. The vessel was then threaded onto the free end of the wire and pulled into position over the centre of the jaw, and the wire then secured underneath the second screw on the same stainless steel jaw.

After this, the second wire could be threaded through the vessel; the jaw attached to the micrometer and containing the artery was then carefully moved closer to the other jaw attached to the force transducer, so that the second wire could be secured to its corresponding screws. The mounting of the artery was done at room temperature, and once finished, the myography chamber was warmed to 37 °C.

2.5.3 Equilibration

The arteries were bathed in PSS at 37 °C for 30 minutes to equilibrate before being normalised. The aim of the equilibration period is to allow the arteries to gradually warm up to experimental temperature and to reset the ion gradients that may have become altered during dissection and the changing of the PSS. The equilibration period also allows for the acquisition of a stable stage of passive tension. When the chamber warmed up to 37 °C, the force transducer was zeroed while two jaws were closed together so that there was no tension from the artery due to stretch.

2.5.4 Normalisation

The objective of the normalisation procedure was to set the artery to standard primary conditions (i.e. resting tension). Normalisation allows arterial force to be accurately measured by determining the internal circumference of the artery, through stretching the artery sequentially and measuring the micrometre and the passive force readings **(figure 2.3)**. At each point of stretching, the wall tension and internal circumference of the vessel is tested to determine the maximum force. The wall tension is an exponential function of the artery's internal circumference. Arteries with an internal circumference

of 0.9 IC_{100} are estimated to be 0.9 times the circumference they would maintain if relaxed and exposed to 100 mm Hg transmural pressure.

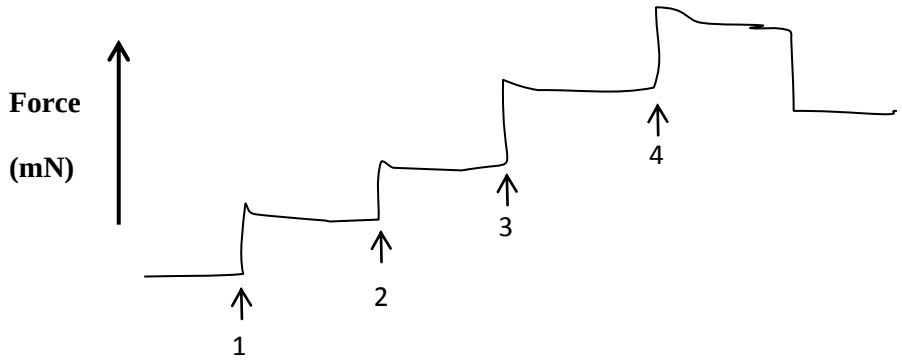

Figure 2.3. Normalisation of mounted arteries. Stepwise increases of jaw distance (and stretching of arteries) were performed (1, 2, 3, and 4) until the wall tension reaches 13.2 kPa (point 4, IC_{100}). Once this is achieved, jaws were brought a little closer to provide 90 % of this value (hence the sudden decrease in the tension in the graph).

2.5.5 Chemicals and solutions

The composition of the main bathing solutions for contraction experiments were as follows (in mM): physiological saline solution (PSS) containing NaCl 137, $NaH_2PO_4H_2O$ 0.44, Na_2HPO_4 0.42, $NaHCO_3$ 4.17, KCl 5.6, $MgCl_2$ 1, HEPES 10, glucose 10 and $CaCl_2$ 2 (pH 7.4); depolarizing high K^+ physiological saline (KPSS) comprising PSS with an equimolar substitution of NaCl by KCl (total 80 mM KCl) (pH

7.4). 20 mM K/ Bay K 8644, a solution that will contract the artery by the opening of L-type Ca^{2+} channels but does not depolarise as much as KPSS, was also used. This solution contained 200 nM ±Bay K8644 dissolved in 20 mM K^+ salt solution (KCl 20, NaCl 117, $NaH_2PO_4H_2O$ 0.44, Na_2HPO_4 0.42, $NaHCO_3$ 4.17, KCl 5.6, $MgCl_2$ 1, HEPES 10, glucose 10 and $CaCl_2$ 2 (pH 7.4)). M-β-CD (10 mM) was dissolved directly in PSS. Ch-MCD (5 mM) was dissolved directly in PSS by heating at 80 °C for 10 minutes using a water bath. 2 mM tetraethylammonium (TEA^+) chloride was dissolved directly in PSS (TEA/PSS) or 20 K/ Bay K (20 K/ Bay K/ TEA). L-N^G-Nitroarginine methyl ester (L-NAME) (250 µM) was dissolved directly in PSS solution or 20 K/ Bay K solution (20 K/ Bay K/ L-NAME). Stock solution of acetylcholine (ACh) (10 mM) was made in distilled water and used at X1000 dilution (final concentration of ACh was 10 µM). NS1619 [1,3-Dihydro-l-[2-hydroxy-5-(trifluoromethyl) phenyl]-5-(trifluoromethyl)-2i/benzimidazol-2-one] was made up as a 10 mM stock solutions in dimethyl sulphoxide (DMSO). Stock solution of sodium nitroprusside (SNP; 10 mM) was made with distilled water. Stock solution of forskolin (FSK; 10 mM) was made using DMSO. Stock solution of isoproterenol (ISO; 10 mM) was made with distilled water. Stock solution of phenylephrine (PE; 10 µM) was made with distilled water. Stock solution of Iberiotoxin (IBTX; 100 µM) was made in distilled water. Finally, the stock solution of filipin (4 µg/ml) was prepared by dissolving in PSS at 37 °C for 10 minutes by using a water bath.

Chapter 3 Ultrastructural Study of Rat Femoral Arteries

3.1 Aim of the chapter

This study was designed to investigate:

- The ultrastructural changes to the cell membrane in the SMCs and ECs of rat femoral arteries after treatment with methyl β-cyclodextrin (M-β-CD), observed using transmission electron microscope (TEM).
- The topological relationship between caveolae and sarcoplasmic reticulum (SR) (caveolae-SR) or caveolae and mitochondria (caveolae-mitochondria) in the SMCs of intact femoral arteries.

The key finding in this chapter

- The results showed that treatment with M-β-CD removed caveolae from SMCs and ECs of rat femoral arteries.

3.2 Introduction

Several studies have provided strong evidence that the SR acts as a major Ca^{2+} store in SMCs (Somlyo et al., 1979, Taggart, 2001). Moreover, numerous other cellular organelles such as mitochondria have been shown to also regulate the Ca^{2+} concentration in SMCs (Patel and Insel, 2009). Recent structural studies of SMCs have reported close proximity of SR to the plasma membrane (15–30 nm), particularly around caveolae (Strehler and Treiman, 2004, Sweeney et al., 2006). Moreover, the relationship between SR/mitochondria-caveolae in vascular SMCs seems to show some interesting nanocontacts (Gherghiceanu and Popescu, 2007). The nanocontacts of caveolae-SR has led some researchers to consider highly localised events in this micro-domain; for example, BK_{Ca} channels are localised in the caveolae micro-domain (Babiychuk et al., 2004, Brainard et al., 2005). BK_{Ca} channels are activated by local SR Ca^{2+} release (Ca^{2+} sparks), and their activation can cause hyperpolarisation and hence changes in the excitability of SMCs. Thus, any disruption of the close links between caveolae-SR may be expected to have an uncoupling effect. On the other hand, a nanocontact has also been shown between mitochondria and caveolae in SMCs (Patel and Insel, 2009). In ECs, the localisation of endothelial NO synthase (eNOS) in the caveolae microdomain is of paramount importance for the effective relaxation of blood vessels (Ghosh et al., 1998, Feron et al., 1996). Nitric oxide (NO) is formed by eNOS and diffuses into SMCs, leading to smooth muscle relaxation. Moreover, caveolae can exist in many different forms, such as rosettes, grape-like clusters and elongated tubules **(figure 3.1)** (Parton et al., 1997, Razani et al., 2002, Yamada, 1955). Interestingly, these different forms of caveolae are mostly present in specific tissues. For instance, vesicles/tubules are highly

abundant in endothelial cells, rosette shapes in adipocytes and grape-like clusters in skeletal muscle cells (Lisanti et al., 1994b, Parton et al., 1997, Simionescu et al., 1975).

Myoendothelial gap junctions (MEGJ) are generally described as forming gap junctions between vascular ECs and vascular SMCs. The endothelial cell membrane forms an eminence through small narrow gaps, 1-1.5 µm in width, in the internal elastic lamina (IEL) to form MEGJs with the SMCs (Wasano and Yamamoto, 1983). Moreover, several studies have proved a physiological role of MEGJ in mesenteric arteries and arterioles where electrical and chemical signals are transmitted from ECs to SMCs (Sandow et al., 2003, Sandow and Hill, 2000, Shimokawa et al., 1996). The elastic tissue of a rat's femoral artery is composed of two distinct layers, the IEL and the external elastic lamina (EEL), and the medial wall or tunica media between the two elastic laminae is filled with layers of SMCs and isolated fragmented elastic fibres (Wasano and Yamamoto, 1983). However, the IEL appears as a plate-like structure, discontinuous in thickness, about 2 µm in width and with several small gaps of about 1-1.5 µm, which serve to allow MEGJ to form. On the other hand, the EEL appears as a slightly undulated sheet-like structure, about 1 µm in thickness, and has small gaps in it of about 3 µm in width, which allow for collagen fibres to pass into the tunica media. Moreover, scanning electron microscopy (SEM) shows the surface of both the IEL and EEL, with several small rounded fenestrations which vary in size from 1 to 5 µm (Wasano and Yamamoto, 1983).

The important physiological role of MEGJs has been studied in different vascular beds (Beny, 1997, Hill et al., 2001, Yamamoto et al., 1999). In guinea-pig mesenteric arterioles, hyperpolarization generated in ECs can be transmitted to the smooth muscle

through MEGJs (Yamamoto et al., 1999). Membrane hyperpolarization can cause smooth muscle relaxation through a decrease in VDCCs open probability.

Cholesterol is an essential component for the assembly of caveolae (Patel and Insel, 2009, Patel et al., 2008b). Cholesterol can be depleted from cell membranes by cholesterol-depleting agents, such as nystatin, saponin, M-β-CD and filipin (Rothberg et al., 1990, Gimpl et al., 1997). M-β-CD is currently the most-used tool for disrupting lipid rafts and caveolae (Barnes et al., 2004). Previous studies have illustrated that the efficiency of M-β-CD is dependent on incubation time, tissue type and temperature (Linder et al., 2005). Caveolae disassembly represents a useful tool to aid in understanding caveolae-dependent physiological processes. Treatment of the tissues with M-β-CD (5-15 mM) for 1 hour at 37 °C alters the cholesterol content of the cell membrane and thereby disrupts caveolae (Pike and Miller, 1998; Kaiser et al., 2002). Cholesterol-depleting agents have been effectively used as a pharmacological tool to demonstrate a role of caveolae in vascular reactivity (Dreja et al., 2002, Je et al., 2004, Bergdahl et al., 2003).

This chapter will focus on the topological relationship between caveolae-SR and caveolae-mitochondria in the SMCs of intact femoral arteries, and on the ultrastructural changes to the cell membrane in the SMCs and ECs of these arteries after M-β-CD treatment, using conventional light and transmission electron microscopy (LM and TEM).

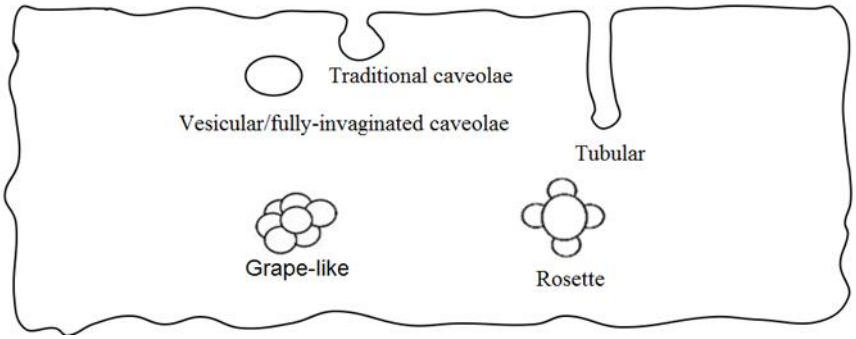

Figure 3.1. A schematic diagram representing the various forms of caveolae in the cell membrane and/or cytoplasm. Caveolae can be found in the forms of tubules, grape-like clusters, rosettes or vesicular. Modified from Razani et al. (2002).

3.3 Results

Intact (control) and 5 mM M-β-CD treated femoral arteries (*n*=5 in each group) were used for the TEM study. For the electron microscopic examination, about 7-8 sections from each animal of both control and treated groups were examined using an H-600 TEM (Hitachi, Pleasanton, California, USA) at an acceleration voltage of 60-120 kV. Then, section of the femoral artery was randomly selected from each group, and captured using an SIS Megaview III camera. These images were taken at different magnifications; X16000, 20000, 26000, 40000 and 60000.

3.3.1 TEM examination of the intact rat femoral artery

Serial cross-sections (70 nm) of the femoral artery were used to show general structure of intact artery walls. The elastic tissue mainly consists of two distinct laminae, the IEL **(figure 3.2 A)** and EEL **(figure 3.3 B)**. Furthermore, the elastic laminae are separated with multiple layers of SMCs, which are punctuated by bundles of collagen fibres **(figures 3.4 and 3.5)**. The IEL appears as a thick and slightly undulated tube, and

includes a few small gaps **(figure 3.2 B),** which vary in size. The gaps are uniformly distributed throughout the IEL. In contrast, the EEL appears as a slightly thin, discontinuous, tube-like structure, which includes several small gaps **(figure 3.3 B)**, which also vary in size. SMCs and ECs were connected with the IEL through contact points, which are located between the cell membranes of both SMC and ECs and the IEL **(figures 3.2, 3.6 and 3.7)**. Furthermore, most of the smooth muscle cells are arranged in parallel to the elastic tissue **(figure 3.3)**.

In the SMCs, TEM analysis revealed that most caveolae appear as omega-shaped invaginations in the plasma membrane, opening to the extracellular space **(figure 3.8)**. The ultrastructure of a SMC consists of a simple network of tubules, encircling caveolae **(figure 3.9)**. Nanocontacts were observed between caveolae-SR and caveolae-mitochondria on close examination of sections of intact rat femoral artery **(figures 3.8 and 3.9)**. Tubules of SR were concentrated at the periphery of the cell close to the cell membrane **(figure 3.9 B)**, whereas mitochondria were easily distinguished near to caveolae **(figure 3.8 B)**. Furthermore, mitochondria were concentrated at the center of the cell, close to the nucleus **(figure 3.8)**.

TEM examination of ECs in intact rat femoral arteries showed that some caveolae present in the ECs **(figure 3.6)** were different in morphology compared with the caveolae present in SMCs. Some caveolae in the cell membrane of the ECs are tubules and some take the regular omega shape. The study also found caveosomes (vesicular/fully-invaginated caveolae) **(figure 3.6 B)**.

3.3.2 TEM examination of rat femoral artery treated with M-β-CD

TEM analysis of femoral arteries was investigated after the disassembly of caveolae from SMCs and ECs. Micrographs of SMCs **(figure 3.10)** and ECs (**figure 3.7)** showed a rarity or absence of caveolae in the M-β-CD-treated artery. These TEM micrographs also show large collagen fibres between the SMCs **(figures 3.4 and 3.5)**, which seem to be inserted into the basement membranes of the SMCs. Nexin (Ne) junctions were also observed between the SMCs of treated vessels **(figure 3.10 B)**.

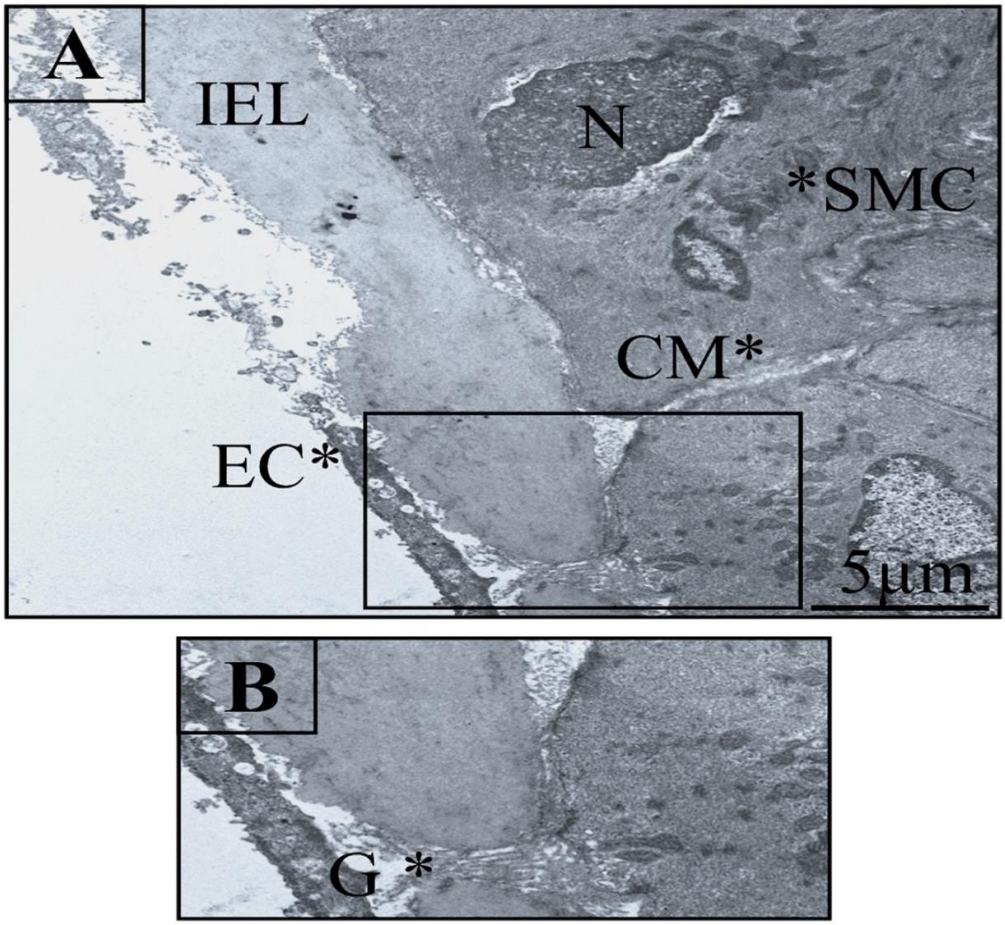

Figure 3.2. Transmission electron micrograph of a cross-section of rat femoral artery showing internal elastic lamina. A. A gap in the IEL, X11500. Scale bar= 5µm. **B.** Detail from square in figure 3.2 A shows a higher magnification image of the gap (G) in the IEL. Note collagen fibre bundles passing through the gap.

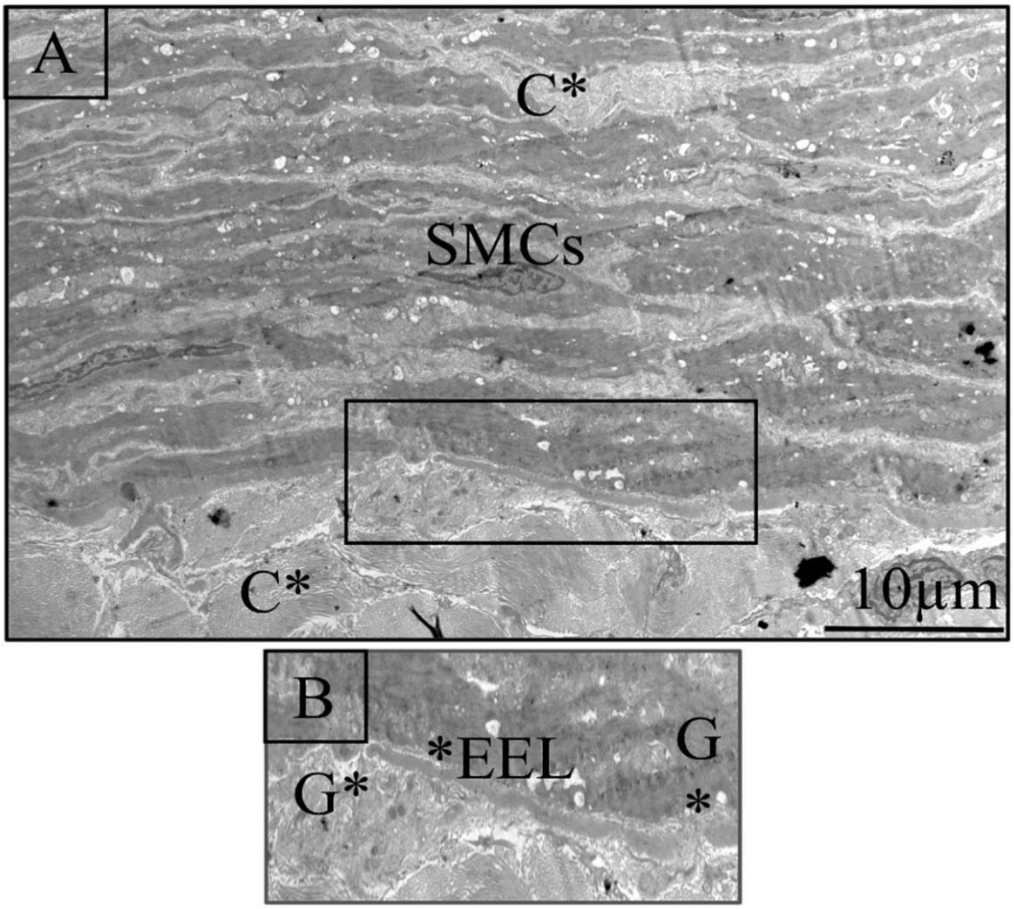

Figure 3.3. Transmission electron micrograph of rat femoral artery showing external elastic lamina (EEL). A. Discontinuous EEL, with small gaps of different width, showing collagen fibres (C) between SMCs, X11500. Scale bar= 10µm. **B**. Detail from marked area in figure 3.3 A shows higher magnification of the gaps (G) in the EEL.

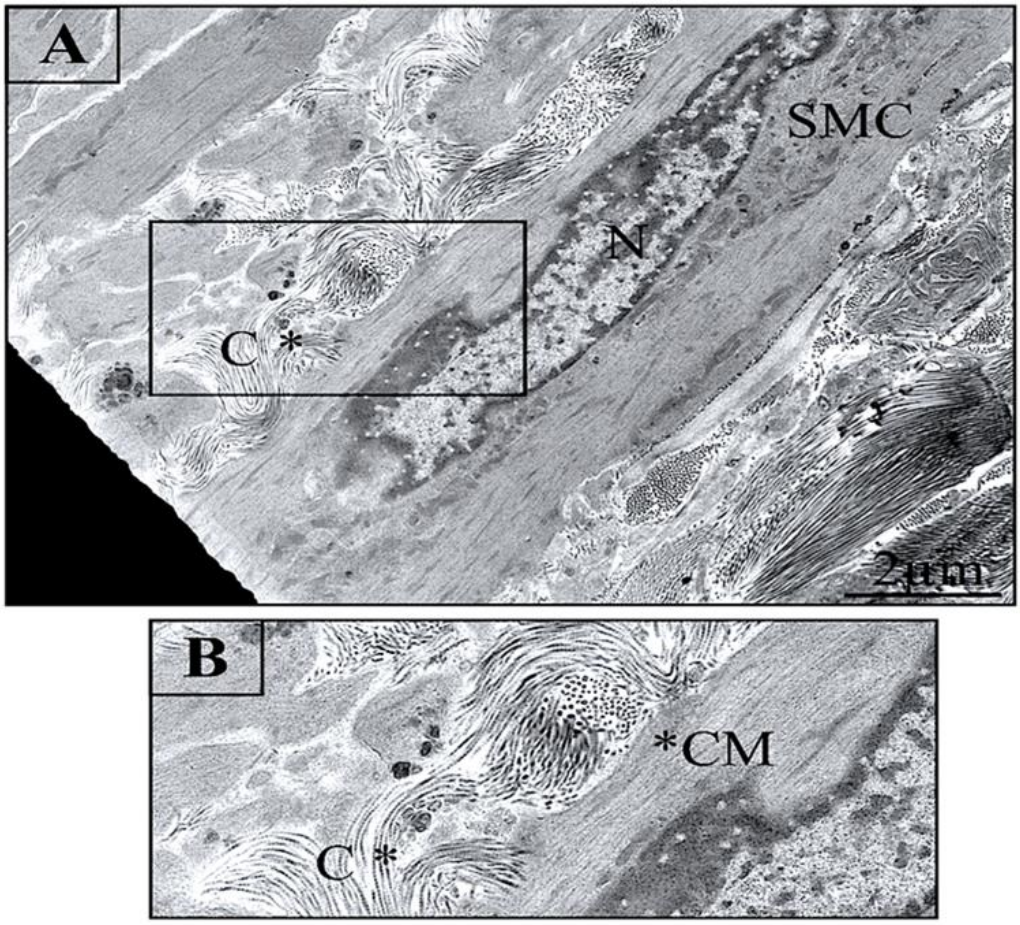

Figure 3.4. Transmission electron micrographs showing cell-matrix linkages in the tunica media of rat femoral artery. A. A complex weave of collagen (C) inserted into a SMC membrane, X27500. Scale bar= 2µm. This artery had been treated with M-β-CD. **B**. Detail from marked area in figure 3.4 A shows parallel collagen (C) fibres inserted into the membranes of the SMCs.

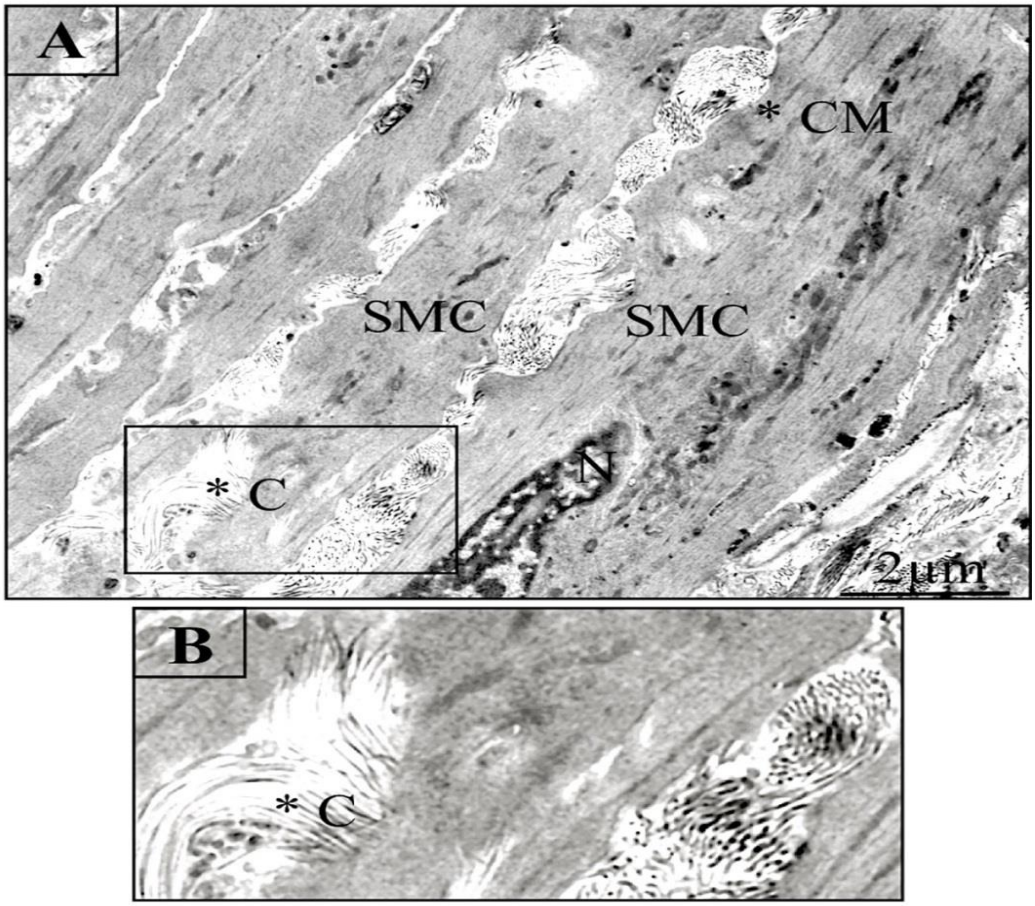

Figure 3.5. Transmission electron micrographs of cell-matrix linkages in the tunica media of rat artery. A. A complex weave of collagen (C) inserted into an SMC membrane, X27500. Scale bar= 2µm. This artery had been treated with M-β-CD. **B**. Detail from marked area in figure 3.5 A shows parallel collagen fibres (C) inserted into the membrane of SMCs.

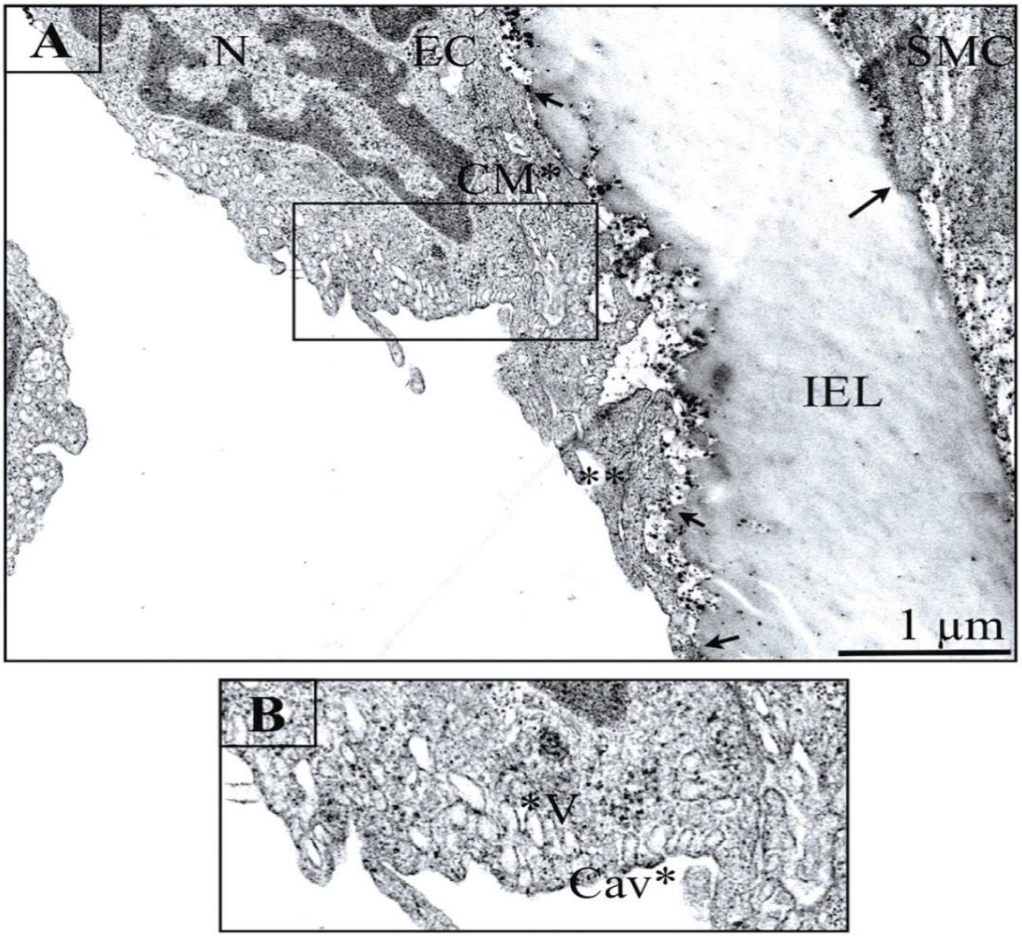

Figure 3.6. Transmission electron micrograph of rat femoral artery ECs showing caveolae. **A**. Caveolae cover most of EC membrane, long arrows show contact of SMCs with IEL, short arrows show contact of ECs with IEL and the double stars show gap junction plaques between two ECs, X60000. Scale bar= 1µm. **B**. Detail from marked area in figure 3.6 A shows caveolae (Cav) and caveosomes (V).

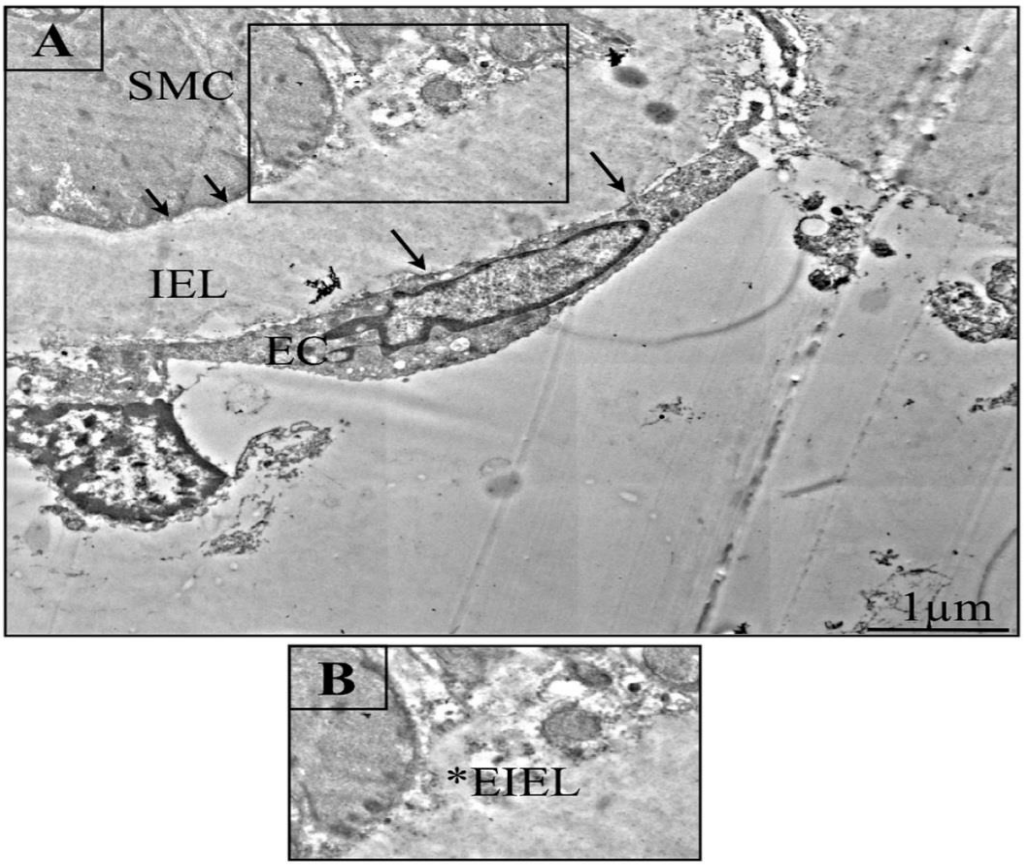

Figure 3.7. Transmission electron micrograph of a cross-section of rat femoral artery treated with 5 mM M-β-CD. A. Cell membranes of SMCs and ECs were free of caveolae, long arrows show contact of ECs with IEL and short arrows show contact of SMCs, X60000. Scale bar= 1µm. **B**. Detail from marked area in figure 3.7 A shows extension of IEL to sides of SMCs (EIEL).

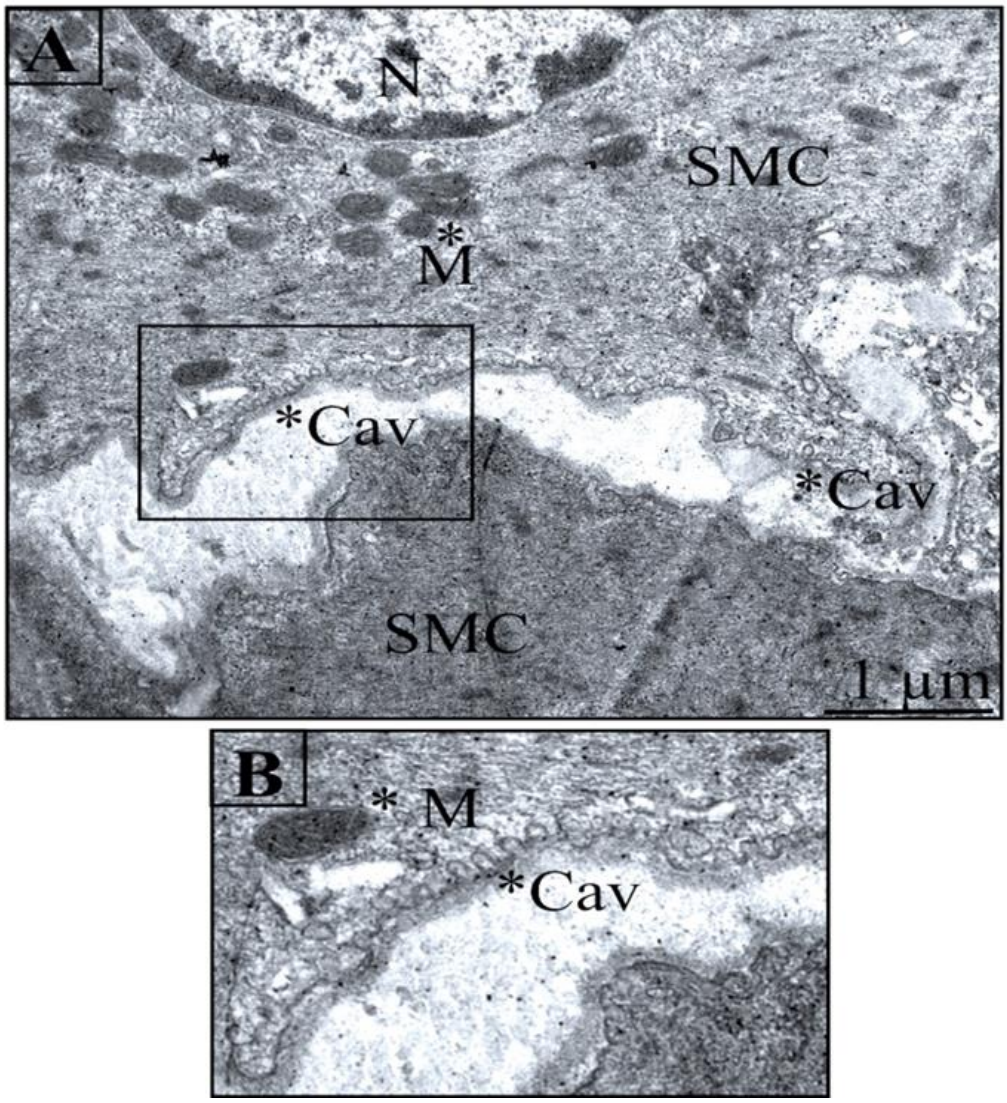

Figure 3.8. Transmission electron micrograph of rat femoral artery SMC showing caveolae and mitochondria. A. Omega-shaped caveolae (Cav) cover most of the SMCs membrane, X60000. Scale bar= 1µm. **B**. Detail from marked area in figure 3.8 A shows mitochondrion (M) close to caveolae.

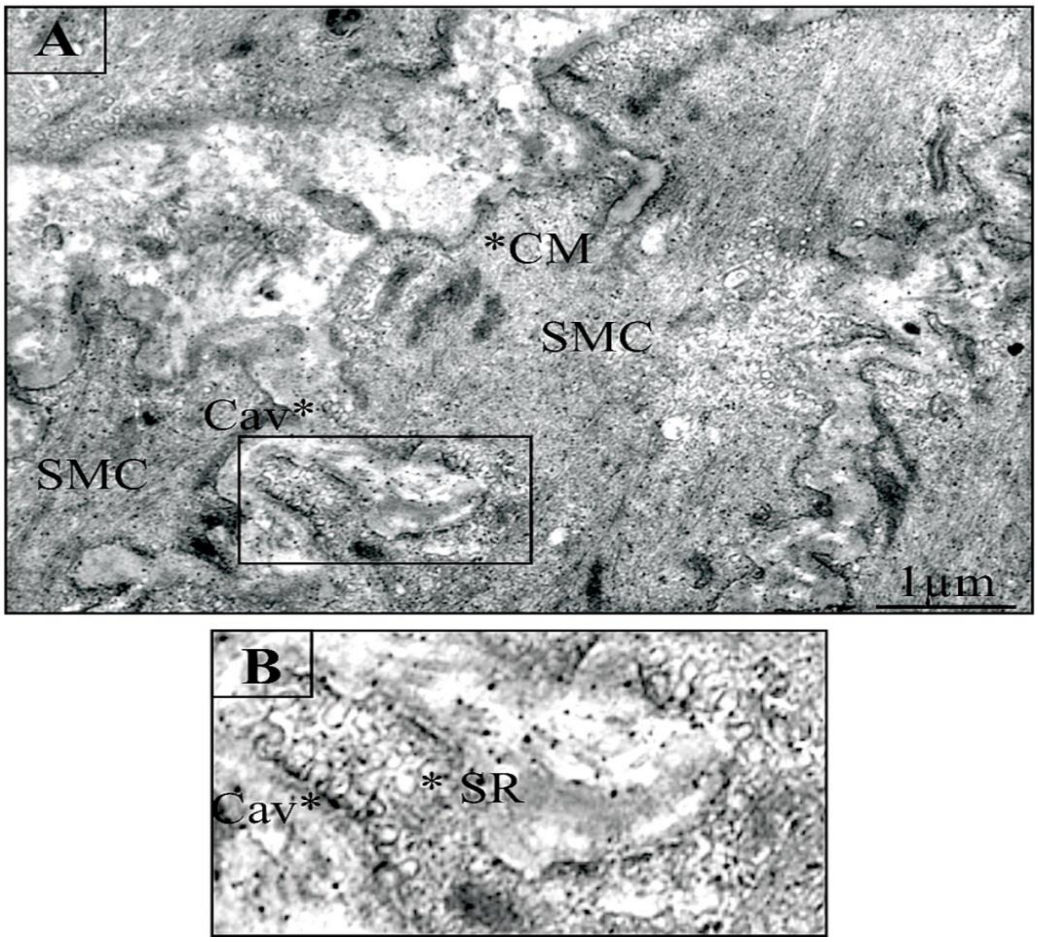

Figure 3.9. Transmission electron micrograph of rat femoral artery SMC showing relationship between caveolae and SR. A. Caveolae (Cav) cover most of the cell membrane of the SMCs, X60000. Scale bar= 1µm. **B**. Detail from marked area in figure 3.9 A. Caveolae are within a few nanometers of the sarcoplasmic reticulum (SR).

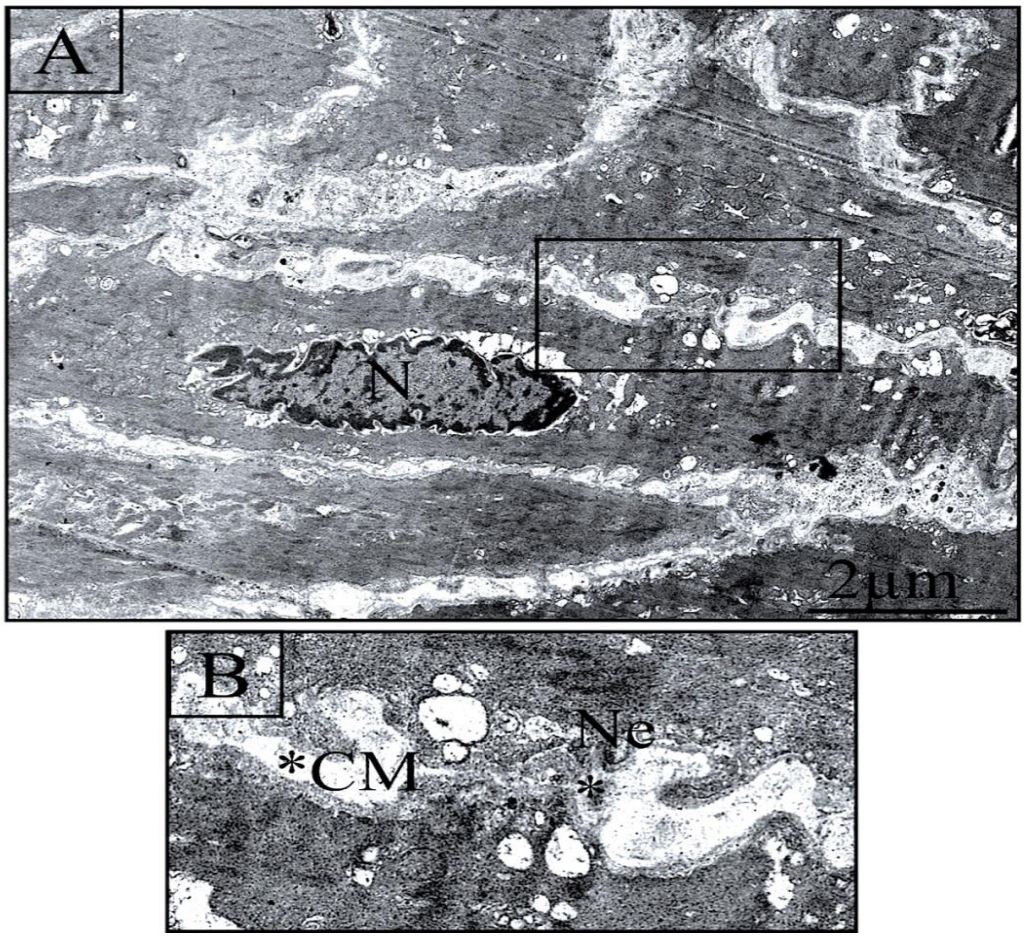

Figure 3.10. Transmission electron micrograph of a cross-section of rat femoral artery treated with M-β-CD. A. SMCs were free of caveolae. Cholesterol extraction with M-β-CD completely abolished caveolae structures from the cell membrane, X27500. Scale bar= 2µm. **B**. Detail from marked area in figure 3.10 A. The cell membrane of SMCs is devoid of caveolae. Note also nexus junctions (Ne) (intercellular connections between two SMCs filled with myofilaments).

3.3.3 Histology of rat femoral arteries

In this technique, four intact rat femoral arteries and four endothelium-denuded arteries were used. Ten sections from each group were examined by conventional light microscope. A random section was selected from both the intact and the endothelium-denuded group, and images captured with an Olympus digital microscope.

3.3.3.1 Histological results of endothelium-intact rat femoral artery

The intact arterial wall consists of three layers, tunica intima, tunica media and tunica adventitia **(figure 3.11 B)**. The tunica intima is composed of a layer of endothelial cells, which have a squamous structure and form a fenestrated face **(figure 3.11B)**. The tunica media is made up of layers of SMCs **(figure 3.11 B)**. SMCs have the ability to stretch up to 1.5 times their length, and then return to their normal length on relaxation. The tunica media is located between the tunica intima on the inside and the tunica adventitia on the outside. The tunica adventitia in arteries is composed mainly of connective tissue (collagen and elastin) **(figure 3.11 B)**. The lumen diameter of a rat femoral artery was about 200 μm **(figure 3.11 A).**

3.3.3.2 Histological results of endothelium-denuded rat femoral artery

The ECs of the femoral artery were mechanically removed by gently rubbing the intimal surface with a human hair **(figure 3.11 C)**. Histology **(figure 3.11 D)** showed the removal of most of the endothelial layer.

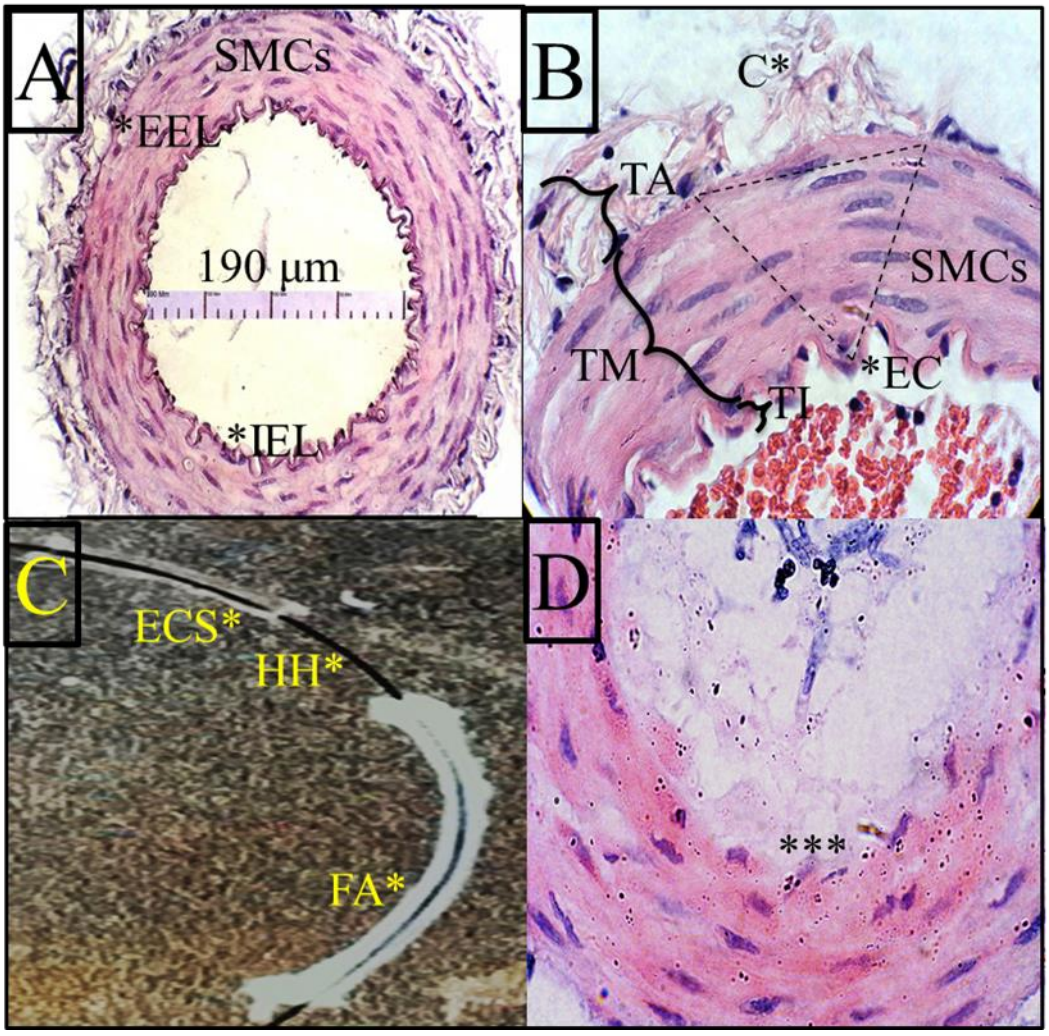

Figure 3.11. Histological analysis of rat femoral artery. A. Photomicrograph of a histological cross-section of an intact artery, X400, internal diameter, 190 µm. **B**. Photomicrograph of magnified cross-section of artery, X600, showing three structural layers: TI, TM and collagen fibre in TA. Picture also shows the layers of SMCs inside the TM in the triangle. **C**. Photograph showing the removal of the endothelial sheath (ECS) from the femoral artery (FA) using a human hair (HH). **D**. Photomicrograph of cross-section of artery showing the lumen of the artery devoid of its sheath of ECs (***), X600.

3.4 Discussion

Studies presented here have focused on the ultrastructure of vascular SMCs in order to examine the strategic relationship between caveolae-SR and caveolae-mitochondria contacts. This micro-architecture of SMCs plays an important role in regulation of Ca^{2+} concentration (Shaw et al., 2006).

Using TEM, the morphology of the cell membrane and the relationships between caveolae-SR **(figure 3.10)** and caveolae-mitochondria in SMCs **(figure 3.10)** and ECs **(figure 3.6)** was examined. TEM revealed that caveolae were often, but not always, in close proximity to peripheral SR or to mitochondria in rat femoral arteries. These results agree with Popescu et al. (2006) who state that caveolae were localised within a few nanometers from the SR and/or from mitochondria in vascular SMCs. Moreover, these results agree with several studies (Taggart, 2001, Dreja et al., 2002, Shaw et al., 2006, Tong et al., 2009) reporting that nanocontacts exist between caveolae-mitochondria and caveolae-SR in the SMCs of different muscular arteries. These studies also report the arrangement of caveolae and underlying peripheral SR in vascular SMCs which regulate Ca^{2+} and contractile activation. Shaw et al. (2006) observed abundant mitochondria in the middle of SMCs, near to the nucleus. These results also agree with our findings **(figure 3.8)**. The current study also shows that some mitochondria in arterial SMCs can be located close to caveolae **(figure 3.10)**. This agreed with the findings of Patel and Insel (2009) who observed nanocotacts between mitochondria and caveolae in pulmonary artery SMCs.

Saliez et al. (2008) demonstrated the presence of caveolae in the ECs of rat mesenteric arteries. TEM examination of intact rat femoral arteries in the current study also showed

numerous caveolae present in the ECs **(figure 3.6)**. These findings were consistent with Xu et al. (2007) who also stated that the integrity of caveolae in ECs is very important in the NO signaling cascade.

The TEM examination of rat femoral arteries showed gaps of different sizes through the IEL **(figure 3.2)** but without an obvious presence of MEGJs from ECs to SMCs. These results agree with reports by Sandow et al. (2002) and Hill et al. (1999) who also confirmed that gaps are present in the IEL of rat femoral arteries without MEGJs from ECs to SMCs. In contrast, they observed the existence of MEGJs in rat mesenteric arteries. Our findings with respect to the IEL contrast with that of Wasano and Yamamoto (1983). They report that the existence of MEGJs that penetrate the IEL of rat femoral arteries, and they found small rounded fenestrations along the IEL and EEL. These fenestrations in the IEL serve to allow diffusion of chemicals or nutrient substances from the vascular lumen into the vascular media. In contrast, the function of fenestrations in the EEL is to pass intercellular collagen fibre bundles between the tunica media and tunica adventitia (Wasano and Yamamoto, 1983). Considering the SEM findings of Wasano and Yamamoto (1983) with respect to fenestrations in the IEL, we suggest that the fenestrations may be pathways for the diffusion of endothelial-derived substances from ECs to SMCs. If this speculation is correct, we also hypothesise that it will explain the effect of the influence of ECs on the relaxation of smooth muscles and the diffusion of NO through connected points between both ECs/SMCs and IEL. Furthermore, connected points between the cell membranes of both SMCs and/or ECs and IEL play an important role in the diffusion of EC relaxation factors, such as NO, to SMCs through the fenestrations located in the IEL. Our results also demonstrated gaps

in the EEL **(figure 3.3)**. Similar gaps in the EEL have been demonstrated by Wasano and Yamamoto (1983) in rat femoral artery SMCs. The function of these gaps may also be to pass macro-molecules, nutrients and other chemical factors directly between SMCs and the tunica adventitia. The present TEM results demonstrate that the SMCs and elastic fibres make a continuous network throughout the tunica media to the tunica adventitia. These results again support Wasano and Yamamoto (1983) who reported that the collagen fibres and SMCs can function as a unit to distribute the intraluminar pressure uniformly around the whole circumference of the vascular walls.

To explore the role of caveolae in femoral artery contractions (see chapters 5 and 6), we used M-β-CD to deplete cholesterol and so the caveolae. TEM analysis showed that caveolae in both SMCs **(figure 3.10)** and ECs **(figure 3.7)** were disassembled from the plasma membrane after the treatment of the vessels with M-β-CD.

In this study, the endothelium was removed from some femoral artery rings (see also chapters 5 and 6) by gently rubbing the intimal surface with a human hair. The morphological integrity of endothelial cells was additionally confirmed by preparing histological preparations of rat femoral artery with standard haematoxylin and eosin staining **(figure 3.11 B)**. Mechanical removal of endothelial cells from the lumen was confirmed by histological techniques **(figure 3.11 D)**. Similar results have been demonstrated in rat femoral artery by Radenkovic et al. (2012) who showed that endothelial cells could be mechanically removed from the intimal surface of artery rings by gently rubbing with a stainless-steel wire. These results were acquired by histology.

3.5 Conclusion

In summary, the details of the ultrastructure of rat femoral arteries was examined using intact artery material, artery that was treated with M-β-CD, and artery that was denuded of ECs with a human hair. The results showed that treatment with M-β-CD removed caveolae and that rubbing the lumen with human hair removed ECs.

Chapter 4 Immunofluorescence and Western blotting Studies of Rat Femoral Artery and Human Coronary Artery Endothelial Cells

4.1 Aim of the study

To investigate the expression of BK_{Ca} channels, cav-1 and cav-3 in rat femoral artery SMCs and ECs and human coronary artery endothelial cells (HCAECs) using three methods: immunohistochemistry, immunocytochemistry and Western blot.

The key findings in this chapter

- Co-expression the BK_{Ca} channels with cav-1 and cav-3 in the SMC layer at tissue level and in individual SMCs in native rat femoral arteries.
- Co-expression of the BK_{Ca} channels with cav-1 in ECs of rat femoral arteries.

4.2 Introduction

To date, expression of three isoforms of caveolin proteins have been found in vascular tissues: cav-1, cav-2, and cav-3 (Drab et al., 2001, Kamishima et al., 2007). As described earlier, the binding of caveolins and partner proteins are thought to occur at CSD of caveolins (Couet et al., 1997, Oka et al., 1997) and caveolin-binding motifs on partner proteins (Dupree et al., 1993, Dietzen et al., 1995) **(figure 4.1)**. Partner proteins for caveolins include ion channels (Nichols and Lippincott-Schwartz, 2001), and mammalian BK_{Ca} channels have two potential cav-1 binding motifs: (^{537}YTEYLSSAF^{545}) and (^{1007}YNMLCFGIY^{1015}) (Alioua et al., 2008).

BK_{Ca} channels are expressed in most vascular cells and play a critical role in the regulation of blood flow (Brenner et al., 2000, Sausbier et al., 2005). Furthermore, BK_{Ca} channels in vascular SMCs are regulated by several vasoconstrictors and vasodilators (Alioua et al., 2008). In addition, studies have shown that BK_{Ca} channels are co-expressed with cav-1 and regulate Ca^{2+} homeostasis in endothelial cells (Wang et al., 2005, Riddle et al., 2011). It seems reasonable, therefore, to postulate that the interaction of BK_{Ca} channels with caveolin 1 and caveolin 3 may play an important role in femoral artery contraction/relaxation.

In this chapter, I aimed to characterise the expression pattern of BK_{Ca} channels, cav-1 and cav-3 using immunohistochemistry, immunocytochemistry and Western blot technique.

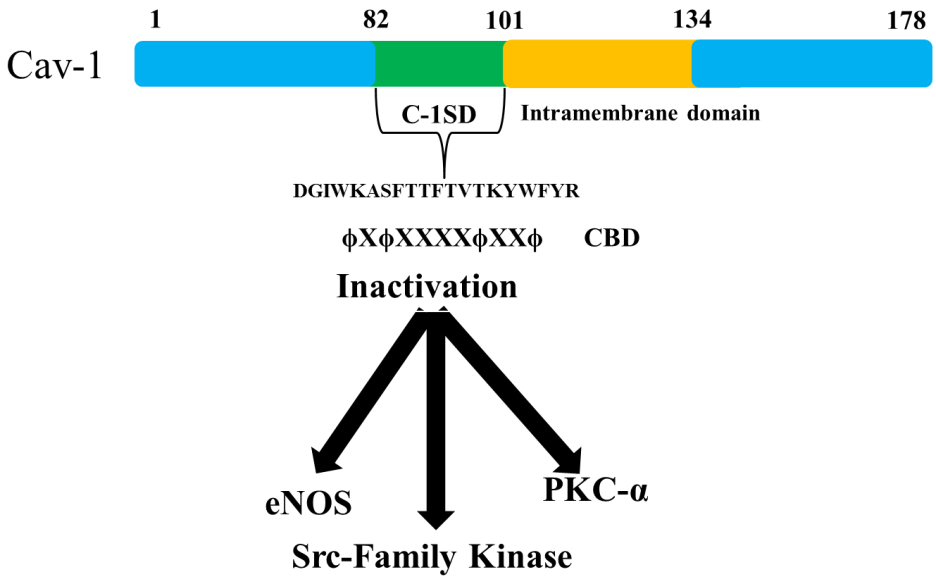

Figure 4.1. Cav-1 scaffolding domain (C-1SD) interacts with the partner proteins (eNOS, Src family kinase and PKC-α) through consensus caveolin-binding motif (CBM). Modified from Okamoto et al. (1998).

4.3 Results

4.3.1 Immunohistochemistry results of rat femoral arteries

4.3.1.1 Expression of α-actin and vWF in the SMCs and ECs of rat femoral arteries

Results from the previous chapter using the traditional histology technique showed that transverse sections of whole femoral arteries are a useful preparation to study SMC layers and EC layers. The results described here further extend such approach and aim to identify the expression pattern of proteins of interest in specific regions. Thus, the artery slice was first stained with antibodies against α-actin and vWF, signature proteins of SMCs and ECs, respectively. Mouse anti-α-actin and rabbit anti-vWF were then visualised using AF-594 (red) and AF-488 (green). Areas stained in red (anti-α-actin) localised to the SMCs layers **(figure 4.2 A)** while those in green (anti-vWF) were the ECs layer **(figure 4.2 B)**. Overlay image **(figure 4.2 C)** showed little overlap (which would have appeared as yellow) between α-actin and vWF stained areas.

For semi-quantitative analysis, a line was drawn across the artery wall **(figure 4.2 C)** in order to assess the signal strength of fluorescence across the SMC and EC layers using Leica Lite confocal software **(figure 4.3)**. Green fluorescence shows the expression of vWF at a high level in the EC layer compared to the SMC layer. Red fluorescence shows the expression of α-actin at high levels in the SMC layers compare to the ECs layer.

To confirm the positive immunostaining result, two negative controls were undertaken. For the first control, secondary antibody was mis-matched against wrong primary antibody (eg. anti-rabbit secondary used against mouse primary). A visual examination

of the mis-match experiments showed a low signal suggesting there is a little cross-reactivity among two animal species (eg. anti-rabbit secondary does not bind to a mouse primary) **(figure 4.2 D)**. For the second control, secondary antibodies were applied without primary antibody incubation. A visual examination of the section stained only with secondary antibodies showed a low signal showing that there is little direct binding of the secondary antibody to tissue slices **(figure 4.2 E)**. A bright field of the rat femoral artery is also shown in **figure 4.2 F**. The cell specific antibodies were used along with antibodies against cav-1, cav-3 and BK_{Ca} channels in order to access the cell types where these proteins are expressed.

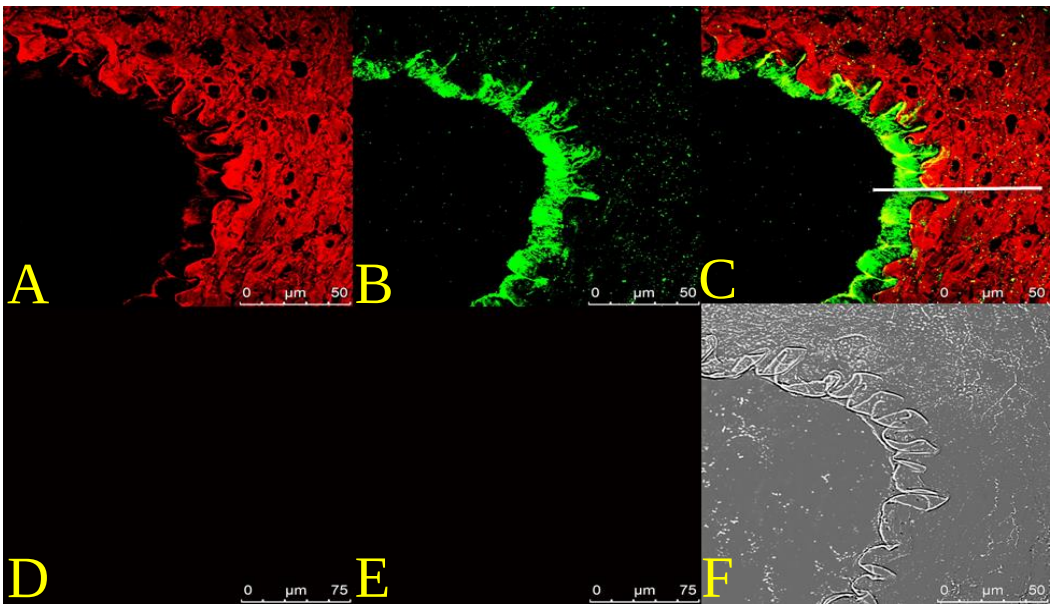

Figure 4.2. Representative confocal images of frozen sections (11 µm) of rat femoral arteries stained with mouse anti α-actin (x300) and rabbit anti-vWF (x300) and visualised with AF-594 (x500) and AF-488 (x500), respectively. A. Expression of α-actin (red) at high levels in the SMCs. **B**. Expression of vWF (green) in ECs at high levels. **C**. An overlay of A and B showed little overlap of red and green fluorescence. **D**. A negative control section of rat femoral artery stained with secondary antibody against mis-matched primary antibody. **E**. A negative control section of rat femoral artery stained with secondary antibodies only. **F**. A bright field section of rat femoral artery. A, B, C and F: scale bar represents= 50 µm, D and E: scale bar represents= 75 µm.

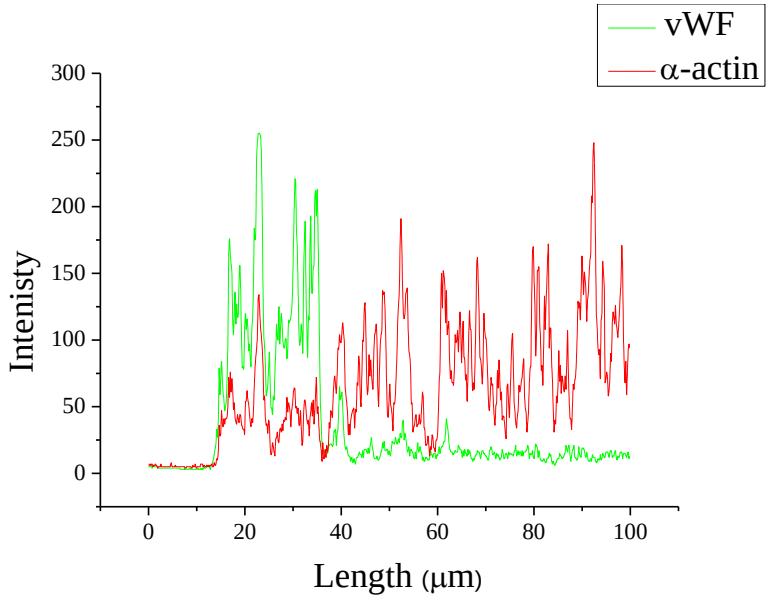

Figure 4.3. Fluorescence intensity profile for the vWF and α-actin signals along the white line shown in figure 4.2 C. Green fluorescence indicates expression of vWF at high levels in ECs, and red fluorescence indicates expression of α-actin at high levels in SMCs.

4.3.1.2 Expression of cav-1 in ECs from rat femoral arteries

The expression of cav-1 in ECs was examined using mouse anti-cav-1 primary antibody indirectly labeled with AF-488 (green) and rabbit anti-vWF indirectly labeled with AF-594 (red). As before, the red signal mainly appeared in the EC layer **(figure 4.4 A)**. A visual examination of anti-cav-1 staining indicates that the green signal appears in both SMCs and ECs layers **(figure 4.4 B)**. Indeed the overlay image **(figure 4.4 C)** showed the cav-1 overlapped with vWF, which appeared yellow. Fluorescence intensity profile taken along the white line in **figure 4.4 C** is shown in **figure 4.5**. The semi-quantitative analysis clearly shows that cav-1 is expressed at high levels in both SMC and EC layers. To confirm the positive immunostaining results, two negative controls, mis-match of primary and secondary antibody and primary antibody omission, were undertaken. Both results showed low signals **(figure 4.4 D and E)**. A bright field of the rat femoral artery is shown in **figure 4.4 F**. Our results therefore confirm that cav-1 is present in the ECs and SMCs of rat femoral artery tissue.

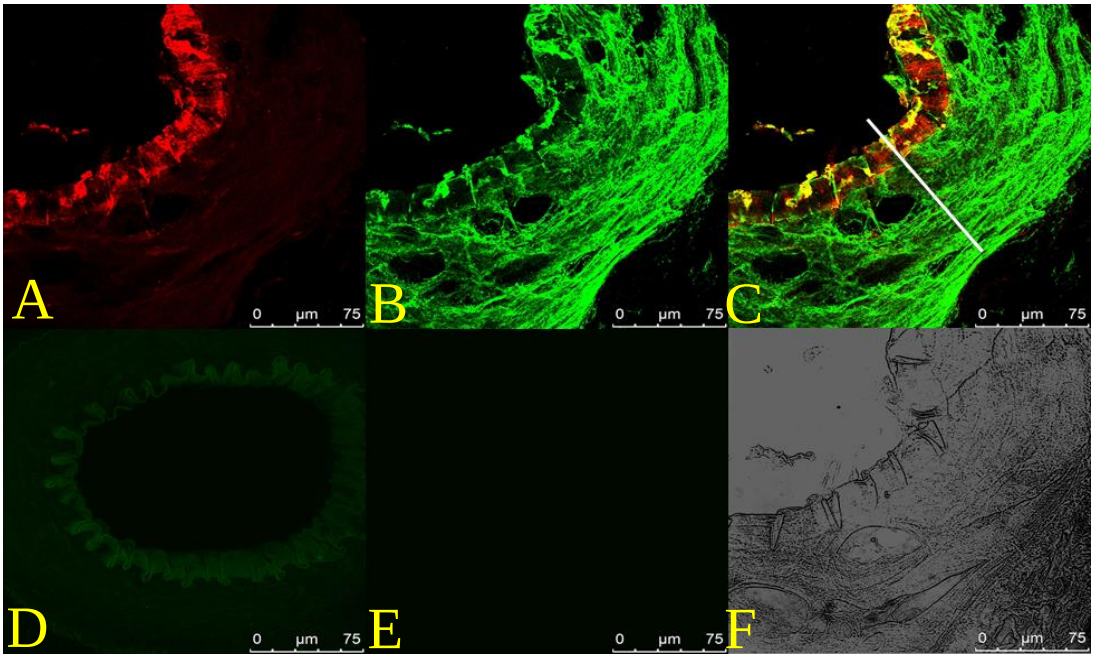

Figure 4.4. Representative confocal images of frozen sections (11 µm) of the rat femoral artery stained with rabbit anti-vWF (x300) and mouse anti-cav-1 (x200) and visualised with AF-594 (x500) and AF-488 (x500) respectively. A. Expression of vWF (red) at high levels in the ECs. **B**. Expression of cav-1 (green) in both SMCs and ECs at high levels. **C**. An overlay of A and B showing overlap of vWF and cav-1 (yellow) in the ECs. **D**. A negative control stained with secondary antibody against wrong primary antibody. E. A negative control stained with secondary antibodies only. **F**. A bright field section of rat femoral artery. Scale bar represents= 75 µm.

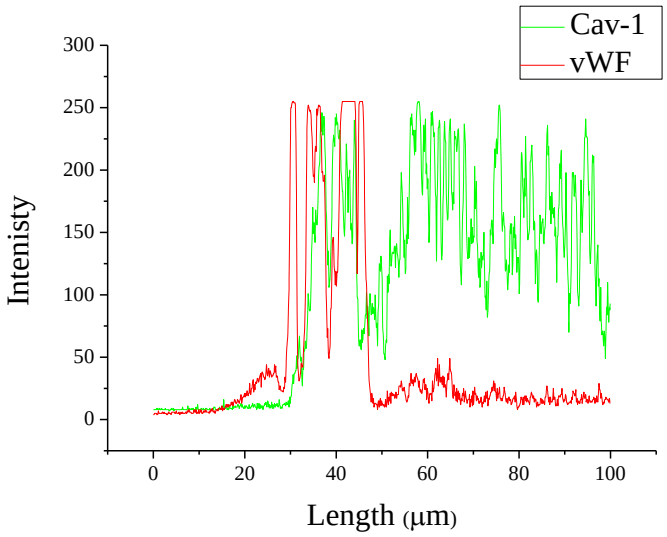

Figure 4.5. Fluorescence intensity profile of cav-1 and vWF along the white line shown in figure 4.4 C. Green fluorescence indicates expression of cav-1 at high levels in both SMCs and ECs.

4.3.1.3 Expression of cav-3 in ECs of rat femoral artery

Expression of cav-3 in ECs was examined using rabbit anti-vWF and mouse anti-cav-3, labeled with AF-594 (red) and AF-488 (green) respectively. A visual examination of the sections indicated that red signal **(figure 4.6 A)** and green signal **(figure 4.6 B)** occur separately. Indeed, an overlay image **(figure 4.6 C)** showed no overlap between vWF and cav-3. Fluorescence intensity profile in the SMCs and ECs along the white line in **figure 4.6 C** is shown in **figure 4.7**. The green fluorescence shows the expression of cav-3 at high levels in the SMC layers, and cav-3 is absent from the EC layer.

To confirm the positive immunostaining result, two negative controls, mis-match of primary and secondary antibody and primary antibody omission, were undertaken. In both cases, there was a low signal **(figure 4.6 D and E)**. A bright field of rat femoral artery is shown in **figure 4.6 F**. Our results therefore confirm that cav-3 is present in the SMCs but not in the ECs of rat femoral artery tissue.

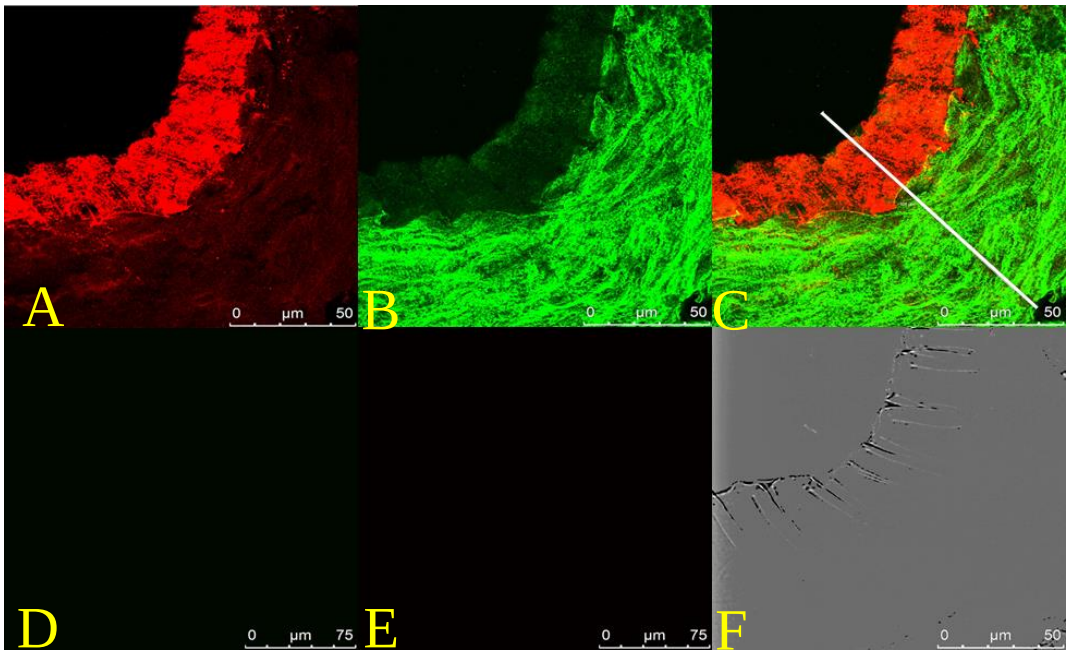

Figure 4.6. Representative confocal images of frozen sections (11µm) of rat femoral arteries stained with rabbit anti-vWF (x300) and mouse anti-cav-3 (x500) and visualised with AF-594 (x500) and AF-488 (x500) respectively. A. Expression of vWF (red) at high levels in the ECs. **B**. Expression of cav-3 at high levels only in the SMCs. **C**. An overlay of A and B showing no overlap of red and green fluorescence in either ECs or SMCs. **D**. A negative control section of rat femoral artery stained with secondary antibody mis-matched with wrong primary antibody. **E**. A negative control section of rat femoral artery stained with secondary antibodies only. **F**. A bright field section of rat femoral artery. A, B, C and F: scale bar represents= 50 µm; D and E: scale bar represents= 75 µm.

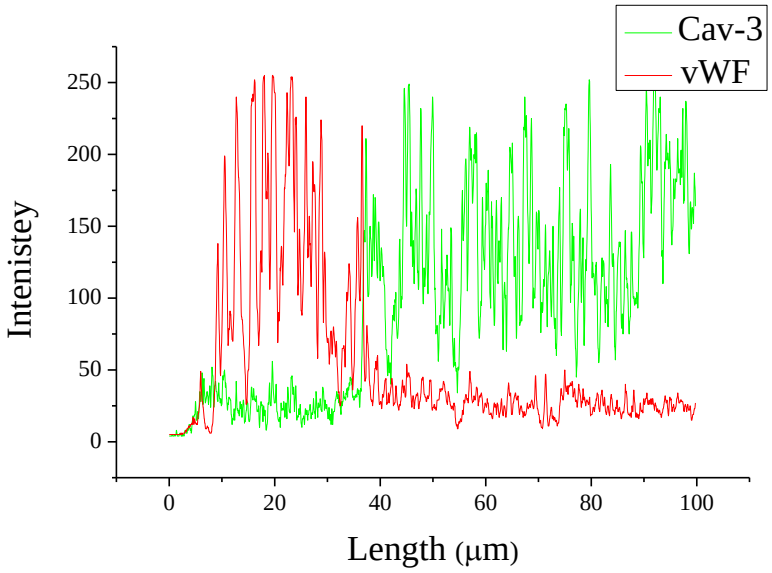

Figure 4.7. Fluorescence intensity profile of cav-3 and vWF along the white line shown in figure 4.6 C. Green fluorescence shows expression of cav-3 at high levels in the SMCs only.

4.3.1.4 Expression of BK_{Ca} channels in the ECs of rat femoral arteries

Expression of BK_{Ca} channels in ECs was examined using rabbit anti-vWF and rabbit anti-BK_{Ca} channels (against the peptide sequence 1184-1200: [C] STANRPNRPKSRESRDK). The former was directly conjugated with Fab AF-594 (red) as described in chapter 2 (2.4.1.1), and the latter was indirectly stained with AF-488 (green). A visual examination of the sections stained with rabbit anti-vWF indicates that the red signal appears in the EC layer **(figure 4.8 A)**. A visual examination of the sections stained with anti-BK_{Ca} channels indicated that the green signal appears in both the SMC and EC layers **(figure 4.8 B)**, with overlay image showing overlap in EC section (yellow, **figure 4.8 C**). The fluorescence intensity profile of the white line shown in **figure 4.8 C** is shown in **figure 4.9**. Green fluorescence shows the expression of BK_{Ca} channels at high levels in both SMC and EC layers.

As before, two negative controls were undertaken by mis-matching primary and secondary antibody **(figure 4.8 D)** and by omitting the primary antibodies **(figure 4.8 E)**. There was little signal detected in either case. A bright field of rat femoral artery is shown in **figure 4.8 F**. Our results therefore showed BK_{Ca} channels are expressed not only in SMCs but also in the ECs of rat femoral arteries.

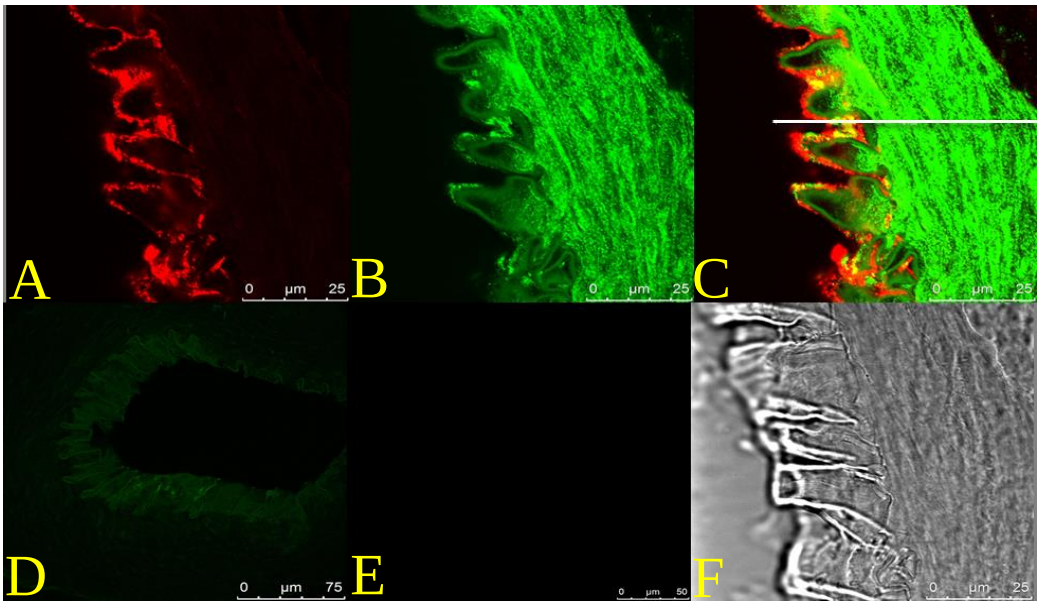

Figure 4.8. Representative confocal images of frozen sections (11 µm) of the rat femoral artery stained with rabbit anti-vWF (x300) and rabbit anti-BK_{Ca} channels (x500) and visualised with AF-594 (x500) and AF-488 (x500) respectively. A. Expression of vWF (red) in the ECs. **B**. Expression of BK_{Ca} channels (green) in both SMCs and ECs at high levels. **C**. An overlay of A and B showing co-expression of vWF and BK_{Ca} channels (yellow spots) in the ECs. **D**. A negative control stained with secondary antibody mis-matched with a wrong primary antibody. **E**. A negative control stained with secondary antibodies only. **F**. A bright field section of rat femoral artery. A, B, C and F: scale bar represents= 25µm; D: scale bar represents= 75µm; E: scale bar represents= 50 µm.

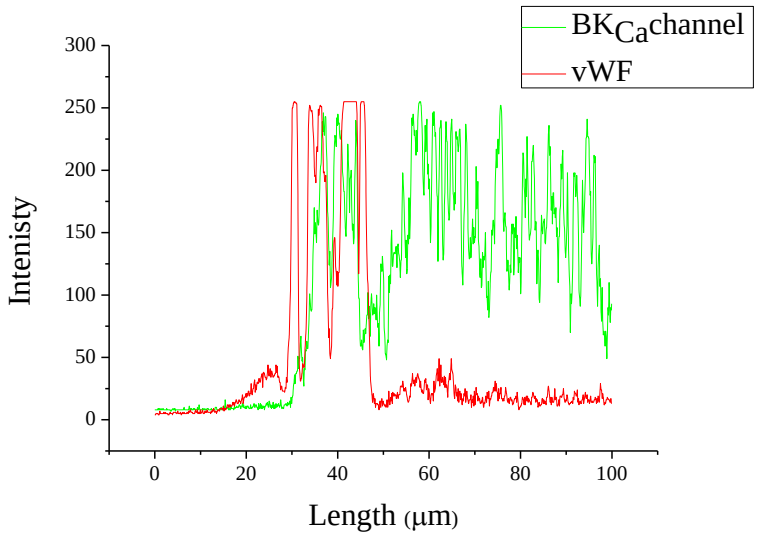

Figure 4.9. Fluorescence intensity profile for BK_{Ca} channels and vWF along the white line shown in figure 4.8 C. Green shows expression of BK_{Ca} channels occurring at high levels in both SMCs and ECs.

4.3.1.5 Expression of BK_{Ca} channels in the SMCs of rat femoral arteries

The expression of BK_{Ca} channels in SMCs was examined by co-staining of rabbit anti-BK_{Ca} channels and mouse anti-α-actin, labeled with AF-488 (green) and AF-594 (red) respectively. A visual examination of the sections stained for BK_{Ca} channels indicated that the green signals occurred in both SMC layer and EC layer (bright green spots above the scale) **(figure 4.10 A)**. Red signal due to the staining with anti-α-actin came from SMC layers **(figure 4.10 B)**. An overlay image (**figure 4.10 C)** showed clear overlap of the BK_{Ca} channels and α-actin (which appeared as yellow). This visual impression was further supported by the fluoresence intensity profile **(figure 4.11)**, taken from the white line shown in **figure 4.10 C**. Thus, this experiment clearly showed that the BK_{Ca} channels are expressed in the SMC layers.

Two negative controls and bright filed image are also shown **(figure 4.10 D, E and F**). Our results therefore confirm that the BK_{Ca} channels is present in the SMCs of rat femoral arteries.

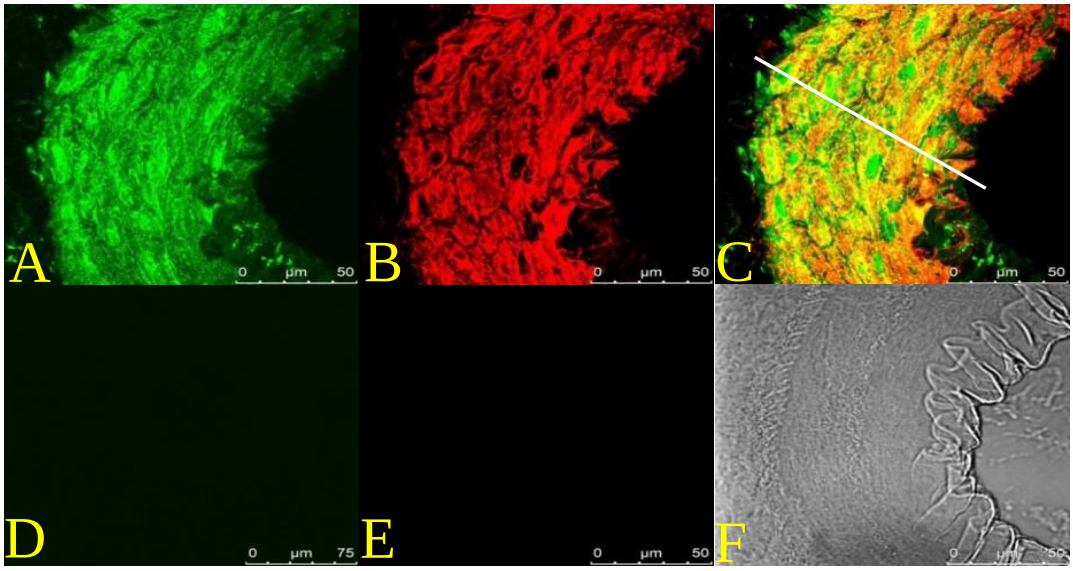

Figure 4.10. Representative confocal images of frozen sections (11 µm) of the rat femoral artery stained with rabbit anti-BK_{Ca} channels (x500) and mouse anti-α-actin (x300) and visualized with AF-488 (x500) and AF-594 (x500) respectively. A. Expression of BK_{Ca} channels (green). Note bright green spots above the scale. **B**. Expression of α-actin (red). **C**. An overlay of A and B showing the co-expression of BK_{Ca} channels and α-actin (yellow) in the SMCs. **D**. A negative control stained with secondary antibody against mis-matched primary antibody. **E**. A negative control stained with secondary antibodies only. **F**. A bright field section of rat femoral artery. A, B, C, E and F: scale bar represents= 50µm, and D: scale bar represents= 75µm.

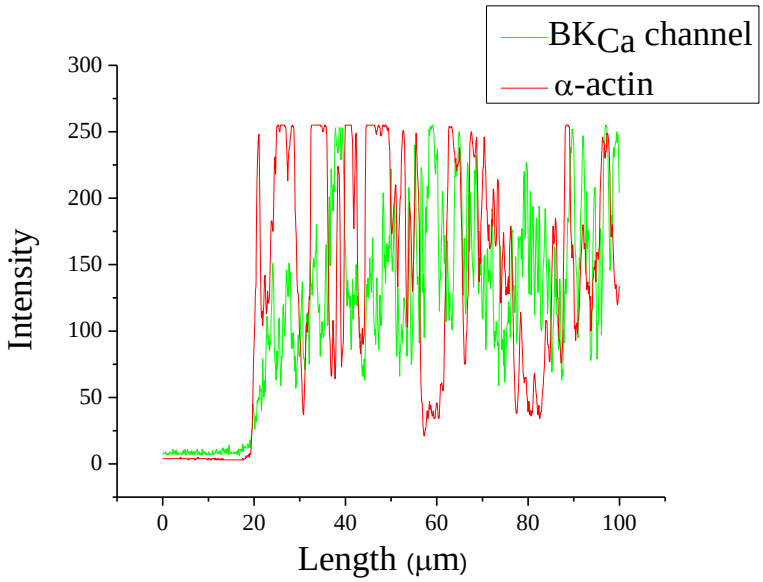

Figure 4.11. Fluorescence intensity profile of BK_{Ca} channels and α-actin along the white line shown in figure 4.10 C. Green fluorescence indicates the expression of BK_{Ca} channels and red fluorescence, that of α-actin.

4.3.1.6 Co-expression of BK_{Ca} channels with cav-1 in rat femoral artery

The next experiment was designed to investigate the co-expression of BK_{Ca} channels with cav-1. Frozen sections (11 μm) of femoral artery stained with mouse anti-cav-1 (AF-488, green) and rabbit anti-BK_{Ca} channels (AF-594, red) are shown in **figure 4.12 A** and **figure 4.12 B**. A visual examination of an overlay image **(figure 4.12 C)** showed the cav-1 co-expressed with BK_{Ca} channels (yellow), and this seems to occur in both SMCs and ECs. Fluorescence intensity profile taken along the white line in **figure 4.12 C** is shown in **figure 4.13**. The expression pattern of cav-1 seems similar to that of BK_{Ca} channels.

As before, two negative controls, mis-match of primary and secondary antibody and omission of primary antibodies, showed low signal **(figure 4.12 D and E)**. A bright field of rat femoral artery section is shown in **figure 4.12 F**. Our results therefore suggest that BK_{Ca} channels and cav-1 are co-expressed, and it seems that this occurs in both SMCs and ECs.

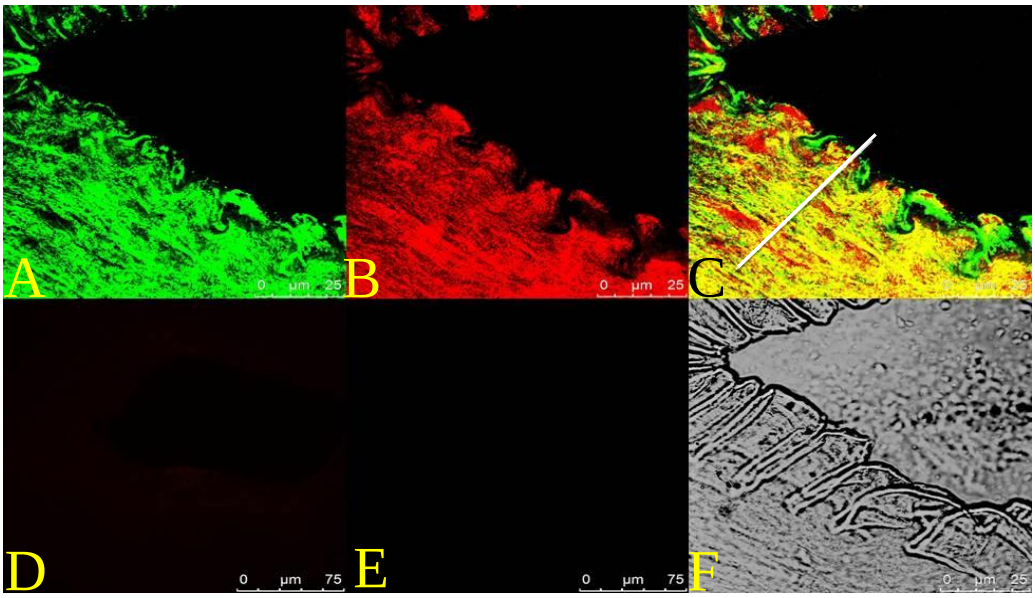

Figure 4.12. Representative confocal images of frozen sections (11µm) of rat femoral artery stained with mouse anti-cav-1 (x200) and rabbit anti-BK_{Ca} channels (x500) and visualised with AF-488 (x500) and AF-594 (x500) respectively. A. Expression of cav-1 (green). **B**. Expression of BK_{Ca} channels (red). **C**. An overlay of the confocal images (A and B) shows co-expression of the cav-1 and BK_{Ca} channels (yellow). **D**. A negative control stained with secondary antibody against wrong primary antibody. **E**. A negative control stained with secondary antibodies only. **F**. A bright field section of rat femoral artery. A, B, C and F: scale bar represents= 25 µm; D and E: scale bar represents= 75µm.

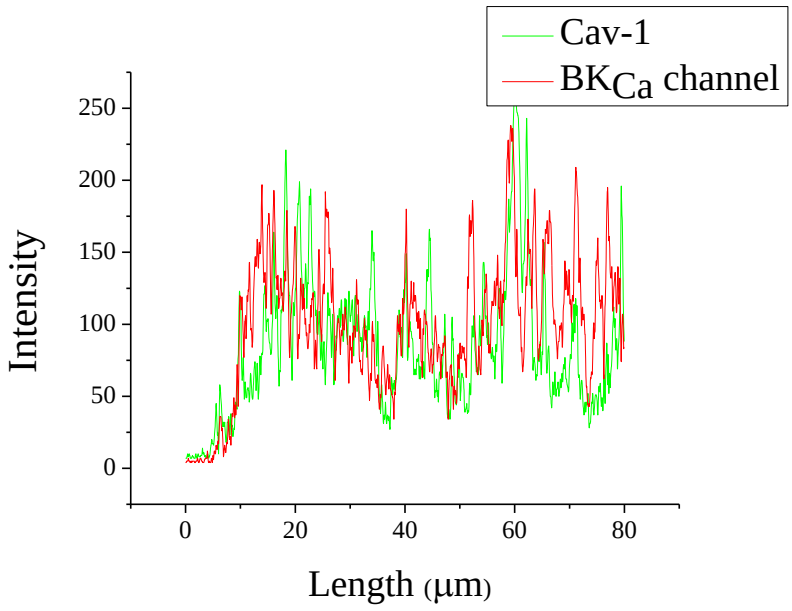

Figure 4.13. Fluorescent intensity profile for cav-1 and BK_{Ca} channels taken along the white line shown in figure 4.12 C. Green fluorescence shows expression of cav-1 while red fluorescence shows expression of BK_{Ca} channels.

4.3.1.7 Co-expression of BK_{Ca} channels with cav-3 in rat femoral arteries

To investigate the co-expression of BK_{Ca} channels with cav-3, rabbit anti-BK_{Ca} channel and mouse anti-cav-3 antibodies were labelled with AF-488 (green) and AF-594 (red) and respectively. A visual examination of the sections stained with anti-BK_{Ca} channels indicated that green signal appears both in the SMC and in the EC layers **(figure 4.14 A)**. A visual examination of the sections stained with anti-cav-3 indicated that the red signal appears in SMC layers **(figure 4.14 B)**. A visual examination of an overlay image **(figure 4.14 C)** showed the co-expression of BK_{Ca} channels with cav-3 in the SMC layers, which appears as yellow, but BK_{Ca} channels are also expressed in areas not stained with red. Fluorescence intensity profile, taken along the white line shown in **figure 4.14 C**, is shown in **figure 4.15**. It was somewhat unexpected that there was some signal measured for cav-3 (length up to 25 µm for red) although visually this area was largely devoid of red staining **(figure 4.14 B)**. Nonetheless, the stronger signal for cav-3 (red) was found in the SMCs.

Two negative controls, mis-match of primary and secondary antibody and omission of primary antibodies, showed low signal **(figure 4.14 D and E)**. A bright field of rat femoral artery is shown in **figure 4.14 F**.

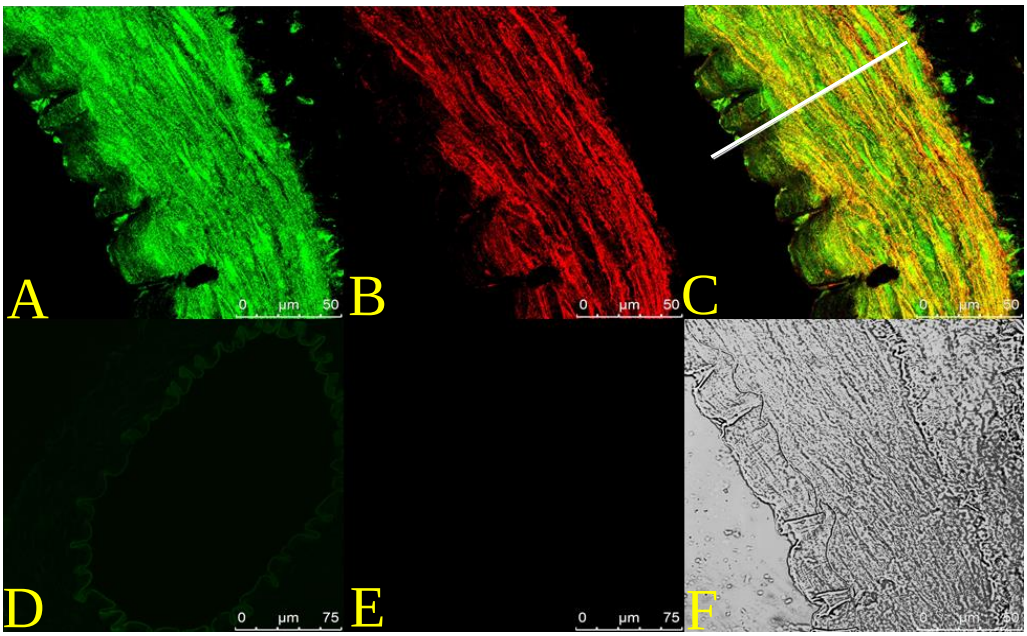

Figure 4.14. Representative confocal images of frozen sections (11 µm) of rat femoral arteries stained with rabbit anti-BK_{Ca} channels (x500) and mouse anti-cav-3 (x500) and visualised with AF-488 (x500) and AF-594 (x500) respectively. A. Expression of BK_{Ca} channels (green) in both SMCs and ECs. **B**. Expression of cav-3 (red) seen in the SMCs. **C**. An overlay of the confocal images showing co-expression of the BK_{Ca} channels and cav-3 (yellow). **D**. A negative control stained with secondary antibody mis-matched against a wrong primary antibody. **E**. A negative control stained with secondary antibodies only. **F**. A bright field section of rat femoral artery. A, B, C and F: scale bar represents= 50 µm; D and E: scale bar represents= 75µm.

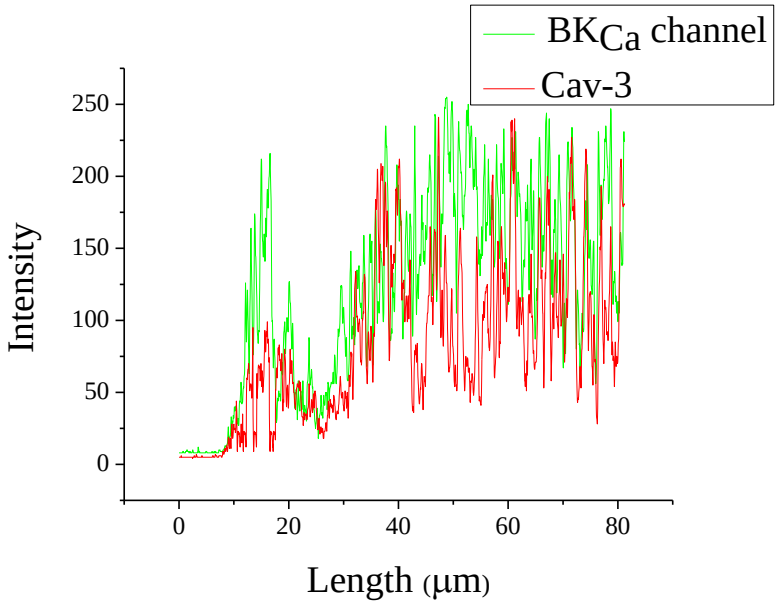

Figure 4.15. Fluorescence intensity profile for BK_{Ca} channels and cav-3 along the white line shown in figure 4.14 C. Green fluorescence shows expression of BK_{Ca} channels and red shows expression of cav-3.

4.3.2 Immunocytochemistry results of rat femoral arteries

4.3.2.1 Co-expression of BK_{Ca} channels with cav-1 in individual SMCs of rat femoral arteries

In this section, immunocytochemistry was used to investigate the co-expression of BK_{Ca} channels with cav-1 and cav-3 at the individual SMC level. Single SMCs were dissociated and then stained with rabbit anti-BK_{Ca} channels and mouse anti-cav-1 and labelled with AF-594 (red) and AF-488 (green) respectively. A visual examination of a cell stained with anti-BK_{Ca} channel antibody indicated that the red signal appears throughout the cell membrane and in the cytoplasm of the SMC **(figure 4.16 A)**. A visual examination of cells stained with anti-cav-1 indicated that the green signal appears throughout the cytoplasm and the cell membrane of the SMC **(figure 4.16 B)**. A visual examination of an overlay image **(figure 4.16 C)** showed the BK_{Ca} channels co-expressed with cav-1, appearing yellow. Fluorescence intensity profile, taken along the white line shown in **figure 4.16 C,** is shown in **figure 4.17**. Both red and green signals show peaks at the edges of the cell, suggesting high levels of expression of both BK_{Ca} and cav-1 in the cell membrane area of the SMC.

Two negative controls, mis-match of primary and secondary antibody and omission of primary antibodies, showed low signal **(figure 4.16 D and E)**. A bright field of a SMC is shown in **figure 4.16 F**.

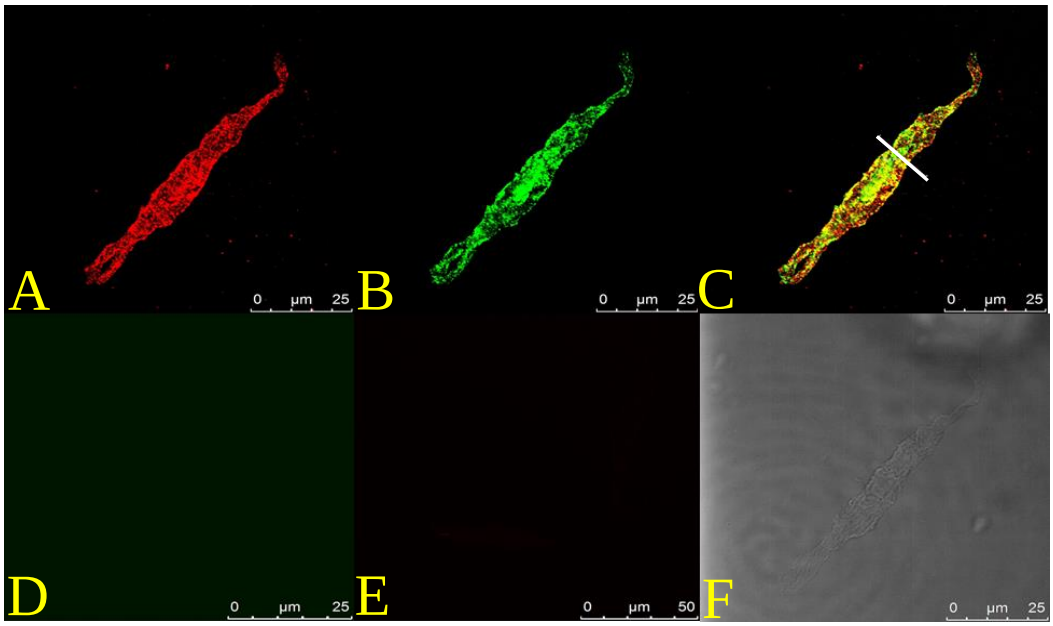

Figure 4.16. Representative confocal images of a single rat femoral artery SMC stained with anti-BK_{Ca} channels (x500) and anti-cav-1 (x200) and labelled with AF-594 (x500) and AF-488 (x500) respectively. A. Expression of BK_{Ca} channels (red). **B**. Expression of cav-1 (green). **C**. An overlay of the confocal images (A and B) showing co-expression of the BK_{Ca} channels with cav-1 (yellow spots). **D**. A negative control of SMC stained with secondary antibody against wrong primary antibody. **E**. A negative control of individual SMC stained with secondary antibodies only. **F**. A bright field section of an individual SMC. A, B, C, D and F: scale bar represents= 25 µm; E: scale bar represents= 50 µm.

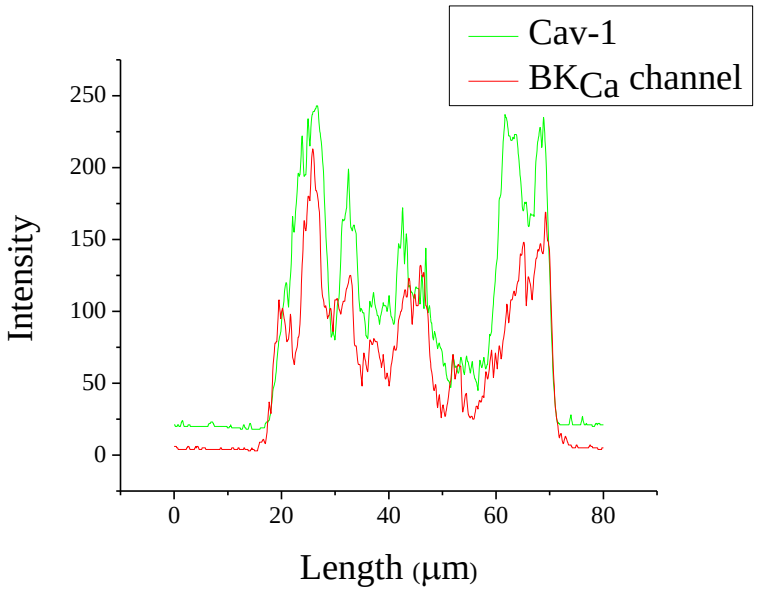

Figure 4.17. Fluorescence intensity profile of cav-1 and BK_{Ca} channels taken along the white line shown in figure 4.16 C. Peaks in green and red fluorescence occur at the edge of the SMC.

4.3.2.2 Co-expression of BK_{Ca} channels with cav-3 in individual SMCs of rat femoral arteries

Individual SMCs were stained with rabbit anti-BK_{Ca} channel and mouse anti-cav-3 and labelled with AF-594 (red) and AF-488 (green), respectively. A visual examination of a cell stained with anti-BK_{Ca} channel antibody indicated that the red signal appears in the cell membrane and in the cytoplasm of the SMC **(figure 4.18 A)**. A visual examination of a cell stained with anti-cav-3 antibody indicated that the green signal appears in the cytoplasm and cell membrane of the SMC **(figure 4.18 B)**. An overlay image **(figure 4.18 C)** showed the BK_{Ca} channels co-expressed with cav-3, showing yellow. The fluorescent intensity profile, taken along the white line shown in **figure 4.18 C**, is shown in **figure 4.19**. Clear peaks in both red and green fluorescence indicate high expression level of both BK_{Ca} channels and cav-3 in the cell membrane although some signal is also seen from the interior of the cell.

Two negative controls, mis-match of primary and secondary antibody and omission of primary antibodies, showed a low signal **(figure 4.18 D and E)**. A bright field of a single SMC is shown in **figure 4.18 F**.

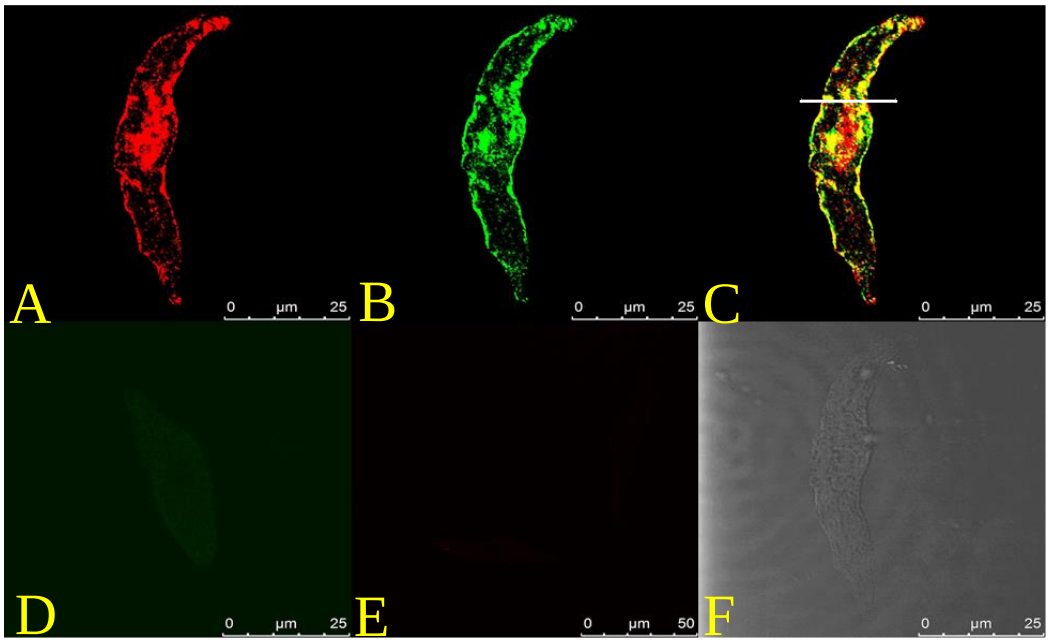

Figure 4.18. Representative confocal images of isolated rat femoral artery SMCs stained with anti-BK_{Ca} channels (x500) and anti-cav-3 (x500) and labelled with AF-594 (x500) and AF-488 (x500) respectively. A. The expression of BK_{Ca} channels (red). **B**. The expression of cav-3 (green). **C**. An overlay of the previous confocal images (A and B) showing co-expression of the BK_{Ca} channels with cav-3 (yellow). **D**. A negative control stained with secondary antibody mis-matched against wrong primary antibody. **E**. A negative control stained with secondary antibodies only. **F**. A bright field of an individual SMC. A, B, C, D and F: scale bar represents= 25 µm; E: scale bar represents= 50 µm.

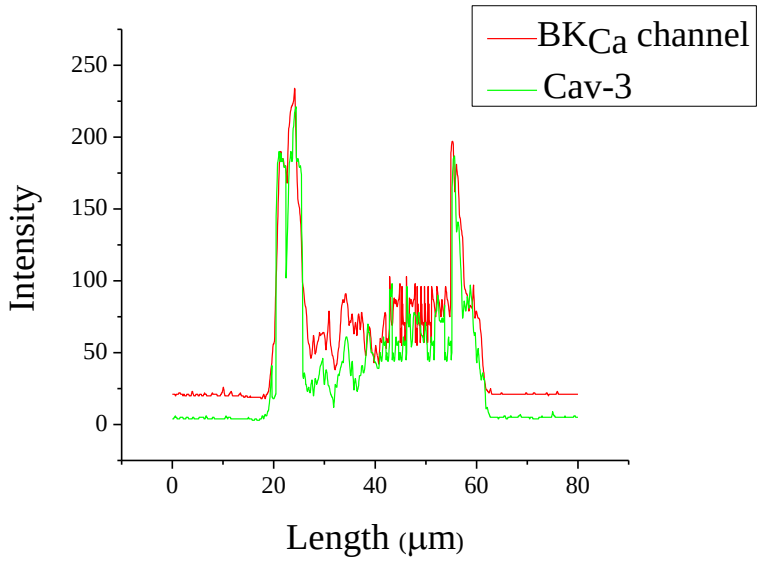

Figure 4.19. Fluorescent intensity profile of BK_{Ca} channels and cav-3 along the white line shown in figure 4.18 C. Red fluorescence shows the expression of BK_{Ca} channels and green fluorescence shows the expression of cav-3. Both signals peak at the cell membrane area.

4.3.3 Immunocytochemistry results of HCAECs

Single cell dissociation of artery smooth muscle cells is a widely used procedure (Kamishima et al., 2007). However, isolation of single ECs from arteries without contaminating other cell types is difficult. Therefore, in order to examine possible co-expression of BK_{Ca} channels with cav-1 and/or cav-3 in individual ECs, I used cultured human coronary artery endothelial cells (HCAECs) as an EC model.

4.3.3.1 Expression of vWF in HCAECs

Even though HCAECs are marketed as ECs, it was necessary to characterise these cells first to confirm that they are indeed ECs. HCAECs were positively stained with anti-vWF **(figure 4.20 A)**. The fluorescent intensity profile, taken along the white line in **figure 4.20 A**, is shown in **figure 4.21**. These results suggest that cultured HCAECs still express a signature protein (vWF) of ECs.

Two negative controls, mis-match of primary and secondary antibody and omission of primary antibody, showed a low signal **(figure 4.20 B and C)**.

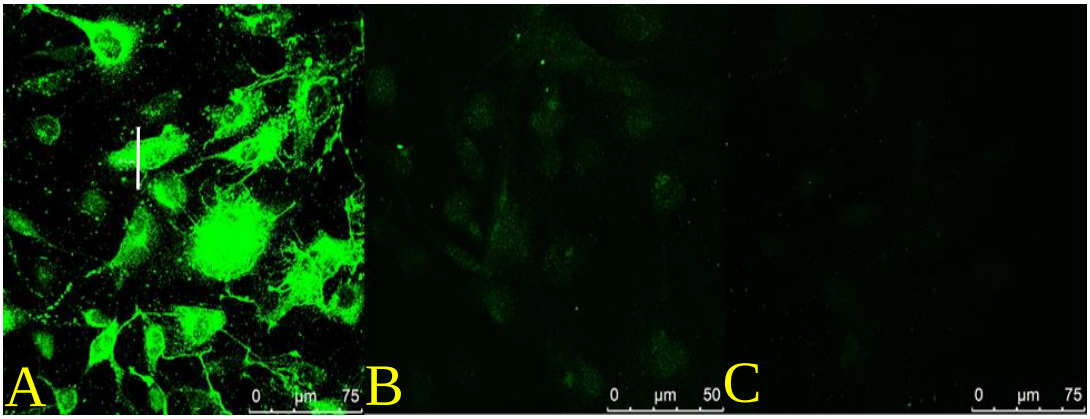

Figure 4.20. Representative confocal images of HCAECs stained with anti-vWF antibody (x300) and visualized with AF-488 (x500). A. Expression of anti-vWF (green) in HCAECs. **B**. A negative control of HCAECs stained with secondary antibody against wrong primary antibody. **C**. A negative control of HCAECs stained with secondary antibodies only. A and C: scale bar represents= 75 µm; B: scale bar represents= 50 µm.

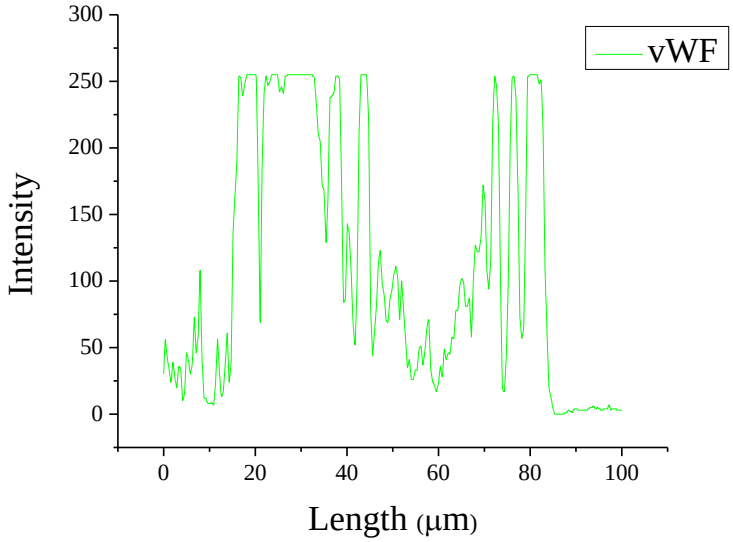

Figure 4.21. Fluorescent intensity profile of vWF taken along the white line shown in figure 4.20 A.

4.3.3.2 Co-expression of BK_{Ca} channels with cav-1 in HCAECs

The co-expression of BK_{Ca} channels with cav-1 in HCAECs was next examined. HCAECs were stained with rabbit anti-BK_{Ca} channels and mouse anti-cav-1 and labelled with AF-594 (red) and AF-488 (green) respectively. A visual examination of the HCAECs stained with anti-BK_{Ca} channels indicates that staining appears in the central portion of the cell **(figure 4.22 A)**. A visual examination of the HCAECs stained with anti-cav-1 showed punctuating signals in the cell membrane area **(figure 4.22 B)**. A visual examination of an overlay image (**figure 4.22 C)** showed no evidence for co-expression of the BK_{Ca} channels with cav-1 staining, i.e. little yellow signal. Fluorescent intensity profile taken along the white line shown in **figure 4.22 C** is shown in **figure 4.23**. Red shows the expression of BK_{Ca} channels in the central portion of HCAECs. Green fluorescence shows the expression of cav-1 at the cell membrane area.

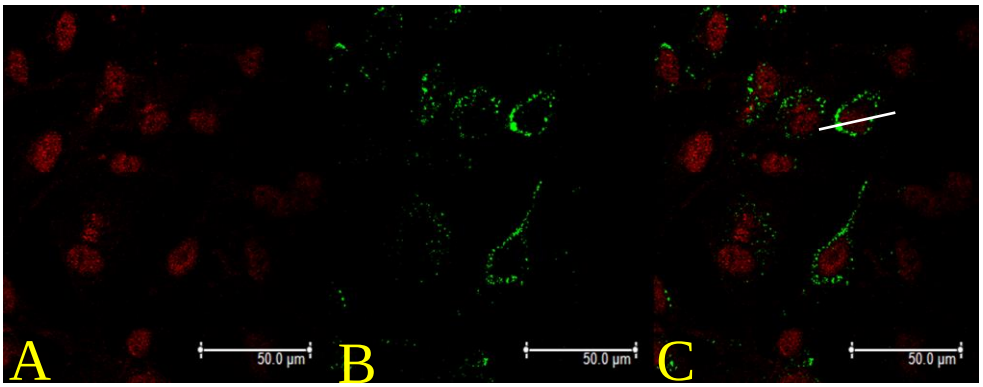

Figure 4.22. Representative confocal images of HCAECs stained with anti-BK_{Ca} channels (x500) and anti-cav-1 (x200) and visualised with AF-594 (x500) and AF-488 (x500) respectively. A. Expression of BK_{Ca} channels (red). **B**. Expression of cav-1 (green). **C**. An overlay of the confocal images (A and B) showing no evidence for co-expression of BK_{Ca} channels with cav-1 (yellow spots are absent). A, B and C, scale bar represents= 50µm.

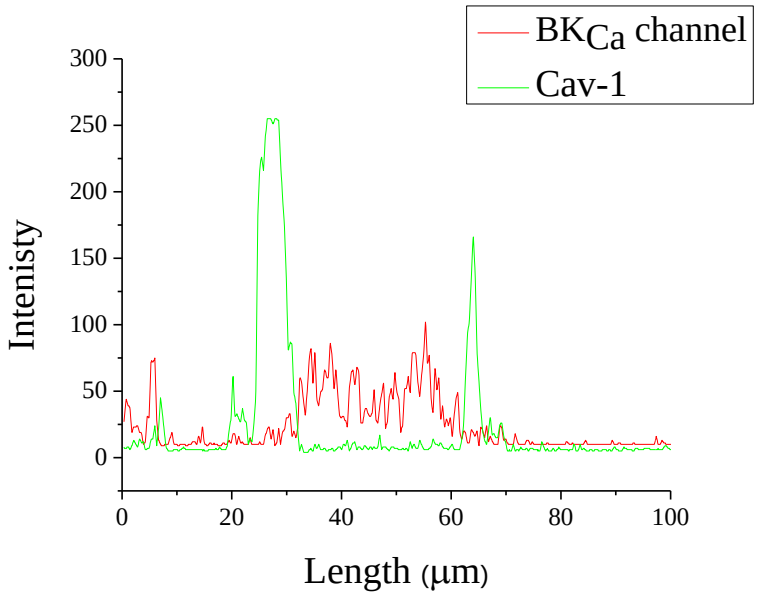

Figure 4.23. Fluorescence intensity profile of BK_{Ca} channels and cav-1 taken along the white line shown in figure 4.22 C. Red fluorescence showed expression of BK_{Ca} channels at low levels in the central portion of the HCAECs. Green fluorescence showed expression of cav-1 at high levels in the cell membrane area of HCAECs with little overlap with red signal.

4.3.3.3 Co-expression of BK_{Ca} channels with cav-3 in HCAECs

Next, possible co-expression of BK_{Ca} channels with cav-3 was examined in HCAECs. Cells were stained with rabbit anti-BK_{Ca} channels and mouse anti-cav-3 and labelled with AF-594 (red) and AF-488 (green) respectively. A visual examination of HCAECs stained with anti-BK_{Ca} channels indicated that the red signal appears in the central portion of the cell **(figure 4.24 A)**. A visual examination of HCAECs stained with anti-cav-3 indicated that there was very little green signal **(figure 4.24 B)** resulting in no overlap in the overlay image **(figure 4.24 C)**. The result that cav-3 is not expressed in HCAECs is further supported by the fluorescent intensity profile **(figure 4.25)**, taken along the white line shown in **figure 4.24 C**. This result is compatible with the previous immunohistochemistry results showing no expression of cav-3 in the ECs of rat femoral arteries.

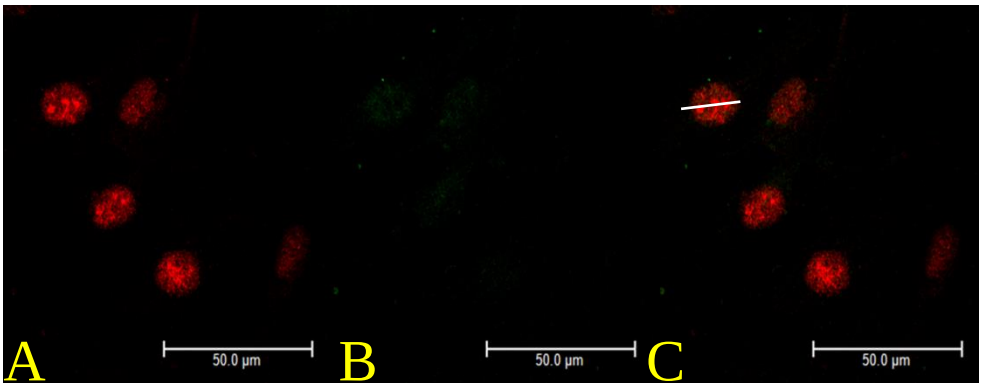

Figure 4.24. Representative confocal images of HCAECs stained with anti-BK_{Ca} channels (x500) and anti-cav-3 (x500) and visualised with AF-594 (x500) and AF-488 (x500) respectively. A. Expression of BK_{Ca} channels (red). **B**. Expression of cav-3 (green). **C**. An overlay of the confocal images (A and B) showing no overlap between cav-3 and BK_{Ca} channels. A, B and C: scale bar represents= 50 µm.

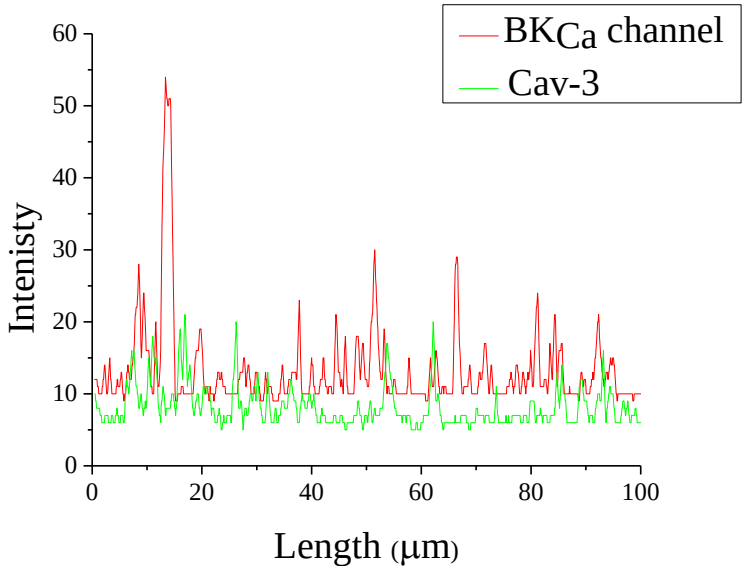

Figure 4.25. Fluorescent intensity profile of BK_{Ca} channels and cav-3 along the white line shown in figure 4.24 C. Little green fluorescence indicates that there is little expression of cav-3.

4.3.4 Results of the Western blot

Several primary antibodies were used for immunochemical experiments, but the detection of signals does not necessarily confirm the presence of target proteins. Primary antibodies are designed to exploit a unique sequence of a target protein, but such sequence may be shared with other proteins. Thus, Western blotting was performed using lysates of rat femoral arteries to access the size of proteins detected by antibodies against cav-1, cav-3, BK_{Ca} channels and α-actin. If a single band with predicted size can be detected, then the Western blot results can validate the usefulness of primary antibodies. Experiments with the mouse monoclonal anti-cav-1 antibodies showed a single band at 24 kDa **(figure 4.26, lane A)**. Experiments with anti-cav-3 antibody showed a single band at 18 kDa **(figure 4.26, lane C)**. Rabbit polyclonal anti-BK_{Ca} channel antibody was also used in Western blotting, and results showed a single band at 97 kDa **(figure 4.26, lane E)**. The essentially same sized band was detected using anti-BK_{Ca} channel primary antibody on rat brain lysates **(figure 4.26, lane F)**.

Re-blotting with anti-α-actin antibody after stripping the nitrocellulose membrane first blotted against anti-cav-1 showed a single band of α-actin at 42 kDa **(figure 4.26, lane B)**. Re-blotting with anti-α-actin antibody after the membrane was blotted for anti-cav-3 showed a single band of α-actin at 42 kDa **(figure 4.26, lane D)**. These results validate the primary antibodies used in the immunohistochemistry and immunocytochemistry.

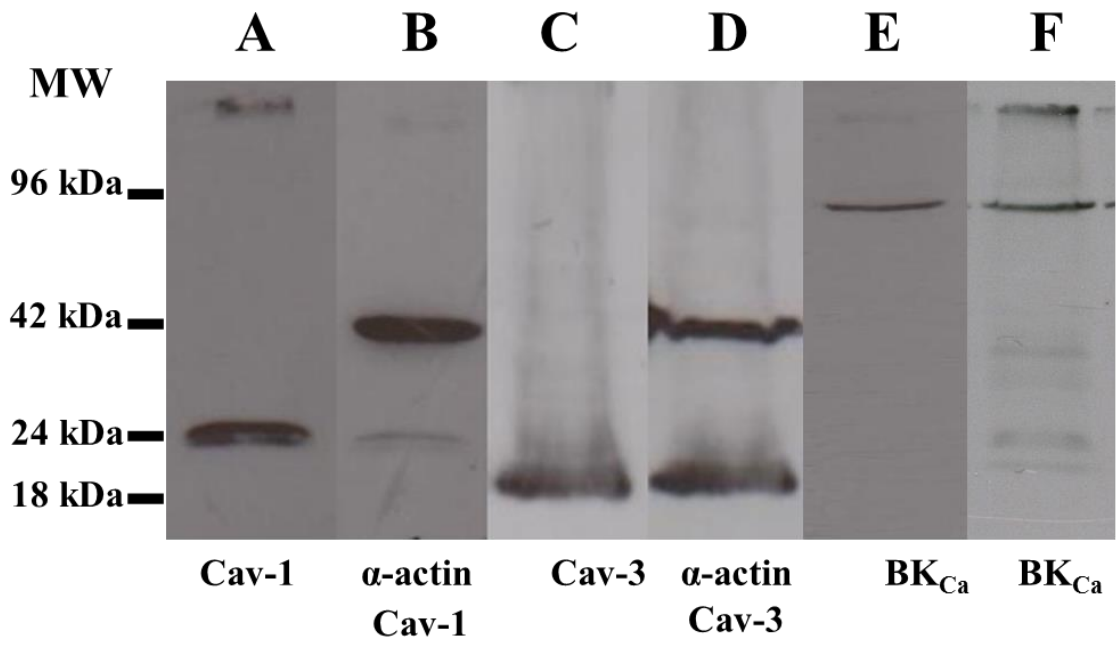

Figure 4.26: Western blot results using cav-1, cav-3, α-actin and BK_{Ca} primary antibodies on rat femoral artery and brain lysates. Lanes A, B, C, D and E: rat femoral artery protein lysates; **Lane F:** rat brain protein lysate. **Lane A** shows a single band of cav-1 at 24 kDa. **Lane B** shows two bands, α-actin at 42 kDa and a light band of cav-1 at 24 kDa remaining after the stripping of the nitrocellulose membrane. **Lane C** shows a single band of cav-3 at 18 kDa. **Lane D** shows two bands, α-actin at 42 kDa and a band of cav-3 at 18 kDa remaining after stripping of the nitrocellulose membrane. **Lanes E** and **F** show a single band of BK_{Ca} channels at 96 kDa for each lane. The dark "band" in Lanes A and F at the top is an artifact, and corresponds to the top of the gel.

4.4 Discussion

The mammalian caveolin family comprises of cav-1, cav-2 and cav-3, expressed in different arterial beds (Kamishima et al., 2007, Riddle et al., 2011). Caveolins are caveolae signature proteins that associate with and regulate a variety of signalling proteins, including ion channels (Alioua et al., 2008, Riddle et al., 2011). Several recent studies have focused on the co-expression of BK_{Ca} channels with cav-1/cav-3 in different vascular beds (Alioua et al., 2008, Riddle et al., 2011). However, the relationship of cav-1/cav-3 with the function of BK_{Ca} channels has not been previously examined either in rat femoral arteries or HCAECs.

In this chapter, we hypothesised that the BK_{Ca} channels and cav-1 and/or cav-3 may interact with each other in rat femoral arteries and HCAECs. Three complementary methods were used to test this hypothesis: immunohistochemistry, immunocytochemistry and Western blot. The major findings of the present study are as follows: (i) co-expression of BK_{Ca} channels with cav-1 in both SMCs and ECs and co-expression of BK_{Ca} channels with cav-3 in the SMCs of rat femoral artery frozen slices; (ii) co-expression of BK_{Ca} channels with cav-1 and cav-3 in isolated SMCs; (iii) no evidence for co-expression of the BK_{Ca} channels with cav-1 or cav-3 in the cultured HCAECs; (iv) Western blot results confirming the protein expression of BK_{Ca} channels, cav-1, cav-3 in protein lysates of rat femoral arteries and brain.

These results may suggest a role for caveolins in regulating signalling pathways through BK_{Ca} channels in vascular ECs and SMCs of rat femoral arteries.

The co-expression of BK_{Ca} channel with caveolins may occur at the C terminus of the channel showing consensus caveolin binding motif (^{1007}YNMLCFGIY^{1015}). Our results

agree with Riddle et al. (2011), who reported the co-expression of BK_{Ca} channels with cav-1 in both the SMCs and ECs of native gracilis resistance arterioles of rats from immunohistochemistry experiments. Furthermore, Alioua et al. (2008), reported the expression of both cav-1 and BK_{Ca} channels in native freshly-dissociated aortic myocytes using immunohistochemistry. Furthermore, our findings also agreed with Brainard et al. (2005) who reported the co-expression of BK_{Ca} channels with cav-1 in human myometrial SMCs (cultured cells) using immunocytochemistry.

Several studies have reported that the expression of cav-3 is muscle-specific (Engelman et al., 1998b). Furthermore, Kamishima et al. (2007) suggested that cav-3 is important in the Ca^{2+} removal of resistance artery SMCs. However, the role of cav-3 in regulating ion channels in SMCs is still controversial. Here in this chapter, immunolabelling experiments revealed the co-expression of BK_{Ca} channels with cav-3 at tissue level in SMCs from rat femoral arteries using immunohistochemistry **(figure 4.14 C)**, as well as the co-expression of BK_{Ca} channels with cav-3 at the level of individual SMCs using immunocytochemistry **(figure 4.18 C)**. Semi-quantitative analysis of immunohistochemistry **(figure 4.15)** and immunocytochemistry **(figure 4.19)** for cav-3 and BK_{Ca} channels revealed an overlap of the signals demonstrating the co-expression of BK_{Ca} channels with cav-3 in the SMC layer of femoral tissues and in the individual SMC. As with cav-1, this co-expression suggests that the cav-3 scaffolding domain (DGVWRVSYTTFTVSKYWCYR, amino acid residues 55–74) may interact with caveolin binding motifs in the C terminus of the BK_{Ca} channels of rat femoral artery SMCs.

To further examine whether the BK_{Ca} channels are co-expressed with cav-1 and cav-3 in human vascular ECs, immunohistochemistry experiments were performed on HCAECs. Immunofluorescence imaging demonstrated no evidence for co-expression of the BK_{Ca} channels with cav-1 in HCAECs **(figure 4.21 C)**. Semi-quantitative analysis of results of this immunostaining **(figure 4.23)** revealed a low level of expression of BK_{Ca} channels with cav-1 proteins compared with the expression levels of BK_{Ca} channels and cav-1 in native rat femoral artery ECs. This may be due to a loss of protein expression in the cultured cells compared with native tissues. Immunofluorescence imaging indicated no overlap occurs between cav-3 and BK_{Ca} channels in HCAECs **(figure 4.24 C)** due to the fact that cav-3 is not expressed in HCAECs. Semi-quantitative analysis of this immunostaining **(figure 4.25)** revealed the expression of BK_{Ca} channels at a low level and no expression of cav-3 proteins in HCAECs. The findings of the current study agree with those of Jow et al. (1999), who reported the absence of BK_{Ca} channels from human aortic endothelial cells (HAEC) (cultured cells), by using patch clamp, RT-PCR, calcium imaging (Jow et al., 1999). In contrast, our results disagree with those of Wang et al. (2005), who reported the co-expression of BK_{Ca} channels and cav-1 in membrane of bovine aortic endothelial cells (cultured cells) by using confocal immunofluorescence microscopy. Generally, presence and expression of plasmalemmal BK_{Ca} channels in vascular endothelial cells is controversial as reviewed by Sandow and Grayson (2009).

Analysis of the Western blot results **(figure 4.26)** of the whole rat femoral artery lysates showed the correct bands for cav-1 (24 kDa), cav-3 (18 kDa), α-actin (42 kDa), and BK_{Ca} channels (96 kDa). Our results agreed with Feher et al. (2010) who demonstrated the expression of cav-1, BK_{Ca} channels and α-actin in the coronary arteries of lean and

obese rats using Western immunoblotting (Feher et al., 2010). Furthermore, Alioua et al. (2008) reported the expression of cav-1 and BK_{Ca} channels in the lysates of rat aorta and in the lysates of human embryonic kidney 293 cells (cell line) using Western blot. Additionally, our findings agreed with Sampson et al. (2004) who showed the expression of cav-1 and cav-3 in the lysate of rat arterial tissues using Western blot.

4.5 Conclusion

In conclusion, we confirm the co-expression the BK_{Ca} channels with cav-1 and cav-3 in the SMC layer at tissue level and in individual SMCs in native rat femoral arteries, as well as the co-expression of the BK_{Ca} channels with cav-1 in ECs of rat femoral arteries.

Chapter 5 The Effect of Caveolae Disruption by M-β-CD on the Contraction of Femoral Artery Rings

5.1 Aim of the chapter:

The aim of this chapter was to study the effects of caveolae disruption on rat femoral artery contraction before and after endothelium removal.

The key findings in this chapter

- Caveolar disruption by a cholesterol depleting agent caused a significant increase in the contraction response of intact rat femoral arteries to 20 K/ Bay K.
- Caveolar disruption also abolished the release of basal NO production/release from the ECs.
- BK_{Ca} channels may have a limited effect on smooth muscle contraction in these arteries in the absence of basal NO release.

5.2 Introduction

SMCs and ECs of muscular distributing arteries such as the femoral artery show cell membranes covered with caveolae (Okamoto et al., 1998, Cohen et al., 2004), also see chapter 3). Caveolar domains contains various molecules such as BK_{Ca} channels, nitric oxide synthase (eNOS), and GPCRs (Drexler et al., 1993, Oh and Schnitzer, 2001, Hardin and Vallejo, 2009).

Several studies provided the evidence that caveolae and caveolins play important role in the regulation of vascular tone and signal transduction pathways necessary for normal blood vessel function (Drexler et al., 1993, Flavahan and Vanhoutte, 1995, Parton, 2001). The role of caveolae and the caveolins in organising signalling pathways means that they influence myogenic tone directly by affecting smooth muscle contractility and indirectly by modifying the release of vasodilator factors, including NO, from the endothelium (Xu et al., 2008, Hardin and Vallejo, 2006). Caveolae are particularly prevalent in ECs where they regulate NO production by interacting with eNOS at the scaffolding domain located between amino acids 82 and 101 of cav-1 (Bucci et al., 2000, Minshall et al., 2003, Cohen et al., 2004, Gratton et al., 2004).

Cholesterol-extracting agents such as M-β-CD and filipin have been widely used to evaluate the role of lipid rafts/caveolae (Darblade et al., 2001, Dreja et al., 2002, Kaiser et al., 2002, Gschwend et al., 2003, Linder et al., 2005, Wijetunge and Hughes, 2005, Xu et al., 2007, Xu et al., 2008, Sandow and Grayson, 2009, Radenkovic et al., 2012). Treatment with M-β-CD is thought to selectively extract cholesterol from the plasma membrane (Kilsdonk et al., 1995, Yancey et al., 1996), leading to disruption of caveolae (Babiychuk et al., 2004, Smith et al., 2005, Jie et al., 2007).

The disruption of caveolae by M-β-CD has been reported to cause an impairment of endothelium-dependent relaxation (Cohen et al., 2004) and increased contraction of blood vessels (Xu et al., 2008). The decrease of membrane capacitance seen with M-β-CD treatment is consistent with the removal of caveolae from the membranes of SMCs (Shaw et al., 2006) and ECs (Yamamoto et al., 2011). Effects of caveolae disruption on ECs may include signalling alterations at the level of the receptors and/or Ca^{2+} mobilising molecules/channels, or via its effect on the interaction of cav-1 with eNOS affecting NO production (Darblade et al., 2001, Linder et al., 2005, Xu et al., 2007). On the other hand, cholesterol-saturated methylcyclodextrin (Ch-MCD) has been reported to have the ability to replenish cholesterol in the membranes of vascular cells that had been depleted by M-β-CD. Thus treatment with M-β-CD leads to loss of basilar artery contractility to endothelin-1, and subsequent treatment with Ch-MCD leads to recovery of the contraction (Bergdahl et al., 2003).

BK_{Ca} channels play a critical role in the function of arteries including the control of blood flow and pressure (Brenner et al., 2000, Sausbier et al., 2005). Immunostaining and electrophysiological studies have shown that BK_{Ca} channels are co-expressed with cav-1 in endothelial cells (Wang et al., 2005, Kamishima et al., 2007, Riddle et al., 2011). Furthermore, mammalian BK_{Ca} channels have two potential binding motifs for cav-1 (Alioua et al., 2008, Lu et al., 2010). Activation of BK_{Ca} channels leads to membrane hyperpolarisation, inhibition of L-type Ca^{2+} channels and vascular relaxation (Lacinova, 2005). BK_{Ca} channels are activated by depolarisation and/or increases in locally produced Ca^{2+} transients (sparks) from RyRs in the SR membrane (Marty, 1981). The distance between the caveolae and superficial SR is about 20 nm in SMCs

(Gherghiceanu and Popescu, 2007). The proximity between SR and BK_{Ca} channels within caveolae seems crucial in the coupling of local SR Ca^{2+} release with the opening of BK_{Ca} channels. Furthermore, if the Ca^{2+} sparks are triggered by occasional opening of L-type Ca^{2+} channels, and if L-type Ca^{2+} channels are also located within caveolae, then the disruption of caveolae may also decrease spark frequency/amplitude due to the increased distance between L-type Ca^{2+} channels and RyRs (Lohn et al., 2000).

In the previous chapter, I have established that rat femoral artery expresses BK_{Ca} channels in both ECs and SMCs. I also established that femoral artery ECs express cav-1, and SMCs express cav-1 and cav-3. Here, I used myography to study the effect of cholesterol depletion from the membrane on the contraction of rat femoral arteries, and identify the molecules that are affected by caveolae disruption.

5.3 Results

5.3.1 Contraction of femoral arteries in response to KPSS and 20 K/ Bay K

5.3.1.1 Experimental protocol

After 50 min normalisation, vessels were first contracted with KPSS. Once a plateau was reached and maintained, the arteries were washed with PSS until force returned to baseline. This procedure was repeated three times until reproducible contractions were elicited (**figure 5.1**). Repeated applications of KPSS generally caused a gradual increase of force. Arteries were then contracted with a "standard" contractile solution (20 K/ Bay K). At the plateau of the 20 K/ Bay K contraction, ACh (final concentration, 10 μM) was added. ACh-induced relaxation indicates the functional integrity of the endothelium (**figure 5.1 A)**. Note that 10 μM ACh that causes almost total relaxation in other arteries such as mesenteric artery but normally induces only a partial and transient relaxation in rat femoral arteries. KPSS (80 mM KCl) causes substantial depolarisation which activates VDCCs. Partial depolarisation caused by 20 mM KCl alone would not be sufficient to induce useful contraction, but addition of Bay K 8644 further facilitates the opening of VDCC. The initial contraction/relaxation using KPSS, 20 K/ Bay K and ACh was important for testing the viability of the arteries to ensure that the isolating and mounting techniques had no adverse effect on responses. If an artery failed to contract to either KPSS or to 20 K/ Bay K, or did not relax in response to ACh, it was excluded from the study.

As a control, the effect of repeated contractions with 20 K/ Bay K was also tested. After completing the preliminary contractions as shown in **figure 5.1 A**, arteries were

contracted with 20 K/ Bay K three times (**figure 5.1 B**). The contraction induced by 20 K/ Bay K was not significantly altered by repeated applications of 20 K/ Bay K (**figure 5.2**).

5.3.1.2 Data analysis

All data are presented as a mean ± standard error of mean. The contraction force is expressed in mN. n is number of observations. Statistical significances were determined using the either paired Student's t-test (for two data sets) or ANOVA (for multiple comparison) (Graphpad, Instat). A value of $P<0.05$ was considered to be statistically significant.

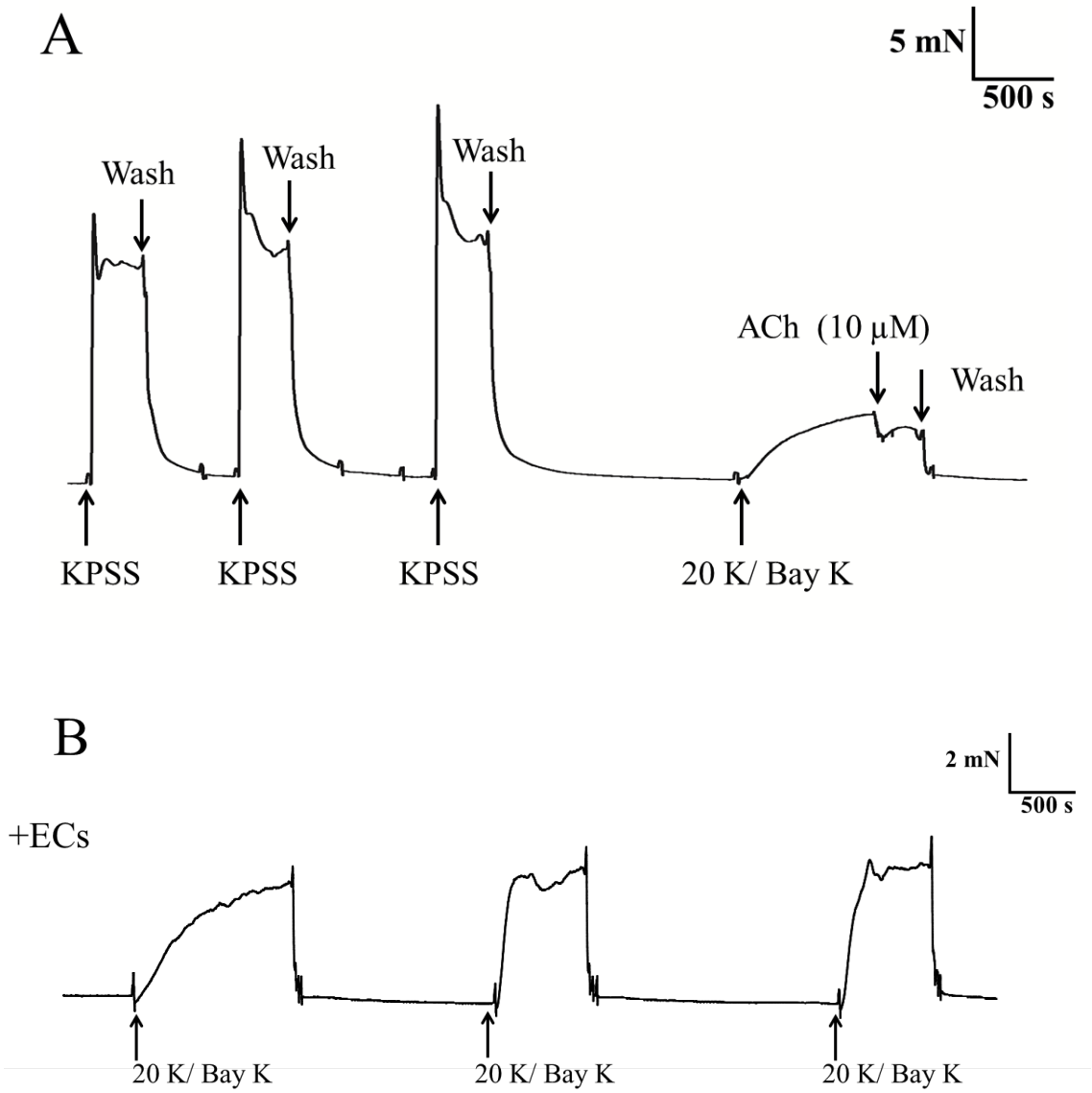

Figure 5.1. Protocol for testing viability of femoral artery for contraction experiments. A. Control contraction with KPSS, followed by 20 K/ Bay K contraction and testing of the intact endothelium using ACh. **B**. Test repeat applications of 20 K/ Bay K on contraction force.

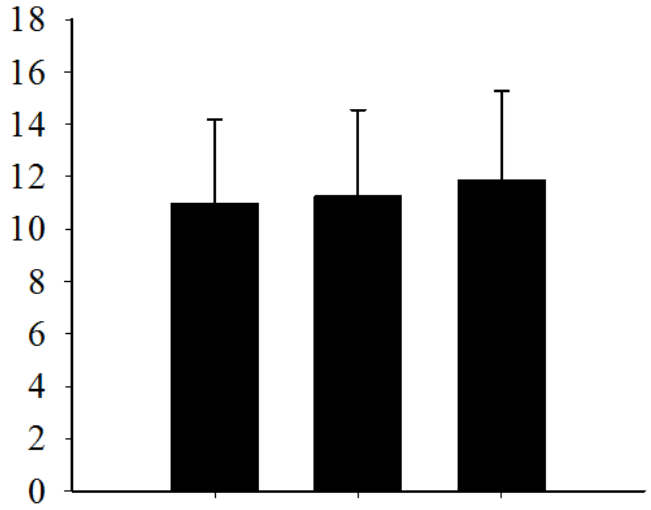

Figure 5.2. Effect of repeated contraction with 20 K/ Bay K on rat femoral artery. Mean data showing the effects of repeat contraction on the response to 20 K/ Bay K. No statistical significance was seen. n=6.

5.3.2 The effects of caveolar disruption by M-β-CD on rat femoral artery contraction

5.3.2.1 Experimental protocol

After completing the preliminary contractions as shown in **figure 5.1 A**, arteries were incubated with 5 mM M-β-CD for 1 hour. Afterwards, the vessels were washed with PSS three times to clean cholesterol debris from the lumen. The vessels were then left for 10 min to recover before the next step. The vessels were then contracted with 20 K/ Bay K. Afterward, 20 K/ Bay K was washed out with PSS. The arteries were left for 10 min to recover. Vessels were stimulated with KPSS at the end to examine the effect of M-β-CD treatment on KPSS induced contraction.

5.3.2.2 Analysis

Incubation of femoral arteries with 5 mM M-β-CD for 1 hour augmented contraction in response to 20 K/ Bay K but not to KPSS (**figure 5.3 A**). Force increased in response to 20 K/ Bay K from 11.84 ± 1.30 mN to 18.25 ± 2.00 mN (n= 14, **P< 0.01). In contrast, the contraction induced by KPSS was not significantly altered by M-β-CD (33.10 ± 1.43 mN to 33.36 ± 2.02 mN, n= 14, ns) (**figure 5.3 B**).

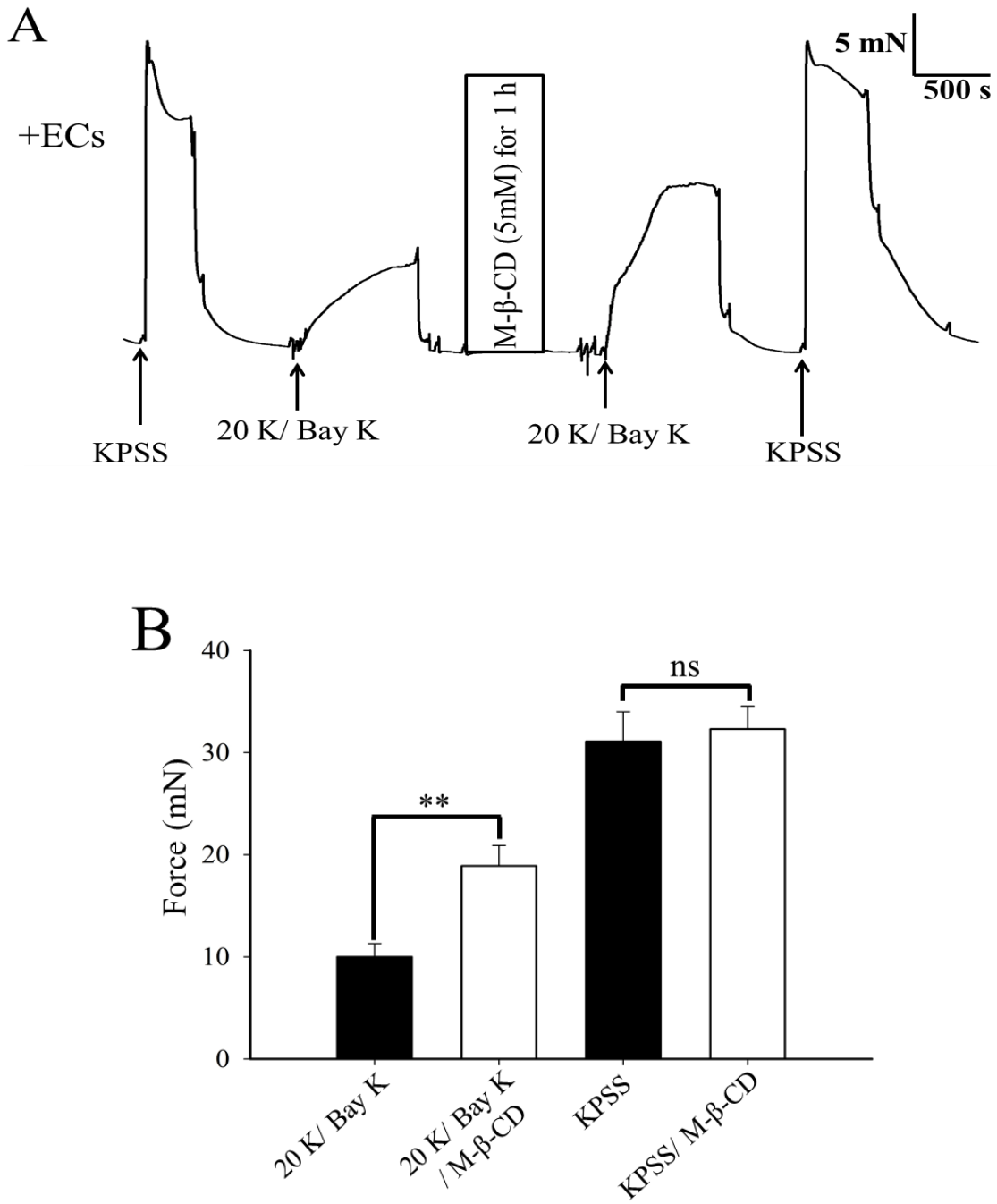

Figure 5.3. Effect of caveolar disruption with M-β-CD on rat femoral artery contractions. **A**. Original traces show that treatment with 5 mM M-β-CD augments contraction in response to 20 K/ Bay K but not to KPSS. **B**. Mean data showing the effects of cholesterol depletion on the response to 20 K/ Bay K and KPSS. Statistically significant difference was detected using Student's *t*-test: *n*=14, **P< 0.01 and ns=non-significant difference, respectively.

5.3.3 The effects of caveolar disruption by filipin on rat femoral artery contraction

5.3.3.1 Experimental protocol

Next, caveolae was disrupted using another cholesterol depleting agent, filipin. After completing the same preliminary contraction shown in **figure 5.1 A**, arteries were incubated with filipin (4 µg/ml, 1 hour). Afterwards, the vessels were washed with PSS three times, left for 10 min to recover, and contracted with 20 K/ Bay K. Arteries were then left for 10 min to recover and stimulated with KPSS.

5.3.3.2 Analysis

The results obtained with filipin were very similar to those with M-β-CD. Filipin treatment augmented contraction to 20 K/ Bay K but not to KPSS (**figure 5.4 A**). Incubation with filipin increased the force produced in response to 20 K/ Bay K from 5.36 ± 1.30 mN to 9.36 ± 2.21 mN (n= 12, *P< 0.05). In contrast, the contraction induced by KPSS was not significantly altered by filipin treatment (18.60 ± 2.90 mN to 18.73 ± 3.12 mN, n= 12, ns) (**figure 5.4 B**).

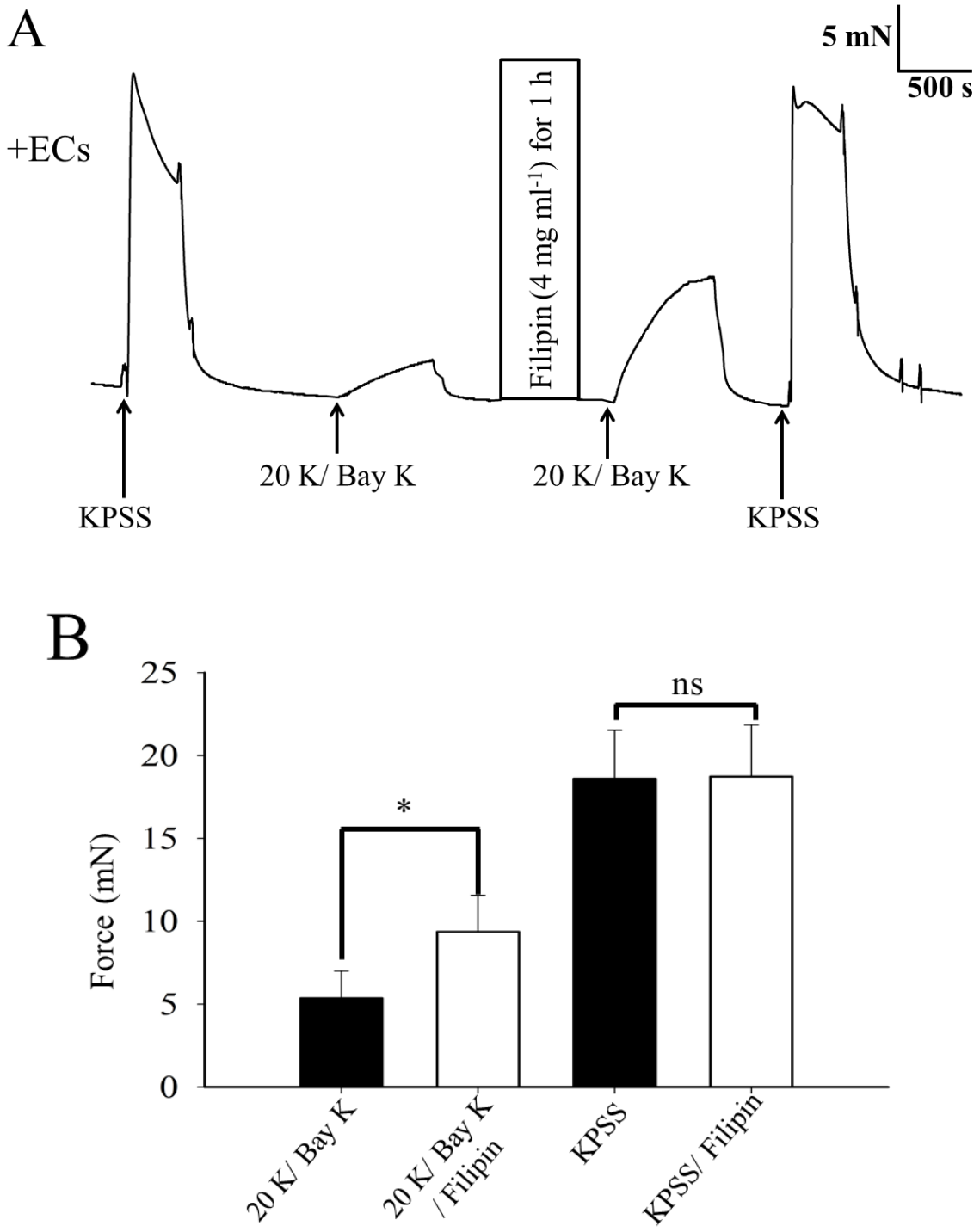

Figure 5.4. Effect of caveolar disruption with filipin. A. Filipin treatment augments contraction in response to 20 K/ Bay K but not to KPSS. **B.** Mean data showing the effects of filipin treatment on the response to 20 K/ Bay K and KPSS. Statistical significance was detected using Student's *t*-test: *n*=12, * P< 0.05.

5.3.4 The effects of Ch-MCD after caveolar disruption by M-β-CD

5.3.4.1 Experimental protocol

Next, Ch-MCD was used to reverse the effects of cholesterol depletion by M-β-CD. After completing the experimental protocol shown in **figure 5.1 A**, the vessels were incubated with Ch-MCD (5 mM) for 1 hour to replenish cholesterol. The vessels were then washed with PSS three times, left for 10 min to recover, and contracted with 20 K/ Bay K. Arteries were then washed with PSS, left for 10 min and stimulated with KPSS.

5.3.4.2 Analysis

Ch-MCD reversed the effect of M-β-CD on 20 K/ Bay K contractions (**figure 5.5 A**). Incubation of arteries in M-β-CD for 1 hour increased force generated in response to 20 K/ Bay K from 3.50± 0.62 mN to 5.73± 1.35 mN, *n*=16), but not to KPSS. Subsequent incubation of arteries with Ch-MCD reversed the effect of M-β-CD (2.74 ± 0.59 mN after Ch-MCD, *n*=12).

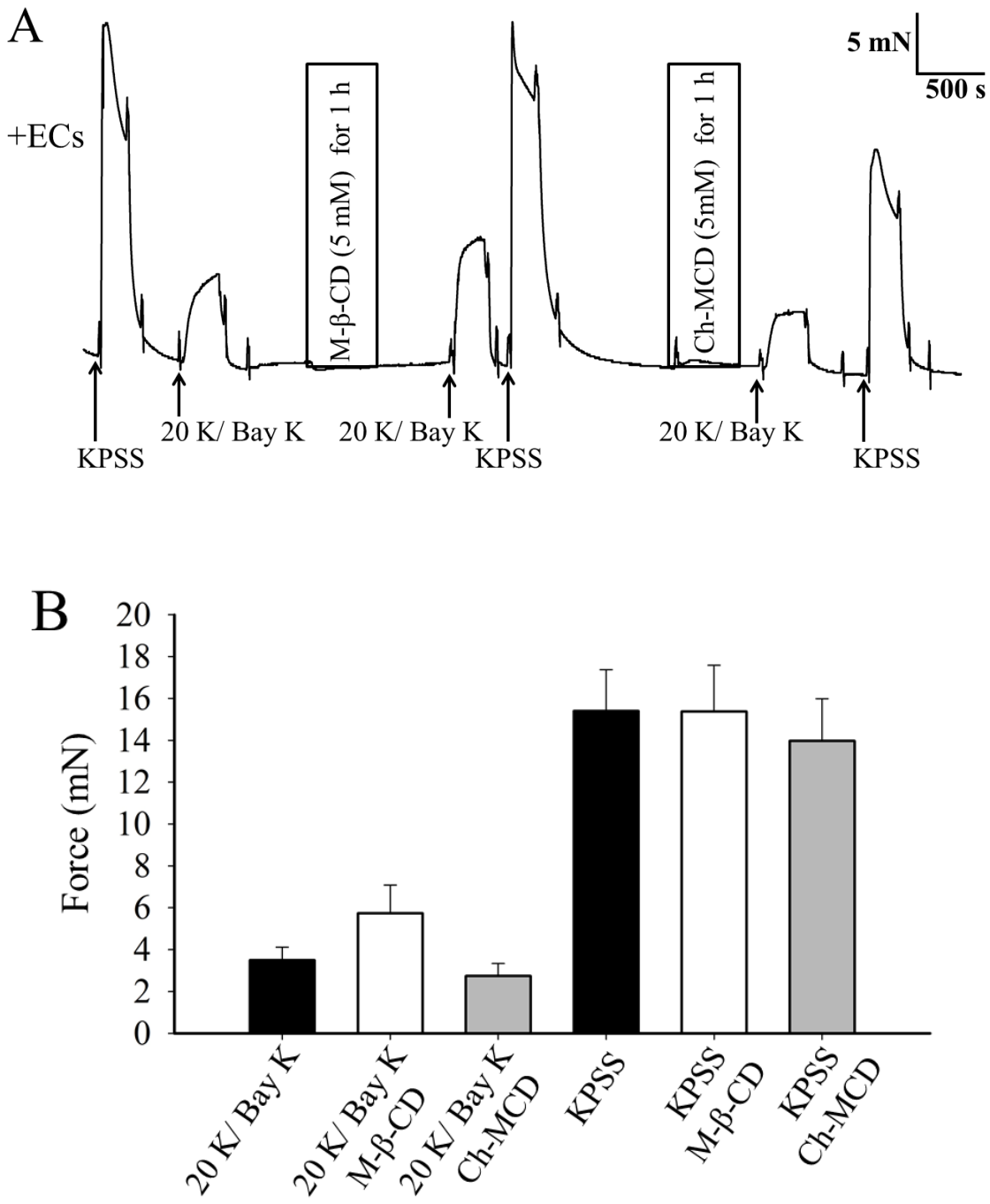

Figure 5.5. Reversibility of the M-β-CD effect on contractions by Ch-MCD. A. M-β-CD treatment augments contraction to 20 K/ Bay K and Ch-MCD reverses this effect. **B.** Mean data showing the effect of M-β-CD and Ch-MCD on 20 K/ Bay K and KPSS contractions. M-β-CD treatment enhanced 20 K/ Bay K contraction. After re-admission of cholesterol, contraction returned to levels seen before application of M-β-CD. Contractions induced with KPSS were not affected by M-β-CD or Ch-MCD. *n*=12.

5.3.5 The effects of Ch-MCD on the 20 K/ Bay K contractions

5.3.5.1 Experimental protocol

Next, whether Ch-MCD exerts direct effects on contraction with 20 K/ Bay K (i.e. in the absence of prior treatment by M-β-CD) was tested. After completing the protocol shown in **figure 5.1 A**, the vessels were incubated with Ch-MCD (5 mM) for 1 hour. Afterwards, the vessels were washed with PSS three times, left for 10 minutes to recover, and contracted with 20 K/ Bay K.

5.3.5.2 Analysis

Incubation of arteries with Ch-MCD had no effect on its own on 20 K/ Bay K-induced force (**figure 5.6 A**). Mean data are shown in **figure 5.6 B** (3.15 ± 0.45 mN to 2.98 ± 0.59 mN, *n*= 6, ns).

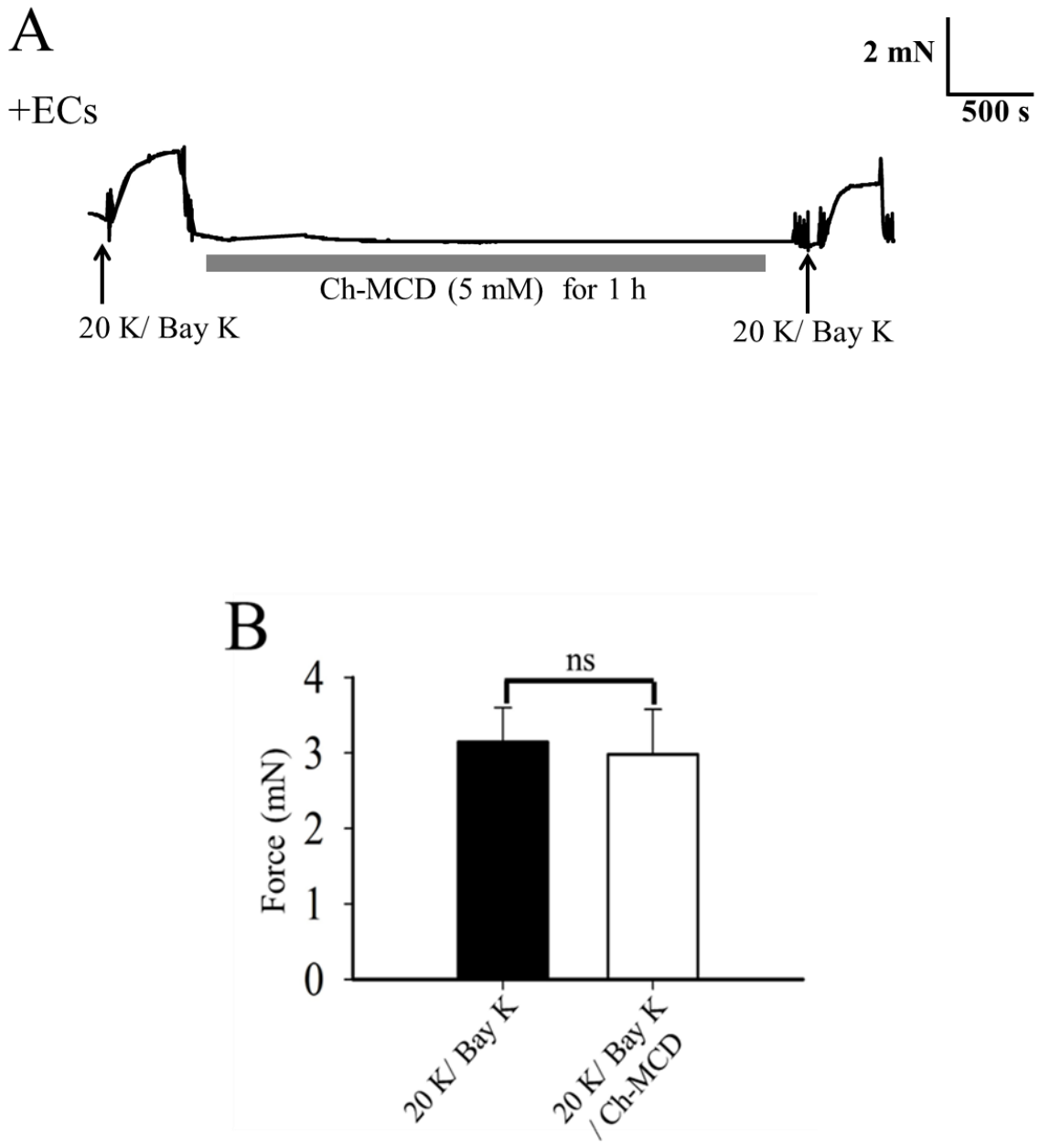

Figure 5.6. Effect of Ch-MCD on contractions with 20 K/ Bay K. A. Incubation with Ch-MCD did not alter the contraction response to 20 K/ Bay K. **B**. Mean data showing the effect of Ch-MCD. Statistical significance was examined using Student's *t*-test: *n*=6, ns.

5.3.6 The effects of endothelial removal on the response to M-β-CD

5.3.6.1 Experimental protocol

Next, whether the endothelium removal would have effects on the change seen with caveolar disruption was tested. After establishing the viability or arteries, the endothelium was mechanically removed. The vessels were then washed with PSS three times and left to recover. Vessels were contracted again with 20 K/ Bay K, then at the plateau of 20 K/ Bay K contraction, ACh (10 μM) was added to confirm the removal of the endothelium. Afterwards, the vessels were washed and left for about 10 min to recover. In order to deplete cholesterol, the vessels were incubated with M-β-CD (5 mM) for 1 hour. Subsequently, the vessels were washed with PSS three times, left for 10 min, and contracted with 20 K/ Bay K.

5.3.6.2 Analysis

After endothelial removal, M-β-CD no longer augmented contraction to 20 K/Bay K (**figure 5.7 A**). Analysis showed that M-β-CD treatment did not significantly alter force generated in response to 20 K/ Bay K in the absence of endothelium (6.61 ± 0.91 mN to 7.40 ± 1.07 mN, *n*= 14, ns) **(figure 5.7 B)**. This indicates that effect of M-β-CD on 20 K/ Bay K contraction using rat femoral artery is mediated by endothelial cells.

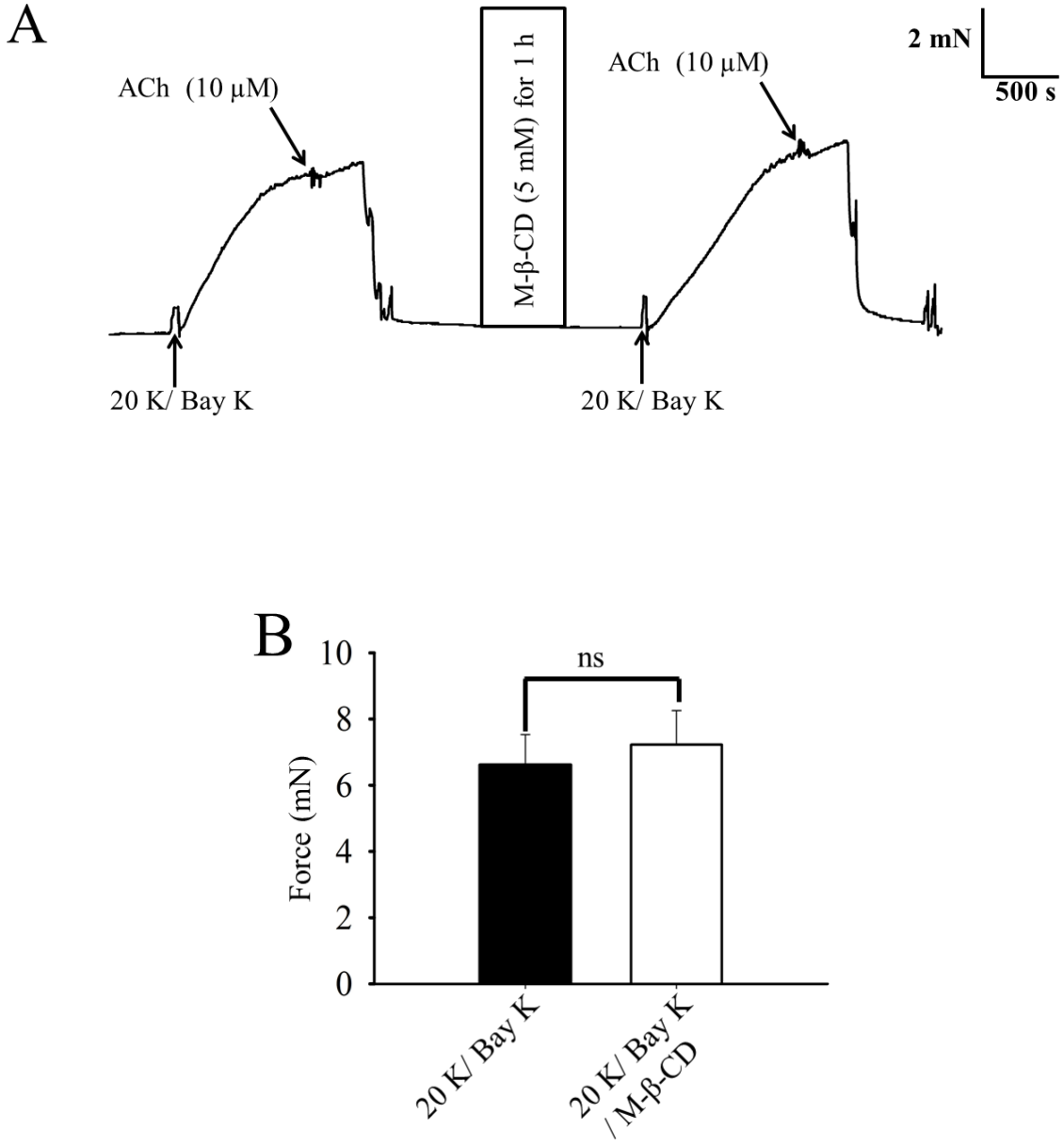

Figure 5.7. Effect of M-β-CD on endothelium-denuded femoral artery. A. After endothelial denudation, incubation with M-β-CD did not augment the contraction response to 20 K/ Bay K. ECs were mechanically removed prior to contracting the artery with 20 K/ Bay K, as shown by the absence of relaxation to ACh. **B**. Mean data showing no significant difference in the contractions of endothelium-denuded arteries stimulated with 20 K/ Bay K following M-β-CD treatment. Statistical significance was examined using Student's *t*-test: *n*=14, ns.

5.3.7 The effects of L-NAME and M-β-CD are not additive

5.3.7.1 Experimental protocol

In the previous section, the effect of M-β-CD was shown to be largely endothelium-dependent. As eNOS is known to be localised in caveolae, and caveolar loss reduces the effectiveness of endothelium-dependent vasodilators (Xu et al., 2008), my results could be explained by the effect of M-β-CD on NO production. Thus, I first investigated the effects of basal NO release on contractions. After completion of the preliminary contraction to 20 K/ Bay K, the vessels were incubated in L-NAME (250 μM), an eNOS inhibitor, for 10 min. Afterwards, the vessels were contracted again using 20 K/ Bay K in the presence of L-NAME. At the plateau of 20 K/ Bay K/ L-NAME contraction, ACh (10 μM) was added to test the effect of L-NAME on endothelium-dependent vasodilation. The vessels were then washed and left about for 10 min to recover. In order to disrupt caveolae the vessels were incubated with M-β-CD (5 mM) for 1 hour. The vessels were then washed with PSS three times and contracted with 20 K/ Bay K. At the plateau of 20 K/ Bay K contraction, ACh was added. Afterwards, the vessels were washed and left for about 10 min to recover. The vessels were then pre-incubated in L-NAME (250 μM) for 10 min and contracted with 20 K/ Bay K/ L-NAME.

5.3.7.2 Analysis

Application of L-NAME augmented contraction to 20 K/ Bay K. Note that, in the presence of L-NAME, application of ACh caused contraction, rather than relaxation. This result is consistent with L-NAME inhibiting basal NO release from the endothelium in this artery. When arteries were subsequently incubated in M-β-CD,

contraction to 20 K/ Bay K was enhanced (**figure 5.8 A**). Note after M-β-CD treatment, ACh application no longer causes relaxation (**figure 5.8 A**). L-NAME no longer had an additional contractile effect after M-β-CD treatment. This could be explained if both M-β-CD and L-NAME act on the same pathway, most likely inhibiting basal NO release from the endothelium. Analysis of the results showed that incubation of arteries with L-NAME caused a significant increase in the force generated in response to 20 K/ Bay K, from 6.82 ± 1.61 mN to 14.90 ± 2.76 mN (*n*= 6, **P< 0.01). However, when arteries were treated with M-β-CD, L-NAME no longer caused significant additional contraction (17.70 ± 2.73 mN to 16.00 ± 3.19 mN (*n*= 6, ns) (**figure 5.8 B**). Overall, these results support the previous observation that the action of M-β-CD is endothelium-dependent, and that M-β-CD and L-NAME both increase force by eNOS inhibition.

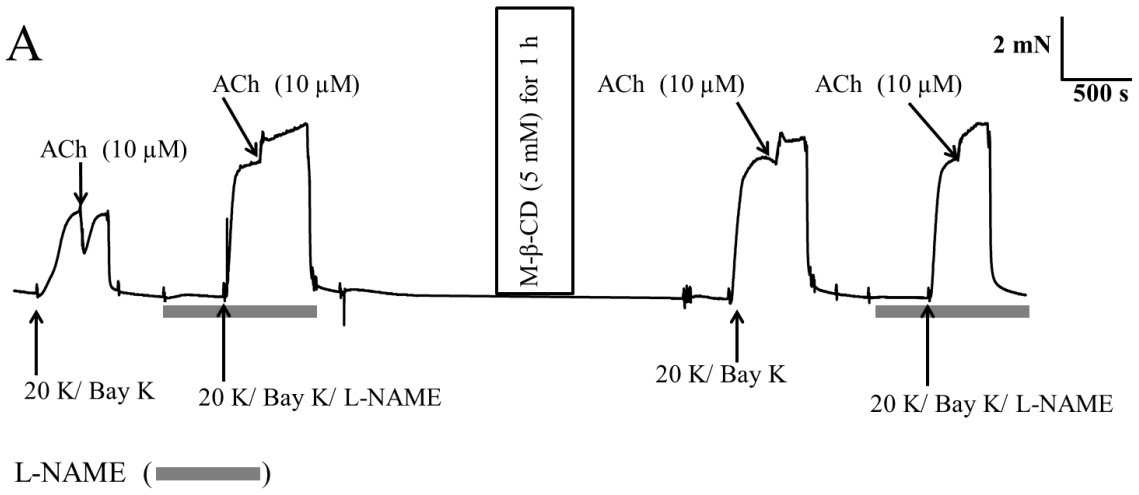

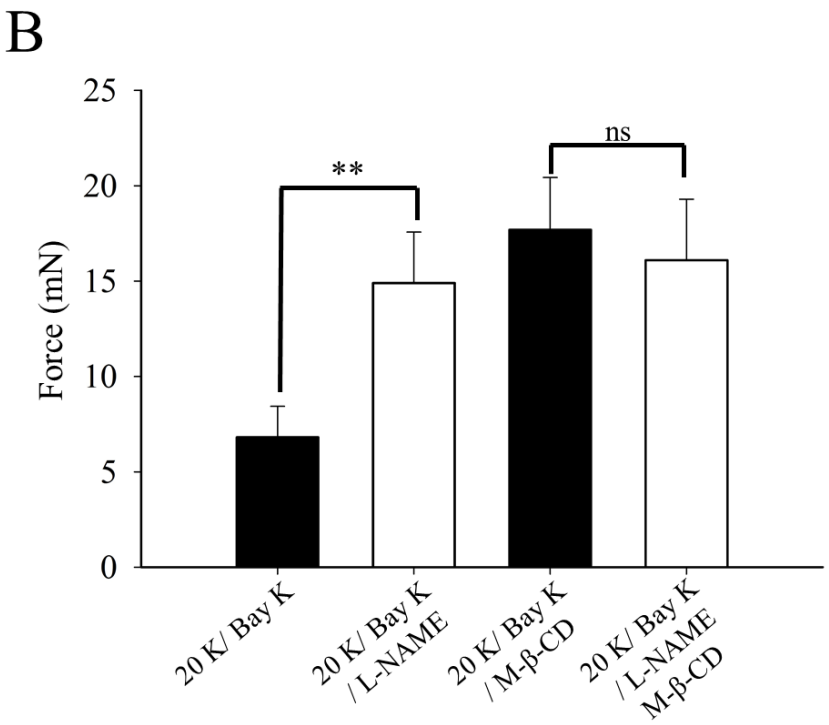

Figure 5.8. Effect of inhibition of NO synthase by L-NAME on femoral artery contractions. A. Incubation with 250 µM L-NAME augmented contraction response to 20 K/ Bay K. When arteries were incubated with M-β-CD, contraction with 20 K/ Bay K was enhanced. However, L-NAME no longer had an additional contractile effect after M-β-CD treatment. **B**. Mean data showing 250 µM L-NAME significantly increases the contraction response to 20 K/ Bay K. L-NAME did not enhance the contraction after M-β-CD treatment. Statistical significance was examined using Student's *t*-test: n=6, **P< 0.01.

5.3.8 Effect of L-NAME on rat femoral artery rings pre-contracted with phenylephrine

Although useful in its simplicity, contraction induced with 20 K/ Bay K may not necessarily reflect the events during more physiological contractions. Here, the effect of L-NAME was further examined using arteries contacted with an α-adrenergic agonist, phenylephrine (PE).

5.3.8.1 Experimental protocol

After the vessels were constricted with 20 K/ Bay K, and ACh was added to confirm the presence of the endothelium, they were contracted with cumulative doses of PE (0.1 µM, 0.3 µM, 1 µM, 3 µM, 10 µM and 30 µM) **(figure 5.9 A)**. Artery rings were then pre-incubated with L-NAME (250 µM) for 10 minutes and then contracted again with cumulative doses of PE (0.1-30 µM) in the presence of L-NAME **(figure 5.9 A)**.

5.3.8.2 Analysis

The response to cumulative doses of PE was measured at the peak of each contraction component. Values are expressed as means ± SEM. PE concentration-response curves were constructed before and after treatment with L-NAME.

Concentration-response curves shifted to the left after incubation with L-NAME **(figure 5.9 B)**, i.e. a given concentration of PE was more effective after L-NAME treatment. These results indicate that PE causes contraction in rat femoral artery and that incubation with L-NAME augments PE-induced contraction, possibly by inhibiting basal endothelial NO release.

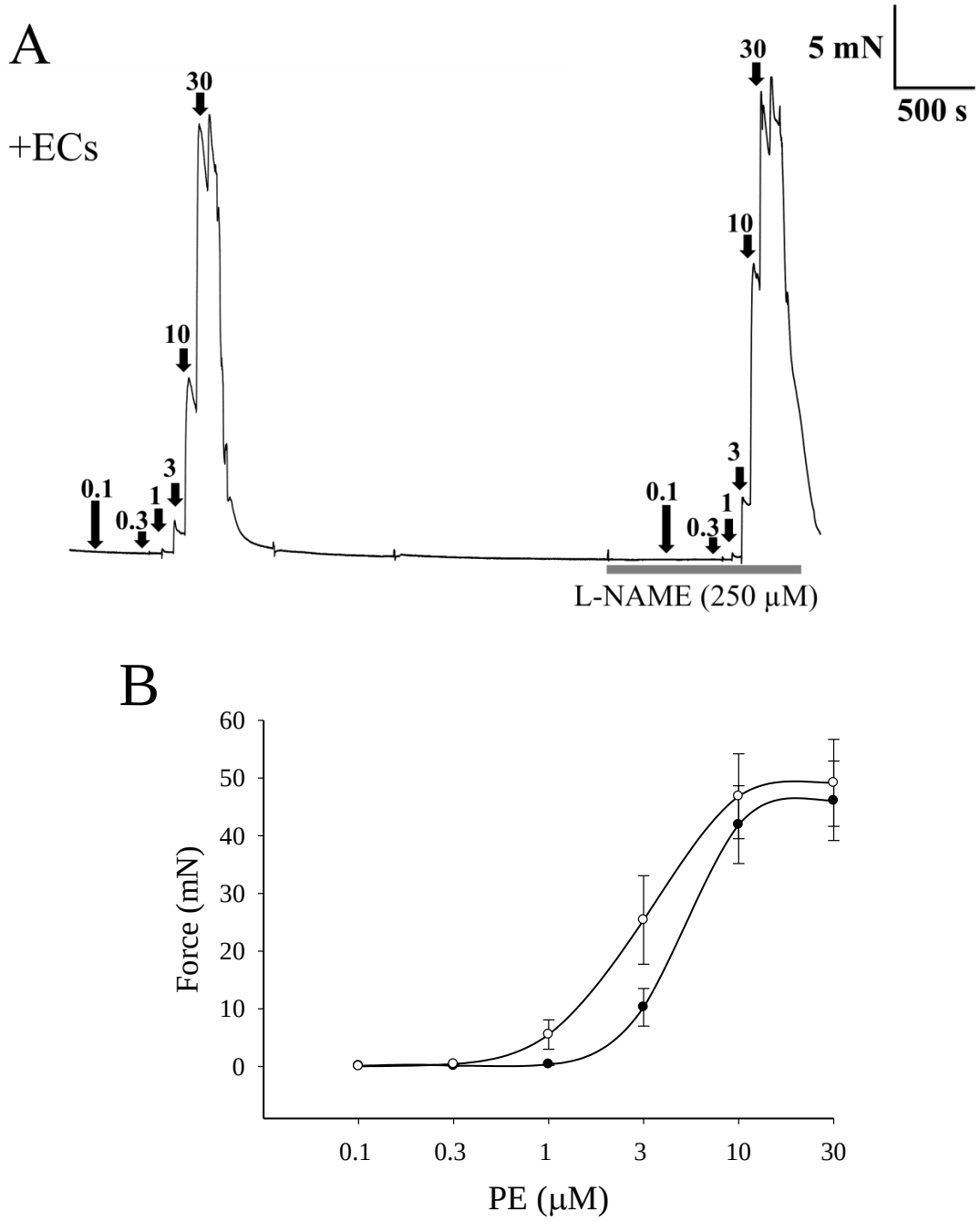

Figure 5.9. Effect of L-NAME on PE-induced femoral artery contraction. A. Traces show phenylephrine contractions (0.1 - 30 μM) before and after incubation with L-NAME (250 μM) **B**. Phenylephrine concentration-response curves before (●) and after (○) incubation with L-NAME. Data are expressed as mean ± SEM (*n*=6).

5.3.9 The disruption of caveolae by M-β-CD is associated with the impairment of BK_{Ca} channel function in rat femoral arteries

The function of the BK_{Ca} channel is reported to be influenced by caveolar location and interaction with caveolins. In this experiment, I tested whether the observed change in contraction by disrupting caveolae is mediated by the BK_{Ca} channel. As BK_{Ca} channels were found in both endothelial and smooth muscle cells in rat femoral artery (see chapter 4), I designed two experiments to examine: (i) the effect of BK_{Ca} channel inhibition by tetraethylammonium ions (TEA^+) on the contraction of femoral arteries in response to 20 K/ Bay K before and after treatment with M-β-CD; (ii) the effect of BK_{Ca} channel inhibition by TEA^+ on the contraction of endothelium-denuded femoral arteries in response to 20 K/ Bay K before and after treatment with 5 mM M-β-CD.

5.3.9.1 Experimental protocol A

Endothelium-intact artery rings were contracted with 20 K/ Bay K. They were then pre-incubated in TEA^+ (2 mM), a relatively selective BK_{Ca} channel inhibitor at this concentration (Langton et al., 1991), for 10 min. Vessels were next contracted with 20 K/ Bay K in the presence of 2 mM TEA^+. In order to disrupt caveolae, vessels were incubated with M-β-CD (5 mM) for 1 hour. Subsequently, the vessels were pre-incubated in TEA^+ (2 mM) for 10 minutes and contracted with 20 K/ Bay K/ TEA.

5.3.9.2 Experimental protocol B

The endothelium was mechanically removed from the lumen of the artery and a similar protocol to that applied in **Experimental protocol A** was then used. Vessels were

contracted with 20 K/ Bay K and ACh (10 μM) was added to confirm the absence of the endothelium. Vessels were pre-incubated in TEA^+ (2 mM) for 10 min and contracted with 20 K/ Bay K/ TEA. Vessels were then incubated with M-β-CD (5 mM) for 1 hour, pre-incubated in TEA^+ (2 mM) and contracted with 20 K/ Bay K/ TEA.

5.3.9.3 Analysis

Incubating artery rings with 2 mM TEA^+ caused an increase in the resting force of the artery, and also the contraction force in response to 20 K/ Bay K **(figure 5.10)**. This result suggests TEA^+-sensitive K^+ channels are contributing to the membrane potential at both resting state and when arteries are contacted with 20 K/ Bay K. The two data traces illustrated in **figure 5.10** show different patterns of response. In the upper trace, spikes are superimposed on top of the increase in resting force, indicating TEA^+ is inducing spontaneous oscillations in this vessel. As before, incubating arteries with 5 mM M-β-CD for 1 hour augmented contraction in response to 20 K/ Bay K **(figure 5.10)**. After treatment with M-β-CD, TEA^+ no longer caused significant additional contraction in response to 20K/ Bay K **(figure 5.10)**. Analysis showed that treatment of intact femoral arteries with M-β-CD caused a significant increase in the force generated in response to 20 K/ Bay K, from 7.07 ± 2.05 mN to 15.29 ± 2.84 mN (n=8, **P< 0.01) **(figure 5.11)**. Increases in the resting tension caused by 2 mM TEA^+ alone before and after M-β-CD treatment was 1.15 ± 0.68 mN and 2.15 ± 0.81 mN, respectively (ns, **figure 5.11)**. 2 mM TEA^+ application significantly increased the contraction with 20 K/ Bay K from 7.07 ± 2.05 mN to 18.53 ± 3.25 mN (n=8, *P< 0.05). After the vessels had been incubated with M-β-CD, incubation with TEA^+ (2 mM) caused a non-significant

increase in the force generated in response to 20 K/ Bay K, from 18.53 ± 3.25 mN to 19.54 ± 2.22 mN (*n*=8, ns) **(figure 5.11)**. The observation that TEA^+ increased force before, but not after, M-β-CD treatment suggests caveolar disruption decreases the contribution of a TEA^+-sensitive K^+ channel to the membrane potential.

In endothelium-denuded femoral arteries, application of 2 mM TEA^+ caused a small but non-significant increase in 20 K/ Bay K contraction (from 6.06 ± 1.44 mN to 8.01 ± 1.58 mN (*n*= 8, ns)) **(figure 5.12 B)**. M-β-CD application had no significant effect on 20 K/ Bay K contraction (6.06 ± 1.44 mN to 6.19 ± 1.32 mN (*n*= 8, ns)). **A**fter arteries were incubated with M-β-CD, TEA^+ caused a small, non-significant, additional contraction in response to 20 K/ Bay K /M-β-CD from 6.19 ± 1.32 mN to 7.23 ± 1.61 mN (*n*= 8, ns).

Overall, these results indicate that inhibition of the potassium channels, possibly BK_{Ca} channels, by TEA^+ effectively increases the contraction of rat femoral artery in the presence of endothelial cells. Caveolae disruption by M-β-CD and/or endothelium removal caused TEA^+ to become much less effective at augmenting contraction to 20 K/ Bay K. M-β-CD treatment and removal of endothelium both seem to inhibit basal endothelial NO release. NO is a known activator of BK_{Ca} channels in SMCs, so reduced basal NO release may lead to less active BK_{Ca} channels, so SMC depolarization, and contraction.

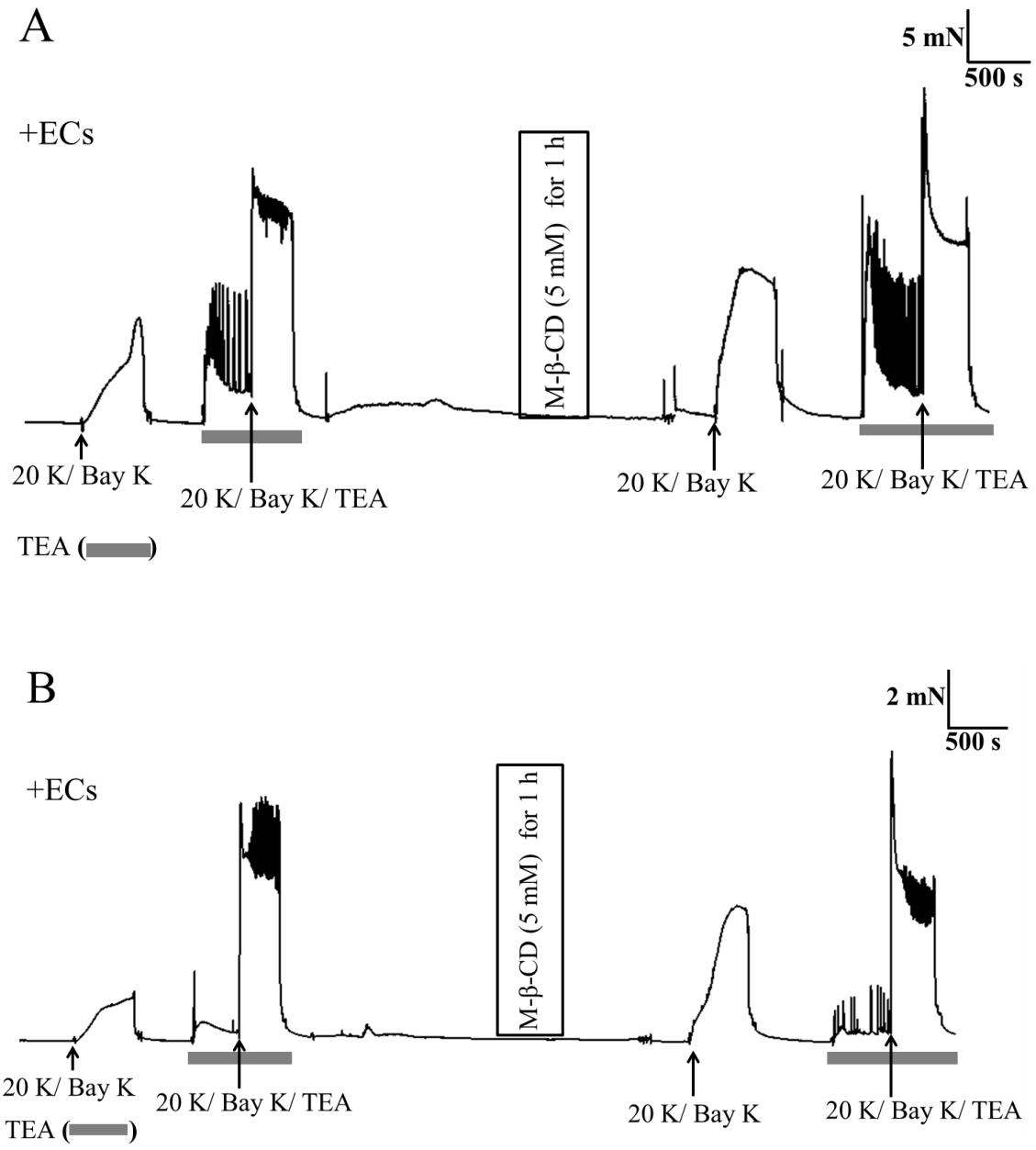

Figure 5.10. Effect of TEA^+ on femoral artery contractions to 20K/ Bay K. Traces show that incubation of arteries with 2 mM TEA^+ by itself causes contraction, and also augments the contraction response to 20 K/ Bay K. In the upper trace (**A**), TEA^+ triggered spontaneous oscillations in force. When arteries were subsequently incubated in M-β-CD, this caused an enhanced contraction in response to 20 K/ Bay K, but this effect of M-β-CD was absent when the arteries were treated with TEA^+. Increases in the basal tension due to TEA^+ application alone were similar before or after M-β-CD treatment.

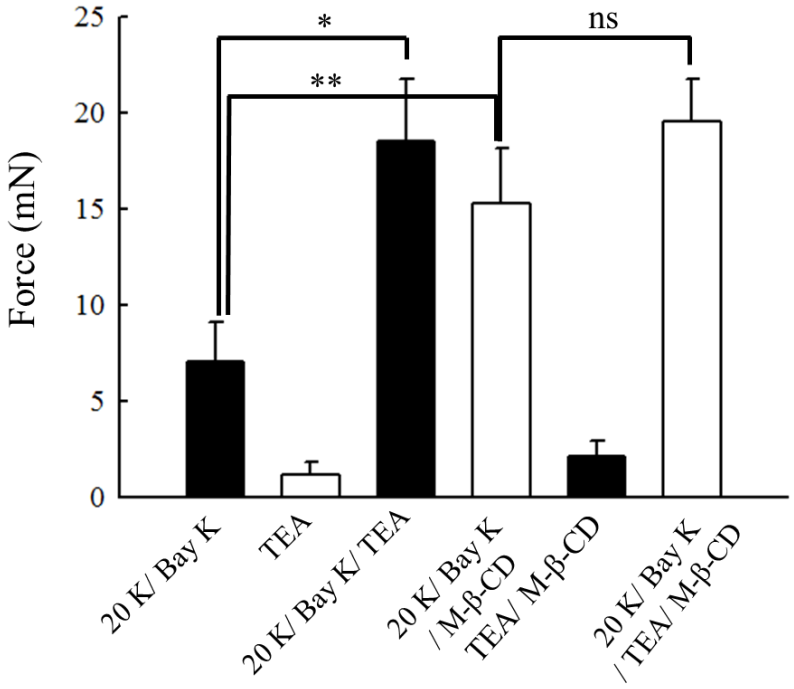

Figure 5.11. Mean data for effect of TEA^+ on femoral artery contractions to 20 K/ Bay K before and after M-β-CD treatment. Data show a significant increase in the contraction in response to 20 K/ Bay K after incubation of the artery with 2 mM TEA^+ before, but not after, treatment with M-β-CD. Statistical significance was examined using ANOVA: *n*=8, * P<0.05 and ** P< 0.01.

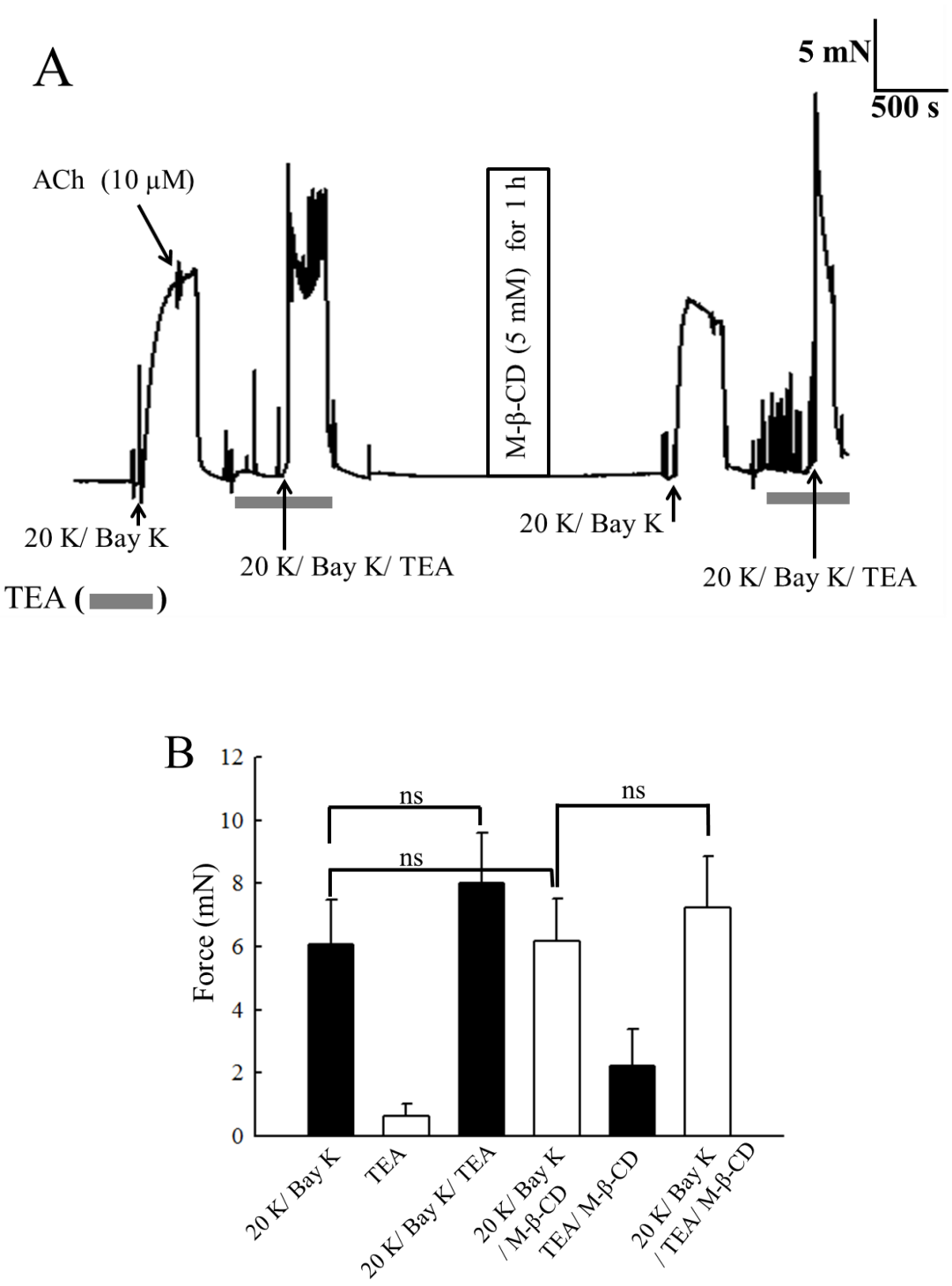

Figure 5.12. Effect of TEA^+ on contractions to 20 K/ Bay K in an endothelium-denuded artery. A. Application of 2 mM TEA^+ or M-β-CD had little effect on 20 K/ Bay K contraction. **B**. Mean data showing a non-significant increase in the contraction response to 20 K/ Bay K by TEA^+ or M-β-CD. Statistical significance was examined using ANOVA *n*=8.

5.3.10 Effect of Iberiotoxin (IBTX) before and after disruption of caveolae by M-β-D

In this experiment, I tested the effect of a more specific inhibitor of BK_{Ca} channels, IBTX, in order to examine whether the observations gained using TEA^+ are re-produced.

5.3.10.1 Experimental protocol

After completion of the preliminary protocol **(figure 5.1 A)**, vessels were pre-incubated in IBTX (100 nM) for 10 minutes. Vessels were then contracted with 20 K/ Bay K in the presence of 100 nM IBTX. The endothelium was then mechanically removed, the vessels washed, left for about 10 minutes to recover, and re-contracted with 20 K/ Bay K. ACh (10 μM) was added to confirm the absence of the endothelium. Vessels were then pre-incubated in IBTX (100 nM) for 10 minutes and contracted with 20 K/ Bay K/ IBTX. Caveolae were then disrupted by incubation with M-β-CD (5 mM) for 1 hour. Afterwards, the vessels were pre-incubated in IBTX (100 nM) for 10 minutes and contracted to 20 K/ Bay K/ IBTX.

5.3.10.2 Analysis

Incubating arteries with 100 nM IBTX for 10 minutes augments contraction to 20 K/ Bay K (**figure 5.13 A)**. After the endothelium removal, incubation of arteries with 100 nM IBTX no longer enhanced 20 K/ Bay K contractions **(figure 5.13 A)**. After arteries were incubated with M-β-CD, IBTX caused no additional contraction in response to 20 K/ Bay K **(figure 5.13 A)**. Application of 100 nM IBTX to endothelium-intact rings

increased contraction with 20 K/ Bay K, from 6.01± 0.09 mN to 11.99 ± 2.66 mN. However, the P value was not quite significant (P=0.0657), presumably due to a small sample size. After removal of ECs, application of IBTX to the arteries caused a small increase in force, from 5.87 ± 0.60 mN to 7.06 ± 1.10 mN. Incubating the vessels with M-β-CD caused a small increase in the force generated in response to 20 K/ Bay K/ IBTX, from 7.06 ± 1.10 mN to 7.57 ± 1.28 mN (*n*=4) **(figure 5.13 B)**.

These results indicate that inhibition of BK_{Ca} channels by IBTX increased contraction to 20 K/ Bay K in femoral artery in the presence of the endothelium. Endothelium removal resulted in abolition of this IBTX effect, as well as that of M-β-CD. These results with IBTX, a very specific BK_{Ca} channel inhibitor, are comparable to those obtained with TEA^+, validating the effects seen with TEA^+, suggesting that they are likely to be mediated by BK_{Ca} channels.

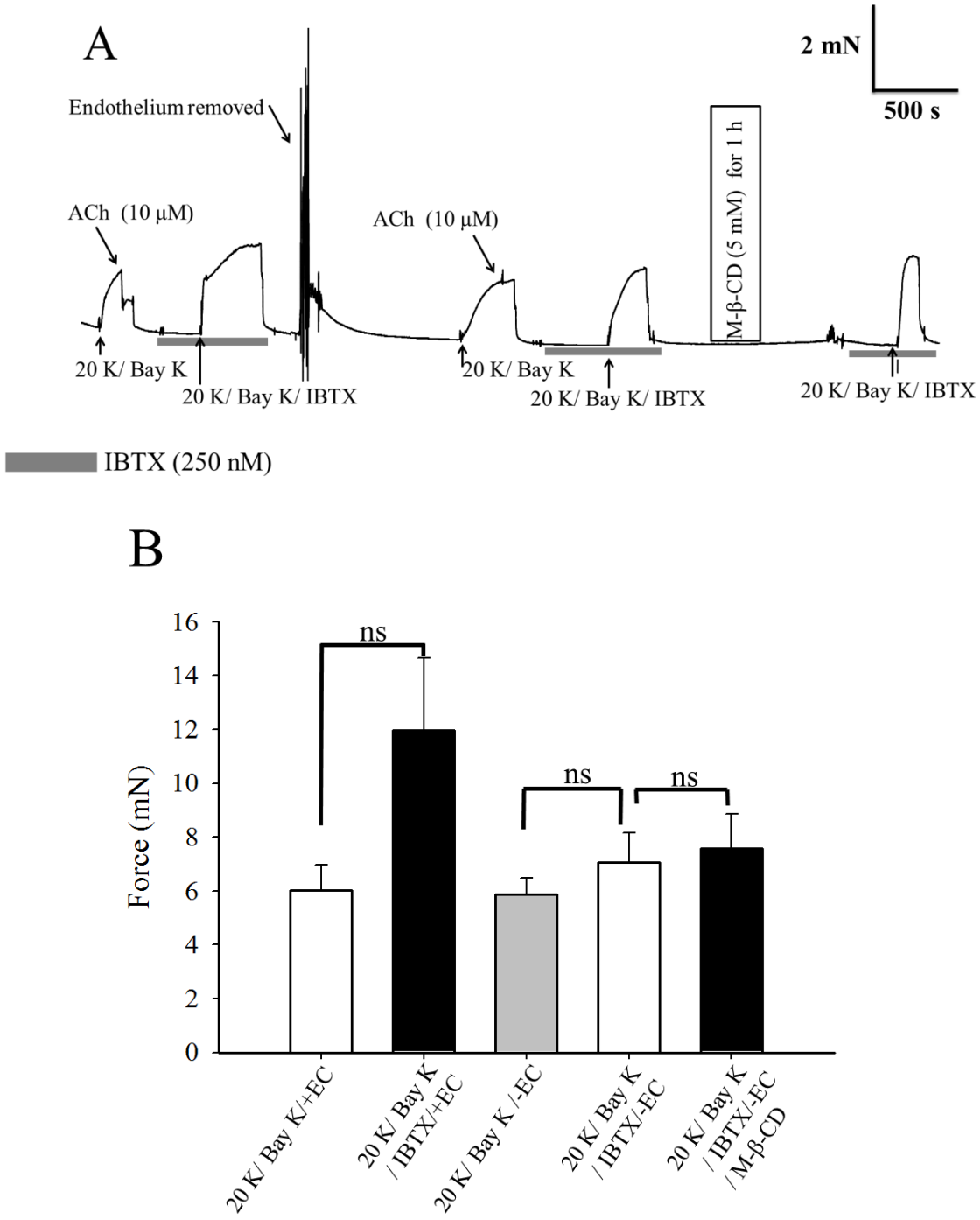

Figure 5.13. Effect of IBTX on femoral artery contractions to 20 K/ Bay K. A. Experimental trace shows incubation of artery with 100 nM IBTX augments contraction in response to 20 K/ Bay K. After endothelial removal, IBTX was no longer effective at increasing force. **B**. Mean data showing an increase in the contraction response to 20 K/ Bay K after incubation of the artery with IBTX when EC is present. *n*=4.

5.3.11 Inhibition of basal release of NO by L-NAME is associated with reduced contraction in response to BK_{Ca} channel inhibition with IBTX

5.3.11.1 Experimental protocol

This experiment was designed to examine whether the effects of L-NAME and IBTX on contraction were additive, an indication that two mechanisms act through different pathways. Vessels were contracted with 20 K/ Bay K and, at the plateau of the contraction, IBTX (100 nM) was added to the chamber. Arteries were then washed and pre-incubated with L-NAME (250 µM) for 10 minutes. Vessels were then contracted using 20 K/ Bay K/ L-NAME, and at the plateau of the contraction, IBTX (100 nM) was added.

5.3.11.2 Analysis

Adding IBTX (100 nM) during 20 K/ Bay K induced further contraction **(figure 5.14 A)**. When arteries were treated with L-NAME, the effect of IBTX was smaller **(figure 5.14 A)**. Analysis of results showed that incubation of arteries with L-NAME by itself caused an increased contraction with 20 K/ Bay K **(figure 5.14 B)**. IBTX (100 nM) caused additional contraction over and above that caused by 20 K/ Bay K of 18.30 ± 0.90 mN and 7.02 ± 2.95 mN in the absence and presence of L-NAME, respectively (n= 4, **P< 0.01) **(figure 5.14 B)**. These results indicate that the inhibition of BK_{Ca} channels by IBTX induces contraction of rat femoral arteries, as shown in the previous section. After incubating arteries in L-NAME, IBTX has less effect on 20 K/ Bay K contractions. Once again, this data is consistent with basal NO release from the endothelium causing activation of BK_{Ca} channels in vascular SMCs. Inhibiting NO

synthesis with L-NAME or BK_{Ca} channels with IBTX (or TEA^{+}) therefore has a similar overall effect on force.

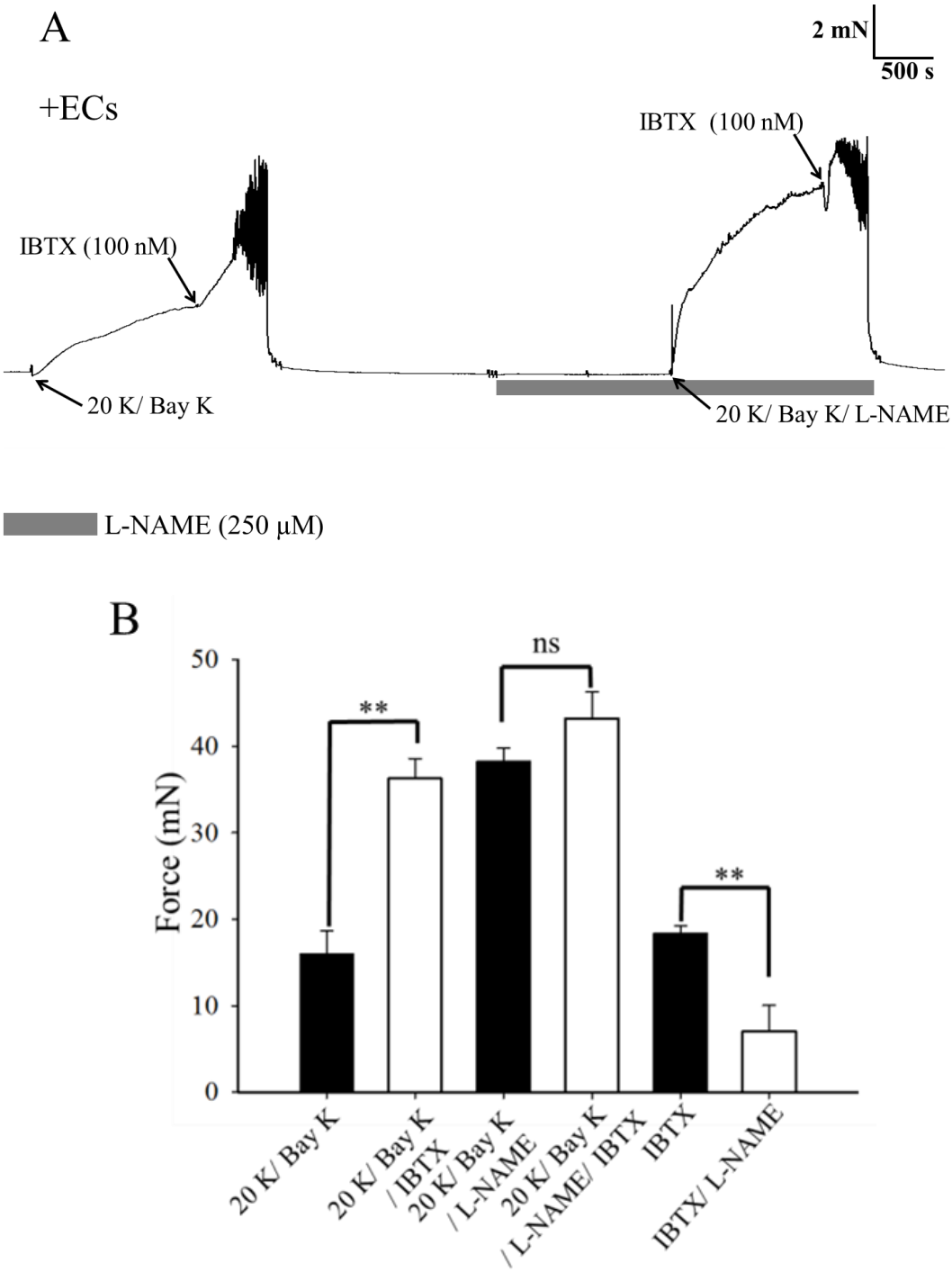

Figure 5.14. Effect of IBTX and L-NAME on contractions with 20 K/ Bay K. A. Addition of 100 nM IBTX induced further contraction to 20 K/ Bay K. When arteries were pre-incubated with 250 µM L-NAME, IBTX was less effective in increasing force. **B**. Mean data showing a significant increase in contraction response to 20 K/ Bay K by IBTX before, but not after, incubation with L-NAME. Statistical significance was established using Student's *t*-test: *n*=4, **P< 0.01.

5.3.12 TEA^+ inhibits relaxation of rat femoral artery to sodium nitroprusside

The results so far indicate that the contraction caused by 20 K/ Bay K is partly dependent on basal release of NO, which subsequently activates BK_{Ca} channels in smooth muscle cells. In other arteries, NO and NO donors have been shown to activate smooth muscle BK_{Ca} channels to cause vasodilation (Mistry and Garland, 1998). In order to test whether a similar mechanism exists in rat femoral artery, experiments were performed to examine the effect of the BK_{Ca} channel inhibitor TEA^+ on relaxations to the NO donor sodium nitroprusside (SNP).

5.3.12.1 Experimental protocol A

To assess the effect of TEA^+ on vasorelaxation, arteries were constricted with 20 K/ Bay K and cumulative doses of SNP added (0.1 µM, 0.3 µM, 1 µM, 3 µM, 10 µM, 30 µM and 100 µM) **(figure 5.15 A).** The protocol was then repeated in the presence of 2 mM TEA^+ (**figure 5.15 A)**.

5.3.12.2 Experimental protocol B

The same protocol as above was repeated on arteries without endothelial cells **(figure 5. 15)**.

5.3.12.3 Experimental protocol C

The same protocol as above was repeated on arteries contracted with KPSS (without ECs) **(figure 5.16)**.

5.3.12.4 Data analysis

SNP (0.1-100 μM) caused concentration-dependent relaxation in endothelium-intact rat femoral arteries contracted with 20 K/ Bay K, before and after incubation with 2 mM TEA^+ **(figure 5.15 A)**. Concentration-response curves show the vasorelaxation response to SNP was inhibited after incubation with 2 mM TEA^+, however, the data were only significantly different at 30 μM SNP (*n*=8, *P<0.05) **(figure 5.15 B)**.

In the endothelium-denuded rings, SNP caused concentration-dependent relaxation **(figure 5.16 A)**. In the presence of TEA^+, SNP was less effective. Concentration-response curves show the vasorelaxation response to SNP was significantly inhibited in the presence of TEA^+ at concentration of SNP of 1 μM and above (1 μM SNP, P<0.01; 3 - 100 μM SNP, P<0.001, *n*=8) **(figure 5.17)**. Vasorelaxation in response to SNP was also attenuated in arteries contracted with KPSS (1 μM SNP, P<0.01; 3 - 100 μM SNP, P<0.001, *n*=8) **(figures 5.16 B and 5.17)**. The latter result is also consistent with K^+ channel activation being involved in SNP relaxations, with BK_{Ca} channel being the most likely candidate.

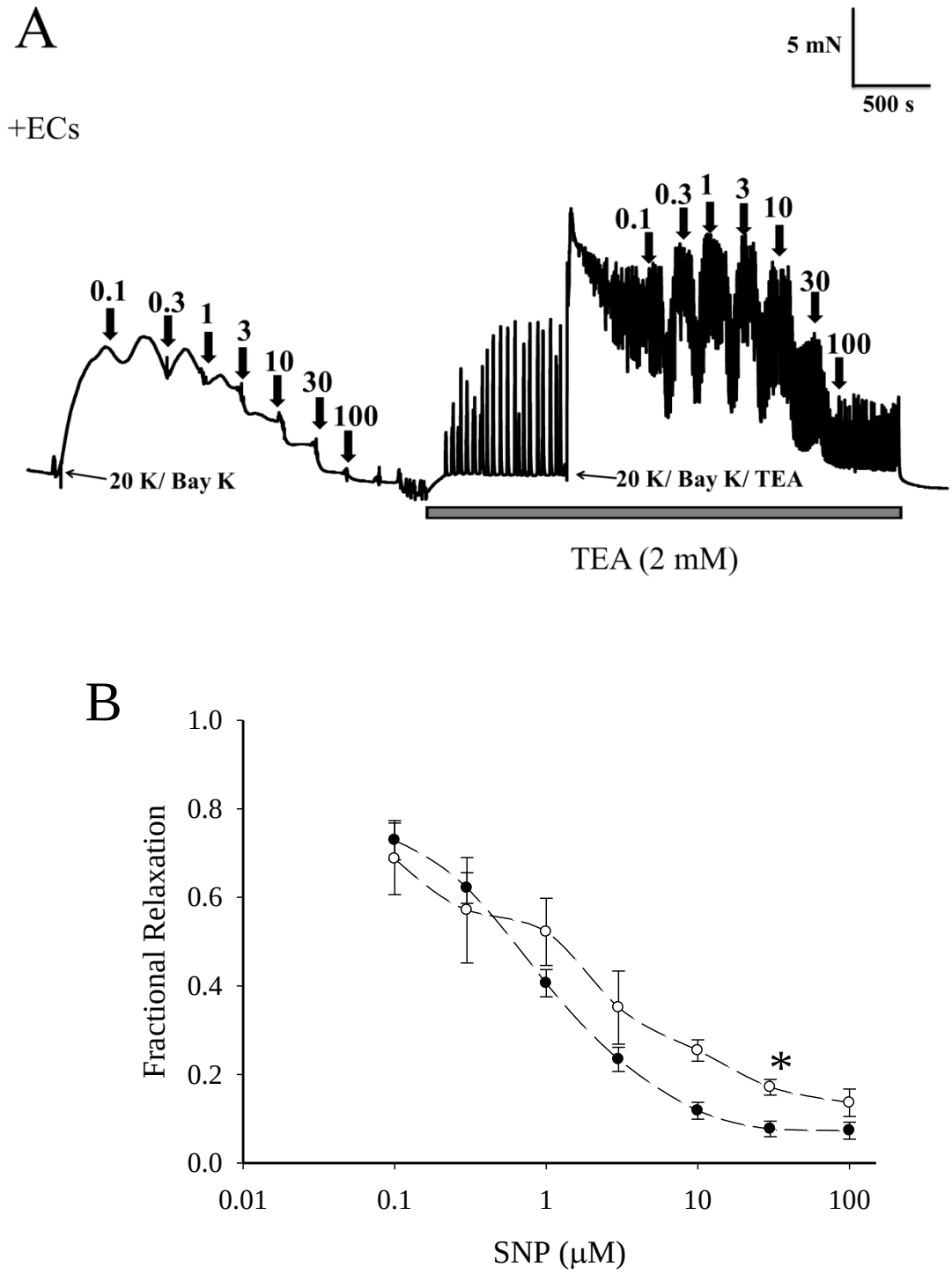

Figure 5.15. Effect of TEA^+ on SNP-induced relaxation of endothelium-intact rat femoral artery. A. Experimental trace showing vasorelaxation in an artery contracted by 20K/ Bay K. SNP (0.1 to 100 μM) before and after the treatment with TEA^+ (2 mM). **B**. Comparison of fractional relaxation induced by SNP in femoral artery before (○) and after (●) the treatment with 2 mM TEA^+.

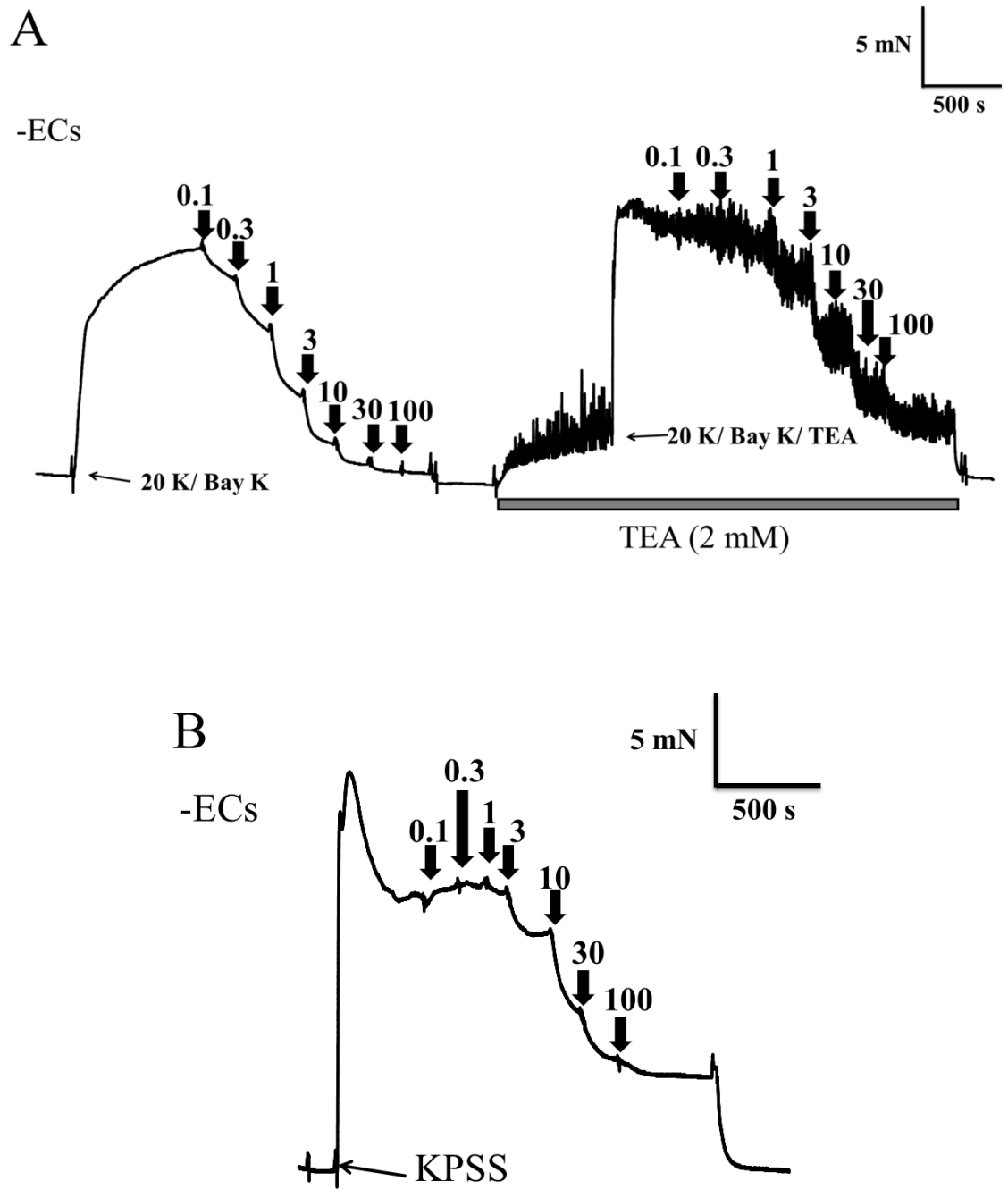

Figure 5.16. Effect of TEA^+ on SNP-induced relaxation of endothelium-denuded femoral artery. A. Traces showing vasorelaxation in an artery pre-contracted by 20K/ Bay K. SNP (0.1 - 100 μM) produced relaxation before and after treatment with 2 mM TEA^+; **B** Trace showing vasorelaxation produced by SNP (0.1 - 100 μM) in an artery contracted with KPSS.

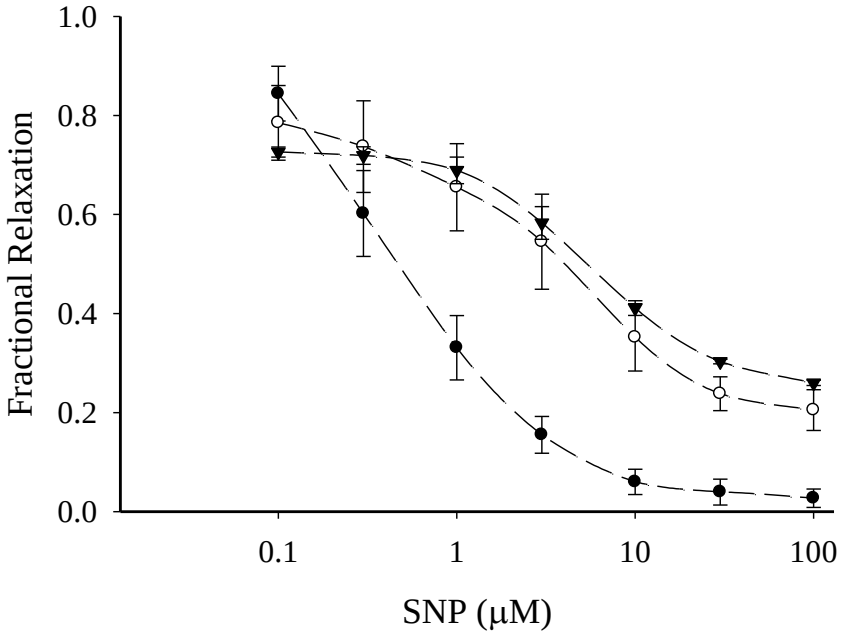

Figure 5.17. Effect of TEA^+ on SNP concentration-response curves in endothelium-denuded femoral artery. Vasorelaxation induced by SNP in arteries contracted with 20 K/ Bay K, before (●) and after (○) the treatment with 2 mM TEA^+ and in arteries contracted with KPSS (▼).

5.4 Discussion

Contraction of vascular SMCs is initiated by an increase in the intracellular Ca^{2+} concentration ($[Ca^{2+}]_i$). $[Ca^{2+}]_i$ can rise from two sources, the extracellular space (Ca^{2+} influx) and intracellular stores (Ca^{2+} release) (Yamamura et al., 2013). Excitatory hormones and neurotransmitters often trigger a combination of Ca^{2+} influx and Ca^{2+} release (McFadzean and Gibson, 2002). Ca^{2+} influx occurs through Ca^{2+} permeable channels, either voltage dependent (L-type Ca^{2+} channels (McFadzean and Gibson, 2002), or voltage independent. The latter includes the receptor-activated calcium channels (ROCCs, activated by agonists acting on GPCRs) and store-operated calcium channels (SOCCs, activated by depletion of the Ca^{2+} stores) (McDaniel et al., 2001).

Activation of L-type Ca^{2+} channels was used as the primary source of contraction here as they play a major role in rat femoral artery (Fransen et al., 2012). I investigated the effects of cholesterol-binding agents and inhibitors of BK_{Ca} channels in the presence and absence of ECs on a simple contraction induced by 20 K/ Bay K. My results collectively suggest that basal NO release from ECs is a key determinant of the size of 20 K/ Bay K contraction, and that BK_{Ca} channels play a critical role in this NO-dependent femoral artery contractility. NO is a well established vasodilator (Cohen et al., 1999, Fransen et al., 2012), but the mechanisms by which NO exert its effects are not completely understood (Cohen et al., 1999).

In this study, two principal methods were used for eliciting contraction, KPSS and 20 K/ Bay K (Dreja et al., 2002, Xu et al., 2007, Yamamura et al., 2013). KPSS, a high K^+ solution (80 mM), was used to depolarize the SMC membrane (Fransen et al., 2012). Isometric contraction can be increased until maximal force is generated by

elevating K^+ to 50 mM K^+ (Fransen et al., 2012). 20 K/ Bay K causes a partial depolarization (20 mM KCl) and activation of L-type Ca^{2+} channels (Bay K 8644) (Yamamoto et al., 1984). Both KPSS and 20 K/ Bay K cause the artery to contract by triggering an influx of Ca^{2+} into the SMC via VDCCs (Yamamura et al., 2013). However, there is a critical difference in contraction induced by KPSS and 20 K/ Bay K. If the arteries are contracted with the former, the opening of K^+ channels cannot cause hyperpolarisation and thus will not lead to artery relaxation. If the arteries are contracted with the latter, opening of K^+ channels can still cause hyperpolarisation and so it will lead to artery relaxation. Together, these two similar but distinctive approaches will aid in untangling the possible role played by K^+ channels in the changes caused by application of M-β-CD and filipin (Darblade et al., 2001, Xu et al., 2007). More specifically, TEA^+ and IBTX were used as inhibitors of BK_{Ca} channels (Szado et al., 2001) to identify the K^+ channel involved. In addition, ACh (to activate eNOS) and L-NAME (to inhibit eNOS) were used to assess the role of NO.

The results in this chapter demonstrate that caveolae disruption using either M-β-CD or filipin causes significant increases in the isometric force of femoral arteries in response to 20 K/ Bay K but not to KPSS **(figures 5.2 A and 5.4 A)**. The fact that contractions were unaffected in response to KPSS also suggests that L-type Ca^{2+} channels might be located outside of the caveolae. A similar result was reported by Dreja et al. (2002). Also, it has been demonstrated that the function of L-type Ca^{2+} channels is independent of caveolae (Lohn et al., 2000). Furthermore, the presence of intact endothelium seems crucial in the change seen with cholesterol depletion. The role of caveolae in ECs has been described previously by several studies (Darblade et al., 2001, Isshiki et al., 2002, Linder et al., 2005, Xu et al., 2007).

The effect of M-β-CD was reversed with application of Ch-MCD **(figure 5.5 A)**. A similar result was reported in the endothelin-1 contraction using basilar arteries of rats (Bergdahl et al., 2003). Thus, although M-β-CD may have other effects, the functional read-out used here (isometric force) can reflect its supposed effect, cholesterol depletion.

Based on a previous study which indicated that NO has a predominant role in mediating relaxation in large arteries (Saliez et al., 2008), I compared the 20 K/ Bay K contractions using endothelium-denuded femoral artery before and after treatment with M-β-CD. The results clearly show that M-β-CD no longer augmented contraction to 20 K/ Bay K in the absence of endothelium (**figure 5.7 A**), suggesting that effect of M-β-CD is endothelium-dependent.

The endothelium regulates smooth muscle tone by producing and releasing relaxing and contracting factors (Moncada et al., 1991, Cohen and Vanhoutte, 1995). Amongst these factors, NO is considered to hold a key position as the major vasodilator (Kikkawa et al., 1999). In some isolated arteries, but not in all, inhibition of the basal NO release by L-NAME significantly increased maximum contraction to various vasoconstrictors (Tabernero et al., 1996). In order to further investigate whether the increased 20 K/ Bay K contraction occurred as a result of "removal" of the tonic inhibitory effect due to basal NO release, I compared contractions in arteries pre-incubated in L-NAME, an eNOS inhibitor **(figure 5.8 A)**. Incubation of arteries with L-NAME caused enhanced contractions to 20 K/ Bay K. When the arteries were subsequently incubated in M-β-CD, this caused increased contraction to 20 K/ Bay K. However, L-NAME no longer enhanced contractions after M-β-CD treatment. In addition, relaxation with ACh was impaired after treatment with M-β-CD or incubation with L-NAME. Thus, it seems that both M-β-CD and L-NAME act

on the same pathway. These results suggest that the basal NO release and diffusion into SMCs cause a tonic endothelium-dependent relaxation, and that inhibition of this process thus increases the contraction, at least in the femoral arteries I investigated. The findings of the current study are consistent with those of Kikkawa et al. (1999) who found that constriction of canine basilar artery rings was increased after incubation with L-NMMA pre-contracted with 40 mM KCl. They suggested that L-NMMA selectively inhibited basal NO release. DiCarlo et al. (1995) found that the maximal vasoconstrictor responses to phenylephrine is enhanced in the presence of L-NAME in iliac artery of rat. They suggested that L-NAME has a negative effective on α_1-adrenoceptor-mediated contraction due to inhibition of the basal release of NO. Our results showing enhanced contraction to PE in the presence of L-NAME **(figure 5.9)** are also consistent with this result.

Findings in this chapter can be compared with several previous studies looking at NO release in response to endothelium-dependent vasodilators such as ACh. Darblade et al. (2001) found that treating rabbit aorta rings with either M-β-CD or filipin impaired endothelium-induced relaxation by ACh. In guinea pig aorta, treatment with either M-β-CD or filipin impaired endothelium-dependent relaxation (Kaiser et al., 2002). The findings are also consistent with those of Chen et al. (2012), who confirmed the cav-1-mediated inhibition of activated eNOS in cultures of human ECs using fluorescence resonance energy transfer and co-immunoprecipitation analyses. Also, the present findings seem consistent with Blair et al. (Blair et al., 1999), who found that disrupting caveolae with oxidised low-density lipoprotein (a cholesterol-binding agent), causes eNOS to leave the caveolae and inhibits ACh-induced activation of the enzyme in pulmonary artery endothelial cells.

Relatively few works have examined the relationship between BK_{Ca} channels and caveolae. I initially hypothesised that changes in caveolae structure might affect BK_{Ca} channels in smooth muscle. However, M-β-CD treatment no longer caused increase in 20 K/ Bay K contraction in the absence of endothelium (**figure 5.7 A**). This indicates that the contractile function of vascular SMCs was only slightly, if at all, altered by treatment with M-β-CD in the absence of the endothelium. Nonetheless, the molecules that reside within SMCs are the final point of action where the contractility of an artery is determined. Thus, the possible role played by BK_{Ca} channels was examined by using specific inhibitors of this channel. Contraction of intact arteries in response to 20 K/ Bay K/ TEA was first compared before/after the treatment with M-β-CD **(figure 5.10)**. This showed a significant increase in the contraction force in intact arteries after treatment with TEA^+, presumably as a result of blocking of potassium channels in SMCs **(figure 5.11)**. After treatment with M-β-CD, TEA^+ no longer had a large contractile effect **(figure 5.11)**. The effect of TEA^+ on 20 K/ Bay K contractions was also compared in endothelium-denuded artery rings, before and after M-β-CD treatment **(figure 5.11 A)**. This result showed a non-significant contraction by TEA^+ in response to 20 K/ Bay K, both before and after treatment with M-β-CD **(figure 5.12 B)**. Thus the effect of TEA^+, along with that previously shown for M-β-CD, is endothelium-dependent.

To summarise, these results indicated that application of TEA^+ is effective at increasing the contraction of rat femoral artery only in presence of the endothelial cells. Caveolae disruption by M-β-CD and/or endothelium removal both reduced the effectiveness of TEA^+ to increase contraction. The simplest explanation is that endothelial cells release a substance, NO, that activates BK_{Ca} channels in smooth muscle cells to cause vasorelaxation. M-β-CD treatment and/or endothelium removal

abolish NO release. TEA^+ has a similar effect to M-β-CD because it blocks BK_{Ca} channels, leading to loss of the effective influence of K^+ channels on membrane potential and L-type Ca^{2+} channels.

Because TEA^+ is sometimes regarded as a relatively non-selective K^+ channel inhibitor, the experiments were repeated with the selective K_{Ca} channel inhibitor IBTX, and similar results were obtained (**figures 5.12 and 5.14**). As with TEA^+, the effect of IBTX was examined before and after removal of endothelial cells, and before and after disruption of caveolae by M-β-CD **(figure 5.13)**. Inhibition of BK_{Ca} channels by IBTX effectively increased the contraction of rat femoral artery in the presence of the endothelium. After caveolae were disrupted by M-β-CD or after the endothelium was removed, this caused IBTX to be less effective in increasing contraction force in response to 20 K/ Bay K **(figure 5.13)**. These results mirrored those obtained with TEA^+.

Further experiments were designed to find out whether the effects both of L-NAME and IBTX on vascular contractility of rat femoral arteries were additive **(figures 5.14)**. Inhibition of BK_{Ca} channels by IBTX enhanced vascular contraction to 20 K/ Bay K, as shown previously. Inhibition of eNOS by L-NAME enhanced vascular contraction to 20 K/ Bay K, as shown previously. However, IBTX caused a much smaller contraction in the presence of L-NAME than in its absence, suggesting both share the same pathway. Inhibiting release of basal NO by L-NAME may cause decreased sGC/cGMP/PKG activity in SMCs, so BK_{Ca} channels may be in a less activated state, causing depolarisation, activation of L-type Ca^{2+} channels and contraction.

As a final test of this hypothesis, the role of BK_{Ca} channels in vasorelaxation to SNP, a nitric oxide donor, was investigated. SNP was used in this experiment to induce

vascular relaxation in endothelium-intact and in the endothelium-denuded artery rings before/after blocking potassium channels with TEA^+. SNP has similar effects to NO on smooth muscle cells (Bonaventura et al., 2007). Endothelium-derived NO or that produced by the metabolism of SNP can promote smooth muscle relaxation through stimulation of guanylyl cyclase activity to increase the synthesis of guanosine 3',5'-cyclic monophosphate (cGMP). Increased cGMP regulates vascular tone via multiple mechanisms, including reducing cytosolic $[Ca^{2+}]_i$ (Bonaventura et al., 2007) and activation of vascular BK_{Ca} channels (Archer et al., 1994). TEA^+ was used in this experiment as an inhibitor of BK_{Ca} channels in vascular SMCs (Langton et al., 1991). Vasorelaxation to SNP in the endothelium-denuded rings was inhibited following by TEA^+ **(figures 5.16 and 5.17)**. These results suggest that blocking potassium channels in SMCs by TEA^+ led to decreased vasorelaxation. Incubation of blood vessels with TEA^+ can abolish endogenous nitric oxide-induced endothelium-mediated hyperpolarization in vascular smooth muscle, and consequently causes vascular spasm (Bialecki and Stinson-Fisher, 1995, Dorigo et al., 1999).

The effect of SNP in relaxing the artery was at least partially endothelium dependent; **(figures 5.15 A and 5.17**). The results suggest that endothelium-derived relaxing factors modulates SNP-induced relaxation. Our results also supported those of a study by Bonaventura et al. (Bonaventura et al., 2008), who found that the relaxation induced by SNP in vascular smooth muscle cells is potentiated by endothelial production of NO. Also they reported that incubation of rat aorta with L-NAME reduces the increase in Ca^{2+} concentration in endothelial cells induced by SNP. These results were acquired by organ bath and confocal microscopy.

Our results also showed that the SNP-induced vasorelaxation was limited in endothelium-denuded femoral rings pre-contracted by KPSS. This result suggested that vascular smooth muscle hyperpolarization by SNP might be mediated by potassium channel activation. A similar result was reported by Callera et al. (2004), who reported that the relaxation induced by SNP in carotid artery, whether endothelium-intact or endothelium-removed, was attenuated in arteries contracted with KPSS.

5.5 Conclusion

Our results suggest that caveolar disruption by a cholesterol depleting agent caused a significant increase in the contraction response of intact rat femoral arteries to 20 K/ Bay K, resulting from: (i) the abolishment of the release of the basal NO from the ECs (ii) a consequent reduction of the effective influence of BK_{Ca} channels on L-type Ca^{2+} channels in the SMCs, so increasing the contraction force. BK_{Ca} channels may have a limited effect on smooth muscle contraction in these arteries in the absence of basal NO release.

Chapter 6 The Effect of Caveolae Disruption by M-β-CD in Femoral Arteries on the Response to Vasodilators

6.1 Aim of the chapter

The goal of the present chapter was to examine the effect of caveolae disruption by M-β-CD on intact and endothelium-denuded femoral arteries in response to several types of vasodilator agents which are thought to act via opening of BK_{Ca} channels to induce SMC relaxation.

The key findings in this chapter

- Caveolae are important for the vasorelaxation of femoral artery in response to the BK_{Ca} channel opener NS-1619.

6.2 Introduction

Membrane hyperpolarization of vascular SMCs has been shown to be an important mechanism for producing vasodilatation (Holland et al., 1996). Activation of BK_{Ca} channels can cause hyperpolarization and then vasorelaxation. BK_{Ca} channels are considered one of the most important types of potassium channels in vascular tissues, and their dual modulation by membrane potential and/or calcium sparks allows then to regulate tone in arterial smooth muscle (Brayden and Nelson, 1992). Further, BK_{Ca} channels can mediate vascular SMCs relaxation through the direct activation by several types of vasodilators, such as NS-1619 (Feher et al., 2010), or indirect activation through GPCR receptors, such as β-adrenergic receptors, which act via second messenger systems (Sadoshima et al., 1988, White et al., 2000).

Stimulation of β-adrenergic receptors by several vasodilator agents, such as isoproterenol (ISO), leads to activation of AC, resulting in an increase in intracellular cAMP concentration $[cAMP]_i$. Additionally, adenylyl Cyclase (AC) can be directly activated by forskolin (FSK). Increase in $[cAMP]_i$ activates cAMP-dependent protein kinase (also known as protein kinase A, PKA), allowing it to phosphorylate BK_{Ca} channels. Phosphorylation by PKA results in BK_{Ca} channel activation, with the consequent hyperpolarization, closure of VDCCs, reduced global $[Ca^{2+}]_i$ and vasodilation (Sadoshima et al., 1988, White et al., 2000). On the other hand, increased intracellular cGMP through stimulation of soluble guanylate cyclase (sGC) by NO, leads to increases in intracellular cGMP concentration $[cGMP]_i$. sGC can also be activated by nitric oxide donors, such as SNP (Khan et al., 1998, Robertson et al., 1993). Increased $[cGMP]_i$ activates cGMP-dependent protein kinase (also known as protein kinase G, PKG). This can also phosphorylate and activate BK_{Ca} channels, inducing vascular SMC relaxation (Khan et al., 1998, Robertson et al.,

1993). In this regard, it has also been demonstrated that cAMP-stimulating agents can increase the activity of BK_{Ca} channels through cross-activation of PKG in vascular SMCs (White et al., 2000).

As well as activating BK_{Ca} channels through protein phosphorylation, activation of PKA and PKG by cAMP and cGMP-stimulating agents can lead to an increase in the activity of BK_{Ca} channels via increasing the frequency of local Ca^{2+} sparks through RyR channels in the SR (Porter et al., 1998). Additionally, PKA and PKG also increase activity of the SR Ca^{2+}-ATPase (SERCA), which leads to transfer of Ca^{2+} from the cytosol of the cell to the lumen of the SR. This occurs through phosphorylation of phospholamban, which then dissociates from SERCA, allowing it to pump Ca^{2+} into the SR more quickly (Porter et al., 1998).

In this chapter, I will use myography to assess the effect of caveolae disruption by M-β-CD on the femoral artery vasorelaxation in response to vasodilators known to activate BK_{Ca} channels.

6.3 Results

The effect of caveolae disruption on the response of femoral artery to three types of vasodilators was studied with myography.

6.3.1 The effects of caveolar disruption by M-β-CD on intact and endothelium-denuded femoral artery vasorelaxant response to NS-1619

This experimental series tested the hypothesis that the femoral artery vasorelaxation response to the BK_{Ca} channel opener NS-1619 would be attenuated post-caveolar disruption.

6.3.1.1 Experimental protocol A

The first protocol was designed to assess the effect of endothelial removal on the vasorelaxant response to NS-1619. Arteries were pre-constricted with 20 K/ Bay K, and, at the plateau of the maximum contraction to 20 K/ Bay K, ACh (10 μM) was added to the myography chamber to check the functional integrity of the endothelium. Vessels were re-contracted with 20 K/ Bay K, and, at the plateau to 20 K/ Bay K contraction, cumulative doses of NS-1619 (0.1 μM, 0.3 μM, 1 μM, 3 μM, 10 μM and 30 μM, and 100 μM) were added to the chamber to induce concentration-dependent vasorelaxation in endothelium-intact rings **(figure 6.1 A)**. Afterword, the endothelium was mechanically removed from vessels (see 2-3-2 in chapter 2). Then, vessels were re-contracted with 20 K/ Bay K and ACh (10 μM) added to check absence of the endothelium. Vessels were re-contracted with 20 K/ Bay K, and at the plateau to 20 K/ Bay K contraction, cumulative doses of NS-1619 were added to induce concentration-dependent vasorelaxation **(figure 6.1 A)**. Vehicle controls

showed that at the highest dose of NS-1619 (DMSO = 1%) the arteries relaxed and therefore these data have been omitted from the concentration-response curves.

6.3.1.2 Experimental protocol B

This protocol was designed to assess the effect of caveolar disruption by M-β-CD on the vasorelaxant response to NS-1619 in endothelium-intact artery rings. Endothelium-intact arteries were contracted with 20 K/ Bay K, and, at the plateau of the contraction, cumulative doses of NS-1619 (0.1 μM-100 μM) were added to induce concentration-dependent vasorelaxation **(figure 6.2 A)**. Vessels were then incubated with M-β-CD (5 mM) for 1 hour to disrupt caveolae. Vessels were re-contracted with 20 K/ Bay K and cumulative doses of NS-1619 added to induce concentration-dependent vasorelaxation **(figure 6.2 B)**.

6.3.1.3 Experimental protocol C

To assess the effect of caveolar disruption by M-β-CD on the response to NS-1619 after endothlium removal, endothelium-denuded arteries were contracted with 20 K/ Bay K, and cumulative doses of NS-1619 (0.1-100 μM) were added to induce concentration-dependent vasorelaxation **(figure 6.3 A)**. Vessels were then incubated with M-β-CD (5 mM) for 1 hour, re-contracted with 20 K/ Bay K and cumulative doses of NS-1619 added to induce vasorelaxation **(figure 6.3 A)**.

6.3.1.4 Experimental protocol D

To investigate the membrane permeability mechanisms involved in NS-1619 vasorelaxation KPSS was used to contract vessels. At the plateau of KPSS contraction cumulative doses of NS-1619 were added to the myograph chamber to

induce concentration-dependent vasorelaxation in endothelium-intact rings **(figure 6.4 A)**.

6.3.1.5 Data analysis

The force response (in mN) to cumulative doses of vasodilator was measured in rat femoral artery rings pre-constricted with KPSS and/or 20 K/ Bay K. Responses are expressed as the fractional relaxation, that is the fraction of the maximum contraction to either KPSS and/or 20 K/ Bay K obtained at a given concentration of vasodilator. Experiments were performed at 7 concentrations (0.1-100 μM). All values are expressed as mean ± SE. Student's *t*-test for paired samples was used to compare values.

6.3.1.5.1 Results

NS-1619 (0.1-100 μM) caused concentration-dependent relaxation in endothelium-intact (control) arteries contracted with 20 K/ Bay K **(figure 6.1 A)**. Relaxation was transient at lower concentrations of NS-1619 and sustained at higher concentrations. In the endothelium-denuded rings, no transient dilation was seen at lower doses of NS-1619 (0.1–3 μM), while higher doses (10-100 μM) still caused relaxation. Concentration-response curves show that the vasorelaxation response to NS-1619 was significantly inhibited after removal of the endothelium **(figure 6.1 B)** at 0.1, 0.3, 1 and 30 μM NS-1619.

In endothelium-intact rings treated with M-β-CD **(figure 6.2 A)**, doses of NS-1619 from 0.1 to 30 μM now caused a sustained increase in the force. The concentration-effect curves show that the vasorelaxation response to NS-1619 in the endothelium-

intact artery was significantly inhibited following exposure to M-β-CD at 1, 3, 10 and 30 μM NS-1619 (**figure 6.2 B**).

In endothelium-denuded rings treated with M-β-CD there were less obvious changes in the response to NS-1619 **(figure 6.3 A)**. Concentration-effect curves show the vasorelaxation response to NS-1619 was only significantly attenuated at 1 μM NS-1619 following the treatment with M-β-CD **(figure 6.3 B)**.

To investigate the role of K^+ channels in the NS-1619 relaxation, arteries were induced to contract with KPSS **(figure 6.4 A)**. In endothelium-intact rings contracted with KPSS, the vasorelaxation response to NS-1619 was slight, with maximum fractional relaxation responses reaching only 0.60±0.08 **(figure 6.4 B)**. This result indicated that NS-1619 is only partially effective in relaxing KPSS contractions.

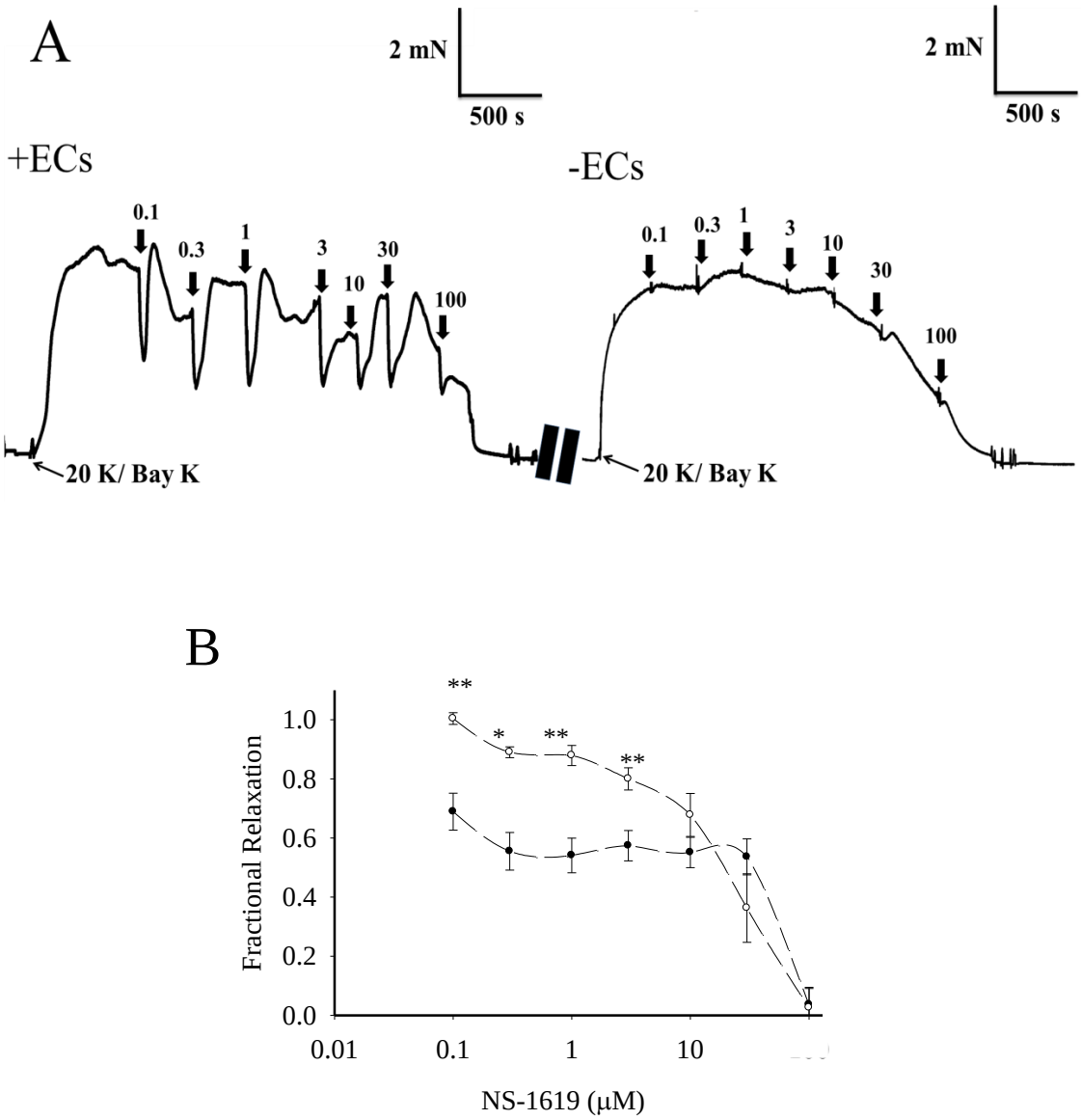

Figure 6.1. Effect of NS-1619 (0.1 - 100 μM) in femoral artery pre-contracted with 20K/ Bay K before and after endothelial removal. A. Recordings show response of control (endothelium-intact) rings and endothelium-denuded artery rings to cumulative doses of NS-1619. **B**. Concentration-response curve for NS-1619 in endothelium-intact rings (●) and endothelium-denuded rings (○). Data are expressed as fractional relaxation. Significance was established using Student's *t*-test *; P<0.05, **; P<0.01**,** *n*=6.

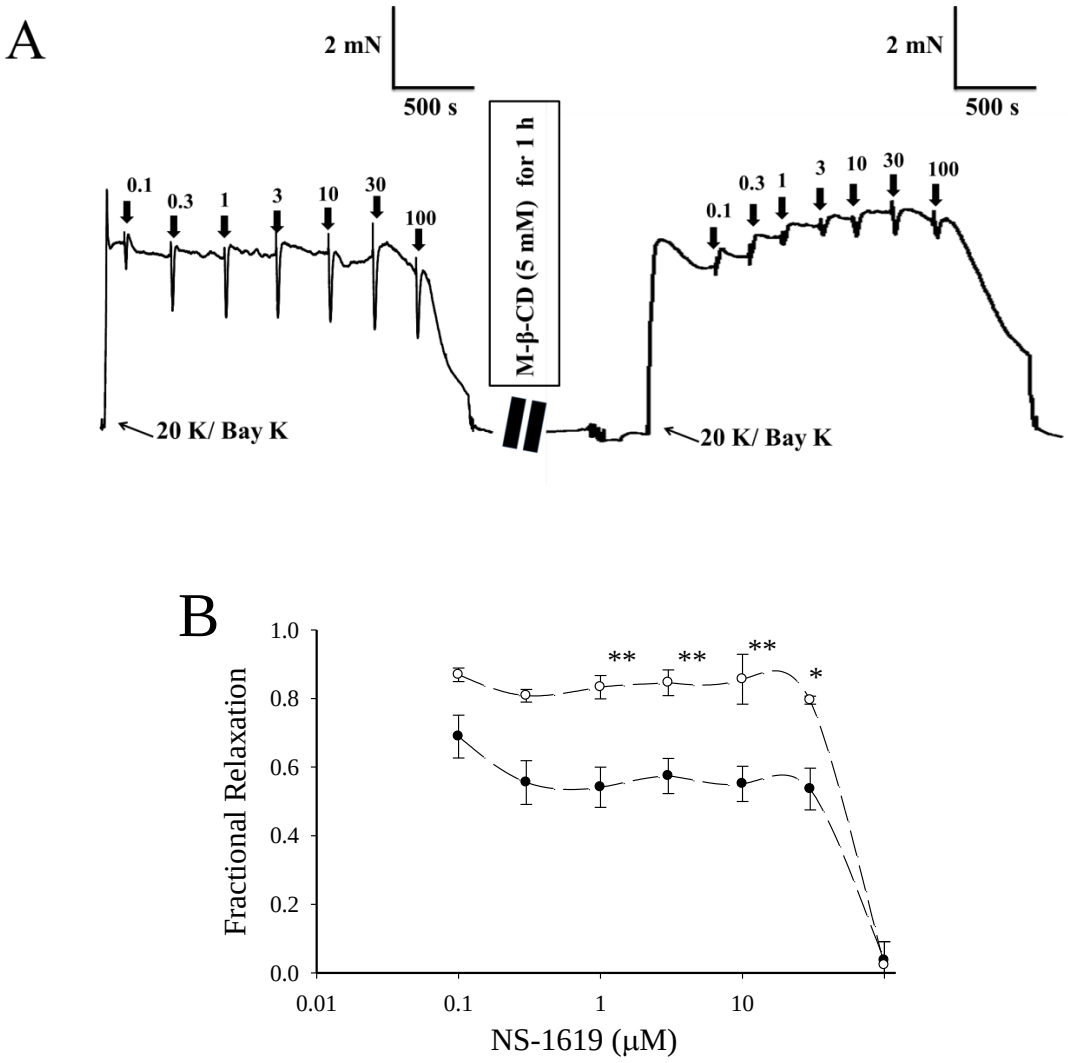

Figure 6.2. Effect of M-β-CD on NS-1619 relaxation of femoral artery. A. Recordings show effect of NS-1619 (0.1 - 100 μM) on control (endothelium-intact) rings before and after the treatment with M-β-CD. **B**. Concentration-response curve for NS-1619 in endothelium-intact artery before (●) and after (○) M-β-CD treatment. Data for before M-β-CD treatment are reproduced from figure 1B for comparison. Data are expressed as fractional relaxation. Significance was established using Student's *t*-test *; P<0.05, **; P<0.01, *n*= 6.

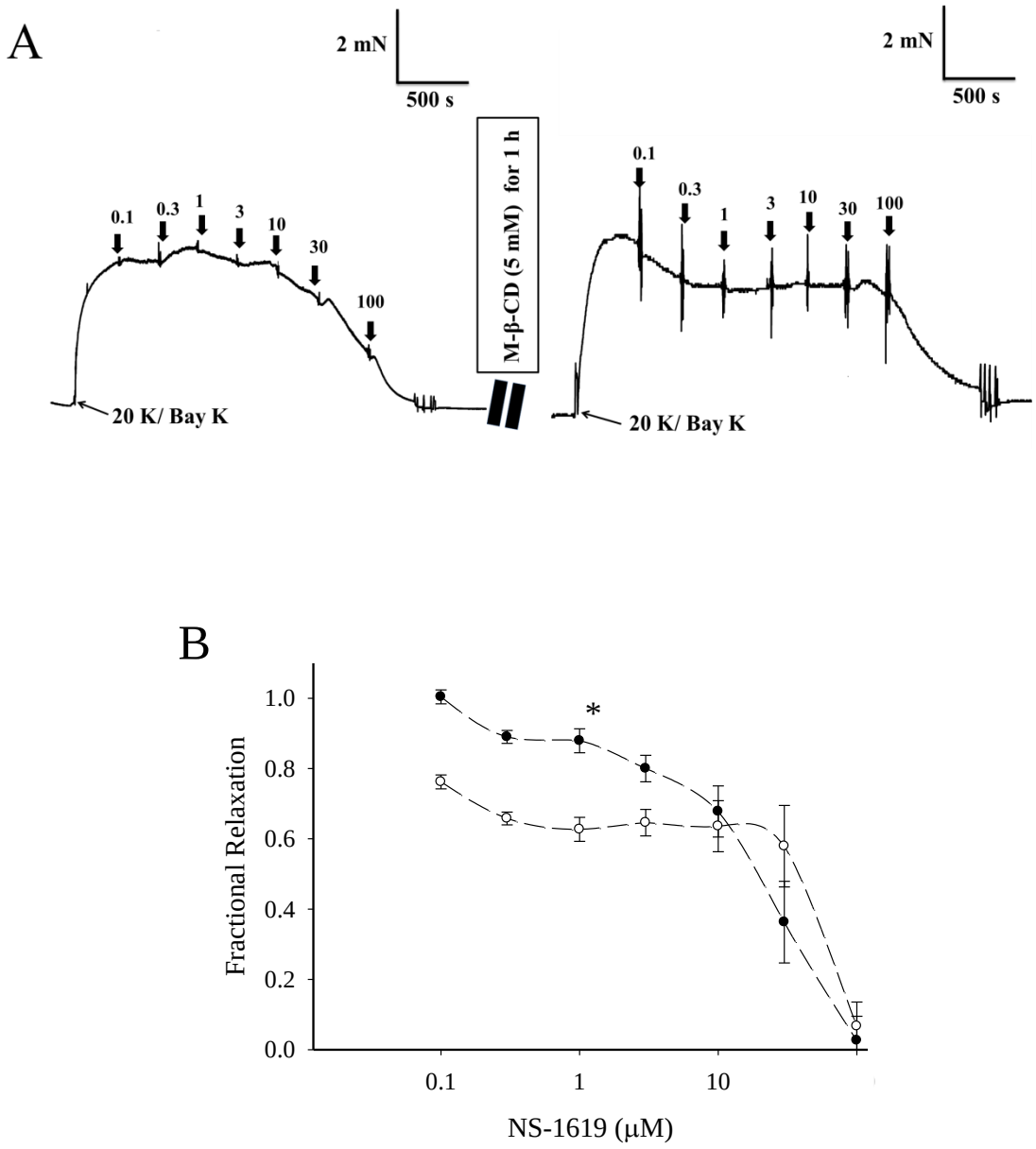

Figure 6.3. Effect of M-β-CD on NS-1619 induced relaxation of endothelium-denuded femoral artery. A. Recordings show effect of NS-1619 (0.1 - 100 μM) on endothelium-denuded rings before and after the treatment with M-β-CD. **B**. Cumulative concentration-response curve for NS-1619 in endothelium-denuded rings before (●) and after (○) treatment with M-β-CD. Data for before M-β-CD treatment and are reproduced from figure 6.1 B for comparison. Data are expressed as fractional relaxation. Significance was established using Student's *t*-test; *; P<0.05**,** *n*= 6.

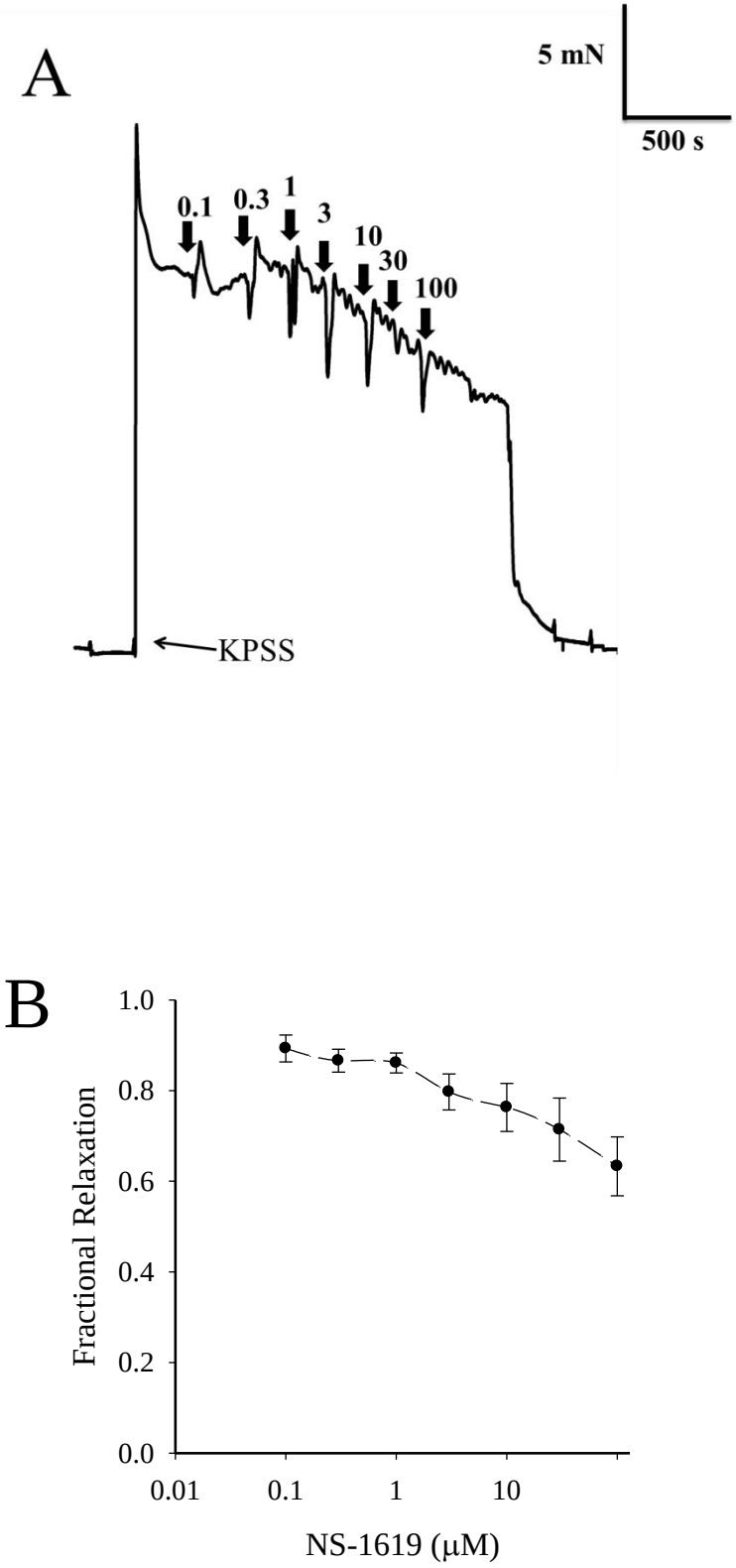

Figure 6.4. NS-1619 relaxation of KPSS contractions in rat femoral artery. A. Experimental trace shows vasorelaxation in an artery pre-contracted with KPSS. NS-1619 (0.1 to 30 μM) produced a slight relaxation **B**. Mean data expressed as fractional relaxations, *n*= 4.

6.3.2 The effects of caveolar disruption by M-β-CD on intact and endothelium-denuded femoral artery vasorelaxant response to isoproterenol

Isoproterenol (ISO) binds β-adrenergic receptors to cause vasodilation. Binding results in activation of adenylate cyclase, generation of cAMP, and activation of PKA, which may cause vasodilation by activating BK_{Ca} channels (see Introduction to this chapter). This experiment was designed to test the hypothesis that the femoral artery vasorelaxation response to ISO would be attenuated post-caveolar disruption.

6.3.2.1 Experimental protocol

The arteries were pre-constricted with 20 K/ Bay K, and, at the plateau of the 20 K/ Bay K contraction, cumulative doses of ISO (0.1 μM, 0.3 μM, 1 μM, 3 μM, 10 μM, 30 μM, and 100 μM) were added to induce concentration-dependent vasorelaxation in endothelium-intact rings and in endothelium-denuded rings before and after treatment with M-β-CD (5 mM) for 1 hour to disrupt caveolae **(figures 6.5 and 6.6)**. To provide evidence for the membrane permeability mechanism and for comparison, the artery rings were contracted with KPSS, and, at the plateau of the contraction, cumulative doses of ISO were added to induce concentration-dependent vasorelaxation in endothelium-denuded rings **(figure 6.7 A)**.

6.3.2.2 Analysis

In endothelium-intact arteries pre-contracted with 20 K/ Bay K, ISO (0.1-100 μM) caused partial relaxation at low concentrations (0.1 -10 μM) **(figure 6.5 A and 6.5 C**). At higher concentrations of ISO (30-100 μM) contraction was seen. After removal of the endothelium, ISO still relaxed the artery rings **(figure 6.5 B)**. However, ISO relaxations were reduced by endothelial removal at ISO

concentrations between 3-100 μM **(figure 6.5 C)**. In endothelium-denuded arteries, caveolar disruption with M-β-CD had little effect on the overall pattern of the response to ISO **(figure 6.6**). Vasorelaxation in response to ISO was absent in endothelium-denuded arteries contracted with KPSS **(figure 6.7)**. The latter result suggests K^+ channel activation may be involved in ISO relaxations.

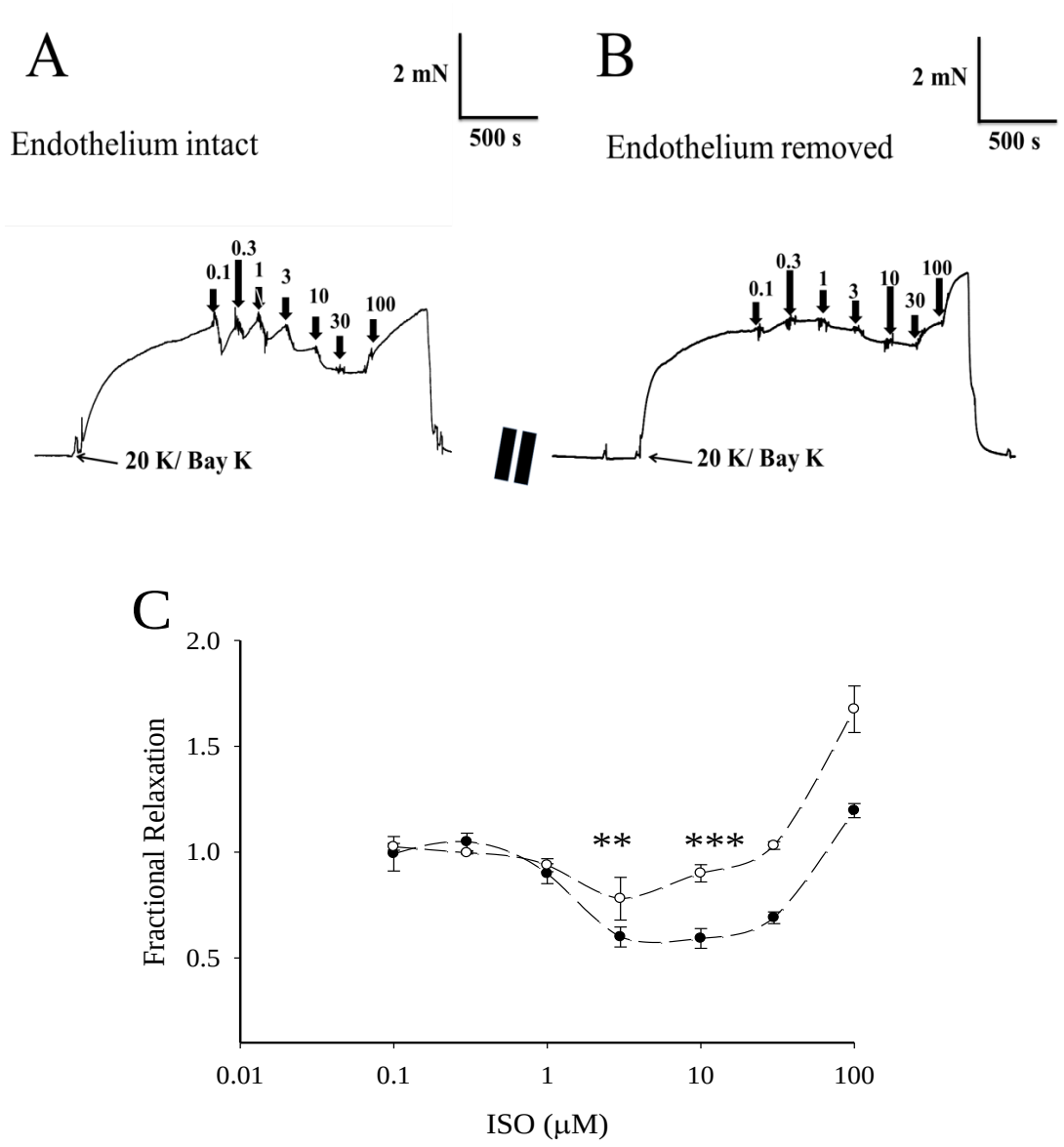

Figure 6.5. Effect of isoproterenol on rat femoral artery before and after endothelium removal. Experimental traces shows the effect of ISO (0.1 - 100 μM) in an artery contracted with 20K/ Bay K in **A.** Control (endothelium-intact) rings ,and **B.** Endothelium-denuded arteries. **C**. Concentration-response curve for ISO before (●) and after (○) endothelial removal. Data are expressed as fractional relaxation. Significant was established using Student's *t*-test *; P<0.05, **; P<0.01; ***; P<0.001**,** *n*= 6.

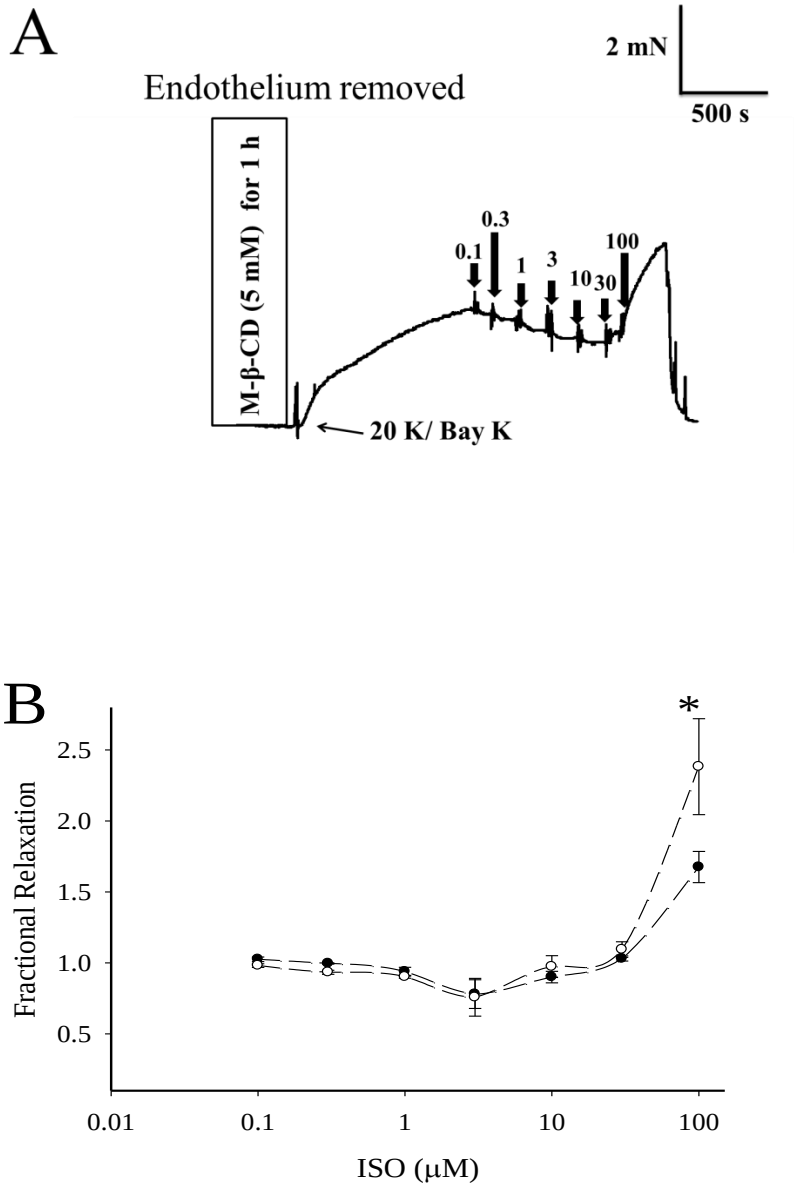

Figure 6.6. Effect of M-β-CD on isoproterenol relaxations in endothelium-denuded rat femoral artery. A. Experimental traces show the effect of ISO (0.1 - 100 μM) on arteries after treatment with M-β-CD. **B**. Concentration-response curve for ISO in endothelium-denuded rings before (●) and after (○) treatment with M-β-CD. Data are expressed as fractional relaxations. Significance was established using Student's *t*-test *; P<0.05**,** *n*= 6.

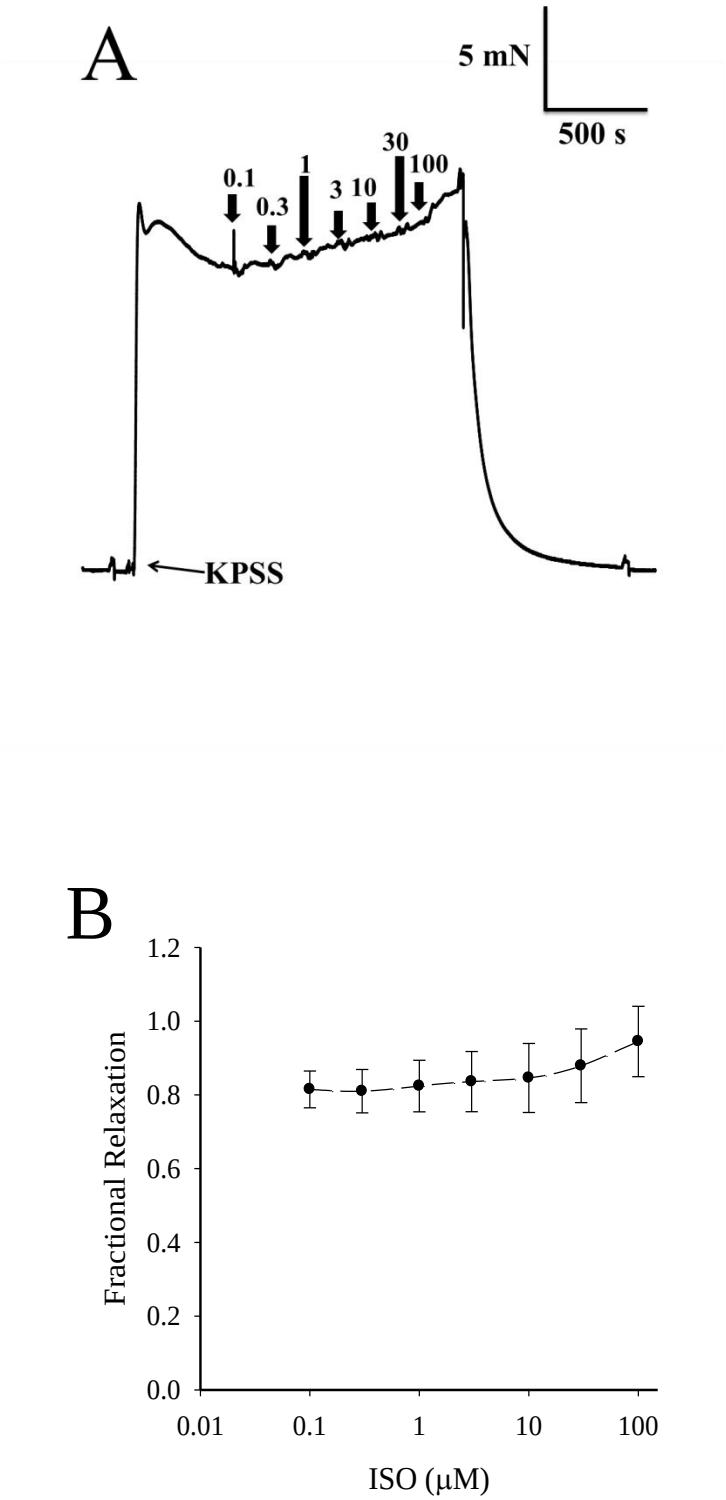

Figure 6.7. Absence of isoproterenol relaxation of KPSS contractions in rat femoral artery. A. Experimental trace shows effect of ISO (0.1-100 μM) in an artery pre-contracted with KPSS. **B**. Mean data expressed as fractional relaxations, *n*= 6.

6.3.3 The effects of caveolar disruption by M-β-CD on femoral artery vasorelaxant response to forskolin

In the previous section I have studied the ability of ISO, an AC/cAMP/PKA coupled vasodilator, to induce vasorelaxation in femoral arteries, and studied the effects of caveolar disruption by M-β-CD on this relaxation. However, the action of ISO appeared complex, with relaxations at low concentrations and contractions at higher concentrations **(figure 6.5)**. Furthermore, the relaxing action of ISO depended partly on the endothelium. In order to simplify the experiments, FSK was used to directly activate AC to induce vasorelaxation, thus by-passing receptor(s)-ISO interaction. ECs were mechanically removed. The experiment was designed to test the hypothesis that caveolar disruption by M-β-CD would attenuate vasorelaxation in femoral artery in response to FSK.

6.3.3.1 Experimental protocol

The endothelium was mechanically removed from vessels (see 2-3-2 chapter 2). Vessels were contracted with 20 K/ Bay K, and, at the plateau of the contraction, cumulative doses of FSK (0.1 μM, 0.3 μM, 1 μM, 3 μM, 10 μM, 30 μM, and 100 μM) were added to the chamber to induce concentration-dependent vasorelaxation **(figure 6.8 A)**. Vessels were then incubated with M-β-CD (5 mM) for 1 hour, re-contracted with 20 K/ Bay K, and cumulative doses of FSK were added to induce concentration-dependent vasorelaxation **(figure 6.8 B)**.

6.3.3.2 Analysis

In 20 K/Bay K contracted arteries, FSK (0.1-100 μM) produced full relaxation **(figure 6.8 A)**. However, FSK caused similar concentration dependent relaxation of

arteries whether before or after the treatment with M-β-CD **(figure 6.8 B)**. Although BK_{Ca} channels are known to be activated by PKA, further experiments are required to determine the role of BK_{Ca} channels in FSK-induced vasodilation in this artery, and effects of caveolar disruption on this process.

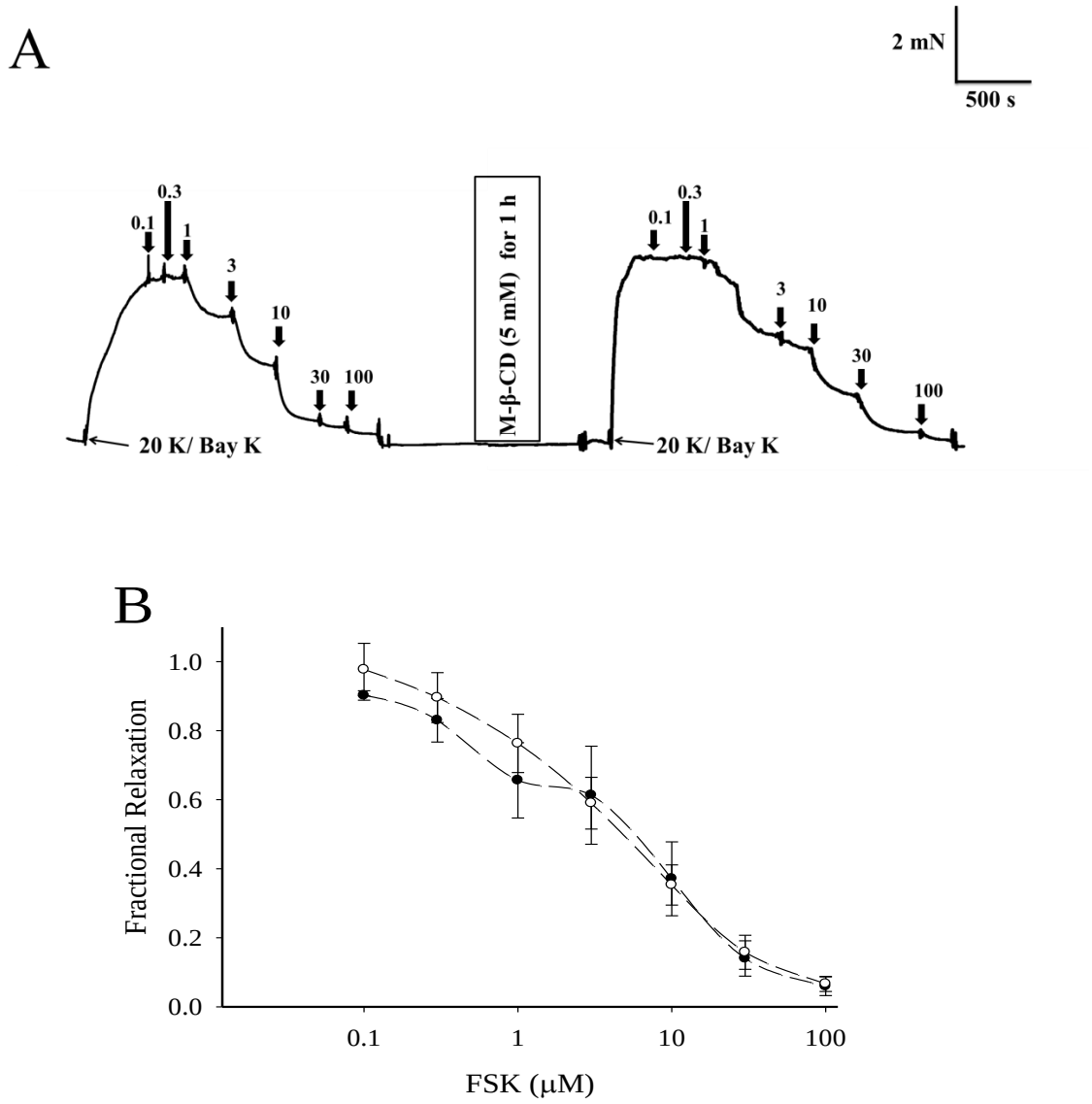

Figure 6.8. Effect of FSK (0.1 - 100 μM) in rat femoral artery pre-contracted with 20 K/ Bay K. A. Recordings show endothelium-denuded rings before and after the treatment with M-β-CD. **B**. Concentration-response curve for FSK before (●) and after (○) treatment with M-β-CD. Data are expressed as fractional relaxation. Results were not statistically significantly different at any concentration of FSK**,** *n*= 8.

6.4 Discussion

The overall goal of this in vitro study was to assess the involvement of caveolae in inducing vasorelaxation of femoral arteries in response to NS-1619, ISO, and FSK, all of which are known to activate BK_{Ca} channels. For this purpose, myography was used to assess the vasorelaxation response before and after caveolae disruption by M-β-CD. Moreover, these vasodilators were tested for their efficacy before and after removing the endothelial layer, to determine whether the vasorelaxation was dependent on endothelial factors. NS-1619 was chosen based on its published ability to directly activate the BK_{Ca} channels and then cause vasorelaxation (Holland et al., 1996). ISO was chosen as this activates β-adrenergic receptors, increases vascular cAMP levels and then activates BK_{Ca} channels (White et al., 2000, Tanaka et al., 2003). FSK was chosen to induce the vasorelaxation as it directly activates AC.

Initially, I tested the effect of the known BK_{Ca} channel activator NS-1619 to induce vasorelaxation in endothelium-intact artery rings. NS-1619 (0.1-100 μM) led to full relaxation of arteries pre-contracted with 20 K/ Bay K **(figure 6.1 A)**, while it was only partially effective in relaxing KPSS contraction, up to a maximal relaxation of 0.60±0.08 **(figure 6.4)**. These results suggest that the femoral artery is significantly sensitive to K^+ channel activation to induce vasorelaxation under control conditions. In relation to the 20 K/ Bay K contraction, Bay K-8644 is dependent on its ability to promote Ca^{2+} influx via L-type VDDCs, thus inducing contraction. VDCCs can be closed via the membrane hyperpolarisation that follows activation of BK_{Ca} channels (see chapter 5*)*. In contrast, when arteries were contracted with KPSS, the potassium gradient across the plasma membrane is reduced and the membrane is completely depolarized. In this situation, activation of potassium channels will have limited effective on membrane potential, consequently limited effect on vascular tone and

therefore, potassium channel opening will not be effective to induce vasodilation (Meisheri et al., 1990). The findings of the current study are partially consistent with those of (Holland et al., 1996), who reported that the NS-1619 induced concentration-dependent relaxation of rat basilar artery rings contracted with both 5-HT and histamine. However, they also reported that NS1619 produced concentration-dependent relaxation artery contracted with a salt solution containing 80 mM K^+. This latter result disagrees with our finding that NS1619 produce only partial relaxation of rat femoral artery contracted with KPSS.

Removal of the endothelium from femoral artery abolished the transient vasorelaxation in response to NS-1619 at low concentrations (0.1 to 10 μM) whilst leaving the relaxation at higher concentrations (100 μM) unchanged **(figure 6.1)**. In this experiment, endothelium removal might have inhibited the femoral artery relaxation at low concentrations of NS-1619 by abolishing release of NO or other endothelium-dependent vasodilator. The findings of the current study are consistent with those of (Feher et al., 2010), who reported endothelium-dependent vasorelaxation in rat aorta in response to NS-1619. In contrast (Feng et al., 2008) showed that NS-1619 induced relaxations of human coronary arterioles were not altered with endothelium removal, suggesting BK_{Ca} channel function is endothelium-independent. Similarly (Geary et al., 1998) reported that NS-1619 induced vasorelaxation in intact and endothelium-denuded rat tail artery rings.

Further studies investigated the effect of caveolae disruption on NS-1619 relaxation. In endothelium-intact rings treated with M-β-CD, vasorelaxation was markedly inhibited compared to the control in response to doses of NS-1619 from 0.1 to 30, but the artery fully relaxed with the highest dose (100 μM) **(figure 6.2)**. The effects of M-β-CD at low doses of NS-1619 may be due to loss of a vasoactive compound

produced by the endothelium such as NO, and/or loss of MEGJs, although further experiments, such as pre-incubation of the artery with a NOS inhibitor such as L-NAME, are required to test this hypothesis. In endothelium-denuded rings treated with M-β-CD **(figure 6.3)** the vasorelaxation was partially inhibited compared to that seen before treatment with M-β-CD, but the relaxation was only significantly different at 1 μM NS-1619.

Overall, the results support the idea that low concentrations of NS-1691 cause an endothelium-dependent vasorelaxation of rat femoral artery and that this relaxation is dependent on the presence of caveolae. The results may point to a role for endothelial BK_{Ca} channels in vasorelaxation to NS-1619. This would be consistent with the immunohistochemistry and immunocytochemistry results in chapter 4 showing the presence of BK_{Ca} channels in endothelial cells. However, discovering the precise role of emdothelial BK_{Ca} channels requires additional experiments, such as pre-incubation of arteries with BK_{Ca} channel inhibitors such as TEA^{+} and IBTX before NS-1619 application.

In contrast to NS-1619, ISO relaxes arteries via activation of second messenger systems. In a step to find out if vasorelaxation response to ISO would be attenuated post-caveolar disruption the vasorelaxation in response to ISO was tested before and after removal of the endothelium, and after caveolae disruption in endothelium-denuded rings. Our results show that ISO in endothelium-intact arteries caused relaxation at low concentrations (0.1-10 μM) while at higher concentrations (30-100 μM) contraction was seen **(figure 6.5 A).** Higher concentrations (30-100 μM), may lead to activation of other vasoconstrictor receptors, such as α-adrenoreceptors or even 5-HT receptors. Antagonists of these receptors could be used to investigate this

possibility. After removal of the endothelium, ISO relaxations were reduced at ISO concentrations between 3-100 µM **(figure 6.5 B)**.

In endothelium-denuded arteries, caveolar disruption with M-β-CD had little effect on the overall pattern of the response to ISO **(figure 6.6**). Vasorelaxation in response to ISO was abolished in endothelium-denuded rings pre-contracted with KPSS **(figure 6.7)**. This suggests K^+ channel activation may be involved in ISO relaxations. The findings of the current study are partially consistent with those of (Yoshida et al., 1999), who reported marked inhibition of vasorelaxation in pulmonary arterioles of dogs in response to ISO after removal of the endothelial layer.

In an attempt to by-pass the complexities of receptor(s)-ISO interaction, AC was directly activated by forskolin to induce vasorelaxation (Vanhoutte, 1989). FSK fully relaxed arteries before and after M-β-CD treatment and no significant difference was seen following treatment with M-β-CD **(figure 6.8)**. This result suggested that vasorelaxation in the femoral artery in response to FSK is endothelium-independent and caveolae disruption has little effect on the relaxation. The findings of the current study are consistent with those of (Yoshida et al., 1999), who reported that the FSK induced vasorelaxation in endothelium-intact and endothelium-denuded pulmonary artery of dog, and that these relaxations were endothelium-independent.

6.5 Conclusion

Although several studies have shown BK_{Ca} channel-mediated vasorelaxation in blood vessels (Meisheri et al., 1990, Holland et al., 1996, Geary et al., 1998), the effect of caveolae disruption in response to different vasodilators has not been reported, at least in the femoral artery. This study demonstrated for the first time that

the integrity of caveolae are important for the vasorelaxation of femoral artery in response to the BK_{Ca} channel opener NS-1619. The relative role of endothelial and smooth muscle cell BK_{Ca} channels in this relaxation requires further study.

Chapter 7

Chapter 8 Final Discussion

8.1 Overview of thesis results

This study was prepared to assess the functional role of caveolae in regulating the contractility of rat femoral artery, with particular emphasis on how the signature proteins of caveolae, the caveolins, may control the activity of Ca^{2+} and voltage-activated large conductance potassium channels and thus vascular contractility.

Femoral artery was chosen in this study due to the importance of this blood vessel in delivering blood and oxygen to the muscles and superficial tissues of the legs, especially during exercise (Mulvany and Aalkjaer, 1990). Many studies have been carried out to investigate the role of caveolae on vascular tissues, using several different techniques (Razani and Lisanti, 2001b, Ostrom and Insel, 2006). However, this is the first study to look specifically at the effects of caveolae in regulating contractility in femoral arteries.

In this thesis I have addressed my aims. Initially, I wanted to establish the presence of caveolae using transmission election microscopy, and then to look at the effect of cholesterol removal by cholesterol depleting agents on caveolae in both ECs and SMCs of femoral artery. TEM has been used extensively to study caveolae in vascular tissues (Minshall et al., 2003, Shaw et al., 2006). The results showed that caveolae were present in both ECs and SMCs, and when cholesterol was depleted the caveolae disappeared. Several contractility studies were designed to examine the effect of caveolae on BK_{Ca} channel function in the presence and absence of endothelial layers in chapters 5 and 6. However, to establish a method to identify the presence of endothelium in the artery, histology was performed before and after the

removal of endothelium. It was shown histologically that the endothelium layer can be removed by gentle rubbing the interior lumen of the artery. After confirming the presence of caveolae by TEM, other techniques have been used to investigate the presence and the co-expression of BK_{Ca} channels to the caveolar domain in the cell membrane of SMCs and ECs. These included the methods of immunohistochemistry, immunocytochemistry, and Western blot. BK_{Ca} channels were found to be co-expressed with cav-1 and cav-3 in the SMC layer both at the tissue level and in individual SMCs, and co-expression of BK_{Ca} channels with cav-1 was seen at the tissue level in ECs in rat femoral artery. One explanation for these results is that caveolin scaffolding domains serve as anchor sites for BK_{Ca} channels within caveolae in vascular cells. These findings support the results in the preceding chapter, which showed caveolae in the cell membrane of SMCs and ECs of rat femoral artery tissue using TEM, and provide novel background information for understanding the physiological function of BK_{Ca} channels in the regulation of vascular contractility.

In the next section of my thesis, in order to determine the physiological role of caveolae in femoral arterial contractility, myography techniques were used. The effects of the removal of cholesterol from the SMC and EC cell membrane using M-β-CD, which would disrupt caveolae, were studied. Prior to my thesis, some studies had investigated the effect of caveolae disruption by M-β-CD in regulation of arterial contraction and relaxation (Darblade et al., 2001, Xu et al., 2007). Cholesterol depletion by M-β-CD causes inhibition of release of NO from ECs (Darblade et al., 2001). Cholesterol depletion can also cause increased contraction in response to stimulation with agonists such as PE (Tabernero et al., 1996). Furthermore, some of these studies showed that when NO release is inhibited by blocking eNOS activity,

this has a similar effect to M-β-CD, also causing increased contraction in response to contractile agonists (Jiang et al., 2005). On the other hand, studies in single SMCs using patch clamp show a direct effect of cholesterol depletion by M-β-CD on inward Ca^{2+} currents, causing an increased influx of Ca^{2+} via VDDCs and a decreased efflux of K^+ through BK_{Ca} channels (Prendergast et al., 2010). These results therefore suggest caveolar depletion can have effects on both ECs and SMCs (Bialecki and Stinson-Fisher, 1995).

Caveolar disruption by the cholesterol depleting agents M-β-CD and filipin caused a significant increase in the contraction force in response to 20 K/ Bay K in endothelium-intact rat femoral arteries (chapter 5). This could result from: (i) Reduced release of a vasodilator, or enhanced release of a vasoconstrictor, from ECs. (ii) loss of communication between ECs and SMCs (MEGJs). (iii) A direct effect of caveolar disruption on SMCs, such as abolishment of the effective influence of BK_{Ca} channels on L-type Ca^{2+} VDDC. As there was no significant change in force development to 20 K/ Bay K when I compared endothelium-denuded arteries before and after treatment with M-β-CD, this suggests that the main contractile effects of caveolar disruption were due to changes in the synthesis or release of an endothelial factor.

Further experiments were designed to assess the role of NO in the changes in contractility seen after caveolar disruption by M-β-CD. I compared the contraction of endothelium-intact femoral arteries in response to 20 K/ Bay K in the presence of the NO synthase inhibitor L-NAME, before and after treatment with M-β-CD. These results showed that the incubation with L-NAME caused the arteries to contract more to 20 K/ Bay K. When the arteries were subsequently incubated in M-β-CD, this, as had previously been shown, also enhanced 20 K/ Bay K contraction.

However, L-NAME no longer had a contractile effect after M-β-CD treatment (i.e. the two effects were not additive). In addition, there was impaired relaxation to ACh, whether after treatment with M-β-CD or incubation with L-NAME, as previously shown by many groups (Darblade et al., 2001, Xu et al., 2007). Overall, these results suggested that the influx of Ca^{2+} via L-type channels in response to 20 K/ Bay K causes the contraction of SMCs. The abolishment of a vasodilator effect of NO due to caveolae disruption by M-β-CD and/or blocking eNOS by L-NAME increased the contraction in response to 20 K/ Bay K. Therefore inhibition of synthesis and/or release and/or diffusion of NO by caveolar disruption caused aberrations in endothelium-dependent relaxation, thus increasing the contraction. The increase of force by eNOS inhibition also shows basal release of endogenous NO in this artery segment.

To directly investigate the role of BK_{Ca} channels in the increased arterial contraction in response to caveolar disruption I compared the contractions of endothelium-intact arteries in response to 20 K/ Bay K before/after the treatment with M-β-CD in the presence of TEA^+ and IBTX, selective blockers for BK_{Ca} channels. Incubation of artery rings with TEA^+ or IBTX caused an augmentation in the contraction to 20 K/ Bay K. After treatment with M-β-CD, TEA^+ or IBTX no longer had a significant contractile effect. I interpret these results as follows: in the absence of M-β-CD basal NO release from the endothelium leads to activation of BK_{Ca} channels in smooth muscle cells. After M-β-CD treatment, NO release is inhibited and therefore there is less influence of SMC BK_{Ca} channels on femoral artery contraction. TEA^+ and IBTX have the same apparent effect as M-β-CD as they cause inhibition of BK_{Ca} channels, in this case by directly binding and inhibiting channel activity.

The possibility of an effect of SMC caveolar disruption on BK_{Ca} channels should not be overlooked. Our results demonstrated a (small) increase in the contractile force in response to 20 K/ Bay K in endothelium-denuded arteries after treatment with M-β-CD. This result might indicate that the contractile function of vascular SMCs was partly altered by treatment with M-β-CD. BK_{Ca} channels might be re-distributed away from the plasma membrane adjacent to the sarcoplasmic reticulum after the treatment with M-β-CD, due to disruption of the caveolar-SR microdomain. The increase in contraction might therefore be partly due to the absence of the effective influence of Ca^{2+} 'sparks' on BK_{Ca} channels, hence causing depolarisation, activation of VDCCs and increasing the contraction force. However, my results showing that endothelium removal largely abolishes the effect of M-β-CD suggest that this mechanism may not be dominant in rat femoral arteries.

The above results led to further examination of the influence of NO on BK_{Ca} channels in modulating vasorelaxation in femoral artery using SNP, an NO donor. SNP has been shown to induce smooth muscle cell hyperpolarization and thus vasorelaxation via activation of BK_{Ca} channels in some vascular tissues (Bialecki and Stinson-Fisher, 1995). To test this in the rat femoral artery, I compared the relaxation of arteries to SNP before and after inhibition of BK_{Ca} channels by TEA^+ treatment. TEA^+ caused significant inhibition of relaxation.

Taken together, the results of chapter 5 provide evidence for the importance of endothelium-derived relaxing factors, specifically NO, in activating BK_{Ca} channels in SMCs, so inducing hyperpolarization and vasorelaxation of rat femoral arteries. However, it is unclear whether changes in the regulatory function of caveolae on BK_{Ca} channels have an influence on vasodilation under other conditions. So, I set out the last results chapter in my thesis to examine the role of caveolar disruption by M-

β-CD in modulating the response to several vasodilators agents which have been previously shown to activate BK_{Ca} channels.

Prior to my thesis, some studies have demonstrated the role of BK_{Ca} channel activation in mediating vasorelaxation in different blood vessels in response to NS-1619, FSK and ISO (Meisheri et al., 1990, Holland et al., 1996, Geary et al., 1998). Initially, I investigated the effect of caveolar disruption by M-β-CD on vasorelaxation of femoral artery in response to NS-1619, M-β-CD significantly inhibited vasorelaxation, indicating it may have affected the ability of BK_{Ca} channels to induce the hyperpolarization. When I compared relaxations before and after treatment with M-β-CD, the transient vasodilation seen at low concentrations of NS-1619 was reduced. This suggests that endothelium-derived relaxing factors may be important for NS-1619 vasorelaxation in this artery.

ISO was also used as a vasodilator. ISO has been shown extensively to induce vasorelaxation via activation of β-adrenergic receptors (Yoshida et al., 1999). The increased intracellular cAMP concentration ($[cAMP]_i$) and subsequent activation of PKA opens BK_{Ca} channels, inducing hyperpolarization, which leads to vasorelaxation (Ahn et al., 1995). To determine effect of caveolae disruption on vasorelaxation I compared responses before and after the treatment with M-β-CD. Although relaxations to ISO were partially reduced by M-β-CD treatment, the complex response of these arteries seen in response to ISO application, with relaxation at low concentrations and contraction at higher concentrations, made further interpretation difficult. In order to simply the experimental protocol, FSK was used to directly activate AC. However, there was no effect of caveolar disruption on FSK-induced vasorelaxation.

8.2 Physiological significance and clinical translation

It is well-known that the femoral artery has an important role in blood supply to lower part of the human body, especially during physical activity and exercise performance, which is characterized by significant cardiovascular alteration such as increase blood flow through femoral artery to distal organs.

Caveolae have been shown to be involved in the regulation of many signaling cascades, ion channels and receptors in ECs and SMCs. Furthermore, it has been shown that caveolae depletion from cell membrane of these cells leads to inhibition of the release of NO, which is important clinically and physiologically to induce vascular relaxation. Potentially, therefore, caveolar disruption can alter the function of the endothelial cells and may lead to vascular dysfunction. I found that removal of caveolae from the endothelium by M-β-CD leads to an increase in the contraction of vascular smooth muscle in response to 20 K/ Bay K. I also found that after removal of the endothelium there was no effect of M-β-CD on the contractility. This suggests the vital role of caveolae in endothelial cells in the maintenance of vascular function. In addition, caveolae disruption causes impairment of vasorelaxation via potassium channels. In contrast, I found that incubating endothelium-intact artery rings with Ch-MCD for one hour, causes attenuated contraction force generated by 20 K/ Bay K. It is known that atherosclerosis can narrow the blood vessels and block the endothelial layer resulting in vascular pathogenesis (Nordestgaard, 1996, Cohen et al., 2004). If the atherosclerosis affects the blood vessels then the vascular function may be affected.

8.3 Future work

To extend the TEM studies described in chapter 3, it was my original intention to attempt to localise BK_{Ca} channels at high resolution with immunogold staining to see, for example, whether the channels were localised to caveolae. However, results from preliminary studies were unclear. In few samples, I have seen some BK_{Ca} channels stained in caveolae, but it was not clear in other samples. Therefore, it would be of interest to increase the *n* number to confirm the exact location of BK_{Ca} channels.

To extend the contraction studies, it would be interesting to examine the role of caveolae and the BK_{Ca} channels in human arteries. Finally, in one part of my study I have incubated some endothelium intact artery rings with Ch-MCD, which attenuated the contraction force generated by 20 K/ Bay K. This might be an interesting area for further experiments, as it is a model of hypercholesterolemia.

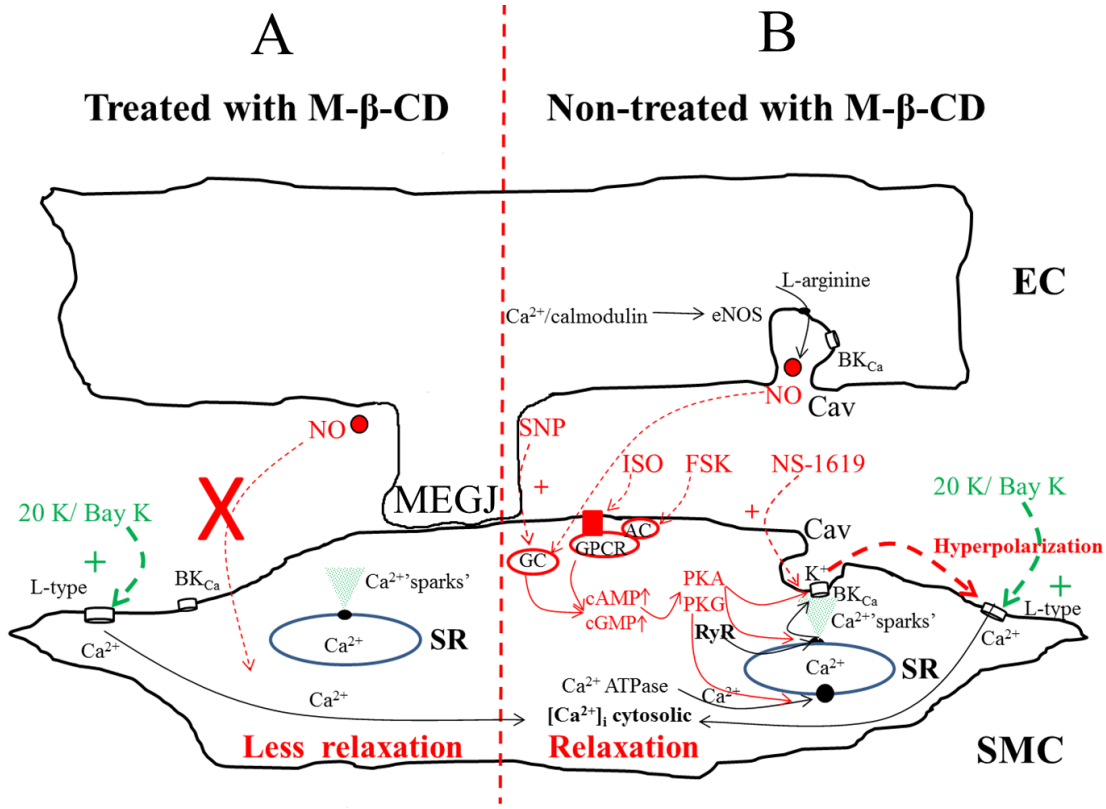

Figure 8.1. Proposed mechanisms of action of the vasodilators and basal NO on Ca^{2+} sparks, BK_{Ca} channels and MEGJ mediated hyperpolarization. A. Shows caveolae disruption by M-β-CD leads to inhibition of basal NO release from the EC. Also re-distribution of the location of the BK_{Ca} channels away from the SR in cell membrane of SMC may occur. Absence of basal NO release leads to reduced SMC relaxation, seen as a vasoconstriction. **B**. Basal NO release leads to increased production of cGMP through activated GC, which in turn stimulates PKG. Activation of PKG (and PKA) have a direct activatory effect on the BK_{Ca} channel, increasing its open probability. PKA and PKG may also act on the SR to increase Ca^{2+} sparks through RyR receptors. Increased Ca^{2+} spark activity leads to increased activity of the BK_{Ca} channel, causing hyperpolarization, which lead to closure of L-type Ca^{2+} channels. This leads to reduced cytosolic Ca^{2+} and SMC relaxation. In addition, hyperpolarization generated in ECs can be transmitted to the smooth muscle through MEGJs. Therefore, membrane hyperpolarization can cause smooth muscle relaxation through a decrease in VDCCs open probability.

References

AARONSON, P. I. & WARD, J. P. T. 2007. *The cardiovascular system at a glance,* Oxford, Blackwell.

ABOULAICH, N., VAINONEN, J. P., STRALFORS, P. & VENER, A. V. 2004. Vectorial proteomics reveal targeting, phosphorylation and specific fragmentation of polymerase I and transcript release factor (PTRF) at the surface of caveolae in human adipocytes. *Biochem J,* 383**,** 237-48.

ADEBIYI, A., NARAYANAN, D. & JAGGAR, J. H. 2011. Caveolin-1 assembles type 1 inositol 1,4,5-trisphosphate receptors and canonical transient receptor potential 3 channels into a functional signaling complex in arterial smooth muscle cells. *J Biol Chem,* 286**,** 4341-8.

AHN, D. S., JEONG, Y. K., LEE, Y. H. & KANG, B. S. 1995. Activation of Ca(2+)-activated K+ channels by beta agonist in rabbit coronary smooth muscle cells. *Yonsei Med J,* 36**,** 232-42.

ALBERTS , J. A., LEWIS J, ET AL. 2002. *Molecular Biology of the Cell. 4th edition.,* New York, New York: Garland Science.

ALIOUA, A., LU, R., KUMAR, Y., EGHBALI, M., KUNDU, P., TORO, L. & STEFANI, E. 2008. Slo1 caveolin-binding motif, a mechanism of caveolin-1-Slo1 interaction regulating Slo1 surface expression. *J Biol Chem,* 283**,** 4808-17.

ALIOUA, A., MAHAJAN, A., NISHIMARU, K., ZAREI, M. M., STEFANI, E. & TORO, L. 2002. Coupling of c-Src to large conductance voltage- and Ca2+-activated K+ channels as a new mechanism of agonist-induced vasoconstriction. *Proc Natl Acad Sci U S A,* 99**,** 14560-5.

ANDERSON, R. G. 1998. The caveolae membrane system. *Annu Rev Biochem,* 67**,** 199-225.

ANDERSON, R. G., KAMEN, B. A., ROTHBERG, K. G. & LACEY, S. W. 1992. Potocytosis: sequestration and transport of small molecules by caveolae. *Science,* 255**,** 410-1.

ARCHER, S. L., HUANG, J. M., HAMPL, V., NELSON, D. P., SHULTZ, P. J. & WEIR, E. K. 1994. Nitric oxide and cGMP cause vasorelaxation by activation of a charybdotoxin-sensitive K channel by cGMP-dependent protein kinase. *Proc Natl Acad Sci U S A,* 91**,** 7583-7.

BABIYCHUK, E. B., SMITH, R. D., BURDYGA, T., BABIYCHUK, V. S., WRAY, S. & DRAEGER, A. 2004. Membrane Cholesterol Regulates Smooth Muscle Phasic Contraction. *Journal of Membrane Biology,* 198**,** 95-101.

BAIG, A., BAO, X., WOLF, M. & HASLAM, R. J. 2009. The platelet protein kinase C substrate pleckstrin binds directly to SDPR protein. *Platelets,* 20**,** 446-57.

BARNES, K., INGRAM, J. C., BENNETT, M. D., STEWART, G. W. & BALDWIN, S. A. 2004. Methyl-beta-cyclodextrin stimulates glucose uptake in Clone 9 cells: a possible role for lipid rafts. *The Biochemical journal,* 378**,** 343-51.

BASTIANI, M., LIU, L., HILL, M. M., JEDRYCHOWSKI, M. P., NIXON, S. J., LO, H. P., ABANKWA, D., LUETTERFORST, R., FERNANDEZ-ROJO, M., BREEN, M. R., GYGI, S. P., VINTEN, J., WALSER, P. J., NORTH, K. N., HANCOCK, J. F., PILCH, P. F. & PARTON, R. G. 2009. MURC/Cavin-

4 and cavin family members form tissue-specific caveolar complexes. *J Cell Biol,* 185**,** 1259-73.
BENY, J. 1997. Electrical coupling between smooth muscle cells and endothelial cells in pig coronary arteries. *Pflugers Arch,* 433**,** 364-7.
BERGDAHL, A., GOMEZ, M. F., DREJA, K., XU, S. Z., ADNER, M., BEECH, D. J., BROMAN, J., HELLSTRAND, P. & SWARD, K. 2003. Cholesterol depletion impairs vascular reactivity to endothelin-1 by reducing store-operated Ca2+ entry dependent on TRPC1. *Circ Res,* 93**,** 839-47.
BERNATCHEZ, P. N., BAUER, P. M., YU, J., PRENDERGAST, J. S., HE, P. & SESSA, W. C. 2005. Dissecting the molecular control of endothelial NO synthase by caveolin-1 using cell-permeable peptides. *Proc Natl Acad Sci U S A,* 102**,** 761-6.
BIALECKI, R. A. & STINSON-FISHER, C. 1995. KCa channel antagonists reduce NO donor-mediated relaxation of vascular and tracheal smooth muscle. *Am J Physiol,* 268**,** L152-9.
BLAIR, A., SHAUL, P. W., YUHANNA, I. S., CONRAD, P. A. & SMART, E. J. 1999. Oxidized low density lipoprotein displaces endothelial nitric-oxide synthase (eNOS) from plasmalemmal caveolae and impairs eNOS activation. *J Biol Chem,* 274**,** 32512-9.
BOLOTINA, V. M., NAJIBI, S., PALACINO, J. J., PAGANO, P. J. & COHEN, R. A. 1994. Nitric oxide directly activates calcium-dependent potassium channels in vascular smooth muscle. *Nature,* 368**,** 850-3.
BOLTON, T. B. & IMAIZUMI, Y. 1996. Spontaneous transient outward currents in smooth muscle cells. *Cell Calcium,* 20**,** 141-52.
BONAVENTURA, D., DE LIMA, R. G., VERCESI, J. A., DA SILVA, R. S. & BENDHACK, L. M. 2007. Comparison of the mechanisms underlying the relaxation induced by two nitric oxide donors: sodium nitroprusside and a new ruthenium complex. *Vascul Pharmacol,* 46**,** 215-22.
BONAVENTURA, D., LUNARDI, C. N., RODRIGUES, G. J., NETO, M. A. & BENDHACK, L. M. 2008. A novel mechanism of vascular relaxation induced by sodium nitroprusside in the isolated rat aorta. *Nitric Oxide,* 18**,** 287-295.
BRAINARD, A. M., MILLER, A. J., MARTENS, J. R. & ENGLAND, S. K. 2005. Maxi-K channels localize to caveolae in human myometrium: a role for an actin-channel-caveolin complex in the regulation of myometrial smooth muscle K+ current. *American journal of physiology. Cell physiology,* 289**,** C49-57.
BRAYDEN, J. E. & NELSON, M. T. 1992. Regulation of arterial tone by activation of calcium-dependent potassium channels. *Science,* 256**,** 532-5.
BRENNER, R., PEREZ, G. J., BONEV, A. D., ECKMAN, D. M., KOSEK, J. C., WILER, S. W., PATTERSON, A. J., NELSON, M. T. & ALDRICH, R. W. 2000. Vasoregulation by the beta1 subunit of the calcium-activated potassium channel. *Nature,* 407**,** 870-6.
BRODUSCH, N., DEMERS, H. & GAUVIN, R. 2013. Nanometres-resolution Kikuchi patterns from materials science specimens with transmission electron forward scatter diffraction in the scanning electron microscope. *J Microsc,* 24**,** 12007.
BROWN, D. A. & LONDON, E. 1998. Functions of lipid rafts in biological membranes. *Annu Rev Cell Dev Biol,* 14**,** 111-36.

BUCCI, M., GRATTON, J. P., RUDIC, R. D., ACEVEDO, L., ROVIEZZO, F., CIRINO, G. & SESSA, W. C. 2000. In vivo delivery of the caveolin-1 scaffolding domain inhibits nitric oxide synthesis and reduces inflammation. *Nature medicine,* 6**,** 1362-7.

BURNHAM, M. P., BYCHKOV, R., FELETOU, M., RICHARDS, G. R., VANHOUTTE, P. M., WESTON, A. H. & EDWARDS, G. 2002. Characterization of an apamin-sensitive small-conductance Ca(2+)-activated K(+) channel in porcine coronary artery endothelium: relevance to EDHF. *Br J Pharmacol,* 135**,** 1133-43.

CALLERA, G. E., YOGI, A., TOSTES, R. C., ROSSONI, L. V. & BENDHACK, L. M. 2004. Ca2+-activated K+ channels underlying the impaired acetylcholine-induced vasodilation in 2K-1C hypertensive rats. *J Pharmacol Exp Ther,* 309**,** 1036-42.

CHEN, Z., BAKHSHI, F. R., SHAJAHAN, A. N., SHARMA, T., MAO, M., TRANE, A., BERNATCHEZ, P., VAN NIEUW AMERONGEN, G. P., BONINI, M. G., SKIDGEL, R. A., MALIK, A. B. & MINSHALL, R. D. 2012. Nitric oxide-dependent Src activation and resultant caveolin-1 phosphorylation promote eNOS/caveolin-1 binding and eNOS inhibition. *Mol Biol Cell,* 23**,** 1388-98.

CHENG, X. & JAGGAR, J. H. 2006. Genetic ablation of caveolin-1 modifies Ca2+ spark coupling in murine arterial smooth muscle cells. *Am J Physiol Heart Circ Physiol,* 290**,** 20.

CHIDLOW, J. H., JR. & SESSA, W. C. 2010. Caveolae, caveolins, and cavins: complex control of cellular signalling and inflammation. *Cardiovasc Res,* 86**,** 219-25.

CLOUGH, G. & MICHEL, C. C. 1981. The role of vesicles in the transport of ferritin through frog endothelium. *J Physiol,* 315**,** 127-42.

COHEN, A. W., HNASKO, R., SCHUBERT, W. & LISANTI, M. P. 2004. Role of caveolae and caveolins in health and disease. *Physiological reviews,* 84**,** 1341-79.

COHEN, R. A. & VANHOUTTE, P. M. 1995. Endothelium-dependent hyperpolarization. Beyond nitric oxide and cyclic GMP. *Circulation,* 92**,** 3337-49.

COHEN, R. A., WEISBROD, R. M., GERICKE, M., YAGHOUBI, M., BIERL, C. & BOLOTINA, V. M. 1999. Mechanism of nitric oxide-induced vasodilatation: refilling of intracellular stores by sarcoplasmic reticulum Ca2+ ATPase and inhibition of store-operated Ca2+ influx. *Circ Res,* 84**,** 210-9.

COOK, N. S. 1988. The pharmacology of potassium channels and their therapeutic potential. *Trends in Pharmacological Sciences,* 9**,** 21-28.

COUET, J., LI, S., OKAMOTO, T., IKEZU, T. & LISANTI, M. P. 1997. Identification of peptide and protein ligands for the caveolin-scaffolding domain. Implications for the interaction of caveolin with caveolae-associated proteins. *The Journal of biological chemistry,* 272**,** 6525-33.

CRIBBS, L. L. 2001. *Vascular smooth muscle calcium channels: could "T" be a target?,* Circ Res. 2001 Sep 28;89(7):560-2.

CUI, J., COX, D. H. & ALDRICH, R. W. 1997. Intrinsic voltage dependence and Ca2+ regulation of mslo large conductance Ca-activated K+ channels. *J Gen Physiol,* 109**,** 647-73.

CULLING, C. F. A. 1974. *Handbook of histopathological and histochemical techniques : (including museum techniques) / [by] C. F. A. Culling ; with a foreword by W. L. Dunn,* London, Butterworth.

DARBLADE, B., CAILLAUD, D., POIROT, M., FOUQUE, M., THIERS, J. C., RAMI, J., BAYARD, F. & ARNAL, J. F. 2001. Alteration of plasmalemmal caveolae mimics endothelial dysfunction observed in atheromatous rabbit aorta. *Cardiovasc Res,* 50**,** 566-76.

DART, C. 2010. Lipid microdomains and the regulation of ion channel function. *J Physiol,* 588**,** 3169-78.

DEL POZO, M. A., BALASUBRAMANIAN, N., ALDERSON, N. B., KIOSSES, W. B., GRANDE-GARCIA, A., ANDERSON, R. G. & SCHWARTZ, M. A. 2005. Phospho-caveolin-1 mediates integrin-regulated membrane domain internalization. *Nat Cell Biol,* 7**,** 901-8.

DICARLO, S. E., PATIL, R. D., COLLINS, H. L. & CHEN, C. Y. 1995. Local modulation of adrenergic responses in the hindlimb vasculature of the intact conscious rat. *J Physiol,* 485**,** 817-25.

DIETER, R. S., CHU, W. W., PACANOWSKI, J. P., JR., MCBRIDE, P. E. & TANKE, T. E. 2002. The significance of lower extremity peripheral arterial disease. *Clin Cardiol,* 25**,** 3-10.

DIETZEN, D. J., HASTINGS, W. R. & LUBLIN, D. M. 1995. Caveolin is palmitoylated on multiple cysteine residues. Palmitoylation is not necessary for localization of caveolin to caveolae. *The Journal of biological chemistry,* 270**,** 6838-42.

DOPICO, A. M., BUKIYA, A. N. & SINGH, A. K. 2012. Large conductance, calcium- and voltage-gated potassium (BK) channels: regulation by cholesterol. *Pharmacol Ther,* 135**,** 133-50.

DORIGO, P., MARAGNO, I., SANTOSTASI, G. & FRACCAROLLO, D. 1999. Endothelium is required in the vascular spasm induced by tetraethylammonium and endothelin-1 in guinea-pig aorta. *Br J Pharmacol,* 127**,** 505-13.

DRAB, M., VERKADE, P., ELGER, M., KASPER, M., LOHN, M., LAUTERBACH, B., MENNE, J., LINDSCHAU, C., MENDE, F., LUFT, F. C., SCHEDL, A., HALLER, H. & KURZCHALIA, T. V. 2001. Loss of caveolae, vascular dysfunction, and pulmonary defects in caveolin-1 gene-disrupted mice. *Science (New York, N.Y.),* 293**,** 2449-52.

DREJA, K., VOLDSTEDLUND, M., VINTEN, J., TRANUM-JENSEN, J., HELLSTRAND, P. & SWARD, K. 2002. Cholesterol depletion disrupts caveolae and differentially impairs agonist-induced arterial contraction. *Arterioscler Thromb Vasc Biol,* 22**,** 1267-72.

DREXLER, H., HAYOZ, D., MÜNZEL, T., JUST, H., ZELIS, R. & BRUNNER, H. R. 1993. Endothelial function in congestive heart failure. *American Heart Journal,* 126**,** 761-764.

DUBE, G. P., BAIK, Y. H. & SCHWARTZ, A. 1985. Effects of a novel calcium channel agonist dihydropyridine analogue, Bay k 8644, on pig coronary artery: biphasic mechanical response and paradoxical potentiation of contraction by diltiazem and nimodipine. *J Cardiovasc Pharmacol,* 7**,** 377-89.

DUPREE, P., PARTON, R. G., RAPOSO, G., KURZCHALIA, T. V. & SIMONS, K. 1993. Caveolae and sorting in the trans-Golgi network of epithelial cells. *The EMBO journal,* 12**,** 1597-605.

ENGELMAN, J. A., LEE, R. J., KARNEZIS, A., BEARSS, D. J., WEBSTER, M., SIEGEL, P., MULLER, W. J., WINDLE, J. J., PESTELL, R. G. & LISANTI, M. P. 1998a. Reciprocal regulation of neu tyrosine kinase activity and caveolin-1 protein expression in vitro and in vivo. Implications for human breast cancer. *J Biol Chem,* 273**,** 20448-55.

ENGELMAN, J. A., ZHANG, X., GALBIATI, F., VOLONTE, D., SOTGIA, F., PESTELL, R. G., MINETTI, C., SCHERER, P. E., OKAMOTO, T. & LISANTI, M. P. 1998b. Molecular genetics of the caveolin gene family: implications for human cancers, diabetes, Alzheimer disease, and muscular dystrophy. *American journal of human genetics,* 63**,** 1578-1587.

FALLET, R. W., BAST, J. P., FUJIWARA, K., ISHII, N., SANSOM, S. C. & CARMINES, P. K. 2001. Influence of Ca(2+)-activated K(+) channels on rat renal arteriolar responses to depolarizing agonists. *Am J Physiol Renal Physiol,* 280**,** F583-91.

FAN, J. Y., CARPENTIER, J. L., VAN OBBERGHEN, E., GRUNFELD, C., GORDEN, P. & ORCI, L. 1983. Morphological changes of the 3T3-L1 fibroblast plasma membrane upon differentiation to the adipocyte form. *J Cell Sci,* 61**,** 219-30.

FATT, P. & KATZ, B. 1953. The effect of inhibitory nerve impulses on a crustacean muscle fibre. *J Physiol,* 121**,** 374-89.

FEHER, A., RUTKAI, I., BELEZNAI, T., UNGVARI, Z., CSISZAR, A., EDES, I. & BAGI, Z. 2010. Caveolin-1 limits the contribution of BK(Ca) channel to EDHF-mediated arteriolar dilation: implications in diet-induced obesity. *Cardiovasc Res,* 87**,** 732-9.

FENG, J., LIU, Y., CLEMENTS, R. T., SODHA, N. R., KHABBAZ, K. R., SENTHILNATHAN, V., NISHIMURA, K. K., ALPER, S. L. & SELLKE, F. W. 2008. Calcium-activated potassium channels contribute to human coronary microvascular dysfunction after cardioplegic arrest. *Circulation,* 118**,** 755827.

FERON, O., BELHASSEN, L., KOBZIK, L., SMITH, T. W., KELLY, R. A. & MICHEL, T. 1996. Endothelial nitric oxide synthase targeting to caveolae. Specific interactions with caveolin isoforms in cardiac myocytes and endothelial cells. *J Biol Chem,* 271**,** 22810-4.

FLAVAHAN, N. A. & VANHOUTTE, P. M. 1995. Endothelial cell signaling and endothelial dysfunction. *Am J Hypertens,* 8**,** 28S-41S.

FLEMING, I. & BUSSE, R. 2003. Molecular mechanisms involved in the regulation of the endothelial nitric oxide synthase. *Am J Physiol Regul Integr Comp Physiol,* 284**,** R1-12.

FORBES, M. S. R. M. L. N. E. 1979. Caveolar systems and sarcoplasmic reticulum in coronary smooth muscle cells of the mouse. *JULTR Journal of Ultrastructure Research,* 67**,** 325-339.

FRA, A. M., WILLIAMSON, E., SIMONS, K. & PARTON, R. G. 1995. De novo formation of caveolae in lymphocytes by expression of VIP21-caveolin. *Proc Natl Acad Sci U S A,* 92**,** 8655-9.

FRANK, P. G., PAVLIDES, S. & LISANTI, M. P. 2009. Caveolae and transcytosis in endothelial cells: role in atherosclerosis. *Cell Tissue Res,* 335**,** 41-7.

FRANSEN, P., HOVE, C. E. V., LANGEN, J. V. & BULT, H. 2012. *Contraction by Ca2+ Influx via the L-Type Ca2+ Channel Voltage Window in Mouse Aortic Segments is Modulated by Nitric Oxide*.

FREY, T. G., PERKINS, G. A. & ELLISMAN, M. H. 2006. Electron tomography of membrane-bound cellular organelles. *Annu Rev Biophys Biomol Struct,* 35**,** 199-224.

FUJIMOTO, T., HAGIWARA, H., AOKI, T., KOGO, H. & NOMURA, R. 1998. Caveolae: from a morphological point of view. *J Electron Microsc,* 47**,** 451-60.

GAETE, P. S., LILLO, M. A., ARDILES, N. M., PEREZ, F. R. & FIGUEROA, X. F. 2012. Ca2+-activated K+ channels of small and intermediate conductance control eNOS activation through NAD(P)H oxidase. *Free Radic Biol Med,* 52**,** 860-70.

GALBIATI, F., RAZANI, B. & LISANTI, M. P. 2001. Caveolae and caveolin-3 in muscular dystrophy. *Trends Mol Med,* 7**,** 435-41.

GANITKEVICH, V. & ISENBERG, G. 1990. Isolated guinea pig coronary smooth muscle cells. Acetylcholine induces hyperpolarization due to sarcoplasmic reticulum calcium release activating potassium channels. *Circ Res,* 67**,** 525-8.

GARCIA-CARDENA, G., MARTASEK, P., MASTERS, B. S., SKIDD, P. M., COUET, J., LI, S., LISANTI, M. P. & SESSA, W. C. 1997. Dissecting the interaction between nitric oxide synthase (NOS) and caveolin. Functional significance of the nos caveolin binding domain in vivo. *J Biol Chem,* 272**,** 25437-40.

GE, S., SONG, L., SERWANSKI, D. R., KUZIEL, W. A. & PACHTER, J. S. 2008. Transcellular transport of CCL2 across brain microvascular endothelial cells. *J Neurochem,* 104**,** 1219-32.

GEARY, G. G., DUCKLES, S. P. & KRAUSE, D. N. 1998. Effect of melatonin in the rat tail artery: role of K+ channels and endothelial factors. *Br J Pharmacol,* 123**,** 1533-40.

GHATTA, S., NIMMAGADDA, D., XU, X. & O'ROURKE, S. T. 2006. Large-conductance, calcium-activated potassium channels: structural and functional implications. *Pharmacol Ther,* 110**,** 103-16.

GHERGHICEANU, M. & POPESCU, L. M. 2007. Electron microscope tomography: further demonstration of nanocontacts between caveolae and smooth muscle sarcoplasmic reticulum. *Journal of Cellular and Molecular Medicine,* 11**,** 1416-1418.

GHITESCU, L., FIXMAN, A., SIMIONESCU, M. & SIMIONESCU, N. 1986. Specific binding sites for albumin restricted to plasmalemmal vesicles of continuous capillary endothelium: receptor-mediated transcytosis. *J Cell Biol,* 102**,** 1304-11.

GHOSH, S., GACHHUI, R., CROOKS, C., WU, C., LISANTI, M. P. & STUEHR, D. J. 1998. Interaction between caveolin-1 and the reductase domain of endothelial nitric-oxide synthase. Consequences for catalysis. *J Biol Chem,* 273**,** 22267-71.

GIANGIACOMO, K. M., GARCIA, M. L. & MCMANUS, O. B. 1992. Mechanism of iberiotoxin block of the large-conductance calcium-activated potassium channel from bovine aortic smooth muscle. *Biochemistry,* 31**,** 6719-27.

GIMPL, G., BURGER, K. & FAHRENHOLZ, F. 1997. Cholesterol as modulator of receptor function. *Biochemistry,* 36**,** 10959-10974.

GLENNEY, J. R., JR. 1989. Tyrosine phosphorylation of a 22-kDa protein is correlated with transformation by Rous sarcoma virus. *J Biol Chem,* 264**,** 20163-6.

GLENNEY, J. R., JR. & SOPPET, D. 1992. Sequence and expression of caveolin, a protein component of caveolae plasma membrane domains phosphorylated on tyrosine in Rous sarcoma virus-transformed fibroblasts. *Proc Natl Acad Sci U S A,* 89**,** 10517-21.

GOVERS, R. & RABELINK, T. J. 2001. Cellular regulation of endothelial nitric oxide synthase. *Am J Physiol Renal Physiol,* 280**,** F193-206.

GRAF, G. A., CONNELL, P. M., VAN DER WESTHUYZEN, D. R. & SMART, E. J. 1999. The class B, type I scavenger receptor promotes the selective uptake of high density lipoprotein cholesterol ethers into caveolae. *The Journal of biological chemistry,* 274**,** 12043-12048.

GRATTON, J. P., BERNATCHEZ, P. & SESSA, W. C. 2004. Caveolae and caveolins in the cardiovascular system. *Circ Res,* 94**,** 1408-17.

GRIFFITH, O. W. & STUEHR, D. J. 1995. Nitric oxide synthases: properties and catalytic mechanism. *Annu Rev Physiol,* 57**,** 707-36.

GSCHWEND, S., HENNING, R. H., DE ZEEUW, D. & BUIKEMA, H. 2003. Coronary myogenic constriction antagonizes EDHF-mediated dilation: role of KCa channels. *Hypertension,* 41**,** 912-8.

GUIBERT, C., MARTHAN, R. & SAVINEAU, J. P. 1996. Angiotensin II-induced Ca(2+)-oscillations in vascular myocytes from the rat pulmonary artery. *Am J Physiol,* 270**,** L637-42.

GUSTINCICH, S., VATTA, P., GORUPPI, S., WOLF, M., SACCONE, S., DELLA VALLE, G., BAGGIOLINI, M. & SCHNEIDER, C. 1999. The human serum deprivation response gene (SDPR) maps to 2q32-q33 and codes for a phosphatidylserine-binding protein. *Genomics,* 57**,** 120-9.

HANSEN, C. G., BRIGHT, N. A., HOWARD, G. & NICHOLS, B. J. 2009. SDPR induces membrane curvature and functions in the formation of caveolae. *Nat Cell Biol,* 11**,** 807-14.

HARDIN, C. D. & VALLEJO, J. 2006. Caveolins in vascular smooth muscle: form organizing function. *Cardiovasc Res,* 69**,** 808-15.

HARDIN, C. D. & VALLEJO, J. 2009. Dissecting the functions of protein-protein interactions: caveolin as a promiscuous partner. Focus on "Caveolin-1 scaffold domain interacts with TRPC1 and IP3R3 to regulate Ca2+ store release-induced Ca2+ entry in endothelial cells". *Am J Physiol Cell Physiol,* 296**,** 31.

HAYER, A., STOEBER, M., BISSIG, C. & HELENIUS, A. 2010. Biogenesis of caveolae: stepwise assembly of large caveolin and cavin complexes. *Traffic,* 11**,** 361-82.

HEAD, B. P. & INSEL, P. A. 2007. Do caveolins regulate cells by actions outside of caveolae? *Trends Cell Biol,* 17**,** 51-7.

HENDERSON, R. & UNWIN, P. N. 1975. Three-dimensional model of purple membrane obtained by electron microscopy. *Nature,* 257**,** 28-32.

HENLEY, J. R., KRUEGER, E. W., OSWALD, B. J. & MCNIVEN, M. A. 1998. Dynamin-mediated internalization of caveolae. *J Cell Biol,* 141**,** 85-99.

HESS, P., LANSMAN, J. B. & TSIEN, R. W. 1984. Different modes of Ca channel gating behaviour favoured by dihydropyridine Ca agonists and antagonists. *Nature,* 311**,** 538-44.

HILL, C. E., EADE, J. & SANDOW, S. L. 1999. Mechanisms underlying spontaneous rhythmical contractions in irideal arterioles of the rat. *The Journal of physiology,* 521 Pt 2**,** 507-16.

HILL, C. E., PHILLIPS, J. K. & SANDOW, S. L. 2001. Heterogeneous control of blood flow amongst different vascular beds. *Med Res Rev,* 21**,** 1-60.
HILL, M. A., YANG, Y., ELLA, S. R., DAVIS, M. J. & BRAUN, A. P. 2010. Large conductance, Ca2+-activated K+ channels (BKCa) and arteriolar myogenic signaling. *FEBS Lett,* 584**,** 2033-42.
HILL, M. M., BASTIANI, M., LUETTERFORST, R., KIRKHAM, M., KIRKHAM, A., NIXON, S. J., WALSER, P., ABANKWA, D., OORSCHOT, V. M., MARTIN, S., HANCOCK, J. F. & PARTON, R. G. 2008. PTRF-Cavin, a conserved cytoplasmic protein required for caveola formation and function. *Cell,* 132**,** 113-24.
HNASKO, R. & LISANTI, M. P. 2003. The biology of caveolae: lessons from caveolin knockout mice and implications for human disease. *Mol Interv,* 3**,** 445-64.
HOLLAND, M., LANGTON, P. D., STANDEN, N. B. & BOYLE, J. P. 1996. Effects of the BKCa channel activator, NS1619, on rat cerebral artery smooth muscle. *British Journal of Pharmacology,* 117**,** 119-129.
HORRIGAN, F. T. & ALDRICH, R. W. 1999. Allosteric voltage gating of potassium channels II. Mslo channel gating charge movement in the absence of Ca(2+). *J Gen Physiol,* 114**,** 305-36.
HU, X.-Q. & ZHANG, L. 2012. Function and regulation of large conductance Ca2+-activated K+ channel in vascular smooth muscle cells. *Drug Discovery Today,* 17**,** 974-987.
INSEL, P. A. & PATEL, H. H. 2007. Do studies in caveolin-knockouts teach us about physiology and pharmacology or instead, the ways mice compensate for 'lost proteins'? *Br J Pharmacol,* 150**,** 251-4.
ISSHIKI, M., YING, Y. S., FUJITA, T. & ANDERSON, R. G. 2002. A molecular sensor detects signal transduction from caveolae in living cells. *J Biol Chem,* 277**,** 43389-98.
IZUMI, Y., HIRAI, S., TAMAI, Y., FUJISE-MATSUOKA, A., NISHIMURA, Y. & OHNO, S. 1997. A protein kinase Cdelta-binding protein SRBC whose expression is induced by serum starvation. *J Biol Chem,* 272**,** 7381-9.
JE, H. D., GALLANT, C., LEAVIS, P. C. & MORAN, K. G. 2004. Caveolin-1 regulates contractility in differentiated vascular smooth muscle. *Biophysical Journal,* 86**,** 173A-173A.
JIANG, H., XIA, Q., WANG, X., SONG, J. & BRUCE, I. C. 2005. Luteolin induces vasorelaxion in rat thoracic aorta via calcium and potassium channels. *Pharmazie,* 60**,** 444-7.
JIE, Z., KENDRICK, A., QUENBY, S. & WRAY, S. 2007. Contractility and calcium signaling of human myometrium are profoundly affected by cholesterol manipulation: implications for labor? *Reprod Sci,* 14**,** 456-66.
JOW, F., SULLIVAN, K., SOKOL, P. & NUMANN, R. 1999. Induction of Ca2+-activated K+ current and transient outward currents in human capillary endothelial cells. *J Membr Biol,* 167**,** 53-64.
JU, H., ZOU, R., VENEMA, V. J. & VENEMA, R. C. 1997. Direct interaction of endothelial nitric-oxide synthase and caveolin-1 inhibits synthase activity. *J Biol Chem,* 272**,** 18522-5.
KAISER, R. A., OXHORN, B. C., ANDREWS, G. & BUXTON, I. L. 2002. Functional compartmentation of endothelial P2Y receptor signaling. *Circ Res,* 91**,** 292-9.

KAMISHIMA, T., BURDYGA, T., GALLAGHER, J. A. & QUAYLE, J. M. 2007. Caveolin-1 and caveolin-3 regulate Ca2+ homeostasis of single smooth muscle cells from rat cerebral resistance arteries. *American journal of physiology. Heart and circulatory physiology,* 293**,** H204-14.

KARAKI, H., OZAKI, H., HORI, M., MITSUI-SAITO, M., AMANO, K., HARADA, K., MIYAMOTO, S., NAKAZAWA, H., WON, K. J. & SATO, K. 1997. Calcium movements, distribution, and functions in smooth muscle. *Pharmacol Rev,* 49**,** 157-230.

KHAN, S. A., HIGDON, N. R. & MEISHERI, K. D. 1998. Coronary vasorelaxation by nitroglycerin: involvement of plasmalemmal calcium-activated K+ channels and intracellular Ca++ stores. *J Pharmacol Exp Ther,* 284**,** 838-46.

KIKKAWA, K., HOSHINO, T., YAMAUCHI-KOHNO, R. & MURATA, S. 1999. Characteristics of heterogeneity in the expression of vasoconstriction in response to N(G)-monomethyl-L-arginine in isolated canine arteries. *Eur J Pharmacol,* 379**,** 167-73.

KILSDONK, E. P., YANCEY, P. G., STOUDT, G. W., BANGERTER, F. W., JOHNSON, W. J., PHILLIPS, M. C. & ROTHBLAT, G. H. 1995. Cellular cholesterol efflux mediated by cyclodextrins. *J Biol Chem,* 270**,** 17250-6.

KING, G. L. & JOHNSON, S. M. 1985. Receptor-mediated transport of insulin across endothelial cells. *Science,* 227**,** 1583-6.

KIRKHAM, M., NIXON, S. J., HOWES, M. T., ABI-RACHED, L., WAKEHAM, D. E., HANZAL-BAYER, M., FERGUSON, C., HILL, M. M., FERNANDEZ-ROJO, M., BROWN, D. A., HANCOCK, J. F., BRODSKY, F. M. & PARTON, R. G. 2008. Evolutionary analysis and molecular dissection of caveola biogenesis. *J Cell Sci,* 121**,** 2075-86.

KLABUNDE, R. 2004. *Cardiovascular Physiology Concepts*, Lippincott Williams & Wilkins.

KO, E. A., HAN, J., JUNG, I. D. & PARK, W. S. 2008. Physiological roles of K+ channels in vascular smooth muscle cells. *J Smooth Muscle Res,* 44**,** 65-81.

KOGO, H., ITO, S. Y., MORITOKI, Y., KURAHASHI, H. & FUJIMOTO, T. 2006. Differential expression of caveolin-3 in mouse smooth muscle cells in vivo. *Cell Tissue Res,* 324**,** 291-300.

KORADE, Z. & KENWORTHY, A. K. 2008. Lipid rafts, cholesterol, and the brain. *Neuropharmacology,* 55**,** 1265-73.

KUO, K. H., WANG, L., PARE, P. D., FORD, L. E. & SEOW, C. Y. 2001. Myosin thick filament lability induced by mechanical strain in airway smooth muscle. *J Appl Physiol,* 90**,** 1811-6.

KWOK, K. H., CHAN, N. W., LAU, C. W. & HUANG, Y. 1998. Contractile and relaxant effects of tetrapentylammonium ions in rat isolated mesenteric artery. *Pharmacology,* 57**,** 188-95.

LACINOVA, L. 2005. Voltage-dependent calcium channels. *Gen Physiol Biophys,* 1**,** 1-78.

LAM, R. S., SHAW, A. R. & DUSZYK, M. 2004. Membrane cholesterol content modulates activation of BK channels in colonic epithelia. *Biochim Biophys Acta,* 15**,** 241-8.

LANGTON, P. D. 1993. Calcium channel currents recorded from isolated myocytes of rat basilar artery are stretch sensitive. *J Physiol,* 471**,** 1-11.

LANGTON, P. D., NELSON, M. T., HUANG, Y. & STANDEN, N. B. 1991. Block of calcium-activated potassium channels in mammalian arterial myocytes by tetraethylammonium ions. *Am J Physiol,* 260**,** H927-34.

LATORRE, R. & BRAUCHI, S. 2006. Large conductance Ca2+-activated K+ (BK) channel: activation by Ca2+ and voltage. *Biol Res,* 39**,** 385-401.
LEDOUX, J., WERNER, M. E., BRAYDEN, J. E. & NELSON, M. T. 2006. Calcium-activated potassium channels and the regulation of vascular tone. *Physiology,* 21**,** 69-78.
LEE, U. S. & CUI, J. 2010. BK channel activation: structural and functional insights. *Trends Neurosci,* 33**,** 415-23.
LEVICK, J. R. 2010. *An introduction to cardiovascular physiology,* London, Hodder Arnold.
LI, S., OKAMOTO, T., CHUN, M., SARGIACOMO, M., CASANOVA, J. E., HANSEN, S. H., NISHIMOTO, I. & LISANTI, M. P. 1995. Evidence for a regulated interaction between heterotrimeric G proteins and caveolin. *J Biol Chem,* 270**,** 15693-701.
LINDER, A. E., MCCLUSKEY, L. P., COLE, K. R., 3RD, LANNING, K. M. & WEBB, R. C. 2005. Dynamic association of nitric oxide downstream signaling molecules with endothelial caveolin-1 in rat aorta. *J Pharmacol Exp Ther,* 314**,** 9-15.
LISANTI, M. P., SCHERER, P. E., TANG, Z. & SARGIACOMO, M. 1994a. Caveolae, caveolin and caveolin-rich membrane domains: a signalling hypothesis. *Trends Cell Biol,* 4**,** 231-5.
LISANTI, M. P., SCHERER, P. E., VIDUGIRIENE, J., TANG, Z., HERMANOWSKI-VOSATKA, A., TU, Y. H., COOK, R. F. & SARGIACOMO, M. 1994b. Characterization of caveolin-rich membrane domains isolated from an endothelial-rich source: implications for human disease. *The Journal of cell biology,* 126**,** 111-26.
LIU, L. & PILCH, P. F. 2008. A critical role of cavin (polymerase I and transcript release factor) in caveolae formation and organization. *J Biol Chem,* 283**,** 4314-22.
LOHN, M., FURSTENAU, M., SAGACH, V., ELGER, M., SCHULZE, W., LUFT, F. C., HALLER, H. & GOLLASCH, M. 2000. Ignition of calcium sparks in arterial and cardiac muscle through caveolae. *Circ Res,* 87**,** 1034-9.
LU, T., ZHANG, D. M., WANG, X. L., HE, T., WANG, R. X., CHAI, Q., KATUSIC, Z. S. & LEE, H. C. 2010. Regulation of coronary arterial BK channels by caveolae-mediated angiotensin II signaling in diabetes mellitus. *Circ Res,* 106**,** 1164-73.
MARTY, A. 1981. Ca-dependent K channels with large unitary conductance in chromaffin cell membranes. *Nature,* 291**,** 497-500.
MCDANIEL, S. S., PLATOSHYN, O., WANG, J., YU, Y., SWEENEY, M., KRICK, S., RUBIN, L. J. & YUAN, J. X. 2001. Capacitative Ca(2+) entry in agonist-induced pulmonary vasoconstriction. *Am J Physiol Lung Cell Mol Physiol,* 280**,** L870-80.
MCFADZEAN, I. & GIBSON, A. 2002. The developing relationship between receptor-operated and store-operated calcium channels in smooth muscle. *Br J Pharmacol,* 135**,** 1-13.
MCMAHON, K. A., ZAJICEK, H., LI, W. P., PEYTON, M. J., MINNA, J. D., HERNANDEZ, V. J., LUBY-PHELPS, K. & ANDERSON, R. G. 2009. SRBC/cavin-3 is a caveolin adapter protein that regulates caveolae function. *Embo J,* 28**,** 1001-15.

MEISHERI, K. D., DUBRAY, L. A. & OLEYNEK, J. J. 1990. A sensitive in vitro functional assay to detect K(+)-channel-dependent vasodilators. *J Pharmacol Methods,* 24**,** 251-61.

MICHEL, J. B., FERON, O., SACKS, D. & MICHEL, T. 1997. Reciprocal regulation of endothelial nitric-oxide synthase by Ca2+-calmodulin and caveolin. *J Biol Chem,* 272**,** 15583-6.

MICHEL, T. 1999. Targeting and translocation of endothelial nitric oxide synthase. *Braz J Med Biol Res,* 32**,** 1361-6.

MILLAN, J., HEWLETT, L., GLYN, M., TOOMRE, D., CLARK, P. & RIDLEY, A. J. 2006. Lymphocyte transcellular migration occurs through recruitment of endothelial ICAM-1 to caveola- and F-actin-rich domains. *Nat Cell Biol,* 8**,** 113-23.

MILLER, C. 1995. The charybdotoxin family of K+ channel-blocking peptides. *Neuron,* 15**,** 5-10.

MINAMI, K., HIRATA, Y., TOKUMURA, A., NAKAYA, Y. & FUKUZAWA, K. 1995. Protein kinase C-independent inhibition of the Ca(2+)-activated K+ channel by angiotensin II and endothelin-1. *Biochem Pharmacol,* 49**,** 1051-6.

MINSHALL, R. D., SESSA, W. C., STAN, R. V., ANDERSON, R. G. & MALIK, A. B. 2003. Caveolin regulation of endothelial function. *Am J Physiol Lung Cell Mol Physiol,* 285**,** L1179-83.

MISTRY, D. K. & GARLAND, C. J. 1998. Nitric oxide (NO)-induced activation of large conductance Ca2+-dependent K+ channels (BK(Ca)) in smooth muscle cells isolated from the rat mesenteric artery. *Br J Pharmacol,* 124**,** 1131-40.

MONCADA, S., PALMER, R. M. & HIGGS, E. A. 1991. Nitric oxide: physiology, pathophysiology, and pharmacology. *Pharmacol Rev,* 43**,** 109-42.

MOORE, M. N. 2006. Do nanoparticles present ecotoxicological risks for the health of the aquatic environment? *Environ Int,* 32**,** 967-76.

MOOSMANG, S., SCHULLA, V., WELLING, A., FEIL, R., FEIL, S., WEGENER, J. W., HOFMANN, F. & KLUGBAUER, N. 2003. Dominant role of smooth muscle L-type calcium channel Cav1.2 for blood pressure regulation. *Embo J,* 22**,** 6027-34.

MULVANY, M. J. & AALKJAER, C. 1990. Structure and function of small arteries. *Physiol Rev,* 70**,** 921-61.

MULVANY, M. J. & HALPERN, W. 1977. Contractile properties of small arterial resistance vessels in spontaneously hypertensive and normotensive rats. *Circulation research,* 41**,** 19-26.

MUNDY, D. I., MACHLEIDT, T., YING, Y. S., ANDERSON, R. G. & BLOOM, G. S. 2002. Dual control of caveolar membrane traffic by microtubules and the actin cytoskeleton. *J Cell Sci,* 115**,** 4327-39.

MURATA, M., PERANEN, J., SCHREINER, R., WIELAND, F., KURZCHALIA, T. V. & SIMONS, K. 1995. VIP21/caveolin is a cholesterol-binding protein. *Proc Natl Acad Sci U S A,* 92**,** 10339-43.

MURATA, T., LIN, M. I., HUANG, Y., YU, J., BAUER, P. M., GIORDANO, F. J. & SESSA, W. C. 2007. Reexpression of caveolin-1 in endothelium rescues the vascular, cardiac, and pulmonary defects in global caveolin-1 knockout mice. *J Exp Med,* 204**,** 2373-82.

NA, K., BUM LEE, T., PARK, K. H., SHIN, E. K., LEE, Y. B. & CHOI, H. K. 2003. Self-assembled nanoparticles of hydrophobically-modified polysaccharide bearing vitamin H as a targeted anti-cancer drug delivery system. *Eur J Pharm Sci,* 18**,** 165-73.

NELSON, M. T., CHENG, H., RUBART, M., SANTANA, L. F., BONEV, A. D., KNOT, H. J. & LEDERER, W. J. 1995. Relaxation of arterial smooth muscle by calcium sparks. *Science,* 270**,** 633-7.

NELSON, M. T. & QUAYLE, J. M. 1995. Physiological roles and properties of potassium channels in arterial smooth muscle. *Am J Physiol,* 268**,** C799-822.

NELSON, M. T., STANDEN, N. B., BRAYDEN, J. E. & WORLEY, J. F., 3RD 1988. Noradrenaline contracts arteries by activating voltage-dependent calcium channels. *Nature,* 336**,** 382-5.

NICHOLS, B. J. & LIPPINCOTT-SCHWARTZ, J. 2001. Endocytosis without clathrin coats. *Trends in cell biology,* 11**,** 406-412.

NORDESTGAARD, B. G. 1996. The vascular endothelial barrier--selective retention of lipoproteins. *Curr Opin Lipidol,* 7**,** 269-73.

NORKIN, L. C. 2001. Caveolae in the uptake and targeting of infectious agents and secreted toxins. *Adv Drug Deliv Rev,* 49**,** 301-15.

NORKIN, L. C., ANDERSON, H. A., WOLFROM, S. A. & OPPENHEIM, A. 2002. Caveolar endocytosis of simian virus 40 is followed by brefeldin A-sensitive transport to the endoplasmic reticulum, where the virus disassembles. *J Virol,* 76**,** 5156-66.

OH, P. & SCHNITZER, J. E. 2001. Segregation of heterotrimeric G proteins in cell surface microdomains. G(q) binds caveolin to concentrate in caveolae, whereas G(i) and G(s) target lipid rafts by default. *Mol Biol Cell,* 12**,** 685-98.

OHAYON, S., GRUENBAUM, S. E., ARTRU, A. A., BOYKO, M., GRUENBAUM, B. F., DUBILET, M., LEIBOWITZ, A., SHAPIRA, Y., TEICHBERG, V. I. & ZLOTNIK, A. 2012. Anatomical location of arterial and venous lines significantly affects motor performance in rats. *Anim Sci J,* 83**,** 656-62.

OHNUMA, K., YAMOCHI, T., UCHIYAMA, M., NISHIBASHI, K., YOSHIKAWA, N., SHIMIZU, N., IWATA, S., TANAKA, H., DANG, N. H. & MORIMOTO, C. 2004. CD26 up-regulates expression of CD86 on antigen-presenting cells by means of caveolin-1. *Proc Natl Acad Sci U S A,* 101**,** 14186-91.

OKA, N., YAMAMOTO, M., SCHWENCKE, C., KAWABE, J., EBINA, T., OHNO, S., COUET, J., LISANTI, M. P. & ISHIKAWA, Y. 1997. Caveolin interaction with protein kinase C. Isoenzyme-dependent regulation of kinase activity by the caveolin scaffolding domain peptide. *J Biol Chem,* 272**,** 33416-21.

OKAMOTO, T., SCHLEGEL, A., SCHERER, P. E. & LISANTI, M. P. 1998. Caveolins, a family of scaffolding proteins for organizing "preassembled signaling complexes" at the plasma membrane. *J Biol Chem,* 273**,** 5419-22.

OLESEN, S. P., MUNCH, E., MOLDT, P. & DREJER, J. 1994. Selective activation of Ca(2+)-dependent K+ channels by novel benzimidazolone. *Eur J Pharmacol,* 251**,** 53-9.

OSTROM, R. S. & INSEL, P. A. 2006. Methods for the study of signaling molecules in membrane lipid rafts and caveolae. *Methods Mol Biol,* 332**,** 181-91.

PALADE, G. E. 1953. Fine Structure of Blood Capillaries. . *J. Appl. Phys. ,* 24**,** 1424-1436.

PANYAM, J., SAHOO, S. K., PRABHA, S., BARGAR, T. & LABHASETWAR, V. 2003. Fluorescence and electron microscopy probes for cellular and tissue uptake of poly(D,L-lactide-co-glycolide) nanoparticles. *Int J Pharm,* 262**,** 1-11.

PARK, D. S., RAZANI, B., LASORELLA, A., SCHREIBER-AGUS, N., PESTELL, R. G., IAVARONE, A. & LISANTI, M. P. 2001. Evidence that Myc isoforms transcriptionally repress caveolin-1 gene expression via an INR-dependent mechanism. *Biochemistry,* 40**,** 3354-62.

PAROLINI, I., SARGIACOMO, M., GALBIATI, F., RIZZO, G., GRIGNANI, F., ENGELMAN, J. A., OKAMOTO, T., IKEZU, T., SCHERER, P. E., MORA, R., RODRIGUEZ-BOULAN, E., PESCHLE, C. & LISANTI, M. P. 1999. Expression of caveolin-1 is required for the transport of caveolin-2 to the plasma membrane. Retention of caveolin-2 at the level of the golgi complex. *J Biol Chem,* 274**,** 25718-25.

PARTON, R. G. 1996. Caveolae and caveolins. *Curr Opin Cell Biol,* 8**,** 542-8.

PARTON, R. G. 2001. Cell biology. Life without caveolae. *Science,* 293**,** 2404-5.

PARTON, R. G., WAY, M., ZORZI, N. & STANG, E. 1997. Caveolin-3 associates with developing T-tubules during muscle differentiation. *The Journal of cell biology,* 136**,** 137-54.

PATEL, H. H. & INSEL, P. A. 2009. *Lipid rafts and caveolae and their role in compartmentation of redox signaling*.

PATEL, H. H., MURRAY, F. & INSEL, P. A. 2008a. Caveolae as organizers of pharmacologically relevant signal transduction molecules. *Annu Rev Pharmacol Toxicol,* 48**,** 359-91.

PATEL, H. H., MURRAY, F. & INSEL, P. A. 2008b. Caveolae as organizers of pharmacologically relevant signal transduction molecules. *Annual Review of Pharmacology and Toxicology.* Palo Alto: Annual Reviews.

PELKMANS, L. & HELENIUS, A. 2002. Endocytosis via caveolae. *Traffic,* 3**,** 311-20.

PELKMANS, L. & ZERIAL, M. 2005. Kinase-regulated quantal assemblies and kiss-and-run recycling of caveolae. *Nature,* 436**,** 128-33.

PIKE, L. J. 2009. The challenge of lipid rafts. *J Lipid Res,* 50**,** 27.

PITHA, J., IRIE, T., SKLAR, P. B. & NYE, J. S. 1988. Drug solubilizers to aid pharmacologists: amorphous cyclodextrin derivatives. *Life Sci,* 43**,** 493-502.

POPESCU, L. M., GHERGHICEANU, M., MANDACHE, E. & CRETOIU, D. 2006. Caveolae in smooth muscles: nanocontacts. *J Cell Mol Med,* 10**,** 960-90.

PORTER, V. A., BONEV, A. D., KNOT, H. J., HEPPNER, T. J., STEVENSON, A. S., KLEPPISCH, T., LEDERER, W. J. & NELSON, M. T. 1998. Frequency modulation of Ca2+ sparks is involved in regulation of arterial diameter by cyclic nucleotides. *Am J Physiol,* 274**,** C1346-55.

PRENDERGAST, C., QUAYLE, J., BURDYGA, T. & WRAY, S. 2010. Cholesterol depletion alters coronary artery myocyte Ca(2+) signalling in a stimulus-specific manner. *Cell Calcium,* 47**,** 84-91.

RADENKOVIC, M., STOJANOVIC, M., JANKOVIC, R., TOPALOVIC, M. & STOJILJKOVIC, M. 2012. Combined contribution of endothelial relaxing autacoides in the rat femoral artery response to CPCA: an adenosine A2 receptor agonist. *ScientificWorldJournal,* 143818**,** 19.

RAMOS-VARA, J. A. 2011. Principles and methods of immunohistochemistry. *Methods Mol Biol,* 691**,** 83-96.

RAZANI, B. & LISANTI, M. P. 2001a. Caveolin-deficient mice: insights into caveolar function human disease. *J Clin Invest,* 108**,** 1553-61.

RAZANI, B. & LISANTI, M. P. 2001b. Caveolins and caveolae: molecular and functional relationships. *Exp Cell Res,* 271**,** 36-44.

RAZANI, B., WOODMAN, S. E. & LISANTI, M. P. 2002. Caveolae: from cell biology to animal physiology. *Pharmacol Rev,* 54**,** 431-67.
RHEE, S. W., STIMERS, J. R., WANG, W. & PANG, L. 2009. Vascular smooth muscle-specific knockdown of the noncardiac form of the L-type calcium channel by microRNA-based short hairpin RNA as a potential antihypertensive therapy. *J Pharmacol Exp Ther,* 329**,** 775-82.
RIDDLE, M. A., HUGHES, J. M. & WALKER, B. R. 2011. Role of caveolin-1 in endothelial BKCa channel regulation of vasoreactivity. *American journal of physiology. Cell physiology,* 301**,** C1404-14.
ROBERTSON, B. E., SCHUBERT, R., HESCHELER, J. & NELSON, M. T. 1993. cGMP-dependent protein kinase activates Ca-activated K channels in cerebral artery smooth muscle cells. *Am J Physiol,* 265**,** C299-303.
ROSSELLI, M., KELLER, P. J. & DUBEY, R. K. 1998. Role of nitric oxide in the biology, physiology and pathophysiology of reproduction. *Human reproduction update,* 4**,** 3-24.
ROTHBERG, K. G., HEUSER, J. E., DONZELL, W. C., YING, Y.-S., GLENNEY, J. R. & ANDERSON, R. G. W. 1992. Caveolin, a protein component of caveolae membrane coats. *Cell,* 68**,** 673-682.
ROTHBERG, K. G., YING, Y. S., KAMEN, B. A. & ANDERSON, R. G. W. 1990. Cholesterol controls the clustering of the glycophospholipid-anchored membrane receptor for 5-methyltetrahydrofolate. *Journal of Cell Biology,* 111**,** 2931-2938.
SADOSHIMA, J., AKAIKE, N., KANAIDE, H. & NAKAMURA, M. 1988. Cyclic AMP modulates Ca-activated K channel in cultured smooth muscle cells of rat aortas. *Am J Physiol,* 255**,** H754-9.
SALIEZ, J., BOUZIN, C., RATH, G., GHISDAL, P., DESJARDINS, F., REZZANI, R., RODELLA, L. F., VRIENS, J., NILIUS, B., FERON, O., BALLIGAND, J. L. & DESSY, C. 2008. Role of caveolar compartmentation in endothelium-derived hyperpolarizing factor-mediated relaxation: Ca2+ signals and gap junction function are regulated by caveolin in endothelial cells. *Circulation,* 117**,** 1065-74.
SAMPSON, L. J., HAYABUCHI, Y., STANDEN, N. B. & DART, C. 2004. Caveolae localize protein kinase A signaling to arterial ATP-sensitive potassium channels. *Circ Res,* 95**,** 1012-8.
SANDOW, S. L., BRAMICH, N. J., BANDI, H. P., RUMMERY, N. M. & HILL, C. E. 2003. Structure, function, and endothelium-derived hyperpolarizing factor in the caudal artery of the SHR and WKY rat. *Arteriosclerosis, thrombosis, and vascular biology,* 23**,** 822-8.
SANDOW, S. L. & GRAYSON, T. H. 2009. Limits of isolation and culture: intact vascular endothelium and BKCa. *Am J Physiol Heart Circ Physiol,* 297**,** 1.
SANDOW, S. L. & HILL, C. E. 2000. Incidence of myoendothelial gap junctions in the proximal and distal mesenteric arteries of the rat is suggestive of a role in endothelium-derived hyperpolarizing factor-mediated responses. *Circulation Research,* 86**,** 341-6.
SANDOW, S. L., TARE, M., COLEMAN, H. A., HILL, C. E. & PARKINGTON, H. C. 2002. Involvement of myoendothelial gap junctions in the actions of endothelium-derived hyperpolarizing factor. *Circulation Research,* 90**,** 1108-13.
SARGIACOMO, M., SCHERER, P. E., TANG, Z., KUBLER, E., SONG, K. S., SANDERS, M. C. & LISANTI, M. P. 1995. Oligomeric structure of

caveolin: implications for caveolae membrane organization. *Proc Natl Acad Sci U S A,* 92**,** 9407-11.

SAUSBIER, M., ARNTZ, C., BUCURENCIU, I., ZHAO, H., ZHOU, X. B., SAUSBIER, U., FEIL, S., KAMM, S., ESSIN, K., SAILER, C. A., ABDULLAH, U., KRIPPEIT-DREWS, P., FEIL, R., HOFMANN, F., KNAUS, H. G., KENYON, C., SHIPSTON, M. J., STORM, J. F., NEUHUBER, W., KORTH, M., SCHUBERT, R., GOLLASCH, M. & RUTH, P. 2005. Elevated blood pressure linked to primary hyperaldosteronism and impaired vasodilation in BK channel-deficient mice. *Circulation,* 112**,** 60-8.

SCHERER, P. E., LISANTI, M. P., BALDINI, G., SARGIACOMO, M., MASTICK, C. C. & LODISH, H. F. 1994. Induction of caveolin during adipogenesis and association of GLUT4 with caveolin-rich vesicles. *J Cell Biol,* 127**,** 1233-43.

SCHERER, P. E., OKAMOTO, T., CHUN, M., NISHIMOTO, I., LODISH, H. F. & LISANTI, M. P. 1996. Identification, sequence, and expression of caveolin-2 defines a caveolin gene family. *Proc Natl Acad Sci U S A,* 93**,** 131-5.

SCHERER, P. E., TANG, Z., CHUN, M., SARGIACOMO, M., LODISH, H. F. & LISANTI, M. P. 1995. Caveolin isoforms differ in their N-terminal protein sequence and subcellular distribution. Identification and epitope mapping of an isoform-specific monoclonal antibody probe. *J Biol Chem,* 270**,** 16395-401.

SCHNITZER, J. E. 2001. Caveolae: from basic trafficking mechanisms to targeting transcytosis for tissue-specific drug and gene delivery in vivo. *Adv Drug Deliv Rev,* 49**,** 265-80.

SCHNITZER, J. E., OH, P., PINNEY, E. & ALLARD, J. 1994. Filipin-sensitive caveolae-mediated transport in endothelium: reduced transcytosis, scavenger endocytosis, and capillary permeability of select macromolecules. *J Cell Biol,* 127**,** 1217-32.

SCHRAMM, M., THOMAS, G., TOWART, R. & FRANCKOWIAK, G. 1983. Activation of calcium channels by novel 1,4-dihydropyridines. A new mechanism for positive inotropics or smooth muscle stimulants. *Arzneimittelforschung,* 33**,** 1268-72.

SHAUL, P. W. & ANDERSON, R. G. 1998. Role of plasmalemmal caveolae in signal transduction. *Am J Physiol,* 275**,** L843-51.

SHAW, L., SWEENEY, M. A., O'NEILL, S. C., JONES, C. J., AUSTIN, C. & TAGGART, M. J. 2006. Caveolae and sarcoplasmic reticular coupling in smooth muscle cells of pressurised arteries: the relevance for Ca2+ oscillations and tone. *Cardiovasc Res,* 69**,** 825-35.

SHIMOKAWA, H., YASUTAKE, H., FUJII, K., OWADA, M. K., NAKAIKE, R., FUKUMOTO, Y., TAKAYANAGI, T., NAGAO, T., EGASHIRA, K., FUJISHIMA, M. & TAKESHITA, A. 1996. The importance of the hyperpolarizing mechanism increases as the vessel size decreases in endothelium-dependent relaxations in rat mesenteric circulation. *Journal of cardiovascular pharmacology,* 28**,** 703-11.

SIMIONESCU, N., SIMINOESCU, M. & PALADE, G. E. 1975. Permeability of muscle capillaries to small heme-peptides. Evidence for the existence of patent transendothelial channels. *The Journal of cell biology,* 64**,** 586-607.

SIMONS, K. & EHEHALT, R. 2002. Cholesterol, lipid rafts, and disease. *J Clin Invest,* 110**,** 597-603.

SIMONS, K. & IKONEN, E. 1997. Functional rafts in cell membranes. *Nature,* 387**,** 569-72.
SIMONS, K. & TOOMRE, D. 2000. Lipid rafts and signal transduction. *Nat Rev Mol Cell Biol,* 1**,** 31-9.
SINGER, S. J. & NICOLSON, G. L. 1972. The fluid mosaic model of the structure of cell membranes. *Science,* 175**,** 720-31.
SKOOG, L. & TANI, E. 2011. Immunocytochemistry: an indispensable technique in routine cytology. *Cytopathology,* 22**,** 215-229.
SMART, E. J., GRAF, G. A., MCNIVEN, M. A., SESSA, W. C., ENGELMAN, J. A., SCHERER, P. E., OKAMOTO, T. & LISANTI, M. P. 1999. Caveolins, liquid-ordered domains, and signal transduction. *Mol Cell Biol,* 19**,** 7289-304.
SMART, E. J., YING, Y., DONZELL, W. C. & ANDERSON, R. G. 1996. A role for caveolin in transport of cholesterol from endoplasmic reticulum to plasma membrane. *J Biol Chem,* 271**,** 29427-35.
SMITH, R. D., BABIYCHUK, E. B., NOBLE, K., DRAEGER, A. & WRAY, S. 2005. Increased cholesterol decreases uterine activity: functional effects of cholesterol alteration in pregnant rat myometrium. *Am J Physiol Cell Physiol,* 288**,** 21.
SOMLYO, A. P., SOMLYO, A. V. & SHUMAN, H. 1979. Electron probe analysis of vascular smooth muscle. Composition of mitochondria, nuclei, and cytoplasm. *The Journal of cell biology,* 81**,** 316-35.
SOMLYO, A. P., SOMLYO, A. V., SHUMAN, H., SLOANE, B. & SCARPA, A. 1978. "Electron probe analysis of the sarcoplasmic reticulum and mitochondria in muscle". *Microsc Acta Suppl,* 2**,** 79-91.
SONES, W. R., DAVIS, A. J., LEBLANC, N. & GREENWOOD, I. A. 2010. Cholesterol depletion alters amplitude and pharmacology of vascular calcium-activated chloride channels. *Cardiovasc Res,* 87**,** 476-84.
SOWA, G., PYPAERT, M. & SESSA, W. C. 2001. Distinction between signaling mechanisms in lipid rafts vs. caveolae. *Proc Natl Acad Sci U S A,* 98**,** 14072-7.
SPEDDING, M. & PAOLETTI, R. 1992. Classification of calcium channels and the sites of action of drugs modifying channel function. *Pharmacol Rev,* 44**,** 363-76.
STREHLER, E. E. & TREIMAN, M. 2004. Calcium pumps of plasma membrane and cell interior. *Current molecular medicine,* 4**,** 323-35.
SWEENEY, M., JONES, C. J. P., GREENWOOD, S. L., BAKER, P. N. & TAGGART, M. J. 2006. Ultrastructural Features of Smooth Muscle and Endothelial Cells of Isolated Isobaric Human Placental and Maternal Arteries. *Placenta,* 27**,** 635-647.
SZADO, T., MCLARNON, M., WANG, X. & VAN BREEMEN, C. 2001. Role of sarcoplasmic reticulum in regulation of tonic contraction of rabbit basilar artery. *American Journal of Physiology - Heart and Circulatory Physiology,* 281**,** H1481-H1489.
TABERNERO, A., GIRALDO, J. & VILA, E. 1996. Effect of NG-nitro-L-arginine methylester (L-NAME) on functional and biochemical alpha 1-adrenoceptor-mediated responses in rat blood vessels. *Br J Pharmacol,* 117**,** 757-63.
TAGAWA, M., UEYAMA, T., OGATA, T., TAKEHARA, N., NAKAJIMA, N., ISODONO, K., ASADA, S., TAKAHASHI, T., MATSUBARA, H. & OH,

H. 2008. MURC, a muscle-restricted coiled-coil protein, is involved in the regulation of skeletal myogenesis. *Am J Physiol Cell Physiol,* 295**,** 28.

TAGGART, M. J. 2001. Smooth muscle excitation-contraction coupling: a role for caveolae and caveolins? *News in physiological sciences : an international journal of physiology produced jointly by the International Union of Physiological Sciences and the American Physiological Society,* 16**,** 61-5.

TANAKA, Y., YAMASHITA, Y., YAMAKI, F., HORINOUCHI, T., SHIGENOBU, K. & KOIKE, K. 2003. MaxiK channel mediates beta2-adrenoceptor-activated relaxation to isoprenaline through cAMP-dependent and -independent mechanisms in guinea-pig tracheal smooth muscle. *J Smooth Muscle Res,* 39**,** 205-19.

TANG, Z., SCHERER, P. E., OKAMOTO, T., SONG, K., CHU, C., KOHTZ, D. S., NISHIMOTO, I., LODISH, H. F. & LISANTI, M. P. 1996. Molecular cloning of caveolin-3, a novel member of the caveolin gene family expressed predominantly in muscle. *The Journal of biological chemistry,* 271**,** 2255-61.

THIELE, C., HANNAH, M. J., FAHRENHOLZ, F. & HUTTNER, W. B. 2000. Cholesterol binds to synaptophysin and is required for biogenesis of synaptic vesicles. *Nat Cell Biol,* 2**,** 42-9.

TONG, W. C., SWEENEY, M., JONES, C. J., ZHANG, H., O'NEILL, S. C., PRIOR, I. & TAGGART, M. J. 2009. Three-dimensional electron microscopic reconstruction of intracellular organellar arrangements in vascular smooth muscle--further evidence of nanospaces and contacts. *Journal of Cellular and Molecular Medicine,* 13**,** 995-8.

VANHOUTTE, P. M. 1989. Endothelium and control of vascular function. State of the Art lecture. *Hypertension,* 13**,** 658-67.

WALSER, P. J., ARIOTTI, N., HOWES, M., FERGUSON, C., WEBB, R., SCHWUDKE, D., LENEVA, N., CHO, K. J., COOPER, L., RAE, J., FLOETENMEYER, M., OORSCHOT, V. M., SKOGLUND, U., SIMONS, K., HANCOCK, J. F. & PARTON, R. G. 2012. Constitutive formation of caveolae in a bacterium. *Cell,* 150**,** 752-63.

WANG, X. L., YE, D., PETERSON, T. E., CAO, S., SHAH, V. H., KATUSIC, Z. S., SIECK, G. C. & LEE, H. C. 2005. Caveolae targeting and regulation of large conductance Ca(2+)-activated K+ channels in vascular endothelial cells. *The Journal of biological chemistry,* 280**,** 11656-64.

WASANO, K. & YAMAMOTO, T. 1983. Tridimensional architecture of elastic tissue in the rat aorta and femoral artery--a scanning electron microscope study. *J Electron Microsc (Tokyo),* 32**,** 33-44.

WAY, M. & PARTON, R. G. 1995. M-caveolin, a muscle-specific caveolin-related protein. *FEBS Lett,* 376**,** 108-12.

WELLMAN, G. C. & NELSON, M. T. 2003. Signaling between SR and plasmalemma in smooth muscle: sparks and the activation of Ca2+-sensitive ion channels. *Cell Calcium,* 34**,** 211-29.

WHITE, R. E., KRYMAN, J. P., EL-MOWAFY, A. M., HAN, G. & CARRIER, G. O. 2000. cAMP-dependent vasodilators cross-activate the cGMP-dependent protein kinase to stimulate BK(Ca) channel activity in coronary artery smooth muscle cells. *Circ Res,* 86**,** 897-905.

WIECHEN, K., SERS, C., AGOULNIK, A., ARLT, K., DIETEL, M., SCHLAG, P. M. & SCHNEIDER, U. 2001. Down-regulation of caveolin-1, a candidate tumor suppressor gene, in sarcomas. *Am J Pathol,* 158**,** 833-9.

WIJETUNGE, S. & HUGHES, A. D. 2005. Mechanism of contraction of rat isolated tail arteries by hyposmotic solutions. *J Vasc Res,* 42**,** 93-100.
WULF, H., HAY-SCHMIDT, A., POULSEN, A. N., KLAERKE, D. A., OLESEN, J. & JANSEN-OLESEN, I. 2009. Molecular investigations of BK(Ca) channels and the modulatory beta-subunits in porcine basilar and middle cerebral arteries. *J Mol Histol,* 40**,** 87-97.
XU, Y., BUIKEMA, H., VAN GILST, W. H. & HENNING, R. H. 2008. Caveolae and endothelial dysfunction: filling the caves in cardiovascular disease. *Eur J Pharmacol,* 585**,** 256-60.
XU, Y., HENNING, R. H., VAN DER WANT, J. J., VAN BUITEN, A., VAN GILST, W. H. & BUIKEMA, H. 2007. Disruption of endothelial caveolae is associated with impairment of both NO- as well as EDHF in acetylcholine-induced relaxation depending on their relative contribution in different vascular beds. *Life Sci,* 80**,** 1678-85.
YAMADA, E. 1955. The fine structure of the gall bladder epithelium of the mouse. *The Journal of biophysical and biochemical cytology,* 1**,** 445-58.
YAMAMOTO, H., HWANG, O. & VAN BREEMEN, C. 1984. Bay K8644 differentiates between potential and receptor operated Ca2+ channels. *Eur J Pharmacol,* 102**,** 555-7.
YAMAMOTO, K., FURUYA, K., NAKAMURA, M., KOBATAKE, E., SOKABE, M. & ANDO, J. 2011. Visualization of flow-induced ATP release and triggering of Ca2+ waves at caveolae in vascular endothelial cells. *J Cell Sci,* 124**,** 3477-83.
YAMAMOTO, Y., IMAEDA, K. & SUZUKI, H. 1999. Endothelium-dependent hyperpolarization and intercellular electrical coupling in guinea-pig mesenteric arterioles. *J Physiol,* 514**,** 505-13.
YAMAMURA, A., YAMAMURA, H., GUO, Q., ZIMNICKA, A. M., WAN, J., KO, E. A., SMITH, K. A., POHL, N. M., SONG, S., ZEIFMAN, A., MAKINO, A. & YUAN, J. X. 2013. Dihydropyridine Ca2+ Channel Blockers Increase Cytosolic [Ca2+] by Activating Ca2+-sensing Receptors in Pulmonary Arterial Smooth Muscle Cells. *Circ Res,* 112**,** 640-50.
YANCEY, P. G., RODRIGUEZA, W. V., KILSDONK, E. P., STOUDT, G. W., JOHNSON, W. J., PHILLIPS, M. C. & ROTHBLAT, G. H. 1996. Cellular cholesterol efflux mediated by cyclodextrins. Demonstration Of kinetic pools and mechanism of efflux. *J Biol Chem,* 271**,** 16026-34.
YOSHIDA, K., FLAVAHAN, N. A., HORIBE, M., SMEDIRA, N. G. & MURRAY, P. A. 1999. Endothelial defect mediates attenuated vasorelaxant response to isoproterenol after lung transplantation. *Am J Physiol,* 276**,** H159-66.
YUAN, P., LEONETTI, M. D., PICO, A. R., HSIUNG, Y. & MACKINNON, R. 2010. Structure of the human BK channel Ca2+-activation apparatus at 3.0 A resolution. *Science,* 329**,** 182-6.
ZHANG, S. X. 1999. *An Atlas of Histology,* Springer.